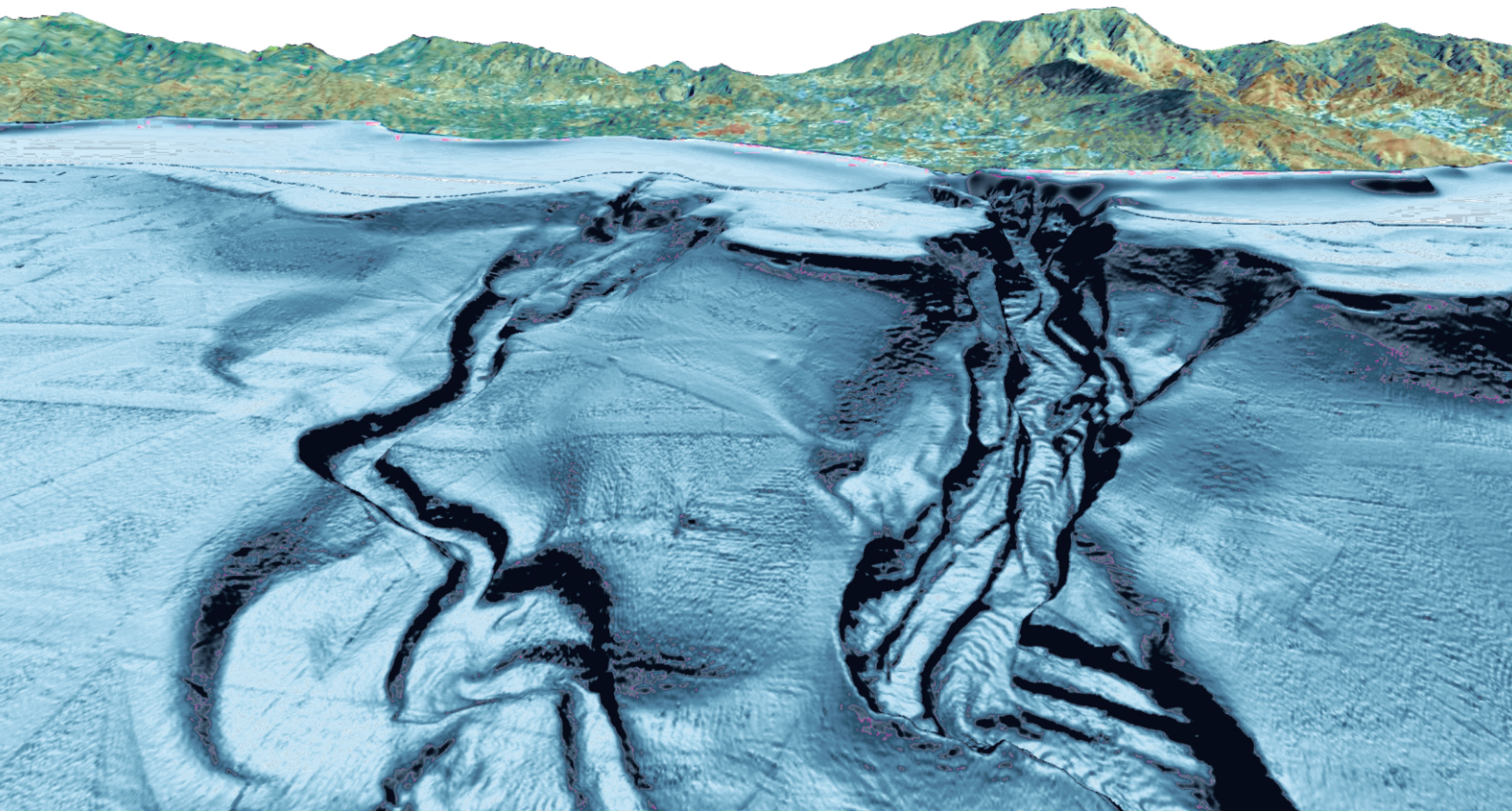


Sedimentary and litter transfer processes in the northern margin of the Alboran Sea:

**The role of shelf-incised submarine canyon
geomorphological characteristics**

Javier Cerrillo Escoriza
PhD Thesis, 2024

Supervisors:
Francisco José Lobo Sánchez
Ángel Puga Bernabéu



Editor: Universidad de Granada. Tesis Doctorales
Autor: Javier Cerrillo Escoriza
ISBN: 978-84-1195-404-4
URI: <https://hdl.handle.net/10481/94624>

A los que quieren entender los secretos del océano
con el fin de preservarlo como se merece

“Only the fact that the canyons are deeply hidden in the darkness of the sea prevents them
from being classed with the world’s most spectacular scenery”

Rachel Carson (The Sea Around Us, 1951)

Agradecimientos

Después de más de cuatro años voy a realizar el depósito de la tesis en el mismo lugar donde todo empezó, en el buque oceanográfico Sarmiento de Gamboa, rodeado de muchos que estuvieron y otros tantos que he conocido ahora. Por fortuna tuve la oportunidad de poder ser elegido para esta aventura y de investigar y trabajar en un tema que me encanta, que empezaría con una estupenda campaña oceanográfica en la costa de Granada y que le seguiría un camino duro. Que recientes estudios alerten sobre el deterioro del estado mental que sufren los estudiantes de doctorado (estrés, depresión, presión constante, pérdida de autoconfianza o insomnio) no es una coincidencia. Creo que esto debe cambiar ya y que todos somos responsables de esta situación. Sin embargo, el ambiente que te rodea es un factor imprescindible respecto a estas situaciones y por mi parte, me gustaría agradecer en primer lugar a mis directores de tesis **Paco** y **Ángel**, que depositaron en mí la confianza en este proyecto y su apoyo fue continuo a lo largo de estos años. Me siento afortunado y muy agradecido de haber tenido a ellos dos como directores y como personas a mi lado.

Me gustaría agradecer a **Paco** sus consejos, sus puntos de vista, su positividad, alegría, y sobre todo su dedicación sea el día que sea para echarme una mano en lo que haga falta. Además, hemos podido compartir varias vivencias como recorreremos toda la península en coche a por muestras sedimentarias. A **Ángel** siempre le estaré agradecido desde el Grado en Geología su confianza en mí. Su preocupación e interés no han cesado desde entonces. Por tantos consejos y ánimos. Tus puntos de vista geológicos hacen que indagar en los temas sea más ameno. Gracias a ambos por esta etapa. Me gustaría agradecer a **Julio** como tutor de esta tesis porque siempre ha tenido tiempo para ocuparse de la burocracia. Además, siempre es agradable estar con él y salir contento por la alegría que transmite.

A mi compañero de piso, **Circón**. El único que ha estado diariamente ahí. El apoyo de un gato y su cariño incondicional ha creado un vínculo muy especial. No concibo esta etapa de la misma manera sin él. **María**, mi agradecimiento especial para ti, ya que una parte es tuya, al haber aprendido tanto de ti. Tú has vivido todas mis frustraciones y mis horas de trabajo en vacaciones, así como los momentos de publicaciones y avances. Gracias por haber estado cerca, aun cuando se está lejos, por el apoyo, por todos los consejos, pero sobre todo por el cariño y el ánimo que he recibido cuando nadie más podía darme.

Y como he dicho, el entorno que nos rodea se ve reflejado también en este trabajo. En especial a mis compañeros del Instituto Andaluz de Ciencias de la Tierra. A mi compañero de

despacho, **Álvaro**, por todos los momentos vividos, numerosas charlas y su apoyo incesante. Por más cervezas así. **Erwin, Sara, Cecilia** y **Adri**, muchas gracias por transmitirme vuestra alegría, por vuestros abrazos y cariño diarios. ¡Hace falta más gente así! A **Rubén, Ricardo** y **Jon**, que siempre estuvieron ahí. Por los numerosos descansos y charlas que sientan tan bien. Al resto de compañeros que han dado y dan vida a los pasillos del IACT: **Bob, Alejandro, Manu, Antonio, Jorge, Dimitris, Manolis, Alpiste, Concha** e **Inma**. Mención especial a **Carolina, Ana** y **Juani**, porque vuestro trabajo de gestión es de agradecer cuando se hace con una sonrisa. Así da gusto venir al IACT.

A todos los compañeros de la Universidad de Granada tanto de la becaría de Estratigrafía y Paleontología como la de Geodinámica, por los buenos momentos que hemos pasado y por los consejos. Mención especial al Departamento de Estratigrafía y Paleontología por darme la oportunidad de formar parte del equipo docente. A **Ángel, Alberto, Fernando** y **Agustín**, por vuestra organización de las clases y/o campos y sus consejos en la docencia.

Esta tesis no había sido posible sin el apoyo de todos los coautores que han participado en las publicaciones durante estos años. En especial a **Jose Luis, Patricia** y **Olga** (IEO Málaga-CSIC), **Isabel** (CIMA), **Noel** (UGR), **Aaron** e **Irena** (UMalta) por vuestra gran dedicación y por vuestros mensajes de ánimo y cariño que han ayudado tanto a esta tesis. A **Marga** (IEO Cádiz-CSIC), que siempre tiene palabras bonitas y de ánimo. A **Ruth** (ICM-CSIC) porque siempre intenta ayudarme en cualquier aspecto incondicionalmente. Mención especial a **Anxo** (UVigo) y su gran acogida en Vigo durante tantas semanas, nuestras charlas variopintas y los furanchos. También me gustaría agradecer a los compañeros de mi estancia en la Universidad de Malta. A **Aaron** por su gran acogida en el *Marine Geology and Seafloor Surveying Group*. A **Irena, Monica, Ariel** y **Andrea** por hacer del centro de trabajo un lugar divertido.

Durante toda mi etapa en Granada, no puedo evitar acordarme de mis compis de grado, a los **Trotamontes**, que siempre estarán ahí para lo que hagan falta. En especial en **Cristina** y **Cecilia**. **Cristina** muchas gracias por todo el apoyo que me has dado todos estos años, por tu preocupación y por todo el cariño, así como los cuidados gatunos. A **Cecilia**, que comparte los cañones submarinos como estudio, siempre tiene tiempo para animarme con la tesis. A **Antonio** que siempre que ha podido ha estado a mi lado. A mi prima **Cristina** que en poco tiempo me hecho sentir tan bien. A **Sergio**, por su felicidad contagiosa, gracias.

A todos mis amigos de Altea, a los que están aquí como **Jake** y **Alex**, siempre en contacto y con su apoyo. A los que siguen allí, **Norberto, Scott, Paco, Marco, Manu, Jaime, Chema, Roberto, Sete, Alberto, Jorge, Fernando** y **Nacho**. Es un placer llegar a la terreta y que te reciban como si no te hubieras ido.

Muchas gracias a toda mi familia que me ha apoyado a lo largo de todos estos años. A mi hermano, que ha sido un amigo de confianza. Pero en especial a mis padres porque es imposible que todos estos años hubieran ocurrido si no hubiera sido por mi madre y mi padre. El agradecimiento más profundo que tengo es para ellos. Aun cuando no entendían bien lo que estudiaba, nunca dejaron de apoyarme en todas las decisiones que tomé. Siempre se han preocupado por el desarrollo de la tesis, me han facilitado todo en mi vida, haciéndome sentir seguro y confiado. Por eso, si puedo ser doctor, es gracias a vosotros. Os quiero mucho.

Funding: This research presented in this Ph. D thesis has been carried out in the Department of Marine Geosciences, at the Instituto Andaluz de Ciencias de la Tierra (CSIC-UGR) and Departamento de Estratigrafía y Paleontología, Facultad de Ciencias, Universidad de Granada. Financial support was provided by a grant *Ayudas para contratos predoctorales para la formación de doctores* with the grant PRE2018-084812 funded by MCIN/AEI/10.13039/501100011033 and *FSE Invierte en tu futuro*, from the *Ministerio de Ciencia e Innovación*, Spanish government. Additional fundings to research activity were provided by the Spanish projects: Alboran Shelf-Slope cOupling processes and deep sediMent trAnsfeR: Source To Sink approaches and implications for biodiversity–ALSSOMAR S2S (CTM2017-88237-P), funded by “Ministerio de Economía y Competitividad”, Spanish government, and Sediment gravity flows and ANthropogenic Impacts in a MEDiterranean deltaic-and-canyon environment: Causal relationships and consequences–SANIMED (PID2021-125489OB-I00) funded by MCIN/AEI/10.13039/501100011033/FEDER, UE.



Cabo de Sacratif, Motril (Granada)

Peter Bojthe

“El mar, quien lo mira lo ve por vez primera, siempre”

Jose Luis Borges

Abstract

Submarine canyons are major morphological features incising continental margins that constitute the main pathways for shelf-to-basin sediment transfer and flux of contaminants and waste during sea-level highstands, as documented in various modern turbidite systems. Factors that control the sedimentary activity in submarine canyons during highstands include the geodynamic setting, the location of the canyon head with respect to the major sediment sources, and the margin width. The northern margin of the Alboran Sea (western Mediterranean Sea) is characterized by a narrow shelf sculpted by the shelf-incised Motril and Carchuna canyons. This thesis aims to establish the factors that control the recent sedimentary activity of the shelf-incised canyons, based on: (1) the geomorphological and sedimentary differences between both canyons, elucidating their respective roles in recent patterns of sediment transport and accumulation between both canyons; (2) the characterization of erosional and depositional bedforms in confined and unconfined settings of the Carchuna Canyon, determining genetic sedimentary processes leading to bedform development in recent times; and (3) the factors that control the distribution of marine litter in the studied submarine canyons, analyzing the litter distribution, density, and origin.

The straight Carchuna Canyon incises the shelf up to 200 m off the coastline and exhibits steep canyon walls featuring narrow terraces, muddy sands with high contents of organic matter along the thalweg, and transported shelf benthic foraminifera in distal settings. The Carchuna Canyon hosts crescentic-shaped bedforms in the axial channel and concentric sediment waves and two scour trails over an overbank deposit, proximal to a channel bend. The Carchuna Canyon thalweg exhibits a density of marine litter up to $8.66 \text{ items} \cdot 100 \text{ m}^{-1}$ with litter hotspots found along the upper reaches of the canyon thalweg. In contrast, the Motril Canyon head is wider and incises the shelf edge, ca. 2 km off the coastline, exhibiting a sinuous morphology and less steep walls, wider terraces, and higher sedimentation rates with muddy sediments along the thalweg. In the Motril Canyon, the density of marine litter is low and the material is scattered, very degraded, and partially buried.

The Carchuna Canyon exhibits a youthful development stage whose activity is more continuous, caused by coarse sediment-laden gravity flows descending from the canyon head and by spillover processes generating sediment waves in the channel bend. More energetic downstream turbiditic flows would exceed the levee crest maximum height, promoting erosion of the overbank deposit and generating scour trains. The high shelf incision of the Carchuna Canyon and its proximity to the coastline favor littoral sediment remobilization and

capture, as well as the formation of gravity flows that transport marine litter along the thalweg toward the distal termination of the channel. In contrast, the Motril Canyon is interpreted as a mature system episodically active which mainly acts as a sediment trap accumulating hemipelagic sediments, where the distant location of the canyon head from the coastline (ca. 2 km) favors fine-grained sediment accumulation from the major regional fluvial source and the input of low amounts of marine litter.

The comparison of the studied shelf-incised canyons with other shelf-incised canyons in narrow and wide margins indicates that: (1) the distance from canyon heads to coastlines exerts the primary control on sediment caliber and flux that is potentially captured by shelf-incised canyons and eventually transported downcanyon; (2) the grade of incision of canyon heads is a key factor driving the recent sedimentary activity of canyons incised in narrow margins; and (3) the physiographic and sediment supply constraints of narrow margins, such as offshore California and the Mediterranean Sea, is a factor controlling the evolution, the sedimentary activity and the high concentration of marine litter in shelf-incised canyons.

Resumen

Los cañones submarinos son rasgos morfológicos que inciden en los márgenes continentales y constituyen las principales vías de transferencia desde la plataforma hasta la cuenca de sedimentos y flujo de contaminantes y residuos, como se ha documentado en varios sistemas turbidíticos modernos. Los factores que controlan la actividad sedimentaria de los cañones submarinos durante los niveles altos del mar incluyen el contexto geodinámico, la localización de la cabecera del cañón con respecto a fuente principal de sedimento y la anchura del margen continental. El margen norte del Mar de Alborán (oeste del Mar Mediterráneo) está caracterizado por una plataforma estrecha incidida por los cañones de Motril y Carchuna. Esta tesis tiene como objetivo establecer los factores que controlan la actividad sedimentaria reciente de los cañones incididos en la plataforma, basado en: (1) las diferencias geomorfológicas y sedimentarias entre ambos cañones, elucidando los patrones recientes de transporte y acumulación de sedimento entre ambos cañones; (2) la caracterización de las formas de fondo erosivas y deposicionales localizadas en contextos confinados y no confinados del Cañón de Carchuna y las implicaciones genéticas en términos de procesos de transporte sedimentario; (3) analizar la distribución, densidad y origen de la basura marina en los cañones submarinos objeto de estudio.

El rectilíneo Cañón de Carchuna incide la plataforma donde su cabecera se localiza a apenas 200 m de la línea de costa; este cañón presenta flancos de elevada inclinación, terrazas estrechas, arenas fangosas con alto contenido de materia orgánica a lo largo del eje del canal y foraminíferos bentónicos de plataforma transportados hacia las zonas distales. El Cañón de Carchuna alberga formas de fondo en forma de media luna en el eje de canal y ondas de sedimentos y trenes de socavaciones sobre los depósitos de desbordamiento cercanos a una curva del canal. Además, el eje de canal presenta una densidad de basura marina de hasta $8.66 \text{ unidades} \cdot 100 \text{ m}^{-1}$ en forma de acumulaciones en las partes superiores del cañón. En contraste, la cabecera del Cañón de Motril es más amplia e incide el borde la plataforma a 2 km de la línea de costa. Presenta una morfología sinuosa y flancos más suavizados, amplias terrazas y tasas de sedimentación más altas con sedimentos fangosos a lo largo del eje del canal. En el Cañón de Motril, la densidad de basura marina es baja y la basura aparece dispersa, muy degradada y parcialmente enterrada.

El Cañón de Carchuna se encuentra en un estado de desarrollo juvenil cuya actividad es relativamente continua, causada por flujos gravitacionales de sedimentos groseros que descienden desde la cabecera y desbordan en las partes inferiores generando ondas de

sedimento sobre un lóbulo deposicional. Eventualmente, flujos turbidíticos de alta energía serían capaces de desplazarse por encima de la cresta del dique, erosionando los depósitos de desbordamiento y generando trenes de socavaciones. La alta incisión en la plataforma del Cañón de Carchuna y su proximidad a la línea de costa favorecería la captura y remobilización del sedimento litoral, así como la formación de flujos gravitacionales que transportan la basura marina a lo largo de todo el valle hacia su terminación distal. En contraste, el Cañón de Motril está en un estadio evolutivo más maduro y muestra una actividad episódica, actuando principalmente como trampa de sedimentos hemipelágicos. La localización aproximadamente a 2 kilómetros de la cabecera a la línea de costa más cercana condicionaría la acumulación de sedimentos de grano fino proveniente de la principal fuente fluvial (i.e., Río Guadalfeo) y la acumulación de bajas cantidades de basura marina.

La comparación de los cañones incididos en la plataforma de estudio con otros cañones que inciden en otras plataformas con extensiones variadas indican que: (1) la distancia desde las cabeceras a la línea de costa ejerce un papel fundamental en el calibre y flujos de sedimentos que pueden ser potencialmente capturados por los cañones incididos en la plataforma y eventualmente transportados hacia las partes profundas del cañón; (2) el grado de incisión de las cabeceras es un factor clave que determina en gran medida la actividad sedimentaria reciente de los cañones que inciden en plataformas estrechas; (3) las condiciones fisiográficas y de aporte sedimentario en los márgenes estrechos, como las que se encuentran en la costa de California y el Mar Mediterráneo, controlan de forma decisiva la actividad sedimentaria reciente y las altas concentraciones de basuras marinas que se observan en los cañones incididos en la plataforma.

Table of contents

| | |
|------------------------------|------|
| <i>Agradecimientos</i> | II |
| Abstract | VI |
| <i>Resumen</i> | VIII |

Part 1

| | |
|--|--------|
| 1. Introduction | 2 |
| 1.1. Importance of the thesis | 3 |
| 1.2. Physiography of submarine canyons..... | 3 |
| 1.3. Global distribution of submarine canyons | 5 |
| 1.4. Sediment transport processes in submarine canyons | 7 |
| 1.4.1. Sediment transport by oceanographic processes | 8 |
| 1.4.2. Sedimentological processes..... | 9 |
| 1.5. Sedimentary products in submarine canyons | 11 |
| 1.6. Controls in the sedimentary activity of submarine canyons | 14 |
| 1.6.1. Type of continental margin | 14 |
| 1.6.2. Sea-level changes | 15 |
| 1.6.3. Degree of canyon shelf incision | 16 |
| 1.6.4. Relationship between canyon heads and major sedimentary sources | 16 |
| 1.7. The human imprint | 17 |
| 1.8. Objectives..... | 19 |
| 1.9. Structure of the thesis..... | 20 |
| 2. Regional setting | 22 |
| 2.1. Geological setting..... | 23 |
| 2.2. The coastal domain..... | 26 |
| 2.3. Submarine geomorphology and deep-water deposits and processes | 27 |
| 2.4. Oceanographic setting | 29 |
| 2.5. Recent to modern sedimentary processes..... | 30 |
| 2.6. Seafloor habitats and biota | 31 |

| | |
|--|-----------|
| 2.7. Anthropogenic activity | 32 |
| 3. Materials and methods..... | 33 |
| 3.1. Bathymetric data | 34 |
| 3.2. Seafloor imagery | 37 |
| 3.3. Sediment samples | 41 |
| 3.3.1. Grain size..... | 41 |
| 3.3.2. Geochemical analysis | 42 |
| 3.3.3. Sedimentation rates | 43 |
| 3.3.4. Surficial foraminifera | 43 |
| 3.4. Sub-bottom profiles | 44 |
| 3.5. Three-dimensional flow simulation | 46 |
| 3.6. Coastal use data..... | 46 |
| 3.7. Maritime traffic data (AIS) | 47 |
| 3.8. Fishing activity data (VMS)..... | 47 |

Part 2

| | |
|--|-----------|
| 4. Morphology and recent sedimentary processes in the shelf-incised Motril and Carchuna canyons: Implications for recent canyon activity..... | 50 |
| Abstract | 51 |
| 4.1. Results | 52 |
| 4.1.1. Geomorphology..... | 52 |
| 4.1.1.1. Major morphological features | 52 |
| 4.1.1.2. Morphometric parameters | 55 |
| 4.1.2. Surficial sediments | 58 |
| 4.1.2.1. Sedimentary facies from seafloor imaging and grain size | 58 |
| 4.1.2.2. Organic matter and carbonate contents | 61 |
| 4.1.3. Sub-surface sediments..... | 62 |
| 4.1.3.1. Sediment cores | 62 |
| 4.1.3.2. Mass accumulation rates | 64 |
| 4.1.3.3. Surficial foraminifera | 64 |

| | |
|---|-----------|
| 4.2. Discussion | 67 |
| 4.2.1. Relation between sedimentary processes and canyon morphology | 67 |
| 4.2.1.1. Comparison with other shelf-incised canyons | 67 |
| 4.2.1.2. Geomorphological differences between Motril and Carchuna canyons | 69 |
| 4.2.2. Implications for canyon activity | 73 |
| 4.3. Conclusions | 77 |
| 5. Bedform development in confined and unconfined settings of the Carchuna Canyon: An example of cyclic steps in shelf-incised canyons | 78 |
| Abstract | 79 |
| 5.1. Results | 80 |
| 5.1.1. Geomorphology and sedimentology of the Carchuna Canyon | 80 |
| 5.1.2. Fine-scale morphology of the Carchuna Canyon | 85 |
| 5.1.3. Sub-surface acoustic facies and architecture of Carchuna Canyon bedforms | 90 |
| 5.1.3.1. Description of acoustic facies | 90 |
| 5.1.3.2. Interpretation of acoustic facies | 93 |
| 5.1.4. Sediment transport simulation..... | 96 |
| 5.2. Discussion | 98 |
| 5.2.1. Development of cyclic steps along the confined setting of the Carchuna Canyon ... | 98 |
| 5.2.1.1. The role of turbidity currents in CSB development | 98 |
| 5.2.1.2. Variability in CSB geometries along the axial channel | 100 |
| 5.2.1.3. Implications of local variability in the slope gradient..... | 101 |
| 5.2.2. Development of cyclic steps along the unconfined setting of the Carchuna Canyon | 102 |
| 5.2.2.1. Factors that control the overflows in the Carchuna Canyon | 102 |
| 5.2.2.2. Sediment waves formed in the overbank deposit of the Carchuna Canyon.. | 105 |
| 5.2.2.3. Scours formed in the overbank deposit of the Carchuna Canyon | 106 |
| 5.2.3. Recent evolution of the Carchuna Canyon..... | 108 |
| 5.2.3.1. High-density turbidity current scenario..... | 108 |
| 5.2.3.2. Low-density turbidity current scenario | 111 |
| 5.3. Conclusions | 113 |

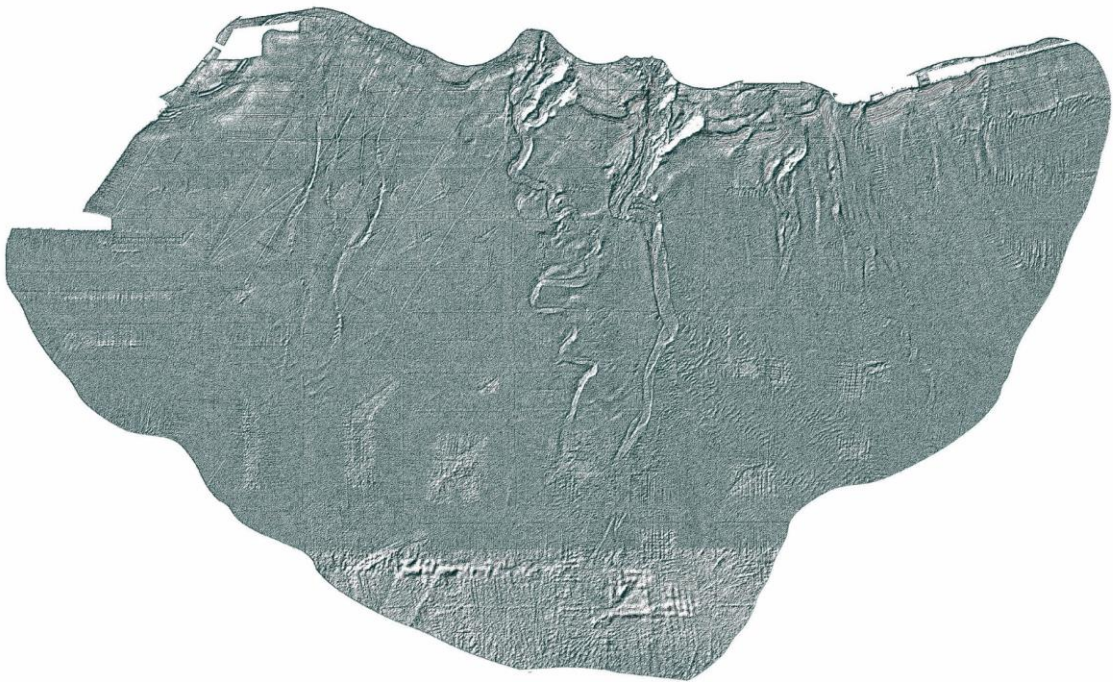
| | |
|---|------------|
| 6. Origin and driving mechanisms of marine litter in the shelf-incised Motril, Carchuna, and Calahonda canyons | 114 |
| Abstract | 115 |
| 6.1. Results | 116 |
| 6.1.1. Overall geomorphology and sedimentology of submarine canyons | 116 |
| 6.1.2. Marine litter distribution | 117 |
| 6.1.3. Other seafloor bottom anthropogenic marks | 123 |
| 6.1.4. Anthropogenic activity regarding the main seafloor habitats | 123 |
| 6.1.5. Mapping of the coastal domain | 126 |
| 6.1.6. Maritime traffic routes | 127 |
| 6.1.7. Mapping of the fishing activity | 128 |
| 6.2. Discussion | 130 |
| 6.2.1. Drivers of the litter abundance | 130 |
| 6.2.2. Drivers of the litter distribution..... | 132 |
| 6.2.3. Litter origin: Coastal uses and marine activities | 133 |
| 6.2.4. Interactions of anthropogenic activity indicators with marine habitats and species | 136 |
| 6.3. Conclusions | 139 |

Part 3

| | |
|---|------------|
| 7. General discussion..... | 142 |
| 7.1. Sedimentary activity in shelf-incised versus blind submarine canyons..... | 143 |
| 7.2. Importance of margin physiography on the sedimentary activity in shelf-incised submarine canyons | 145 |
| 7.2.1. Main sedimentary processes in canyons incised in narrow and wide margins | 146 |
| 7.2.2. Development of bedforms in shelf-incised canyons along narrow versus wide margins | 147 |
| 7.2.2.1. Confined bedforms in shelf-incised canyons in narrow versus wide margins..... | 147 |
| 7.2.2.2. Unconfined bedforms in shelf-incised canyons in narrow versus wide margins..... | 148 |

| | |
|--|------------|
| 7.2.3. Abundance, origin, and distribution of marine litter in shelf-incised canyons in narrow versus wide margins | 149 |
| 7.2.3.1. Abundance of marine litter in shelf-incised canyons in narrow versus wide margins | 149 |
| 7.2.3.2. Origins of marine litter along shelf-incised canyons in narrow versus wide margins | 150 |
| 7.2.3.3. Litter distribution within shelf-incised canyons in narrow versus wide margins | 152 |
| 7.3. Sedimentary processes of shelf-incised canyons in narrow margins | 153 |
| 7.3.1. Relationship between the degree of canyon incision and turbidity current initiation initiation | 153 |
| 7.3.1.1. Shelf-incised canyons fed by river systems in narrow margins..... | 154 |
| 7.3.1.2. Shelf-incised canyons fed by longshore currents in narrow margins..... | 156 |
| 7.3.1.3. Shelf-incised canyons fed by multiple processes in narrow margins..... | 158 |
| 7.3.2. Bedform development in shelf-incised canyons carved in narrow margins | 159 |
| 7.3.3. Relation between the degree of incision of margin canyons and marine litter in narrow margins..... | 160 |
| 7.3.3.1. Relation between the abundance of marine litter and the degree of canyon incision..... | 162 |
| 7.3.3.2. Relation between the origin of marine litter and the degree of canyon incision | 162 |
| 8. Conclusions | 164 |
| 8.1. Conclusions | 165 |
| 8.2. Forthcoming research..... | 167 |
| 9. Supplementary material | 169 |
| 10. References | 172 |

Part 1



1. Introduction
2. Regional setting
3. Materials and methods

Chapter 1

Introduction

1.1. Importance of the thesis

Submarine canyons are common morphological features incised on continental margins (Daly, 1936; Shepard and Emery, 1941; Normark and Carlson, 2003; Harris and Whiteway, 2011) and the major conduits for the transport of sediment, nutrients, and pollutants from shelf to basin, generating deep-sea fans downstream (Shepard, 1981; Canals et al., 2004; Piper and Normark, 2009; Puig et al., 2014; Fisher et al., 2021). Interest in the evolution, occurrence, and distribution of canyons in the oceans has been motivated by various factors, including the need to lay cables and support naval submarine operations (Piper et al., 1999), to understand the geological evolution of continental margins, and to understand oceanographic and ecological processes associated with canyons (Clark et al., 1992; Harris and Whiteway, 2011). In addition, there are progressively more impacts from human activities along the submarine canyons that range from fishing, extraction of natural resources, and as sinks of marine litter (Dissanayake et al., 2023).

There has been a significant advancement in knowledge of modern submarine canyons in recent times due to the fact that the interplay between oceanographic, biological/ecological processes, and bathymetric and topographic features have consequences on the functioning and associated diversity of both pelagic and benthic communities (Paull et al., 2013; Fabri et al., 2017; Fernandez-Arcaya et al., 2017; Symons et al., 2017; Paradis et al., 2021, Zhou et al., 2021; Hernandez et al., 2022, Li et al., 2022; Scacchia et al., 2022; Miramontes et al., 2023; Pearman et al., 2023; Taviani et al., 2023). The advent of Remotely Operated Vehicles (ROV) or Autonomous Under-Water Vehicle (AUV) in the last 20 years opened up a new perspective on submarine canyon research, allowing to explore previously inaccessible parts of the deep ocean. Because of this increased research effort, our understanding of submarine canyons is gradually improving. However, the main limitation remains the technology of surface ships to image, monitor, and sample within these topographically hazardous and inaccessible complex marine environments (Khripounoff et al., 2003; Paull et al., 2002; Xu, 2011; Bailey et al., 2021).

1.2. Physiography of submarine canyons

The striking geomorphic resemblance between submarine canyons and river valleys has led to a shared terminology for their description. The axial channel of submarine canyons often features a well-defined thalweg, which is the line connecting the deepest points along the

canyon, bounded by one or more lower terraces and by sidewalls that separate the upper terraces and the eroded continental slope (Figure 1.1). The physiography of the submarine canyons is diverse, but can be broadly divided into upper, middle, and lower courses (Normark et al., 1993; Amblas et al., 2018, 2021) (Figure 1.1). The upper course is characterized by a canyon head incised into the continental shelf or the shelf edge, exhibiting a V-shaped profile with steep walls frequently covered by gullies and slump scars. The middle course exhibits a U-shaped cross-section with smoother reliefs and wider meandering valleys that erode the upper reaches of the continental slope. Submarine canyons commonly have tributaries feeding their upper and middle courses. The lower canyon course exhibits U-shaped profiles and low reliefs. Lower canyon courses exhibit sinuous paths and confined channels forming channel-levee systems between the lower reaches of the continental slope and the abyssal plain.

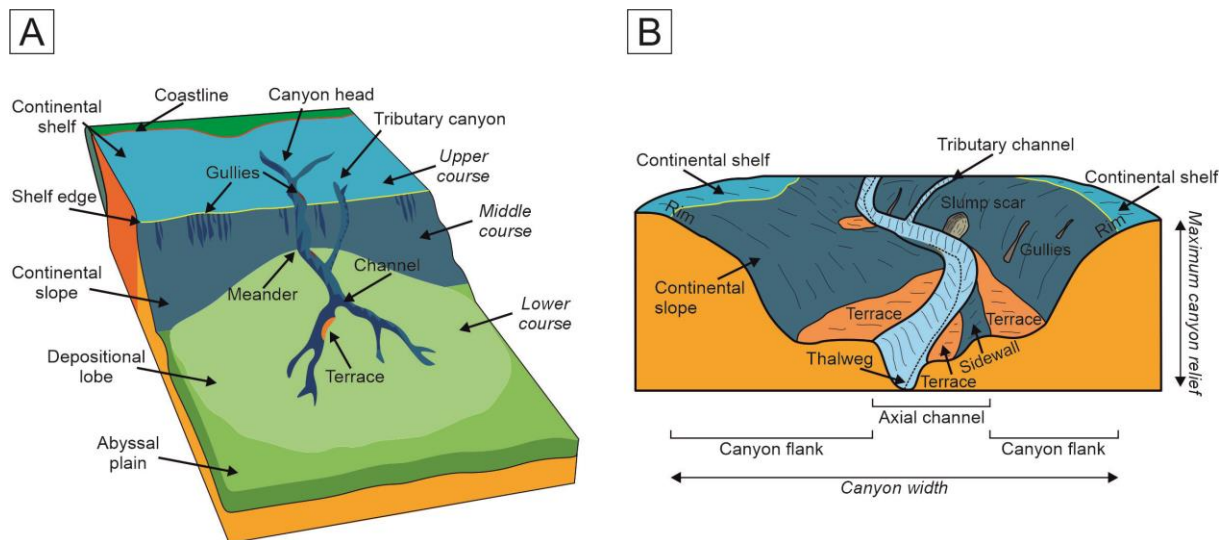


Figure 1.1. (A) Sketch showing the main physiographic elements of a submarine canyon. Modified from IUCN (2019) and adapted from the terminology used by Amblas et al. (2022). (B) 3D schematic diagram of a submarine canyon illustrating the terminology used to describe the major geomorphic features in this thesis. Adapted from the terminology used by Paull et al. (2013) and Tubau et al. (2015a).

Submarine canyons can be classified into three main types according to the distance of the canyon head to the coastline and the absence/occurrence of direct connection to terrestrial fluvial systems (Harris and Whiteway, 2011) (Figure 1.2): 1) shelf-incised canyons having heads connected to a major river system (e.g., Paull et al., 2002; Mazières et al., 2014; Paradis et al., 2021; Marsset et al., 2022); 2) shelf-incised canyons with no clear bathymetric connection to a major river system (e.g., Lastras et al., 2011a; Lo Iacono et al., 2020; Maier et

al., 2020; Dobbs et al., 2023); and 3) blind canyons incised onto the continental slope (Lastras et al. 2011b; Brothers et al. 2013; Huang et al. 2014; Lo Iacono et al. 2014). Shelf-incised canyons are large morphological features that erode into bedrock in their upper courses, with axial channels characterized by coarse-grained sediments (e.g., Smith et al., 2005; Normark et al., 2009b). They have been extensively studied in terms of their sedimentary activity favored by the proximity to sedimentary sources, such as shelf oceanographic processes and/or river systems, which are able to trigger turbidity currents. Sedimentary processes control the morphology and evolution of shelf-incised canyons, which can vary greatly (Walsh and Nittrouer, 2003; Zhu et al., 2009; Jobe et al., 2011; Lastras et al., 2011b; Amblas et al., 2012).

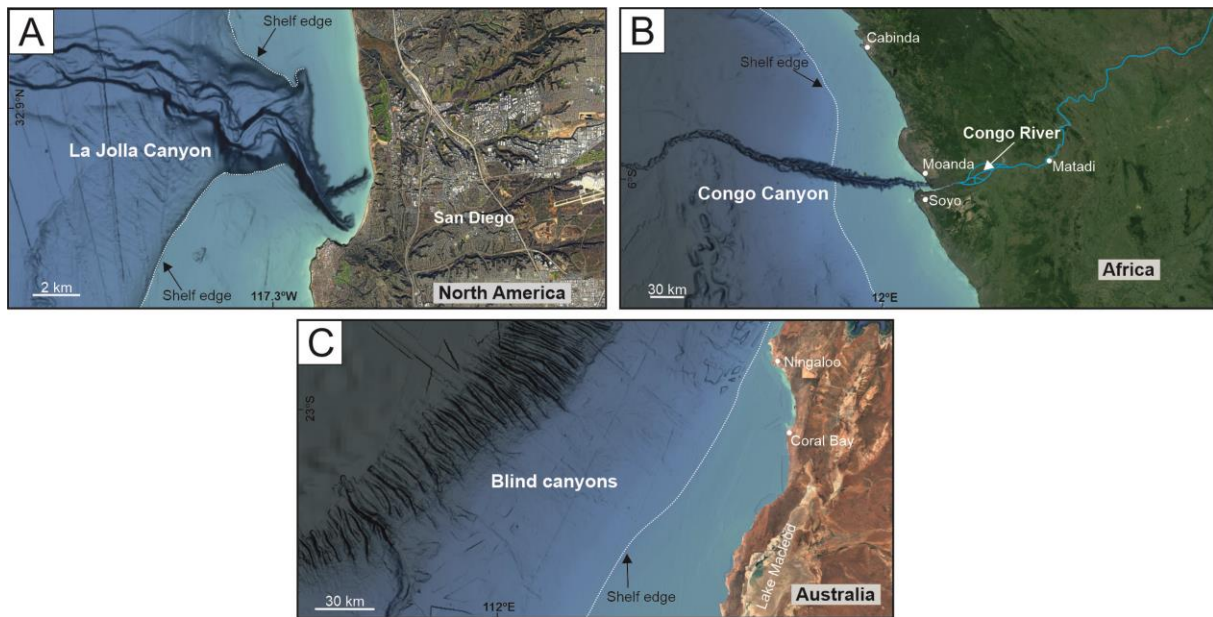


Figure 1.2. Three main types of submarine canyons according to the distance of the canyon head to the coastline and the absence/occurrence of direct connection to terrestrial fluvial systems. (A) Shelf-incised La Jolla Canyon with no bathymetric connection to a major river system. (B) Shelf-incised Congo Canyon with direct connection to the Congo River. (C) Blind canyons incised onto the continental slope in the northwestern Australian margin. Bathymetry extracted from the National Oceanic and Atmospheric Administration (NOAA, 2023) and image land extracted from the General Bathymetric Chart of the Oceans (GEBCO Compilation Group, 2023).

1.3. Global distribution of submarine canyons

Active continental margins contain over 50% more canyons than passive margins (Figure 1.3). Blind canyons are the most common type mapped being the shorter in length (Table 1.1). Shelf-incised canyons are over twice the mean size of blind canyons, longer, and less incised (Harris and Whiteway, 2011; Harris et al., 2014) (Table 1.1). Shelf-incised canyons

associated with rivers are common on active continental margins, specifically on the western margin of South and North America, but they are absent from the margins of Australia and Antarctica (Harris and Whiteway, 2011) (Table 1.1). In contrast, shelf-incised canyons with no connection to a major river system are distributed more or less equally amongst active and passive continental margins (Harris and Whiteway, 2011) (Table 1.1).

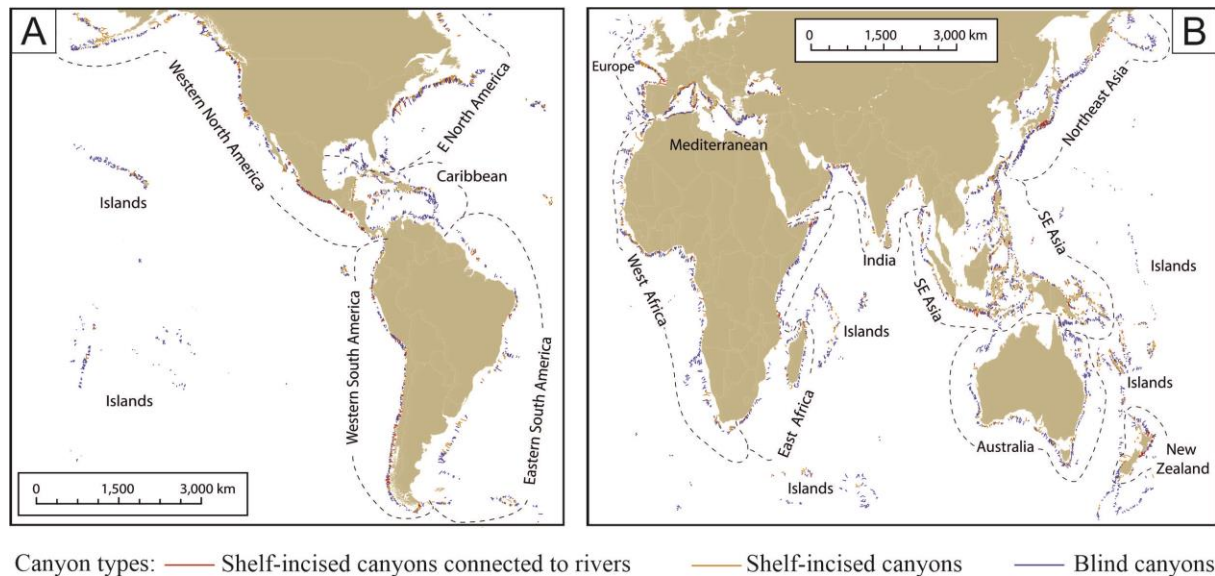


Figure 1.3. Global map showing the location of submarine canyons defined by Harris and Whiteway (2011). Canyon locations are classified into: shelf-incised canyons connected to rivers, shelf-incised canyons with no bathymetric connection to a major river system, and blind canyons incised onto the continental slope. Areas shown are North and South America (A) and Europe, Asia and Africa (B). Both maps are projected in Azimuthal Equidistant.

Mediterranean canyons constitute a well-defined family of submarine canyons at a global scale. Canyons in the Mediterranean and Black seas have the shortest mean length, the lowest incision depth, and the smallest average area compared to other ocean regions, for both shelf-incised and blind canyons (Harris and Whiteway, 2011) (Table 1.1). The distinctiveness of Mediterranean canyons stems from the fact that canyon genesis was dictated by a pronounced sea-level fall and desiccation event during the Messinian Salinity Crisis (Harris and Whiteway, 2011). Specifically, shelf-incised canyons are remarkable in Mediterranean active margins (Bernhardt and Schwanghart, 2021), where: (a) a regional correlation with regionally-averaged sediment discharges to the coast has been found (Harris and Macmillan-Lawler, 2015); and (b) their evolution is largely driven by erosive density currents (Bernhardt and Schwanghart, 2021).

Table 1.1.

Submarine canyon statistics (mean) for abundance, length, slope, sinuosity and canyon type. Based on Harris and Whiteway, 2011.

| | Percent | Length (km) | Slope (°) | Sinuosity | Percent type 1 | Percent type 2 | Percent type 3 |
|--------------------------|-------------|----------------|--------------|-------------|-------------------|-------------------|-------------------|
| Antarctica (P) | 7.83 | 56.1 | 3 | 1.09 | 0 | 39.08 | 60.92 |
| Arctic (P) | 5.90 | 65.2 | 2.7 | 1.07 | 0.29 | 35.07 | 64.64 |
| Australia (P) | 4.38 | 52.6 | 4.9 | 1.15 | 0 | 19.92 | 80.08 |
| Caribbean (A) | 2.86 | 52.1 | 5.2 | 1.14 | 0.43 | 23.50 | 76.07 |
| NE Asia (A) | 6.33 | 43.2 | 4.5 | 1.12 | 2.97 | 20.81 | 76.22 |
| E Africa (P) | 3.27 | 47.1 | 3.8 | 1.14 | 4.71 | 19.90 | 75.39 |
| E N-America (P) | 3.68 | 62.9 | 4.4 | 1.12 | 4.73 | 33.11 | 62.16 |
| E S-America | 3.27 | 49.8 | 4.3 | 1.13 | 1.57 | 24.08 | 74.35 |
| India (P) | 3.40 | 32.7 | 5.2 | 1.10 | 3.52 | 32.16 | 64.32 |
| Islands (A) | 17.40 | 30 | 7.3 | 1.10 | 0.10 | 23.26 | 76.64 |
| Mediterranean (A) | 8.86 | 26.5 | 6.5 | 1.11 | 3.86 | 29.54 | 66.60 |
| New Zealand (A) | 1.42 | 58.6 | 3.6 | 1.19 | 8.43 | 19.28 | 72.29 |
| SE Asia (A) | 15.70 | 36.4 | 5.8 | 1.12 | 2.51 | 37.69 | 59.80 |
| W Africa (P) | 3.83 | 57.1 | 3.4 | 1.09 | 1.34 | 29.91 | 68.75 |
| W Europe (P) | 2.38 | 49.6 | 4.5 | 1.12 | 2.88 | 26.62 | 70.50 |
| W N-America (A) | 4.96 | 60.7 | 4.3 | 1.23 | 8.62 | 25.17 | 66.21 |
| W S-America (A) | 4.55 | 35.6 | 5.1 | 1.26 | 11.65 | 22.93 | 65.41 |
| Type 1 | 2.62 | 80.9 | 3.8 | 1.19 | - | - | - |
| Type 2 | 28.57 | 50.4 | 5.2 | 1.12 | - | - | - |
| Type 3 | 68.82 | 39.1 | 5.2 | 1.11 | - | - | - |

A: Active margin; P: Passive margin; Type 1: shelf-incised canyons connected to river systems; Type 2: shelf-incised canyons with no direct connection with river system; Type 3: blind canyons.

1.4. Sediment transport processes in submarine canyons

Several studies have shown that submarine canyons have higher concentrations of suspended sediments (e.g., Palanques et al., 2006; Haalboom et al., 2021), downward particle fluxes (e.g., Palanques et al., 2005; Tarrés et al., 2022), and sediment accumulation rates (e.g., Puig et al., 2015; Paradis et al., 2021) than the surrounding open-slope regions (Puig et al., 2003). Although the progress in the study of submarine canyon processes has advanced with the ability to collect detailed bathymetric data to document seafloor morphology (Paull et al., 2011; Li et al., 2023; Cerrillo-Escoriza et al., 2024), yet mechanisms involved in transporting sediments into and through submarine canyons are not fully understood (Puig et al., 2014). The following sections are dedicated to outlining the most significant sediment transport mechanisms that have been described in submarine canyons (Figure 1.4).

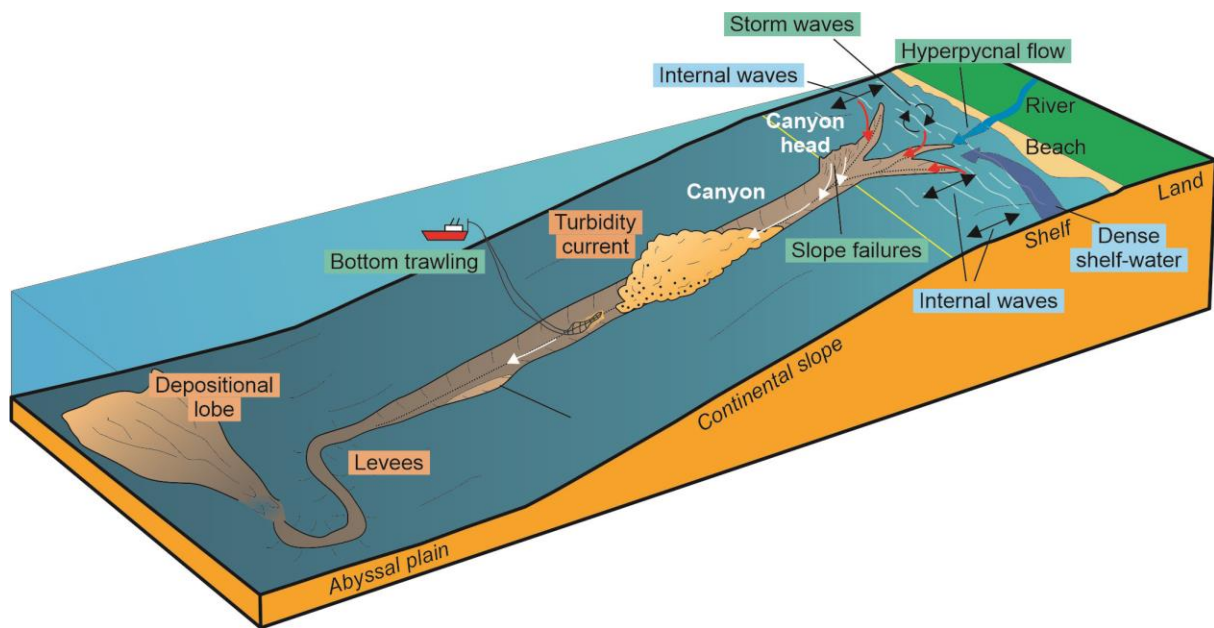


Figure 1.4. Oceanographic (in blue) and sedimentological (in green) transport processes in the shelf-incised submarine canyons.

1.4.1. Sediment transport by oceanographic processes

Submarine canyons affect the lateral movement of water masses along continental margins and the vertical movement within submarine canyons. Oceanographic processes such as dense shelf-water cascading (e.g., DeGeest et al., 2008; Palanques et al., 2012; Saldías and Allen, 2020) and internal waves (e.g., Xu et al., 2010; Puig et al., 2013, 2014; Droghei et al., 2016; Maier et al., 2019) favor particle dispersal within canyons.

Internal waves

Internal waves are oscillations along density boundaries within the water column. Submarine canyons act as effective pathways for funneling open-ocean internal wave energy to shallower waters (Gordon and Marshall, 1976). Increased bottom shear stresses as a result of these intensified internal waves are able to resuspend and subsequently transport sediment (Puig et al., 2004) (Figure 1.4). Periodic internal-wave resuspension has been observed in various submarine canyons, including the Monterey (Xu et al., 2002), Hueneme (Xu et al., 2010), Guadiaro (Puig et al., 2004), and Lisbon canyons (de Stigter et al., 2011).

Dense shelf-water cascading

Dense shelf-water cascading is a meteorologically-driven oceanographic phenomenon in which dense water over the continental shelf moves down the continental slope to greater depths as gravity-driven currents (Killworth, 1983; Ivanov et al., 2004) (Figure 1.4). Cascading events can be intensified by cold, dry winds, which cool and homogenize the shelf water column, enhancing dense water formation (Palanques et al., 2006) that can last from days to several weeks (Canals et al., 2006; Puig et al., 2014; Talling, 2014; Wunsch et al., 2017). Submarine canyons incised on continental shelves where this phenomenon occurs can channelize dense water transporting coarse-grained sediments and can create high sediment fluxes toward greater depths until they reach their neutral density level, causing resuspension and sediment transport (Canals et al., 2006; Puig et al., 2008, 2014).

1.4.2. Sedimentological processes

The main triggering processes of downcanyon sediment transfer are turbidity currents, which are gravity-driven flows in which sediment suspension is supported by turbulence that is denser than the surrounding water (Parsons et al., 2007), causing them to flow downslope as an undercurrent, where they can exchange sediment with the bed (Piper and Normark, 2009). Hence, if they move swiftly enough (favored on steeper slopes and in laterally confined conduits), they can entrain more sediment than they deposit and cause net erosion of the seafloor (Pratson et al., 2000; Mohrig and Marr, 2003; Piper and Normark, 2009). As they descend to lower slopes and/or lose their confinement, they tend to become depositional and eventually die out as the sediment driving their movement settles out (Amblas et al., 2022). There are several ways in which a turbidity current can form (Piper and Normark, 2009) (Figure 1.4): mass failures that may evolve via water entrainment and dilution into turbidity currents (Howarth et al., 2021), discharge or subglacial meltwater can flow hyperpycnal turbidity currents (Mulder and Syvitski, 1995), or storm waves can suspend and transport downslope sediments in bottom boundary layers (Puig et al., 2003; Friedrichs and Wright, 2004).

Sediment failures

Evidence of large slope failures evolving into turbidity currents channelized through submarine canyons comes mainly from data obtained from communication cable breaks

(Babonneau et al., 2017; Schulten et al., 2023). Such turbidity currents are extremely energetic, attaining speeds of tens of meters per second, and are therefore difficult to capture using moored instrumentation. They also have long run-out distances, generally extending along the entire length of the submarine canyon and submarine channel before arriving at the basin seafloor. Earthquakes have been suggested to generate large slope failures triggering turbidity currents in submarine canyons (e.g. Kaikōura Canyon, Mountjoy et al., 2018; Kaoping Canyon, Chiang and Yu, 2022).

Freshwater sediment-laden flows

An hypopycnal flow is a negatively buoyant plume that flows along the seafloor in front of a river mouth as a result of increased sediment concentration (Mulder et al., 2003), where the bulk density of the effluent (sediment and water) is greater than that of the receiving ambient water (Mulder and Alexander, 2001; Piper and Normark 2009). During significant periods of flooding, river discharges can carry large volumes of sediments ultimately transported into nearby canyon heads where they generate turbidity currents. This genetic process has been observed in several canyon heads, such as São Vicente (Serra et al., 2020), Var (Migeon et al., 2006), Saint-Etienne (Babonneau et al., 2013) and Alías-Almanzora canyons (Puig et al., 2017).

Storms

Storm waves can resuspend sediments within the bottom boundary layer that flows downslope, eventually generating turbidity currents (e.g., Paull et al., 2018; Li et al., 2019; Heijnen et al., 2022). In canyon heads, the initiation process during storms involves sand resuspension and ignition of seaward-advecting flows as the seafloor deepens faster than sediment fall out and more sediment is eroded from the canyon floor (Parker, 1982; Piper and Normark, 2009). These turbidity currents do not appear to reach slope fans or distal basin settings (Paull et al., 2005; de Stigter et al., 2007; Xu, 2011). Enhanced sediment transport and increased particle fluxes during storm events have been recorded in many submarine canyons by the advection of resuspended sediments from adjacent shelves, such as Monterey (Xu et al., 2013) and Mugu canyons (Xu et al., 2010).

Anthropogenic activities

Turbidity currents can also be generated by anthropogenic activity, such as bottom trawling (e.g., Martín et al., 2014; Puig et al., 2015; Paradis et al., 2021) (Figure 1.4). Trawling on the margins of submarine canyons leads to sediment suspension that generates dilute, slow-moving turbidity currents that advance along the main canyon axis and overspill the canyon flanks, contributing to the infilling of submarine canyons (Puig et al., 2012).

1.5. Sedimentary products in submarine canyons

The sedimentary products in shelf-incised canyons are mostly associated with lower reaches where depositional lobes are formed, whereas the upper reaches act mainly as sediment bypass areas. However, the axial channel of the canyon heads can act as temporal sediment storage, accumulating MTD triggered by high flanks gradients (e.g., Marsset et al., 2022; Wan et al., 2022) or low tides unloading seabed sediment (e.g., Hughes Clarke et al., 2014; Clare et al., 2016). In addition, other submarine canyons that are characterized by low sedimentary activity act as passive systems that accumulate hemipelagic sedimentation (e.g., Morelli et al., 2022; Cerrillo-Escoriza et al., 2024).

In the lower reaches, depositional lobes are complex morphological features that develop at the mouths of shelf-incised canyons (Figure 1.4) and are fed by terrigenous shallow-marine sediments which are redistributed into deeper water by sediment gravity flows, mainly turbidity currents (Deptuck and Sylvester, 2018). Most depositional lobes of shelf-incised canyons are made up of a combination of submarine channels that progressively build up levees and submarine lobe-like deposits that accumulate where sediment-gravity flows lose channel confinement (Deptuck and Sylvester, 2018). The main channel may be relatively straight and wide, flanked by highly asymmetric levees, as is the case for the Var fan in relatively steep margins (Migeon et al., 2006), or it may be highly sinuous and narrow, flanked by relatively symmetric levees, as is the case of the Congo-Zaire fan (Babonneau et al., 2002). Depositional lobes may be constituted by a series of channel-levee systems that develop through avulsions (Figure 1.5).

The dominance of sedimentary processes in shelf-incised canyons is reflected in the submarine morphology. Broad transitions from proximal erosional zones to distal depositional zones are usually observed (Arzola et al., 2008; Lastras et al., 2009). This along-canyon trend is also observed in thalweg longitudinal downslope profiles canyons that provide information

about the balance between sediment supply and transport (Gerber et al., 2009; Covault et al., 2011), which mainly have very concave shapes due to continuous supply of coarse-grained sediments, regardless of the sea-level stand (Covault et al., 2011). Other characteristic features of shelf-incised canyons include diverse superimposed smaller-scale morphologies which are usually erosional, such as bedforms, terraces, knickpoints, gullies, and scars (e.g., Hagen et al., 1994; Peakall et al., 2000; Wynn and Stow, 2002; Baztan et al., 2005; Mitchell, 2006; Lastras et al., 2007; Tubau et al., 2015a; Mountjoy et al., 2009; Symons et al., 2016). The variable geomorphology may, in turn, influence recent canyon sedimentation patterns (Drexler et al., 2006).

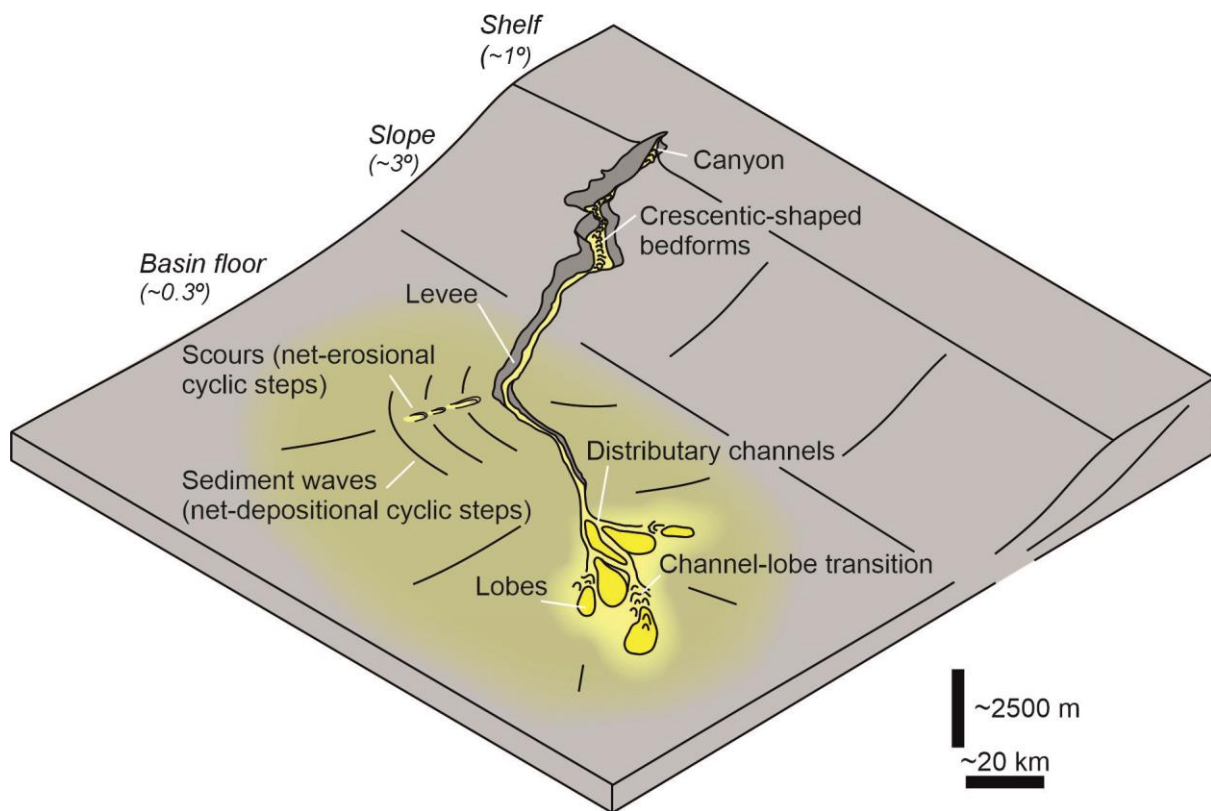


Figure. 1.5. Architectural elements of a canyon-fed continental margin and locations of cyclic steps. Modified from Covault et al. (2017).

The spatial variability of bedforms along submarine canyons is particularly outstanding, as they reflect the recurrent passage of turbidity currents (Peakall et al., 2000; Fildani et al., 2006; Kostic, 2011; Covault et al., 2014, 2017). These bedforms are constituted by different morphological features according to the prevalence of deposition or erosion, such as sediment waves or scours (Symons et al., 2016; Covault et al., 2017; Slooman and Cartigny et al., 2020), and to the confined or unconfined nature of the canyon setting in which bedforms are

formed, such as axial channels, levees, or depositional lobes (e.g., Tubau et al., 2015a; Hage et al., 2018) (Figure 1.5).

Coarse-grained crescentic-shaped bedforms (CSBs) are usually confined along the axial channel of submarine canyons that sustain sediment transport activity (e.g., Smith et al., 2005, 2007; Xu et al., 2008; Paull et al., 2011, 2013; Kostic, 2011; Babonneau et al., 2013; Covault et al., 2014; Mazières et al., 2014; Tubau et al., 2015a) (Figure 1.5). Confined CSBs are typically developed in net-erosion or low aggradation rate settings (Smith et al., 2007; Paull et al., 2010; Hughes Clarke et al., 2014). The imbalance between erosion on the lee side and deposition on the stoss side of CSBs often causes upslope migration (Tubau et al., 2015a; Slooman and Cartigny, 2020), usually in response to relatively brief, high-energy turbidity flow events (Normark et al., 2002; Smith et al., 2005; Xu et al., 2008; Paull et al., 2010; Babonneau et al., 2013; Symons et al., 2016; Hage et al., 2018).

Bedform development is more diverse in unconfined settings of submarine canyon systems, such as backslopes of channel levees, where sediment waves and scours can be found (e.g., Migeon et al., 2000, 2001; Wynn et al., 2000, 2002; Normark et al., 2002; Fildani et al., 2006; Arzola et al., 2008; Kostic, 2014; Symons et al., 2016; Ge et al., 2017; Casalbore et al., 2018; Li and Gong, 2018; Maselli et al., 2019, 2021; Stacey et al., 2019; Zhou et al., 2021; Normandeau et al., 2022; Scacchia et al., 2022) (Figure 1.5). The development of these bedforms depends on the relationship between erosion and deposition (Symons et al., 2016). Net-depositional fine-grained sediment waves are characterized by positive reliefs with straight to sinuous plan-view shapes (Zhong et al., 2015; Symons et al., 2016). In contrast, scours are predominantly net-erosional bedforms that occur as isolated depressions or linear trains. They are characterized by crescentic to enclosed depressions that often form asymmetrical waveforms (Macdonald et al., 2011; Paull et al., 2014; Covault et al., 2014; Zhong et al., 2015; Fildani et al., 2016, 2017).

Sediment waves and scours can be interpreted as cyclic steps (Tubau et al., 2015a; Hage et al., 2018) where the bedforms are bounded by hydraulic jumps of overriding turbidity currents, which are Froude-supercritical over the lee bedform sides and Froude-subcritical over the stoss sides (Covault et al., 2014) (Figure 1.6). The cyclic steps are defined as upstream-migrating bedforms in regions with high gradients and slope breaks (Kostic, 2011). In submarine canyons, cyclic steps can be found in both confined and unconfined settings (Paull et al., 2011; Zhong et al., 2015); cyclic steps can significantly enhance sediment transport efficiency (Sun and Parker, 2005; Taki and Parker, 2005; Slooman and Cartigny, 2020) and

play a key role in their initiation and maintenance (Fildani et al., 2013; Hizzett et al., 2017; Slooman and Cartigny, 2020; Ono et al., 2023). The geometric properties of the cyclic steps (i.e., wavelength, amplitude, and asymmetry) are controlled by different factors such as the gradients of canyon floors, flow thickness and velocity (Cartigny et al., 2011; Kostic, 2011; Slooman and Cartigny, 2020).

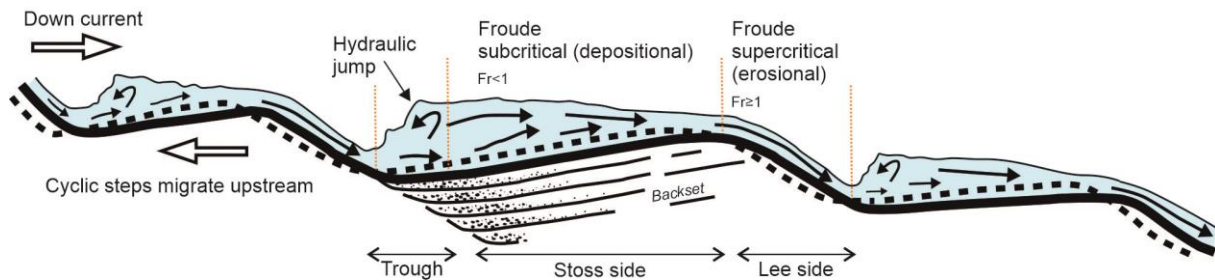


Figure 1.6. Conceptual depositional scheme of generation of cyclic steps in subaerial open-channel flows. Modified from Slooman and Cartigny (2020).

1.6. Controls in the sedimentary activity of submarine canyons

Submarine canyons are dynamic systems that adapt to changes in climatic changes and tectonic forcing, by altering their courses and profiles, becoming more or less active, and filling up with sediments or becoming more deeply incised. Several factors can control their sedimentary activity, such as the margin type, sea-level changes, the degree of canyon head incision in the shelf, or the location of the canyon head with respect to the principal sedimentary source (e.g., Bernhardt et al., 2015; Sweet and Blum, 2016; Bernhardt and Schwanghart, 2021)

1.6.1. Type of continental margin

Passive margins are characterized by wide shelves and high sediment rates (Walsh and Nittouer, 2003; Blum and Hattier-Womack, 2009; Warrick and Farnesworth, 2009; Normark et al., 2009; Harris and Whiteway, 2011; Sweet and Blum, 2016). Passive margins have long, low-gradient submarine canyons, resulting in large canyon incisions by erosive flows across low-gradient, fine-grained shelves (Reading and Richards, 1994; Harris and Whiteway, 2011; Azpiroz-Zabala et al., 2017; Soutter et al., 2021). In contrast, active continental margins tend to be narrower than passive margin shelves and are located adjacent to orogenic mountain belts with steeper catchments that favor the supply of coarser-grained sediments and more

erosive flows (Covault et al., 2007; Harris and Whiteway, 2011; Harris et al., 2014; Soutter et al., 2021). As a consequence, submarine canyons are steeper, shorter, more dendritic, and more closely spaced than those in passive margins (Harris and Whiteway, 2011).

1.6.2. Sea-level changes

Sea-level changes also play an important role in submarine canyon activity, as they modify the accommodation space, the supply of terrigenous sediments and marine surface processes (Amblas et al., 2022). Sequence stratigraphic schemes were initially based on the assumption that canyons were preferentially active during sea-level lowstands, when the continental shelves were subaerially exposed; the fluvial systems delivered directly into canyon heads, establishing a direct link between fluvial and deep-water systems, which helped to funnel large volumes of sand-rich sediments into deep-water setting. (Mitchum, 1985; Vail, 1987; Posamentier and Vail, 1988) (Figure 1.7A). During lowstand conditions, the upper reaches of shelf-incised canyons exhibit straight patterns due to flank erosion by high-density turbidity currents and limited aggradation (Lowe, 1982; Shanmugam, 1997). The channels form laterally migrating sandy depositional lobes at their mouths (Figure 1.7A) (Allin et al., 2016; Zhang et al., 2018; Fisher et al., 2021).

Following this assumption, submarine canyons were considered to be essentially inactive during sea-level highstands, where canyons tend to exhibit highly sinuous plan-view patterns due to the prevailing influence of fine-grained sediment gravity flows (Keevil et al., 2006). Individual channels constrained by muddy levees tend to aggrade, whereas muddy lobes are formed distally in lower canyon reaches (Figure 1.7A) (Zhang et al., 2018; Fisher et al., 2021). There is now strong evidence, however, that many submarine canyons were active during the Holocene highstand, when flows capable of transporting sediments modified canyon axial channels (e.g., Canals et al., 2006; Xu et al., 2008; Zhang et al., 2018). This recent sedimentary activity can vary according to several factors, such as shelf width and steepness.

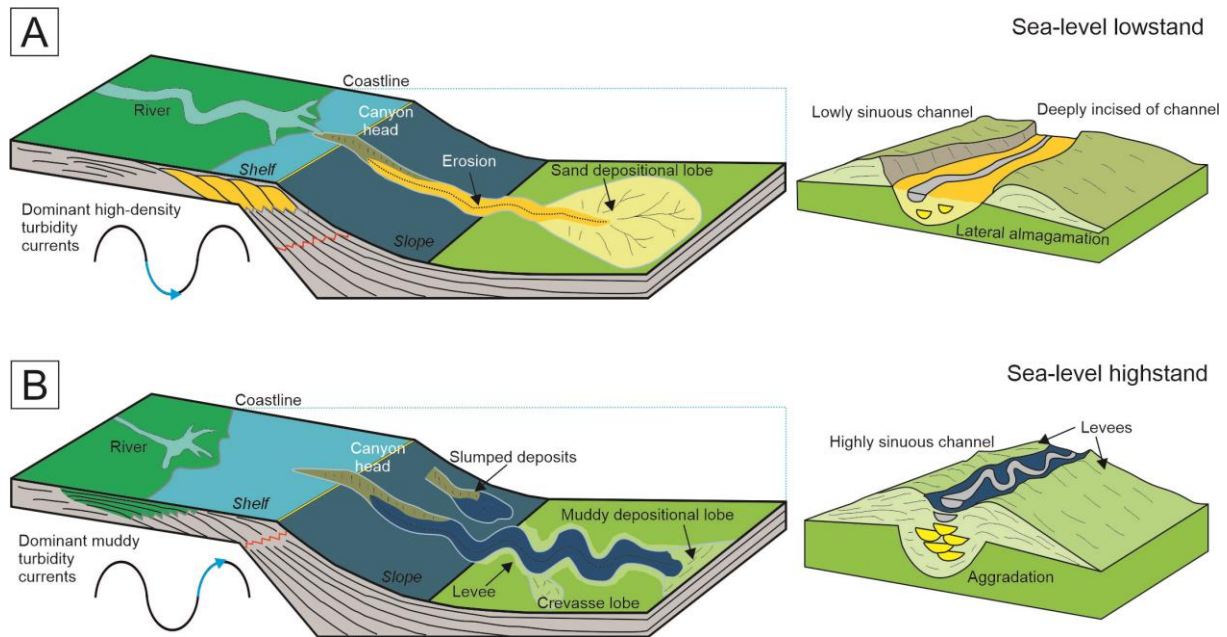


Figure 1.7. Schematic illustrations of the architectural evolution of a shelf-incised submarine canyon in response to sea-level changes. (A) During sea-level lowstands, high-density turbidity currents erode axial channels and transport coarse-grained sediments that construct distal sandy lobes. (B) During sea-level highstands, muddy turbidity currents develop sinuous aggradational channels constrained by muddy levees.

1.6.3. Degree of canyon shelf incision

The degree of canyon shelf incision essentially determines the amount of sediment deposited in shallow water that may be captured by canyons during sea-level highstand (Mullenbach and Nittrouer, 2000; Puig et al., 2014, 2017; Sweet and Blum, 2016). Shelf-incised canyons that show evidence of recent activity tend to have their heads located at few kilometers (<10) from the nearby shorelines, mantled by coarse-grained sediments (e.g., Lewis and Barnes, 1999; Mullenbach and Nittrouer, 2000; Normandeau et al., 2015; Sweet and Blum, 2016). Shelf-incised canyons export high amounts of sediments as they are frequently affected by erosive turbidity flows (Harris and Whiteway, 2011). In contrast, submarine canyons whose heads are remote from the shoreline, such as blind canyons, are generally inactive and characterized by muddy sediments (Harris and Whiteway, 2011; Sweet and Blum, 2016).

1.6.4. Relationship between canyon heads and major sedimentary sources

Shelf-incised canyon activity is also influenced by the location of canyon heads with regard to the main sedimentary source (Bernhardt and Schwanghart, 2021). The functioning of canyon

systems as sediment conduits or traps during highstand conditions will be determined by the balance between erosive flows and hemipelagic deposition in a given canyon domain (Drexler et al., 2006; Arzola et al., 2008; DeGeest et al., 2008). Sediment sources can be riverine (a), deltaic (b), or driven by longshore-drift (c) (Sweet and Blum, 2016):

(a) The highest activity in shelf-incised canyons is usually related to the existence of a direct connection with river systems (Babonneau et al., 2002; Brothers et al., 2013), which can result in the channeling of hyperpycnal turbidity currents (Puig et al., 2017).

(b) Shelf-incised canyons with canyon heads located remote from the coastline but close to river mouths are draped by hemipelagic muds (Normark et al., 2009). Such connections are frequent in active margins characterized by high river discharges (Harris and Whiteway, 2011; Bernhardt and Schwanghart, 2021).

c) Sediments transported by longshore currents can be captured depending on the strength and location of littoral cells and the occurrence of sediment depocenters (Sweet and Blum, 2016). The capture of longshore currents by canyon heads usually occurs in narrow margins due to the proximity of the coastline (e.g., offshore California, Normark et al., 2009), where captured littoral cells can trigger downcanyon-moving turbidity currents (Piper and Normark, 2009).

1.7. The human imprint

The occurrence and accumulation of litter in the marine realm is an environmental problem with potential consequences for marine and coastal ecosystems (Richmond, 1993; Adams, 2005). Of particular importance is the long-lasting presence of plastic litter in the oceans, which exhibits high concentrations and has accumulated in diverse seafloor features, such as submarine canyons, channels, and sedimentary drifts (Goldberg, 1997; Thompson et al., 2004; Kane and Fildani, 2021) (Figure 1.8). Considering the global trends in plastic production, the increased fluxes and areal coverage of plastics can impact seafloor habitats and associated benthic communities (Goldberg, 1997; Thushari and Senevirathna, 2020).

Studies on litter composition provide information about its origin. Plastics usually come from coastal and land sources, whereas other types of marine debris —such as those coming from fishing gears— may indicate human activity in the marine realm (Pham et al., 2014a; Vieira et al., 2015; Alves et al., 2021; Morales-Caselles et al., 2021; Cerrillo-Escoriza et al., 2023) (Figure 1.8). On continental margins, litter density, distribution, and composition are variable

at different scales (Sánchez et al., 2013). Specifically, the spatial distribution of litter is influenced by a multiplicity of factors, including waves and oceanographic currents, seafloor geomorphology, anthropogenic activities, shipping routes, and river inputs (Galgani et al., 2000; Ramirez-Llodra et al., 2013; Pham et al., 2014b; Angiolillo et al., 2015; Gerigny et al., 2019; Dominguez-Carrió et al., 2020; Canals et al., 2021; Bergmann et al., 2022; Hernandez et al., 2022). Interactions of litter artefacts with benthic and demersal organisms are very complex, since litter can provide habitat or coverage for diverse marine species (e.g., Goldberg, 1997; Sánchez et al., 2013; Mecho et al., 2020).

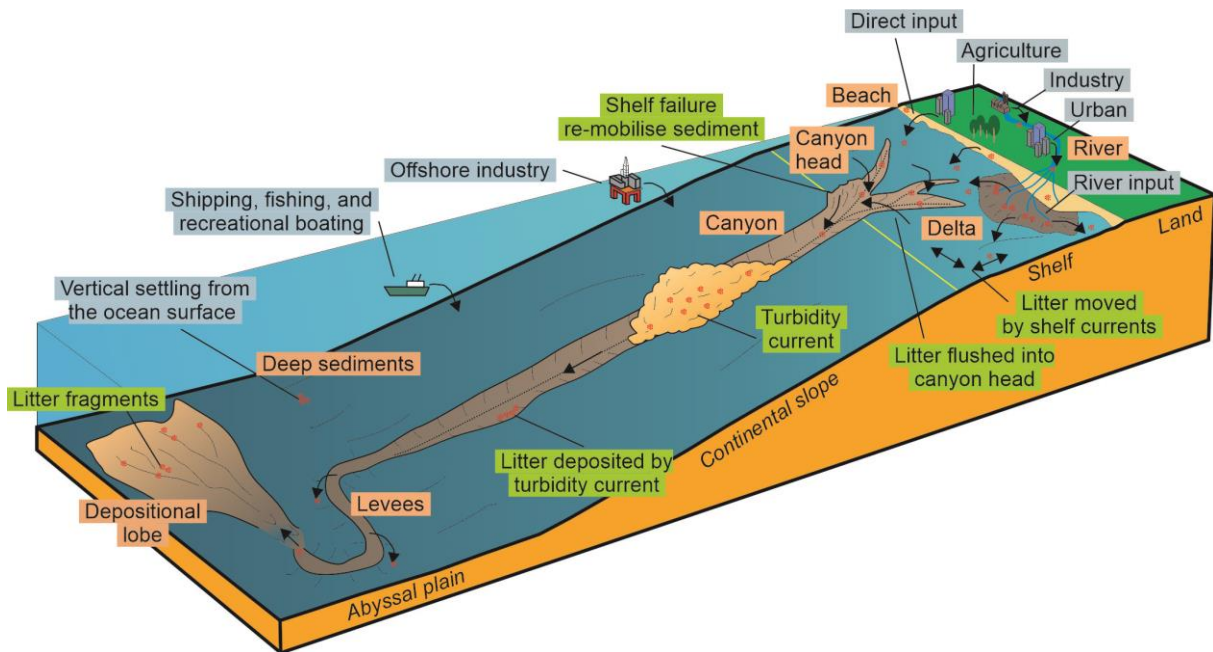


Figure 1.8. Major sources (in blue) and sinks (in orange) of marine litter and microplastics in a shelf-incised submarine canyon. Adapted from Pohl et al. (2020), United Nations (2021), and Hernandez et al. (2022).

Channeled seafloor features such as submarine canyons tend to show patchy but pervasive distributions with local high abundances of marine debris (Galgani et al., 2000; Pham et al., 2014b; Pierdomenico et al., 2019) (Figure 1.8). Shelf-incised canyon heads at short distances from the coasts can act as sinks for diverse types of land-derived litter (Wei et al., 2012; Ramirez-Llodra et al., 2013; Mecho et al., 2020; Cerrillo-Escoriza et al., 2023), whose concentrations are determined by densities of coastal urbanization and population and fluvial inputs (Mordecai et al., 2011; Neves et al., 2015; Tubau et al., 2015b; Cerrillo-Escoriza et al., 2023). In shelf-incised canyons located at longer distances from the coast, litter is mainly marine-sourced (Mordecai et al., 2011). Yet submarine canyons can locally receive human

discards from ships if they are located along shipping routes, mainly in blind canyons (Wei et al., 2012; van den Beld et al., 2017).

Along submarine canyons, litter can be entrained by diverse deep-water flows, such as downslope near-bottom currents (Tubau et al., 2015b; Pierdomenico et al., 2020) or erosional turbidity currents (Zhong and Peng, 2021). In addition, geomorphological canyon complexity may favor litter accumulations along their pathways (Tubau et al., 2015b). Because of the high densities of marine litter usually found in submarine canyons, some benthic habitats and species found in these seafloor features are particularly vulnerable, and interactions between marine debris and sessile organisms are varied, including physical contacts and entanglements (Mordecai et al., 2011; Oliveira et al., 2015). Major disturbances to Vulnerable Marine Ecosystems (VMEs) in submarine canyons, such as cold-water coral banks and gorgonian aggregations, appear to be caused by different types of lost fishing gear (Fabri et al., 2014).

1.8. Objectives

The northern margin of the Alboran Sea (western Mediterranean Sea) exhibits an abrupt character, with a narrow shelf and the sculpting of several sectors by submarine canyons and other valley systems (Vázquez et al., 2015) that receive moderate amounts of marine plastic litter (García-Rivera et al., 2018; Liubartseva et al., 2018). The shelf-incised, sinuous Motril and Calahonda canyons are located ca. 2 km off the shoreline, whereas the straight Carchuna Canyon dissects the entire shelf. Despite their proximity in the same margin, the studied canyons exhibit great geomorphologic, sedimentary, and marine litter abundance and composition differences. In addition, the Carchuna Canyon exhibits bedforms in both confined and unconfined settings, along its axial channel and over an overbank deposit. This thesis aims to establish the factors that control the sedimentary activity within shelf-incised canyons, considering the geomorphological and sedimentary differences and the abundance, origin, and distribution of marine litter, in shelf-incised canyons in the northern margin of the Alboran Sea (western Mediterranean Sea). To achieve this aim, this thesis has three major scientific objectives:

- 1) To highlight geomorphological and sedimentary differences between the nearby Motril and Carchuna canyons and elucidate their respective roles in recent patterns of sediment transport and accumulation in order to: (1) discern the relation between sedimentary processes and canyon morphology; and (2) establish the driving factors of

recent activity in both submarine canyons. The studied canyons exhibit noteworthy geomorphologic and sedimentary differences despite their geographic proximity.

- 2) To improve the understanding of the processes leading to the formation and maintenance of bedforms in submarine canyons, framed by the larger picture of recent canyon evolution: (1) characterize the erosional and depositional bedforms in confined and unconfined settings of the Carchuna Canyon; and (2) determine the genetic constraints on sedimentary processes leading to bedform development along the Carchuna Canyon in recent times.
- 3) To analyze the litter distribution, density, and origin in the Motril, Carchuna, and Calahonda shelf-incised submarine canyons, in order to: (1) characterize and quantify litter type and density in these canyons and, in view of other worldwide submarine canyons, to understand the major factors behind litter accumulation; (2) understand the factors that control the distribution of marine litter in the studied submarine canyons; (3) discern the litter origin (land- versus marine- sourced); and (4) analyze the potential impact of litter on the benthic habitats and communities in the three studied submarine canyons.

1.9. Structure of the thesis

This PhD Thesis volume is organized into three parts and comprises ten chapters. The first part includes a general introduction, objectives, and structure of the thesis, the setting of the study area, and the materials and methods. Part one is arranged as follows:

- I. Chapter 1 provides an overview of submarine canyons, their terminology and physiography, their global distribution, and the controls in the sedimentary record of submarine canyons. Sediment transport processes and sedimentary products in submarine canyons are also reviewed. In addition, the human imprint over these marine systems has been recollected.
- II. Chapter 2 describes the geological and oceanographic setting, the characteristics of the coastal domain and submarine geomorphology, and the recent to modern sedimentary processes. Seafloor habitats and biota and the anthropogenic activity along the study area are also shown.
- III. Chapter 3 explains the materials and methods used in this thesis, mostly collected during an oceanographic survey: bathymetric data, seafloor imagery, sediment samples, and sub-bottom profiles. In addition, ancillary data such as three-dimensional

flow simulations, coastal uses data, maritime traffic, and fishing activity data have also been used.

Part two presents the observations, results, and discussion obtained from the study of the shelf-incised submarine canyons in the study area. Part two is arranged as follows:

- IV. Chapter 4 presents the geomorphological and sedimentary characteristics and differences between the Motril and Carchuna canyons and their implications for recent canyon activity. This chapter is written according to the first major scientific objective.
- V. Chapter 5 deals with the processes leading to the formation and maintenance of bedforms in confined and unconfined settings of the Carchuna Canyon. This chapter is written according to the second major scientific objective.
- VI. Chapter 6 describes the litter distribution, density, and origin in the Motril, Carchuna, and Calahonda canyons. This chapter is written according to the third major scientific objective.

In the third part of this thesis, an integrated discussion, general conclusions, and future perspectives on submarine canyon research are presented. This section is organized as follows:

- VII. Chapter 7 focuses on a general discussion of the main differences in sedimentary processes between shelf-incised canyons in narrow and wide margins. In addition, the implications for bedform development and the abundance, origin, and distribution of marine litter along shelf-incised canyons are also discussed.
- VIII. Chapter 8 summarizes the most relevant results and their implications for the knowledge of the recent activity in shelf-incised submarine canyons. In addition, this chapter highlights some aspects of the investigation on submarine canyons, which, according to the author, could be viable research lines on this topic in the future.
- IX. Chapter 9 provides supplementary material used in this thesis.
- X. Chapter 10 contains the list of references.

Chapter 2

Regional setting

The study area is located in the central sector of the northern Alboran Sea margin, between the towns of Motril and Calahonda (Figure 2.1A, B), and comprises the narrowest shelf (3 km wide) of the entire northern Alboran Sea margin (Figure 2.1), which is deeply incised by the Motril and Carchuna canyons (Figure 2.1B).

2.1. Geological setting

The Alboran Basin is a narrow, elongated basin located in the westernmost part of the Mediterranean Sea, 150 km N–S wide, 350 km W–E long, and with maximum water depths of ca. 1800 m (Figure 2.1A). The basin is surrounded by the Spanish and Moroccan continental margins, and the basin topographic features include the northern shelf, basin slope and apron, the Alboran Ridge and Trough, the Djibouti Ridge and Trough, and several turbiditic systems in the basin northern slope (Figure 2.1A). The Alboran Sea was developed in a convergent tectonic setting between the Eurasian and African plates since the late Oligocene. The compressive tectonic regime triggered folding, reverse fault inversions, and a conjugate system of strike–slip and normal faults (Figure 2.1B) (Comas et al., 1999; Ballesteros et al., 2008). Moreover, the basin has been progressively restricted due to the uplift of the adjacent mountainous reliefs composing the Gibraltar Arc, an arcuate Alpine range comprising the Betic and Rif mountains (Platt and Vissers, 1986; Comas et al., 1992; García-Dueñas et al., 1992; Estrada et al., 1997, Platt et al., 2003).

In the Late Miocene, the seawater exchange between the Atlantic Ocean and the Mediterranean Sea was reduced; as a consequence, an important sea-level lowering and desiccation of the Mediterranean Sea occurred. The Mediterranean waters increased their salinity and most of the basin margins were subaerially exposed; this event is known as the Messinian Salinity Crisis (MSC) (Ryan et al., 1973; Juan et al., 2016; Gómez de la Peña et al., 2021; Miramontes et al., 2023). Fluvial subaerial erosion during this period created incipient canyons that were further reshaped by submarine erosional processes (Frey-Martinez et al., 2004; Maillard et al. 2006). The subsequent opening of the Strait of Gibraltar enabled the flooding of the Mediterranean Basin and the development of a Pliocene-Quaternary sedimentary prism in the margins of the Alboran Sea (Ryan et al., 1973; Campos et al., 1992; Bache et al., 2012). The northern margin of the Alboran Sea is characterized by diverse Quaternary depositional systems, with dominance of siliciclastic sedimentation (Ercilla et al., 1992, 1994; Lobo et al., 2015).

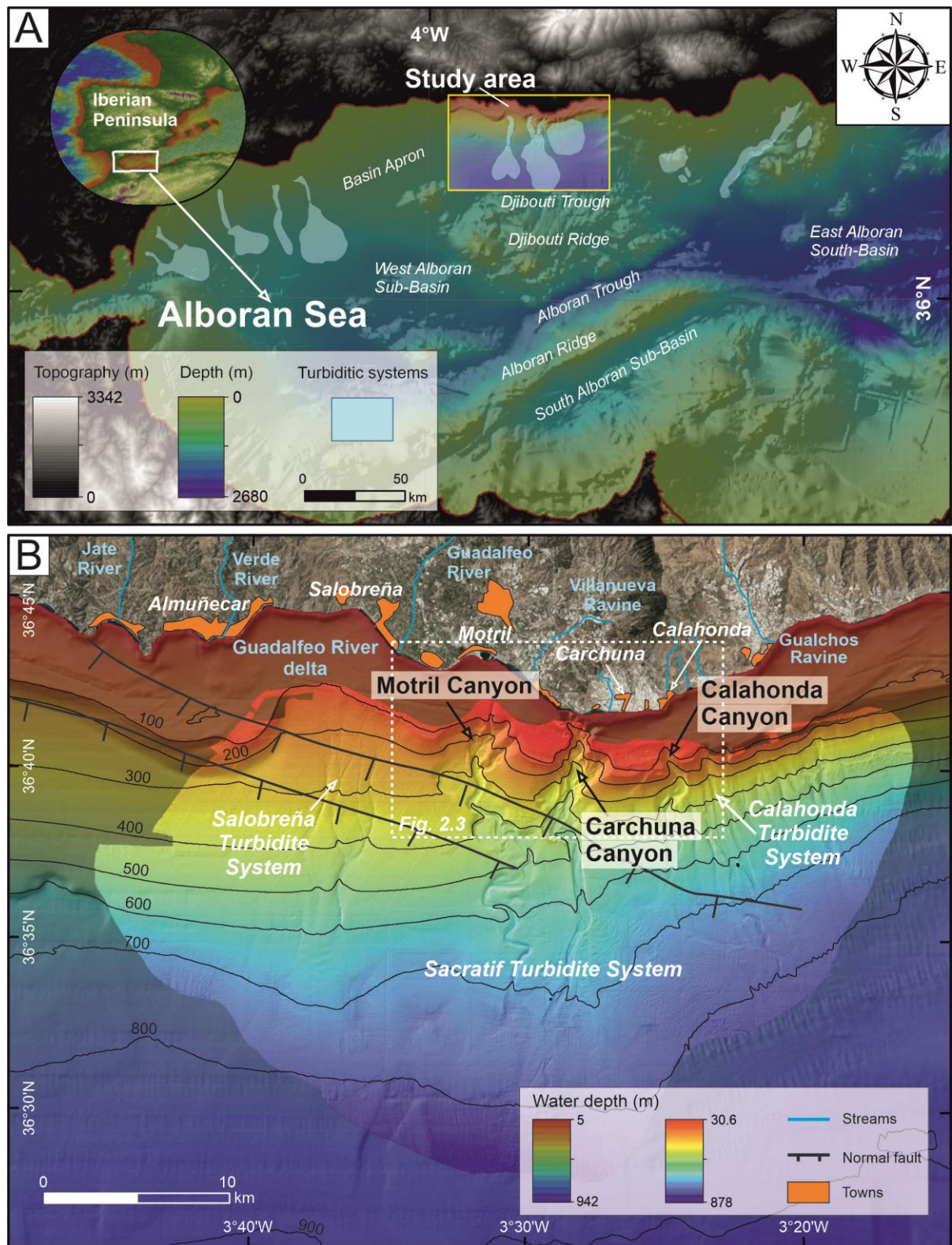


Figure 2.1. (A) Geographic location of the Alboran Sea in the southern Iberian Peninsula. Overview map of the Alboran Sea indicating the study area, main turbidity systems, and main topographic features. (B) 10 m high-resolution bathymetric map constructed with data collected during the ALSSOMAR-S2S survey superimposed on a 50 m cell bathymetric grid, provided by the “Ministerio de Pesca y Cultura”, Spanish Government. The bathymetric grid shows normal faults cutting the studied canyons (after Rodríguez et al., 2017). Bathymetric contour in meters.

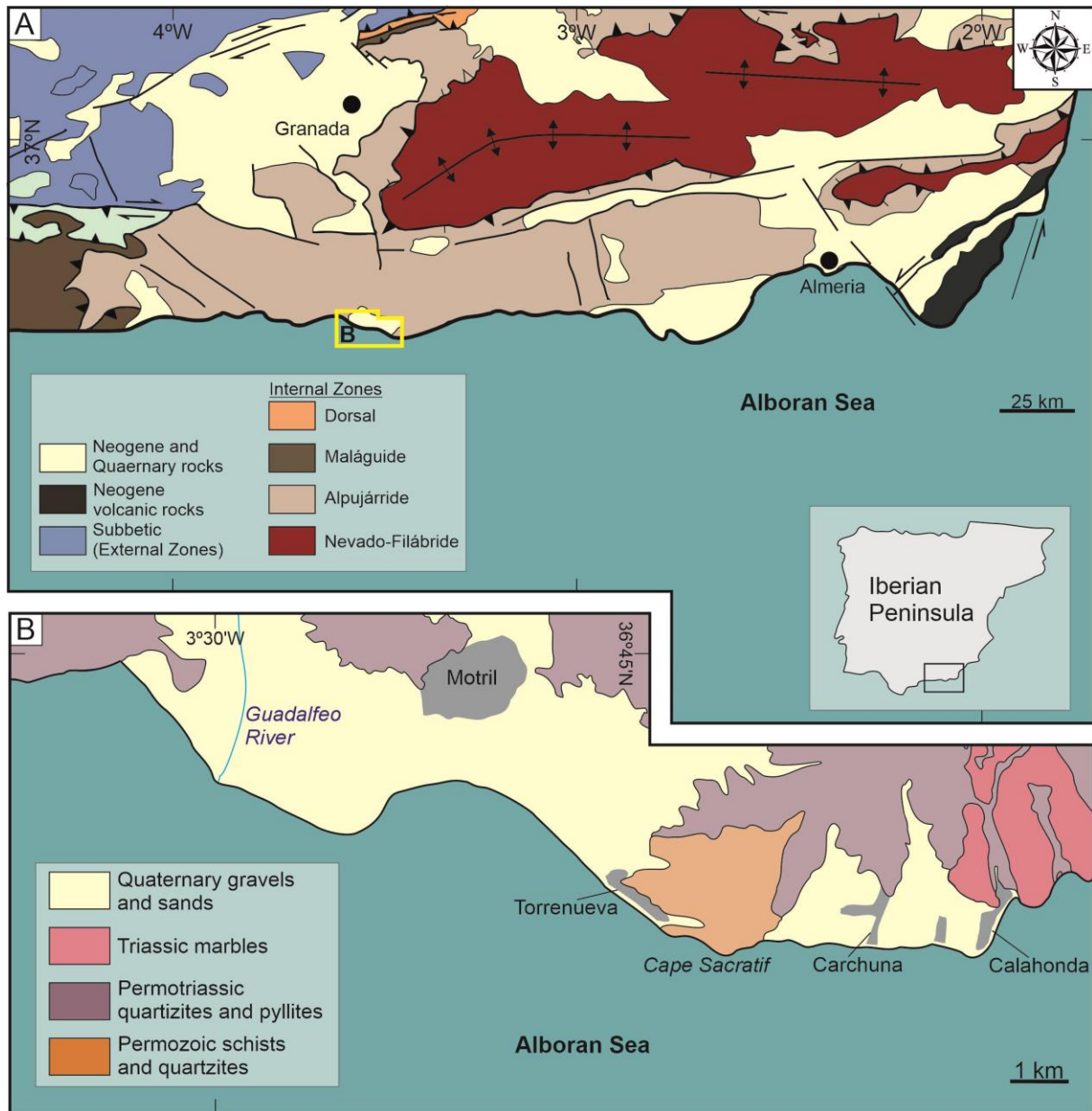


Figure 2.2. (A) Simplified geological map of the northern and northeastern margin of the Alboran Sea. (B) Geological map of the Motril-Calahonda area showing the location of the main towns, Cape Sacratif and the Guadalfeo River.

The geodynamic evolution of the Alboran Domain is mostly controlled by the exhumation of metamorphic core units driven by the African-Eurasian convergence. The metamorphic basement of the Betic Cordillera is made up of three stacked metamorphic complexes, i.e., Nevado-Filabride, Alpujárride, and Maláguide (Figure 2.2A), formed mainly by marbles, micaschists, dark schists, phyllites, quartzites, and dolomites. The coastal geomorphology of the study area is characterized by beaches and coastal plains (Godoy et al., 2020). The Alpujárride metamorphic complex composed of Paleozoic schists, Permo-Triassic phyllites,

and Triassic marbles constitutes the geological basement of the study area (Figure 2.2B) (Aldaya et al., 1979, 1981). The basement is buried by coarse-grained Upper Pleistocene to Holocene alluvial fans, ravines, the deposits of the Guadalfeo River. In addition, gravelly and sandy beaches (Goy et al., 2003, Ercilla et al., 2014) are found between Carchuna and Calahonda towns, and between Torrenueva and the Gualdalfeo River (Figure 2.2B) (Aldaya et al., 1979, 1981). Onshore, the coastal sedimentary record contains sandy Holocene deposits such as spit bars and infralittoral prograding wedges (IPWs) that constitute major progradational phases separated by erosional gaps, generated by coastal drift during the Holocene (Lario et al., 1999; Fernández-Salas et al., 2009; Bárcenas et al., 2011; Ortega-Sánchez et al., 2014).

2.2. The coastal domain

Sediment supply to the coastline along the northern margin of the Alboran Sea has mainly been provided via relatively short, mountainous rivers (Liquete et al., 2005) and ephemeral creeks, active during autumn and winter (Stanley et al., 1975; Fabres et al., 2002; Palanques et al., 2005) that feed different shelf deltaic systems. Inshore of the submarine canyons, there is no significant river- or creek-delta system at present (Liquete et al., 2005). Only two small dry streams with torrential character in the rainy season debouch in the proximity of the study area: the Villanueva Ravine inland from the Motril Canyon, and the Gualchos Ravine east of the study area (Figures 2.1B and 2.3). These ravines are short (<20 km), feature high slopes (>3.6°), and occur in small basins (<120 km²) (Bárcenas et al., 2009).

The Guadalfeo River is a major regional fluvial source located west of the study area (Figures 2.1B and 2.3). The Guadalfeo River catchment has an area of 1252 km², a steep basin and a relatively straight hypsometric curve indicative of a moderately dissected landscape (Jabaloy-Sánchez et al., 2014). The Guadalfeo River has a permanent water flow with an average water discharge of 23.4 m³·s⁻¹ and an average sediment load of 83 kg·s⁻¹ (Liquete et al., 2005; Bárcenas et al., 2015). The river delta is asymmetrically triangular, with a long side (5.8 km) facing southwest and a short side (2.9 km) facing southeast (Figure 2.2A).

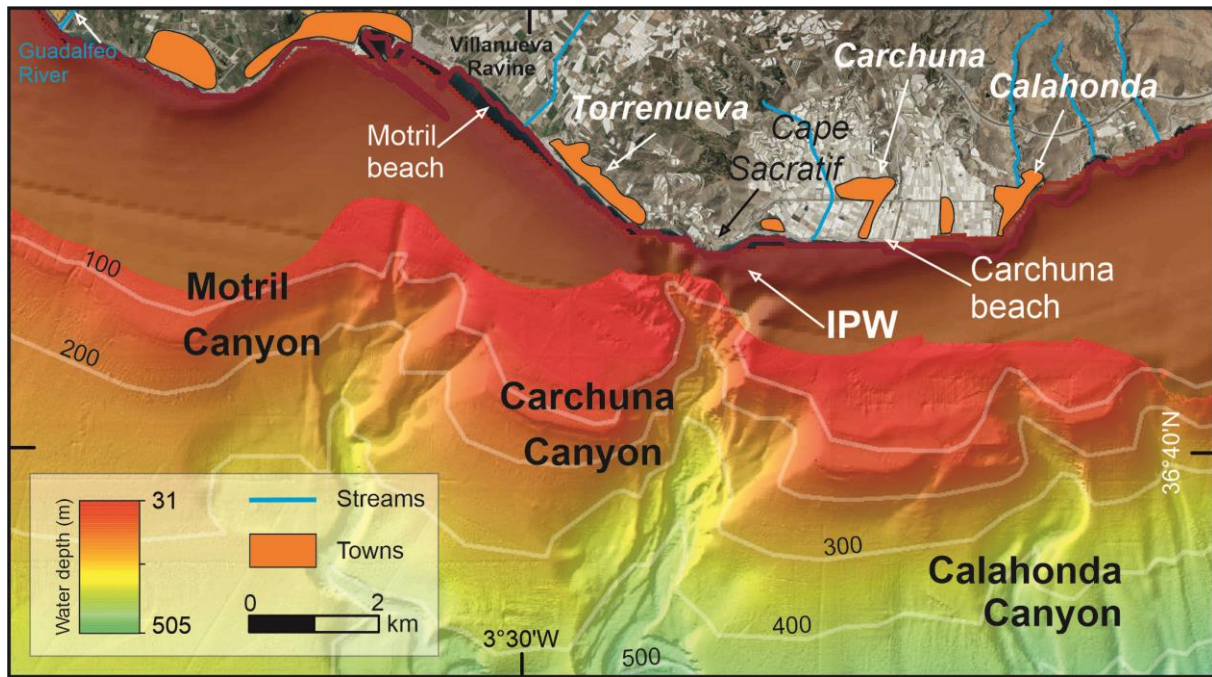


Figure 2.3. Zoom-in of the shelf in the study area where different degrees of incision of the Motril, Carchuna, and Calahonda canyon heads can be observed. An infralittoral prograding wedge (IPW) laterally bounded by the Carchuna Canyon head is also shown. Aerial continental photography shows major rivers and towns. Bathymetric contours in meters.

2.3. Submarine geomorphology and deep-water deposits and processes

The inner shelf of the Alboran Sea is characterized mainly by IPWs (Ercilla et al., 1994; Hernández-Molina et al., 1994, 2000), whereas the outer shelf is covered by a widespread sandy veneer due to the influence of postglacial transgressive erosion (Lobo et al., 2006). The shelf edge is located at a mean water depth of 115 m (Ercilla et al., 1994; Vázquez, 2001). In the study area, the Carchuna IPW —composed of coarse-grained sediments— exhibits a break in the slope at 20 m water depth, and is laterally bounded by the Carchuna Canyon head (Figure 2.3) (Fernández-Salas et al., 2009; Ortega-Sánchez et al., 2014). The submarine prodeltaic system off the Guadalfeo River is located west of the Motril Canyon head over the shelf. The prodelta is predominantly made up of coarse-grained sediments that grade into muds (up to 75%) towards the east (Jabaloy-Sánchez et al., 2014; Lobo et al., 2015).

The northern margin of the Alboran Sea contains several deep-water turbidite systems (Ercilla et al., 1992, 1994, 2016, 2019; Alonso and Ercilla, 2002a), contourite drifts, and mass-transport deposits (Bárcenas et al., 2011; Ercilla et al., 2016, 2019). Turbidite systems are formed by shelf-incised or shelf-edge canyons that evolve downslope into channel-levee

complexes and distally into deep-water fans. In contrast, turbidite ramp systems consist of small-sized straight canyons and gullies eroding the slope and feeding fan lobes through distributary channels (Vázquez et al., 2015). These deep-water systems are grouped into three different sectors (Figure 2.1A): western, middle, and eastern.

The study area is located in the middle deep-water sector off the coast of Granada province and contains several deep-water turbidite systems (Figure 2.1B). The narrow Salobreña Turbidite Ramp System includes a set of gullies that erode the distal part of the Guadalfeo River prodelta and feed a distal unchannelized lobe (Vázquez et al., 2015; Ercilla et al., 2019). The Calahonda Turbidite Ramp System comprises four small shelf-incised canyons and several slope-eroding gullies feeding a large channelized lobe off a coastal segment fed by ephemeral rivers (Pérez-Belzuz and Alonso, 2000a; Pérez-Belzuz et al., 2000; Alonso and Ercilla, 2002b). The main submarine canyon of this turbidite ramp system is the Calahonda Canyon, a shelf-incised canyon located 2.5 km south of Calahonda town with a sinuous valley along the slope (Figures 2.1B and 2.3; Cerrillo-Escoriza et al., 2023).

The Sacratif Turbidite System is located between the above-mentioned systems and includes the Motril and Carchuna canyons (Figures 2.1B and 2.3; Cerrillo-Escoriza et al., 2023, 2024). The Motril Canyon is located 5 km east of the Guadalfeo River mouth, where its main valley exhibiting a sinuous morphology on the slope (Figures 2.1B and 2.3). The straight Carchuna Canyon crosses the shelf and its head is located 200 m offshore Cape Sacratif (Figures 2.1B and 2.3). Both canyons debouch into large lobes fed by distributary channels (Pérez-Belzuz and Alonso, 2000b; Pérez-Belzuz et al., 2000; Cerrillo-Escoriza et al., 2024) having superimposed sediment waves (Muñoz et al., 2017; Cerrillo-Escoriza et al., 2023). Distally, this margin connects with the Motril Basin, which is bounded to the south by several seamounts (Alonso and Maldonado, 1992; Pérez-Belzuz, 1999).

The deep-water systems developed during Pliocene-Quaternary (Alonso and Maldonado, 1992; Ercilla et al., 1992; Estrada et al., 1997; Pérez-Belzuz and Alonso, 2000a, b; Pérez-Belzuz et al., 2000; Vázquez et al., 2015) where the local topography, avulsion processes, and high-frequency glacio-eustatic sea-level changes influenced their evolution (Alonso and Ercilla, 2002b; Ercilla et al., 2021). Deep-water turbiditic deposits alternate with contourites and landslides. Contourite features include both depositional forms, such as plastered, channel-related, mounded confined and mounded, elongate and separated drifts (Ercilla et al., 2021), and erosional forms such as moats and contourite channels (Ercilla et al., 2021). Landslides are mainly associated with seamounts and generate lobate bodies up to 10 km in

length and tens of meters thick (Vázquez et al., 2015). In the Alboran Sea, other deep-water features such as fluid-flow features such as mud diapirs, mud volcanoes, pockmarks, and authigenic carbonates have been found (e.g. Pérez-Belzuz et al., 1997; Somoza et al., 2012; León et al., 2014; Palomino et al., 2016).

2.4. Oceanographic setting

The northern Alboran Sea is a microtidal, low energy wave setting with astronomical tidal ranges between 0.3 m to the west and 0.1 m to the east (Parrilla and Kinder, 1987; Albérola et al., 1995; Arabelos et al., 2011). Tidal currents are of the order of $2 \text{ cm}\cdot\text{s}^{-1}$, increasing with depth to $4 \text{ cm}\cdot\text{s}^{-1}$, due to topographic constriction (Albérola et al., 1995). In addition, meteorological tides exceed 1 m for periods of several days, allowing larger wave run-ups during storms. Easterly winds are more common than westerly ones, especially during spring and summer. However, waves from the west-southwest are somewhat more energetic than easterly ones, dominating during fall–winter storms (Jabaloy-Sánchez et al., 2014). Littoral drift shows substantial variability due to the local coastal morphology and meteorological conditions (e.g., Stanley et al., 1975; Bárcenas, 2013). The coast along the study area is affected by wave trains coming from W, WSW, SW, ESE, and E, oblique to the main E-W coastal trend (Ortega-Sánchez et al., 2014).

The vertical water mass structure exhibits four main layers (Figure 2.4): Surface Atlantic Water (SAW) extends from 0 m to 150-200 m water depth; Western Intermediate Water (WIW) ranges from 150-200 to 300 m water depth; Levantine Intermediate Water (LIW) extends from 300 to 500-600 m water depth; and Western Mediterranean Deep Water (WMDW) lies below 500-600 m water depth (Brankart and Pinardi, 2001; Millot, 2009; 2014). The SAW enters the Mediterranean Sea through the Strait of Gibraltar, where it is mixed with Mediterranean waters and generates the Atlantic Jet (AJ; velocities up to $1 \text{ m}\cdot\text{s}^{-1}$) (Figure 2.4). The trajectory of the AJ exhibits two anticyclonic gyres, Western and Eastern Alboran Gyres (WAG and EAG), and one cyclonic gyre in the Alboran Sea (Tintoré et al., 1988; Perkins et al., 1990; García-Lafuente et al., 1998; Renault et al., 2012). In shallow water, the path of the AJ is controlled to a large extent by the wind regime (Sarhan et al., 2000; Oguz et al., 2017), which can induce the upwelling in the northern sector of the Alboran Sea, and the advection of mesoscale structures ($\sim 20 \text{ km}$ diameter) around the anticyclonic gyres (La Violette, 1984; García-Lafuente et al., 1998)

The Carchuna Canyon head influences coastal swells and storm processes as it increases nearshore wave heights, particularly of western waves, favoring long-term coastal erosion owing to the concentration of energy (Ortega-Sánchez et al., 2014). In addition, a bottom flow distinct to the wind-driven surface flow has been detected in the Carchuna Canyon; in the bottom layer, the currents tend to flow downcanyon, particularly during easterlies dominance, where bottom flow velocities are between 20 and 30 cm·s⁻¹ (Serrano et al., 2020).

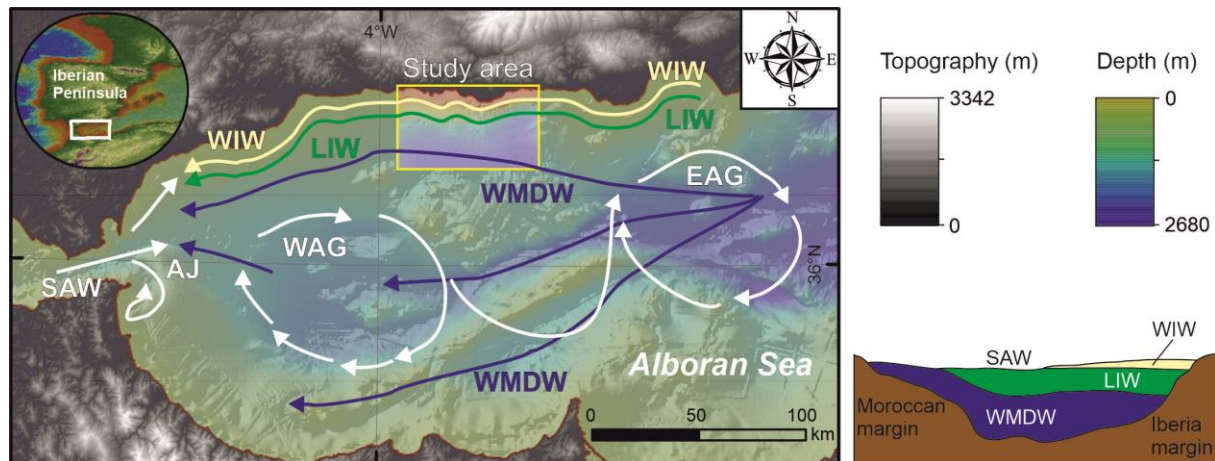


Figure 2.4. General view of the Alboran Sea (left) showing the main water mass pathways and sketch of their vertical distribution (right). SAW, Surface Atlantic Water; AJ, Atlantic Jet; WIW, Western Intermediate Water; LIW, Levantine Intermediate Water; WMDW, Western Mediterranean Deep Water. Adapted from Juan et al. (2016), Ercilla et al. (2016, 2019), and Vargas-Yáñez et al. (2021).

2.5. Recent to modern sedimentary processes

Different sedimentary processes driven by postglacial climatic conditions took place in the Alboran Sea during the Holocene. A first phase of canyon turbiditic activity was marked by an increase of fine-grained detritus due to either local ice melting or increased storminess during the Bølling-Allerød (Weaver and Pujol, 1988; Bozzano et al., 2009). A second phase of reactivation of submarine canyons was linked to glacial meltwater and riverine input during the Younger Dryas (Jimenez-Espejo et al., 2008; Bozzano et al., 2009).

At present, detrital material is delivered to the northern Alboran Sea margin by short rivers and ephemeral creeks, especially during autumn and winter (Stanley et al., 1975; Fabres et al., 2002; Palanques et al., 2005). In shallow water, nepheloid layers may be transported laterally either by littoral drift or the AJ influence (Fernández-Salas et al., 2009). Along submarine canyons, nepheloid fluxes have been related either to river floods (Palanques et al., 2005) or to the interaction of internal waves with the seafloor (Puig et al., 2004). Hemipelagic

deposition is widespread in deep areas (Masqué et al., 2003). Additionally, sediment transport and deposition along the slope, base-of-slope, deep-water basinal areas, and seamount flanks (Ercilla et al., 2016) are generated by near-bottom currents (Fabres et al., 2002). Sediment accumulation rates in deep-water areas vary from 0.2 to 15 cm²·yr⁻¹ (Masqué et al., 2003).

2.6. Seafloor habitats and biota

Cliffs and marine bottoms located between the rocky coastlines of Gualchos and Motril are included in the Special Area of Conservation (SAC) “Acantilados y Fondos Marinos de Calahonda-Castell de Ferro” (Cliffs and Marine Bottoms of Calahonda-Castell de Ferro) (ES6140014) since 2015 (Mateo-Ramírez et al., 2021). The SAC covers an area of ca. 9 km² between the coastline and ca. 65 m water depth and includes littoral habitats, such as sandbanks (Habitat Code (HC) 1110 from the EU Habitat Directive), *Posidonia* beds (HC 1120), large shallow inlets and bays (HC 1160), reefs (HC 1170), and submerged or partially submerged sea caves (HC 8330) (Mateo-Ramírez et al., 2021). In addition, several species with different protection statuses have been found in the area, mostly in infralittoral and circalittoral bottoms, such as the knobbed triton *Charonia lampas*, the noble pen shell (probably extinct since 2017) *Pinna nobilis*, the Mediterranean reef-building vermetid gastropod *Dendropoma lebeche*, the chalice coral *Astroides calycularis* and the orange puffball sponge *Tethya aurantium* (Mateo-Ramírez et al., 2021), most of them included in Annex II of the Barcelona Convention and some classified as “Vulnerable” in the Spanish and Andalusian Lists of Endangered Species (Mateo-Ramírez et al., 2021).

Some poorly known invertebrates that are scarce in other areas of the Mediterranean Sea have been documented in the SAC, such as the hippolytid decapod *Bythocaris cosmetops* and the tropical hermit crab *Pagurus mbizi* (García Raso et al., 2011, 2014). Some bathyal molluscs (e.g., *Poromya granulata*, *Alvania testae*) display populations in the SAC circalittoral zone (Marina et al., 2015). The geographical location of the SAC in a transitional settlement zone for Atlantic species, the heterogeneity of soft bottoms and the occurrence of upwellings may favour the high biodiversity found in the studied soft bottoms. Knowledge of the bathyal habitats and communities where the three studied canyons are located is very scarce. Exceptions include generic studies of fish, decapod and mollusc assemblages of the northern Alboran Sea under the framework of the Marine Litter in the Sea Floor in the Mediterranean

and Black Seas (MEDITS) expeditions (Abelló et al., 2002; García-Ruiz et al., 2015; Ciercoles et al., 2018).

2.7. Anthropogenic activity

Values of plastic debris fluxes in the northern Alboran Sea coast range between 10 and 15 $\text{kg}\cdot\text{km}^{-1}\cdot\text{day}^{-1}$ (Liubartseva et al., 2018) and sea surface plastic concentration is above 3 $\text{g}\cdot\text{km}^{-2}$ (Liubartseva et al., 2018). On the seafloor, the Alboran Sea is the region that exhibits the highest density of litter (25 $\text{kg}\cdot\text{km}^{-2}$) of the entire Spanish Mediterranean Sea (García-Rivera et al., 2018). However, the values of coastal debris fluxes and seafloor litter are not high in the Mediterranean context (Liubartseva et al., 2018). Litter density is higher at water depths lower than 50 m (ca. 25 $\text{kg}\cdot\text{km}^{-2}$) and between 500 and 800 m water depths (ca. 15 $\text{kg}\cdot\text{km}^{-2}$; García-Rivera et al., 2018). These values have been attributed to a multiplicity of coastal uses facing a narrow shelf and to the high level of maritime traffic in open waters (García-Rivera et al., 2018). The beaches located along the coast of the northern Alboran Sea exhibit high plastic item percentages (ca. 88% on the coast of Málaga and ca. 80% on the coast of Almería) (Ministerio para la Transición Ecológica y el Reto Demográfico (MITECO-DGCM), 2021). Inland of the study area, most litter is composed of plastics in Carchuna beach (Figure 1D): 62.4% of >50 cm size items and 80.9% of <50 cm size items. In the vicinity of the study area, Motril beach (Figure 2.1C) exhibits a microplastic concentration of ca. 32 $\text{particles}\cdot\text{kg}^{-1}$ (Godoy et al., 2020). In addition, widespread agricultural activities in the study area such as greenhouses and farming can generate large amounts of waste that can lead to beach pollution (Junta de Andalucía. Consejería de Medio Ambiente, 2019).

The operative fishing fleet registered in 2018 under the modality of artisanal gear amounts to 318 vessels distributed in a total of 11 harbours on the northern Alboran Sea. The largest percentage of artisanal vessels is concentrated along the coasts of the province of Malaga (52%) while the Motril Port accounts for 5.3% (Baro et al., 2021). Bottom trawl, purse seine, and surface longline were the most important fishing techniques in the northern Alboran Sea during 2016 (Baro et al., 2021). In Motril Port, the most relevant fishing techniques are bottom trawl (67.1%), artisanal activity (21.7%), purse seine (10%) and surface longline activity (1.2%) (Baro et al., 2021).

Chapter 3

Materials and methods

Datasets used for this work were mostly collected during the ALSSOMAR-S2S (Alboran Shelf-Slope cOupling processes and deep sediMent trAnsfer: Source To Sink approaches and implications for biodiversity) multidisciplinary expedition carried out from 29 August to 19 September 2019 on board the RV “Sarmiento de Gamboa” (Figure 3.1) in the continental shelf and slope of the northern margin of the Alboran Sea- between Almuñecar and Calahonda towns (Figure. 2.1B).



Figure 3.1. Research vessel “Sarmiento de Gamboa” during the ALSSOMAR-S2S multidisciplinary expedition.

3.1. Bathymetric data

Multibeam bathymetric data were collected along the study area using a quill-mounted Atlas Hydrosweep DSTM multibeam echo sounder operating at frequencies of 14.5 to 16 kHz, providing coverage of up to six times the water depth. Raw multibeam data were processed with Teledyne CarisTM HIPS and SIPS Hydrographic Data Processing System and gridded to obtain Digital Elevation Models with cell sizes of 40, 30, and 10 m at the Instituto Hidrográfico de la Marina, Spanish Government. Processing of multibeam data included corrections for heading, depth, pitch, heave and roll. Tidal and sound velocity corrections were applied and the sounding data were cleaned to remove erroneous soundings. These data were combined with a background Alboran Sea bathymetric grid of 50 m resolution (Ministerio de Pesca, Agricultura y Alimentación, 2002). This multibeam bathymetry acquisition took place in 2002 during cruise Alborán-03 aboard the R/V Vizconde de Eza in the framework of the project entitled Fishing Charts of the Mediterranean (CAPERMA),

which was conducted by the Spanish Institute of Oceanography (IEO) and the General Secretary of Maritime Fisheries (SGPM). These surveys were carried out using a Simrad EM 300 multibeam echosounder in conjunction with differential GPS and the inertial aided system Seapath 200. In addition, the acquired multibeam data were combined with background bathymetric data from the shelf (5 m resolution grid). This multibeam bathymetry acquisition took place from 1999 to 2002 aboard several research vessels in the framework of the project entitled ESPACE (“Estudio de la Plataforma Continental Española”). The purposes of the ESPACE project were to acquire systematic seafloor information on the seafloor from 8-10 to 180 m water depths using high-resolution geophysical techniques.

Bathymetric grids were imported into ArcGIS™ geographic information software and geo-spatial QPS Fledermaus™ software for geomorphological interpretations and detailed morphometric analysis in areas of small-scale morphological variability. The goals were defined in order to identify major sediment transport pathways and to determine the efficiency of sediment dispersal systems from the shelf to the slope through submarine canyons. Geomorphological segments in the Motril and Carchuna canyons were defined according to the orientation of the axial channel and the slope gradient of the flanks.

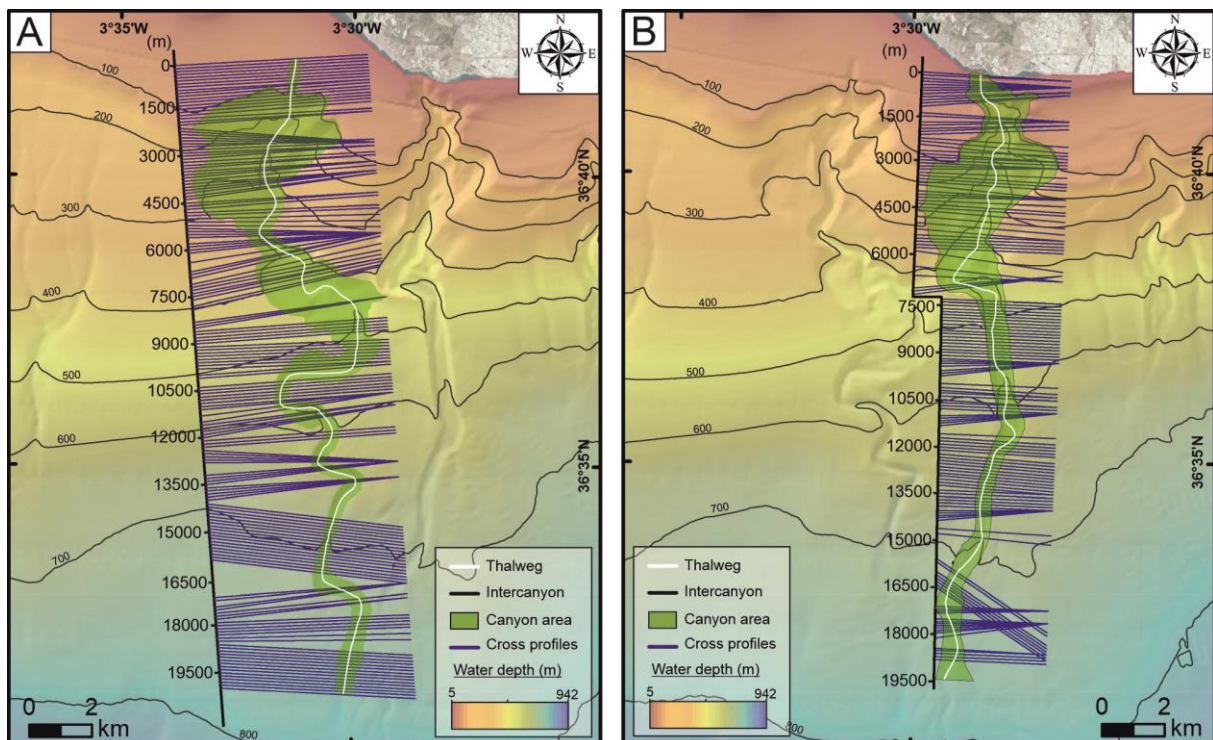


Figure 3.2. Bathymetric grid of the study area showing the cross-sections (in blue) used in the Motril (A) and Carchuna (B) canyons (highlighted in green). Bathymetric contours in meters.

The main canyon morphometric parameters were measured in a number of bathymetric sections. We initially traced two parallel straight lines in intercanyon areas parallel to the path of the submarine canyons; afterwards, perpendicular lines 100 m apart were traced along both submarine canyons (Figure 3.2). Water depth and gradient values were measured each 10 m along the perpendicular lines. Bathymetric profiles along the thalweg of both studied canyons were classified according to Covault et al. (2011).

The main metric and morphologic characteristics of the canyons were measured in order to compare canyon morphologies in the study area. The following parameters were measured: minimum and maximum water depth, total (along the thalweg) and straight canyon length, canyon sinuosity, canyon and canyon floor width, canyon incision (depth difference between the canyon axis and the adjacent interfluves), canyon area (value per cross section), canyon gradient (angle measured between two points along the canyon axis relative to horizontal), gradient of the canyon flanks (average angle measured between the shallowest and deepest points along the canyon wall relative to horizontal), number of gullies that erode the canyon walls (including isolated and merging gullies), and north azimuth. Canyon relief was quantified after Goff (2001) and Green et al. (2007). The average canyon relief was estimated using the RMS relief, which determines the square root of the profile variance between the canyon thalweg and adjacent interfluves.

On the other hand, sediment waves (bedform terminology based on Tubau et al., 2015a) were characterized using the following parameters: amplitude, wavelength, and slope of lee and stoss sides. For the characterization of scours, scour width, length, and headwall height were determined (Figure 3.3). Sets of crescentic-shaped bedforms (CSBs) (designed by letters) have been defined according to CSB crest concavity, considered as high (>0.6) or low (<0.6) according to the length/width ratio. In addition, two sectors of unconfined sediment waves were defined according to their distinctive wavelengths and heights. The bedforms asymmetry was determined by the methodology outlined by Xu et al. (2008), which involves the following steps: (1) selection of bathymetric profiles, (2) profile detrending, (3) calculation of the first derivative, (4) calculation of the H/L (height/wavelength) ratio based on the first derivative function, and (5) calculation of the asymmetry index for each undulation/bedform. A positive index indicates asymmetry towards upcanyon, whereas a negative index indicates asymmetry towards downcanyon.

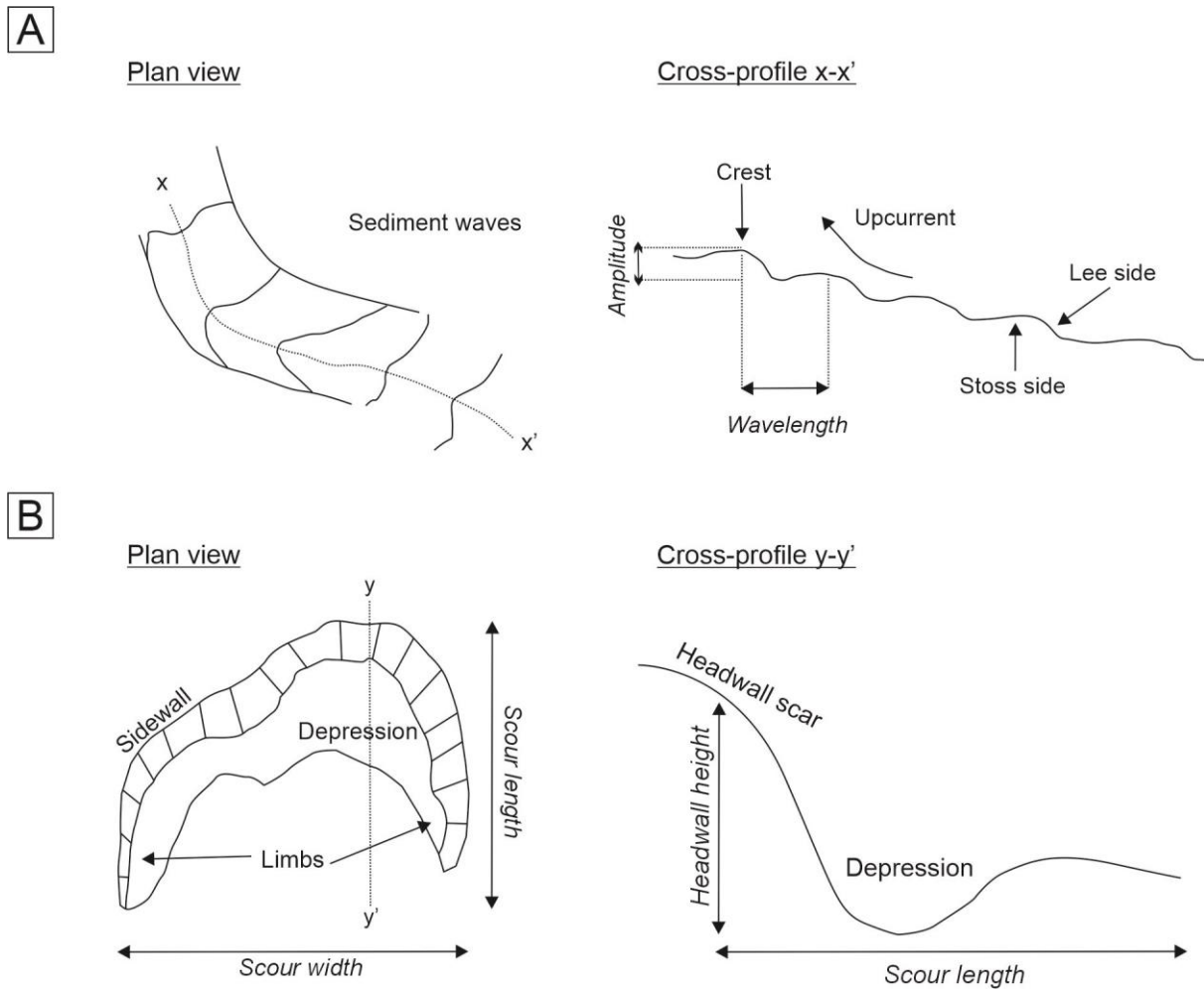


Figure 3.3. Plan views and cross-sections of: (A) a train of sediment waves; (B) and a single scour, illustrating the terminology and main geomorphic parameters used in this study. Modified from Tubau et al. (2015a).

3.2. Seafloor imagery

Acquisition of optical submarine imagery was carried out with the Remotely Operating Vehicle (ROV) Luso (EMEPC— Portuguese Task Group for the Extension of the Continental Shelf) during the ALSSOMAR-S2S oceanographic cruise (2019) (Figure 3.3). The ROV Luso was equipped with an Argus HD-SDI 1/3" standard definition video camera. The high-resolution photos and video footage obtained amount to a total of 70 hours of video recording. The ROV Luso was equipped with two parallel laser beams at a fixed width of 62 cm that provided a reference scale to measure targets during subsequent video analysis. Besides, the ROV was equipped with an ultra-short baseline positioning system (USBL) to ensure detailed records of the ROV tracks where the device moved at an average speed of 0.3 knots.

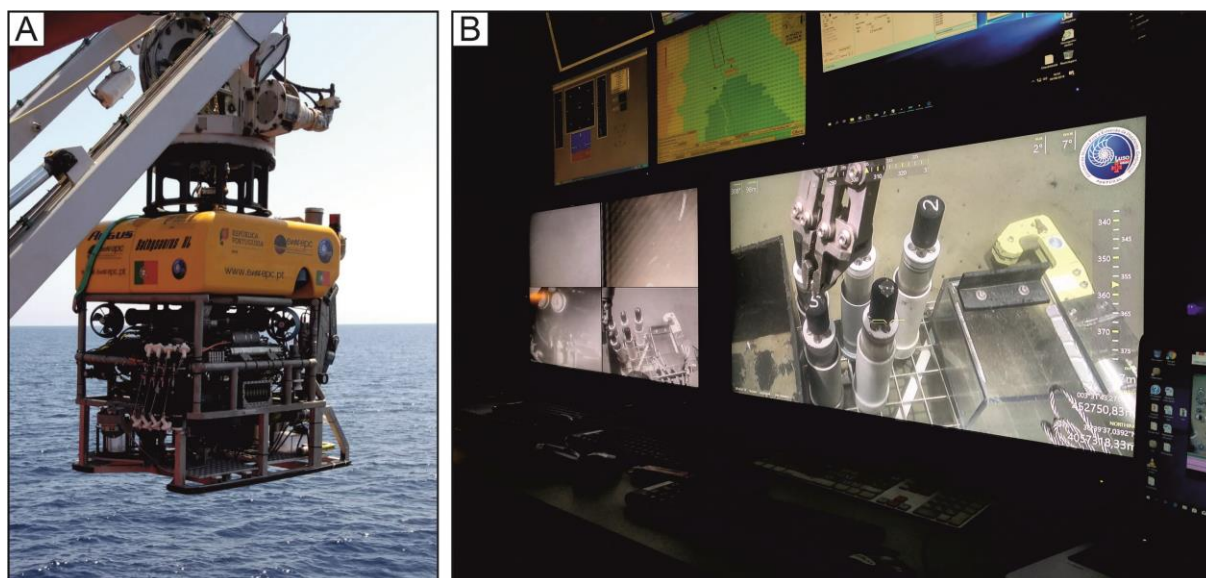


Figure 3.3. (A) ROV Luso (EMEPC— Portuguese Task Group for the Extension of the Continental Shelf) during the ALSSOMAR-S2S oceanographic cruise. (B) Control of the ROV from the research vessel “Sarmiento de Gamboa” during a dive in the ALSSOMAR-S2S oceanographic cruise.

Eleven submarine video dives explored almost 18 km long seafloor transects in the Motril, Carchuna, and Calahonda canyons (Figure 3.4A): (a) the upper segment of the Motril Canyon along two 5 km long continuous dives from 388 m water depth in the canyon thalweg (Dive 01) to 105 m water depth in the canyon head (Dive 02); in between, the dives run along the western canyon flank; (b) the upper (Dives 03, 04, 05, 06, and 11) and lower segments of the Carchuna Canyon (Dives 9 and 10), in a water depth range of 100-750 m and 9 km in total length; and (c) the upper segment of the Calahonda Canyon, in the 115-325 m water depth range and 3 km in total length (Dives 7 and 8).

The images were placed geographically in an ArcGIS environment (Figure 3.4A) to aid in the characterization of submarine canyon features, such as grain size, lithology, sedimentary facies and small-scale bedforms. In addition, the analysis of video footage was aimed to characterize and quantify marine litter type and density, and to analyze the potential impact of litter on benthic habitats in Motril, Carchuna and Calahonda canyons. The length of the ROV dives was calculated and the total number of items for each dive was converted and quantified as linear litter density, in items·100 m⁻¹. Subsequently, the identified marine litter was georeferenced in ArcGIS™. Marine litter classification was based on the Guidance on Monitoring of Marine Litter in European Seas put forth by the Technical Subgroup on Marine Litter (MSFD) (European Commission of the European Union, 2013). A standardized litter classification considers five main categories of material (Table 3.1): plastic, metal, rubber,

glass/ ceramics, and textiles/natural fibers; and four additional categories in the Mediterranean Sea: wood, paper/cardboard, other, unspecific.

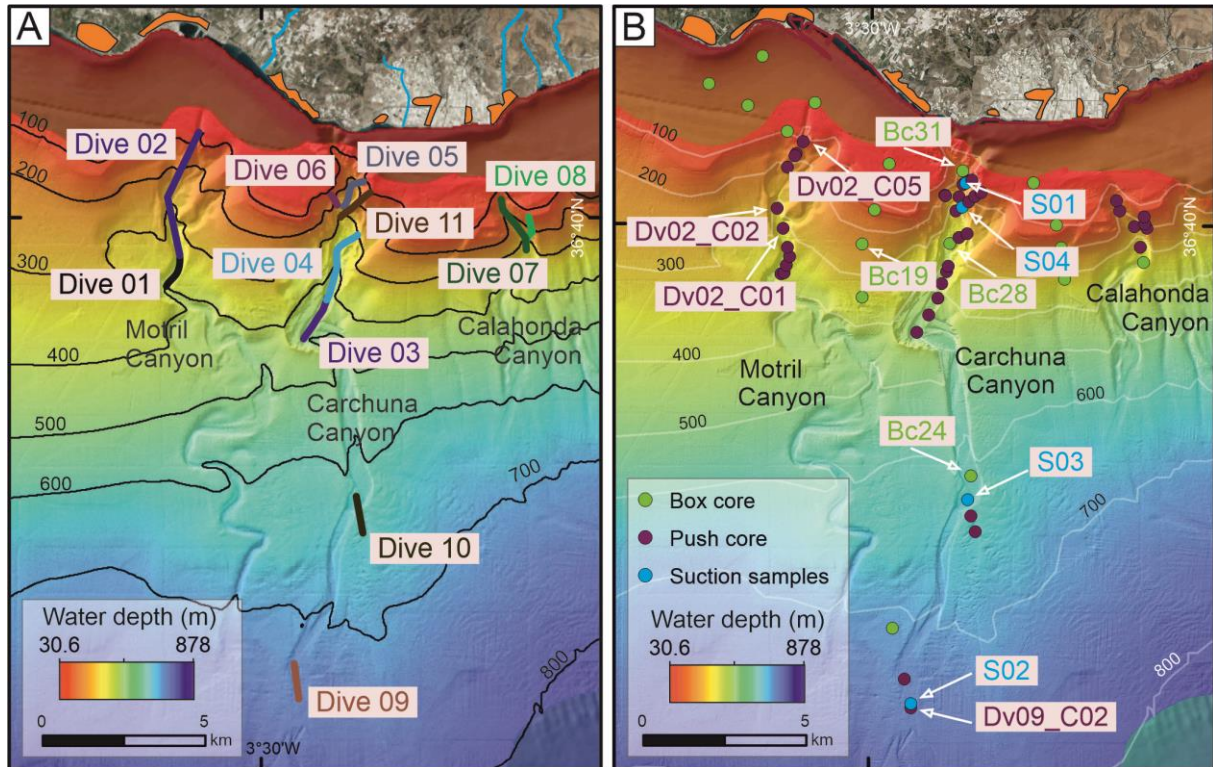


Figure 3.4. Location of Remote Operating Vehicle (ROV) dives, along the Motril, Carchuna, and Calahonda canyons (A) and location of push and box cores and suction samples (B) over a 10 m resolution bathymetric grid acquired during the oceanographic survey ALSSOMAR-S2S 2019. The names of sediment cores used for foraminifera identification and sedimentation rates are indicated. Bathymetric contours in meters.

Seafloor habitats displaying the greatest concentrations of anthropogenic activity were characterized by joining substrate types and the dominant habitat-structuring species identified in ROV underwater images, executed by José Luis Rueda, Olga Sánchez-Guillamón, and José Antonio Caballero-Herrera (Instituto Español de Oceanografía (CSIC), Centro Oceanográfico de Málaga). Annotations of substrate type were made each time a substrate change was detected along dive transects; in specific substrate types, annotations from underwater images were calibrated with data derived from grain size analyses from sediment cores collected with push and box corer devices. Six categories of substrates were identified and compared with surficial sediment samples and grain-size analysis whenever possible (rock, detritic sediment with bioclasts, sand, muddy sand, sandy mud, and mud). Habitat- structuring taxa (mainly megabenthic taxa) and other associated taxa observed in video dives were ranked using a quantification system (0 = absence of species; 1 = 1

individual of a taxa; 2 = 2-5 individuals; 3 = 5-25 individuals; 4 = 25-100 individuals; 5>100 individuals). Those taxa showing the highest average rank along sections of the same dive were interpreted as dominant, but only the dominant habitat-structuring taxa were selected to determine the biological component of the seafloor habitat type. Habitat characterization and nomenclature was carried out whenever possible by combining depth, substrate type, and dominant taxa information. In some cases, facies (interpreted as subtypes or varieties) of the same habitat were detected in some of the underwater images. Habitat classification and nomenclature followed the Reference List of Marine Habitats located in Spain (Templado et al., 2013), which follows a similar hierarchical habitat classification scheme to the EUNIS pan-European habitat identification system from the European Environment Agency. Whenever possible, some habitat types were also linked to the habitat classification of the Barcelona Convention and/or the EU Habitats Directive (Council Directive 92/43/EEC).

Table 3.1.

Litter categories of the Guidance on Monitoring of Marine Litter in Mediterranean Sea (European Commission of the European Union, 2013).

| Type of litter | Examples |
|-------------------------|---|
| Plastics | Bags, bottles, food wrappers, sheets, other plastic objects, fishing nets, fishing lines, other fishing related, ropes/strapping bands, sanitarries (diapers, etc.) |
| Rubber | Tyres, others (gloves, shoes, etc.) |
| Metals | Beverage cans, other food cans/wrappers, middle size containers, large metallic objects, cables, fishing related |
| Glass/ceramics | Bottles, pieces of glass, ceramic jars, large objects |
| Textiles/natural fibers | Clothing (clothes, shoes), large pieces (carpets, etc.), natural ropes |
| Wood (processed) | Construction timbers, pallets, fragments |
| Paper/cardboard | Magazines, boxes |
| Other (specify) | - |
| Unspecified | - |

3.3. Sediment samples

Surficial sediment samples were collected with a suction arm and surficial rock samples were collected with a plier arm, both of them installed in the ROV. A total of 25 sediment cores up to 30 cm long were collected with a push corer also mounted on the ROV, and handled by the plier arm (Figure 3.4B). Additionally, 16 sediment cores up to 50 cm long were collected by deploying a box corer from the ship (Figure 3.4B). Sediment cores were initially split and a visual description of sedimentary facies (lithology, sediment texture and structure, sediment color using the Munsell color chart, bioturbation intensity, and grain size) was undertaken. The top first centimeters of these short sediment cores were subsequently sampled for grain-size analysis and determination of organic matter and carbonate contents, analyses executed by Patricia Bárcenas (Instituto Español de Oceanografía (CSIC), Centro Oceanográfico de Málaga); and for foraminifera identification executed by José Noel Pérez Asensio (Departamento de Estratigrafía y Paleontología, Universidad de Granada) and Isabel Mendes (Centro de Investigação Marinha e Ambiental (CIMA), Universidade do Algarve). Three sediment cores were sampled for the determination of sedimentation rates using ^{210}Pb and ^{137}Cs radioactivity measurements made by Thorbjørn Joest Andersen (Department of Geosciences and Natural Resource Management (IGN), University of Copenhagen). Grain size and geochemical analysis served as ground truth of seafloor imagery and to provide genetic constraints and sediment sources of seafloor sediments and rocks. Foraminiferal assemblages were used to identify transported shelf taxa in deep areas of the submarine canyons. A comparison of sedimentation rates in different bathymetric settings (canyon versus intercanyon) was used to establish the recent activity of submarine canyons.

3.3.1. Grain size

Grain size analysis was executed in the uppermost centimeter of 41 sediment cores (Supplementary Table S1). Surficial sediment samples were dried in the oven at 60°C during 48 hours to reach constant weight. Organic matter oxidation with hydrogen peroxide (H_2O_2 33%) was carried out; later, approximately 10-15 g of sample were weighed. The samples were mixed with pyrophosphate 2% during 24 hours in order to disintegrate and disperse fine sediments. Once the samples were disaggregated, 2 mm mesh size wet sieving was carried out with dispersant. The fraction >2 mm was dried in the oven at 60°C until reaching constant weight during 24-48 h, then weighed and labeled for storage. The fraction <2 mm was

analyzed with a particle size analyzer by laser diffraction (MasterSizer 3000, Malvern®). After this analysis, the samples were poured back into a labeled falcon tube and wet stored.

The grain size distribution was estimated according to the logarithmic Udden-Wentworth grade scale (Udden, 1914; Wentworth, 1922) and plotted as frequency versus grain size. These data were subjected to statistical analysis: mean, sorting, skewness, and kurtosis (Folk and Ward, 1957). Finally, grain size data were plotted according to the textural classification of sediments (Folk, 1954). Sand and gravel were plotted together due to the low gravel occurrences, as only seven samples contained gravel.

3.3.2. Geochemical analysis

Geochemical analysis entailed using the loss on ignition (LOI) method (Dean, 1974; Bengtsson and Enell, 1986) to estimate organic matter and carbonate content of the surficial sediment samples. The LOI method is based on the sequential heating of the samples in a muffle furnace (Figure 3.5).

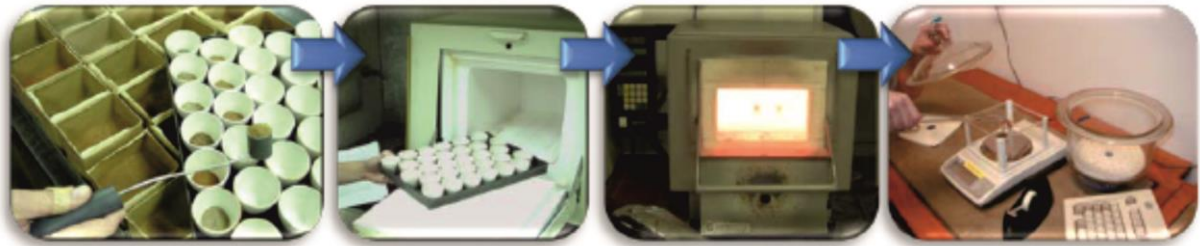


Figure 3.5. Loss on ignition (LOI), method to estimate organic matter and carbonate content of surficial sediment samples based on the sequential heating of the samples in a muffle furnace.

After oven sediment drying to constant weight and determination of the water content (usually 12-24 hours at 100°C), organic matter was combusted to ash and carbon dioxide at 500-550°C during 4 hours. The LOI was then calculated:

$$LOI_{550} = ((DW_{100} - DW_{550}) / DW_{100}) * 100$$

LOI₅₅₀ is provided as a percentage; DW₁₀₀ is the dry weight of the sample in grams after oven drying; and DW₅₅₀ is the dry weight of the sample in grams after heating to 550°C. The weight loss is considered to be proportional to the amount of organic carbon contained in the sample.

In a second knickpoint, carbon dioxide was detached from carbonate (leaving oxide) by heating the samples to 900-1000°C during 2 hours. LOI was calculated as:

$$\text{LOI}_{950} = ((\text{DW}_{550} - \text{DW}_{950}) / \text{DW}_{100}) * 100$$

LOI₉₅₀ is given as a percentage; DW₉₅₀ is the dry weight of the sample after heating to 950 °C.

Assuming a weight of 44 g·mol⁻¹ for carbon dioxide and 60 g·mol⁻¹ for carbonate, the weight loss by LOI at 950°C multiplied by 1.36 should equal the weight of the carbonate in the original sample.

3.3.3. Sedimentation rates

The analyses of sedimentation rates were performed along three short sediment cores located at the same latitude in different physiographic locations: thalweg of the Motril Canyon, thalweg of the Carchuna Canyon, and intercanyon area between the studied canyons. The three sediment cores Dv02_C02, BC19, and BC28 (respectively 18, 20, and 32 cm long) (Figure 3.4B) were sampled each centimeter, and the samples were freeze-dried during 48-72 hours to estimate their water contents.

The samples were subsequently studied to assess the activity of ²¹⁰Pb, ²²⁶Ra, and ¹³⁷Cs via gamma spectrometry at the Gamma Dating Center, Department of Geosciences and Natural Management (University of Copenhagen, Denmark). Measurements were carried out on a Canberra ultralow-background Ge-detector. ²¹⁰Pb was measured via its gamma-peak at 46.5 keV, ²²⁶Ra via the granddaughter ²¹⁰Pb (peaks at 295 and 352 keV), and ¹³⁷Cs via its peak at 661 keV. Chronologies were calculated using the CRS-model by Appleby and Oldfield (1978). Activities in the lower part of the cores were calculated based on regressions of unsupported Pb-210 versus cumulated mass depth following the procedures described by Appleby (2001) and Andersen (2017).

3.3.4. Surficial foraminifera

The uppermost centimeter (0-1 cm) of 4 push cores and 3 box cores collected in the Motril (Dv02_C01, Dv02_C02, and Dv02_C05) and Carchuna canyons (Bc24, Bc28, Bc31, and Dv09_C02) (Figure 3.4B) were used for benthic and planktonic foraminifera identification.

For surficial samples collected with the ROV suction arm, at least 300 benthic foraminifera were counted and identified at the species level in the fraction higher than 125 μm . Relative abundances (%) were calculated from raw counts. Species with a relative abundance higher than 1.5% were included in benthic foraminiferal assemblages. Four suction samples collected by the ROV were studied along the Carchuna Canyon (Figure 3.4B). Two samples were collected from the upper part of the eastern wall (S01 and S04; Figure 3.4B) and two samples were collected from the canyon thalweg of the lower segment (S02 and S03; Figure 3.4B).

Transported shelf taxa include species whose deepest living depth (i.e., the deepest limit of its bathymetric range) was shallower than the sampling depth. These transported shelf taxa were grouped as total transported shelf taxa and identified along the Carchuna Canyon. Furthermore, the percentage of planktonic foraminifera (%P hereafter) was calculated using the following formula: $[P / (P + B)] \times 100$, where P are planktonic foraminifera and B are benthic foraminifera.

3.4. Sub-bottom profiles

The Parasound sub-bottom profiler is based on the parametric effect by simultaneously transmitting two slightly different primary frequencies at high sound pressures into the water column. The interaction of these frequencies generates secondary frequencies confined to the central lobe of the transmitted beam pattern. This effect results in an exceptionally narrow transmission beam, significantly enhancing lateral resolution and enabling the imaging of small-scale structures. This method stands out for its ability to provide good resolution for characterizing sediment layers and their properties in marine geological studies.

Sub-bottom acoustic profiles collected by means of a Teledyne Parasound™ PS-35 echo sounder were used in this study (Figure 3.6). The echo sounder operated with a primary frequency of 18 kHz and a secondary frequency of 4 kHz, resulting in maximum penetrations of about 0.1 s TWTT (Two-Way Travel Time). Processed SEG-Y files (static corrections, gains, and spike removal) were imported in IHS Kingdom™ software for subsequent interpretation. The entire grid of parasound acoustic profiles covers the entire study area. However, only four profiles along the canyon thalweg and an overbank deposit of the Carchuna Canyon have been used (Figure 3.6) to characterize the bedforms developed along the canyon system.

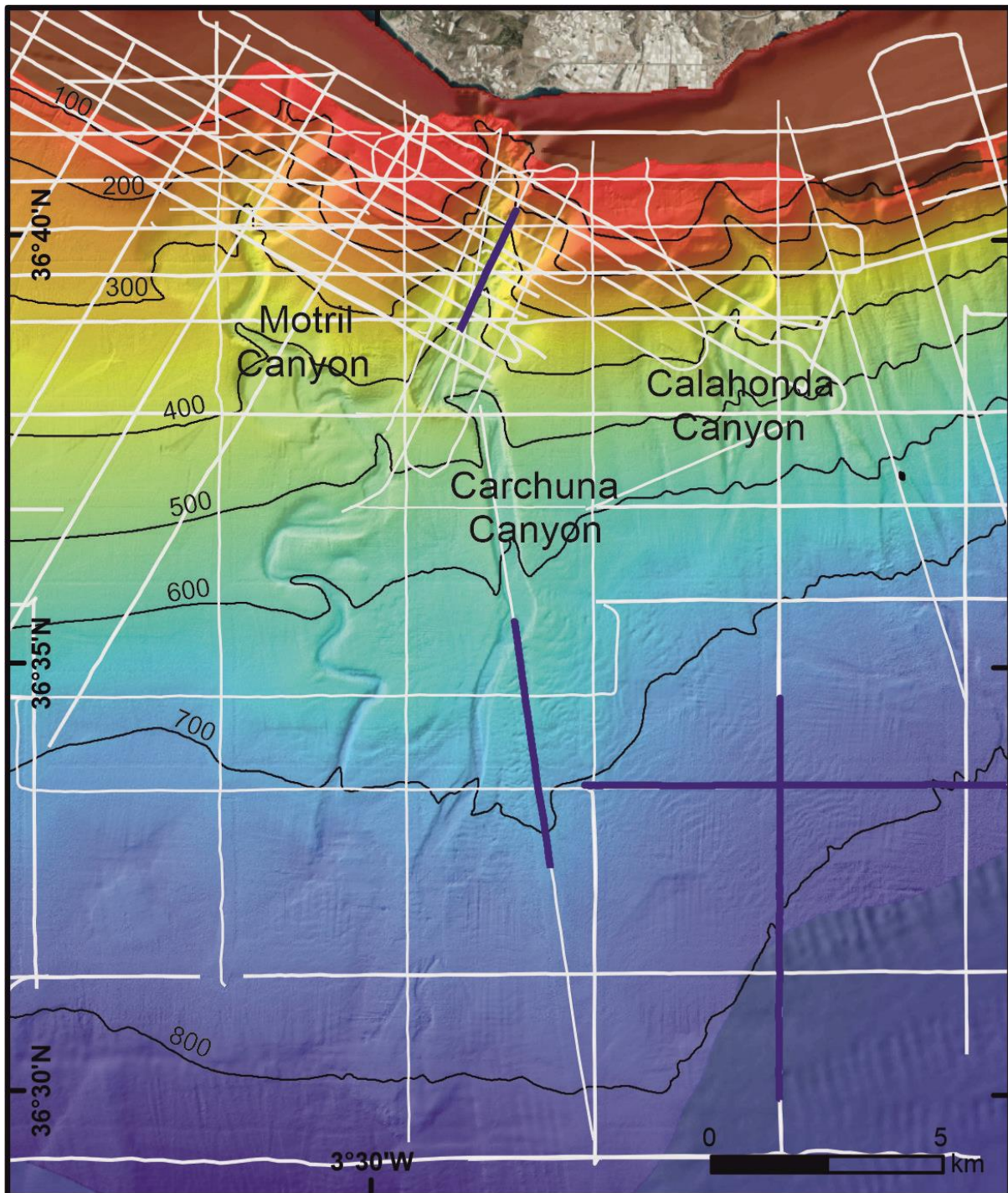


Figure 3.6. Zoomed-in high-resolution bathymetric map of the study area showing the location of acoustic profiles collected (in white), and the location of profiles studied (in blue). Bathymetric contours in meters.

3.5. Three-dimensional flow simulation

The software FLOW-3D® HYDRO (Version 2022R1) was used to simulate different three-dimensional flow scenarios, under the guidance of Irena Schulten (Marine Geology and Seafloor Surveying, Department of Geosciences, University of Malta). This software can use multibeam bathymetric data to reconstruct flow velocities and the Froude number. A grid cell size of 20 m and pre-defined physical models provided in the software were used to reconstruct water flows along the Carchuna Canyon. The following settings were chosen for the simulation: shallow-water model (viscous bed shear stress and turbulent bed shear stress enabled); gravity and non-inertial model (gravitational acceleration in z-direction = $9.81 \text{ m}\cdot\text{s}^{-2}$); turbulence and viscosity model (renormalized group or RNG model to calculate wall shear stress where turbulence mixing length is dynamically computed); and variable density flow model (2nd order monotonicity preserving approximation to density transport equation). For simplification, no submerged flow was considered, and the seafloor was treated as a non-erosional solid medium. This model setting yields velocity values that appear too high for submarine environments (up to $45 \text{ m}\cdot\text{s}^{-1}$). For this reason, the results only distinguish high and low flow velocities. Different flow initiation heights at the canyon head were tested. For the final simulation, the height of fluid flow at the canyon head was set to 30 m, as this height produced the most realistic flow results and agreed well with field observations. Flow 3D post v1.1 was used for postprocessing the data.

3.6. Coastal use data

Land use data from the coastal plain adjacent to the study area (“Consejería de Agricultura, Ganadería, Pesca y Desarrollo Sostenible, Junta de Andalucía”, regional government) were mapped in ArcGIS™. These datasets extend from the Guadalfeo River delta to the east of Calahonda town and cover an extension of 8706 ha. Eleven land uses were considered for classification purposes: beaches, forest, farming, scrubs and pastures, wet areas, areas with low vegetation coverage, greenhouses, roads, industrial infrastructures, mining extraction, and urban. These data were analysed by calculating the area of each individual use and the minimal distance from each use to the coastline to discern the origin of marine litter.

3.7. Maritime traffic data (AIS)

AIS (Automatic Identification System) is the mariner's most significant development in navigation safety since the introduction of radar. AIS works by taking your position and movements via the vessels' GPS system or an internal sensor built into an AIS unit. That information is then collated along with programmable information from the AIS unit and is transmitted in the background at regular intervals whilst also receiving other vessels' AIS information. This is a digital positional awareness system operating in the Very High Frequency (VHF) maritime band. AIS does this by continuously transmitting vessel identity, position, speed, and course along with other relevant information to all other AIS equipped vessels within range. Combined with a shore station, this system also offers port authorities and maritime safety bodies the ability to manage maritime traffic and reduce the hazards of marine navigation.

A maritime traffic density map of the number of routes·km⁻² in the study area for the year 2018 was downloaded from the MarineTraffic© website (www.marinetraffic.com). This website provides information about the current geographic positions of ships, ship characteristics, and weather conditions, among other data. This map was imported and georeferenced in an ArcGIS™ project to describe the position of the ships and the major maritime routes in the study area.

3.8. Fishing activity data (VMS)

Vessel Monitoring System (VMS) data of the main fishing fleets operating in the study area were assessed for the period 2018-2019 (“Ministerio de Pesca, Agricultura y Alimentación”, Spanish government). The VMS database covers the geographic position, date, time (approximately every two hours), and instantaneous velocity of each boat. VMS data included separate data organized by fishing gear of each fleet type, including vessels with licenses for a single gear. Fishing fleets in the study area include artisanal fishing boats, bottom trawling, purse seine, and longline fishing boats. For this work, the fishing activity could only be analysed for bottom trawling, purse seine, and longline fishing boats, as VMS data were not available for the remaining fishing fleets. The three studied fishing fleets are responsible for the largest landings in the Port of Motril, which is the main one in the study area.

This VMS database was imported and georeferenced in the ArcGIS™ project to describe the fishing activity along the studied canyons. The fishing activity in the study area was quantified

in five sectors, from west to east (Figure 3.7): Western Sector, Motril Canyon, Carchuna Canyon, Calahonda Canyon, and Eastern Sector. Depth ranges within each sector included the shelf (0-100 m water depths), shelf edge and uppermost slope (100-200 m water depths), upper slope (200-500 m water depths), and middle slope (below 500 m water depth). The fishing effort was estimated as the average number of fishing days per km² in 2018 and 2019.

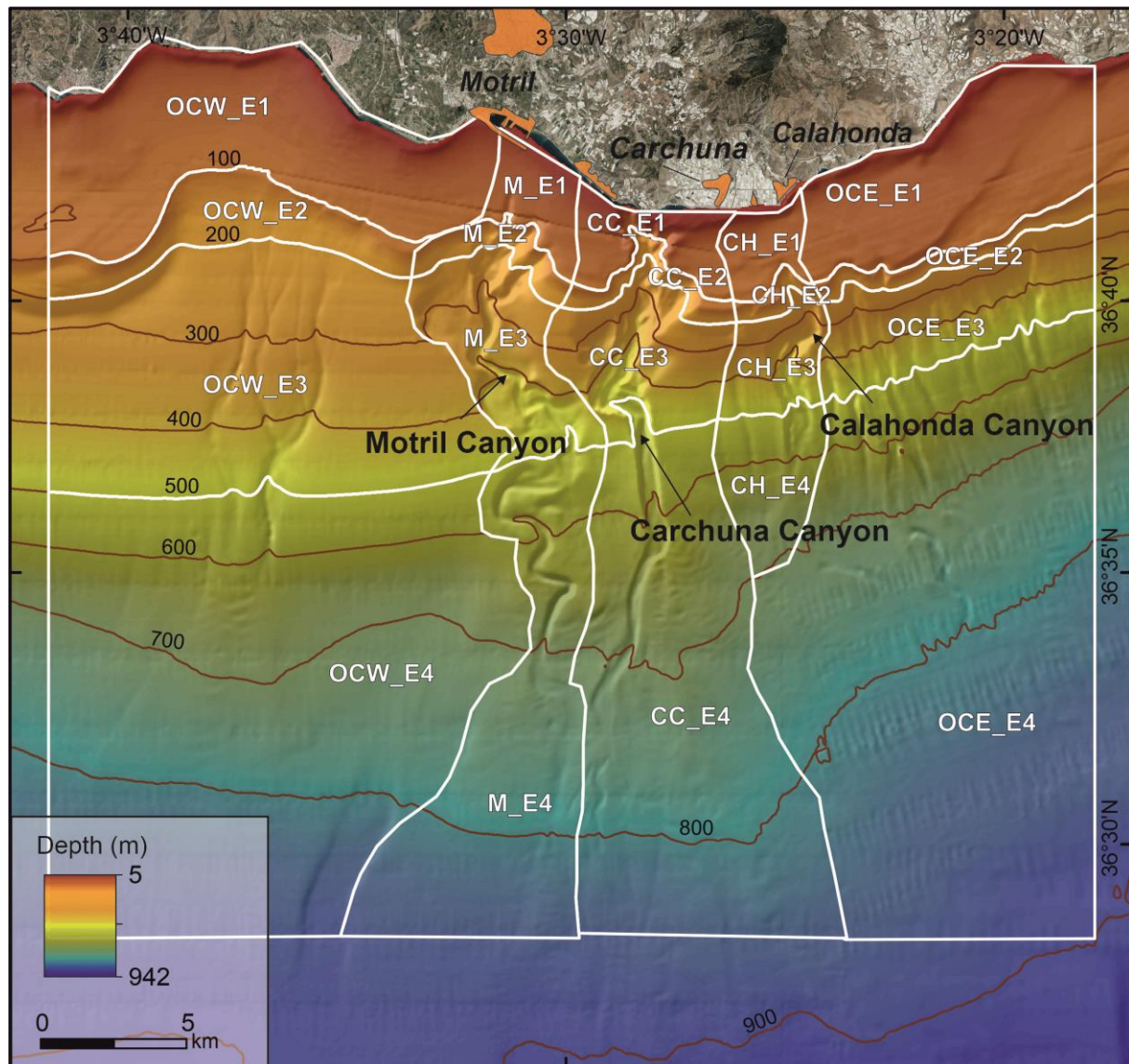


Figure 3.7. Distribution of sectors in order to quantify the fishing activity along the studied shelf-incised canyons. OCW: Western sector of the study area; M: Motril Canyon; CC: Carchuna Canyon; CH: Calahonda Canyon; OCE: Eastern sector of the study area; E1: Shelf; E2: Outer shelf-uppermost slope; E3: Upper slope; E4: Middle slope. Bathymetric contours in meters.

Part 2



4. Morphology and recent sedimentary processes in the shelf-incised Motril and Carchuna canyons:
Implications for recent canyon activity
5. Bedform development in confined and unconfined settings of the Carchuna Canyon: An example of cyclic steps in shelf-incised canyons
6. Origin and driving mechanisms of marine litter in the shelf-incised Motril, Carchuna, and Calahonda canyons

Chapter 4

Morphology and recent sedimentary processes in the shelf-incised Motril and Carchuna canyons: Implications for recent canyon activity

This chapter have been published in *Geomorphology* as:

^{1,2}Cerrillo-Escoriza, J., ¹Lobo, F. J., ²Puga-Bernabéu, ³Bárcenas, P., ⁴Mendes, I., ²Pérez-Asensio, J. N., ⁵Durán, R., ⁶Andersen, T. J., ^{1,2}Carrión-Torrente, ⁷García, M., ²López-Quirós, A., ⁸Luján, M., ⁹Mena, A., ³Sánchez-Guillamón, O., ¹⁰Sánchez, M. J., 2024. Variable downcanyon morphology controlling the recent activity of shelf-incised submarine canyons (Alboran Sea, western Mediterranean). *Geomorphology* 453, 109127. <https://doi.org/10.1016/j.geomorph.2024.109127>

¹Department of Marine Geosciences, Instituto Andaluz de Ciencias de la Tierra (CSIC-UGR), Armilla, Granada Spain, ²Departamento de Estratigrafía y Paleontología, Facultad de Ciencias, Universidad de Granada, Granada, Spain, ³Instituto Español de Oceanografía, Centro Oceanográfico de Málaga (IEO-CSIC), Fuengirola, Málaga, Spain, ⁴Centro de Investigação Marinha e Ambiental (CIMA), Universidade do Algarve, Faro, Portugal, ⁵Institute of Marine Sciences (CSIC), Barcelona, Spain, ⁶Department of Geosciences and Natural Resource Management (IGN), University of Copenhagen, Copenhagen K, Denmark, ⁷Instituto Español de Oceanografía, Centro Oceanográfico de Cádiz (IEO-CSIC), Cádiz, Spain, ⁸Department of Earth Sciences, CASEM – Facultad de Ciencias del Mar y Ambientales, Universidad de Cádiz, Puerto Real, Spain, ⁹Departamento de Xeociencias Mariñas e Ordenacion do Territorio, Facultad de Ciencias do Mar, Universidad de Vigo, Vigo, Spain, ¹⁰Instituto de Oceanografía y Cambio Global (IOCAG), Universidad de Las Palmas de Gran Canaria, Las Palmas de Gran Canaria, Spain.

Abstract

This research aims to distinguish genetic sedimentary processes building canyon geomorphological patterns and the factors driving different sedimentary activities in two nearby Mediterranean shelf-incised submarine canyons (Carchuna and Motril) that exhibit different degrees of incision on the narrow margin of the northern Alboran Sea.

The straight Carchuna Canyon incises the shelf up to 200 m off the coastline and exhibit steep canyon walls featuring narrow terraces, muddy sands with high contents of organic matter along the thalweg, and transported shelf benthic foraminifera in distal settings. The Motril Canyon head is wider and incises the shelf edge, ca. 2 km off the coastline. It exhibits a sinuous morphology and less steep walls, wider terraces, and higher sedimentation rates with muddy sediments along the thalweg. In both canyons, cross-section relief, width, incision, and area decrease downslope, although these parameters increase locally.

The downslope variations of geomorphological parameters are attributed to enhanced erosional/depositional processes promoted by tectonically controlled abrupt changes of the axial channel orientation. The degree of shelf incision, the location of the canyon heads in relation with the local sediment sources, and the seasonally variable hydrodynamic regimes determine the different degrees of recent canyon activity. The Motril Canyon is interpreted as a mature system that reflects episodic activity, collecting fine-grained sediments from the nearby Guadalfeo River. The Carchuna Canyon exhibits a youthful developmental stage whose activity is more continuous and involves sediment trapping of littoral cells and continuous downslope sand transport.

4.1. Results

4.1.1. Geomorphology

4.1.1.1. Major morphological features

The continental margin enclosed in the study area has a main E-W orientation and the shelf is up to 3.5 km wide (Figure 4.1A). The shelf edge is located at 100 to 125 m water depth. The Motril and Carchuna canyons are N-S trending, shelf-incised features that exhibit contrasting morphological configurations (Figure 4.1A).

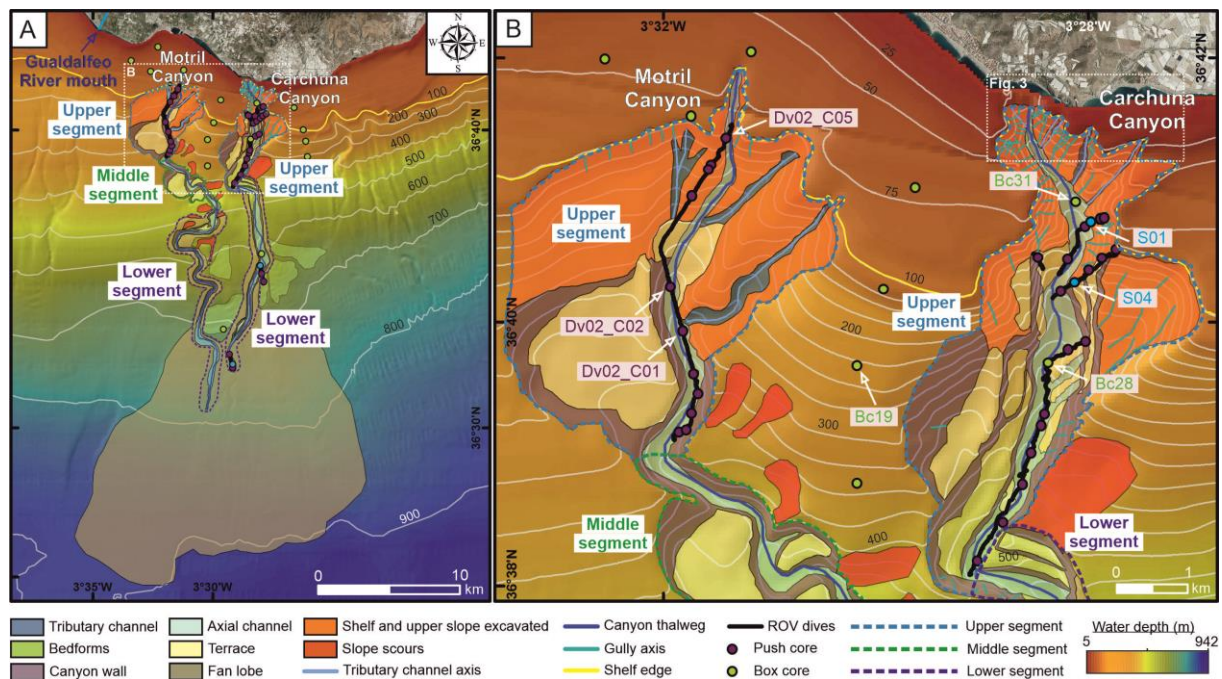


Figure 4.1. (A) Geomorphological mapping of the study area and zoom of the shelf and upper slope (B) over the 50 m resolution bathymetric grid, showing the segment distribution within each canyon. Push and box core location and ROV dives executed during ALSSOMAR 2019 survey are also indicated. Bathymetric contours in meters.

Motril Canyon

The Motril Canyon is incised in the shelf edge, and its head lies at 100 m water depth, 2200 m off the northern coastline and 5500 m southeast of the Guadalfeo River mouth (Figure 4.1A). Three geomorphological segments can be discerned in the Motril Canyon (Figure 4.1; Table 4.1). The upper segment is characterized by a roughly N-S trending axial channel from 75 to 400 m water depths. The canyon head begins with a 950 m long and 140 m wide straight channel that incises the outer shelf up to 100 m water depth (Figure 4.1B; Table 4.1). The amphitheater-like canyon head is excavated in the outer shelf and upper slope down to 275 m

water depth that includes two large tributary channels on the eastern flank, and one tributary channel and wide terrace in the western flank (Table 4.1).

The middle segment starts with an abrupt change in the orientation of the main valley from N-S to NW-SE down to 500 m water depth. Here, the axial channel shows a sinuous path with two large terraces in the southwestern flank (Figure 4.1B; Table 4.1). The lower segment trends N-S from 500 to 750 m water depths, and features six meanders. The width of the axial channel—limited by steep walls (ca. 16°)—decreases downslope from 900 to 300 m (Table 4.1). Away from the axial channel, lateral levees with superimposed bedforms are observed in the eastern flank (Figure 4.1A). Downslope of the channel mouth (up to 900 m water depth), a lobate morphology is observed (Figure 4.1A).

Table 4.1.
Main morphological and sedimentological differences between Motril and Carchuna canyons.

| | Motril Canyon | Carchuna Canyon |
|-------------------------------------|---|---|
| Longitudinal profile | Slightly concave | Very concave |
| Distance from the coastline | 2200 m | 200 m |
| Close to the river mouth | Yes, Guadalfeo River | No |
| Canyon head | 4.3 km wide, U-shaped | 1.5 km wide, V-shaped |
| Tributary channels WF | 1 channel 1.1 km long and 180 m wide | 2 channels up to 700 m long and 50 m wide. Several 300 m long gullies |
| Tributary channels EF | 2 channels up to 2.5 km long and up to 200 m wide | 3 channels up to 1 km long and 125 m wide. Heads cut IPW. Several 500 m long gullies |
| Axial channel | Straight | Straight with bedforms |
| Terraces WF | 1 terrace with 2500 m wide | Up to 900 m and 150 m wide |
| Terraces EF | No | Up to 500 m long and 150 m wide terraces |
| Sedimentary facies | Medium silts in AC. Coarse silts in WF | Very fine sands in canyon head. Coarse silts in AC. Fine sands in WF; Very fine sands in EF |
| Organic matter | High in AC. Low in WF | High in the lower reaches. Low in canyon head |
| Sediment cores | Massive and homogenous muds | Sandy muds along AC. Sands in flanks |
| Mass accumulation rates | 15.21 kg·m ⁻² ·yr ⁻¹ ; 1.45 cm·yr ⁻¹ | 5.40 kg·m ⁻² ·yr ⁻¹ ; 0.49 cm·yr ⁻¹ |
| Surficial foraminifera | Lack of reworked foraminifera downcanyon | Decrease of values of foraminiferal fragments and reworked |
| Axial channel | Sinuuous | |
| Terraces WF | 2 terraces up to 1.5 km ² (3.5° slope gradient) | |
| Terraces EF | Excavated areas disconnected from the AC (17° slope gradient) | |
| Axial channel | Meandering, from 900 to 300 m wide | Straight, from 430 to 150 m wide |
| Levees | Wide | Narrow |
| Superimposed undulations over levee | Yes, NW-SE orientation of the crests | Yes, NW-SE orientation of the crests. Area of 25 km ² |
| Sedimentary facies | - | Very fine sands in AC. Coarse silts in eastern levee |
| Organic matter | - | High in the termination of the channel |
| Sediment cores | - | Muds with interbedded sands along AC |
| Surficial foraminifera | - | High percentage of planktonic foraminifera (%P) |

WF: Western flank; EF: Eastern flank; IPW: Infralittoral prograding wedge; AC: Axial channel.

Carchuna Canyon

Two geomorphological segments were distinguished in the Carchuna Canyon (Figure 4.1; Table 4.1). In the upper segment, the canyon is deeply incised in the shelf, as its head is located just 200 m off the coastline at 30 m water depth (Figures 4.1B and 4.2). This segment is defined by an axial channel with a main N-S orientation down to 500 m water depth. The canyon head starts with an axial channel that widens from 70 to 150 m down to 200 m water

depth and it widens to as much as 550 m. The uppermost axial channel exhibits bedforms that may reach 2 m in height and 15-30 m in length (Figure 4.2). The eastern flank in the shelf-incised section harbors three tributary channels, whose heads are incised into shelf infralittoral prograding wedges (Figure 4.2; Table 4.1).

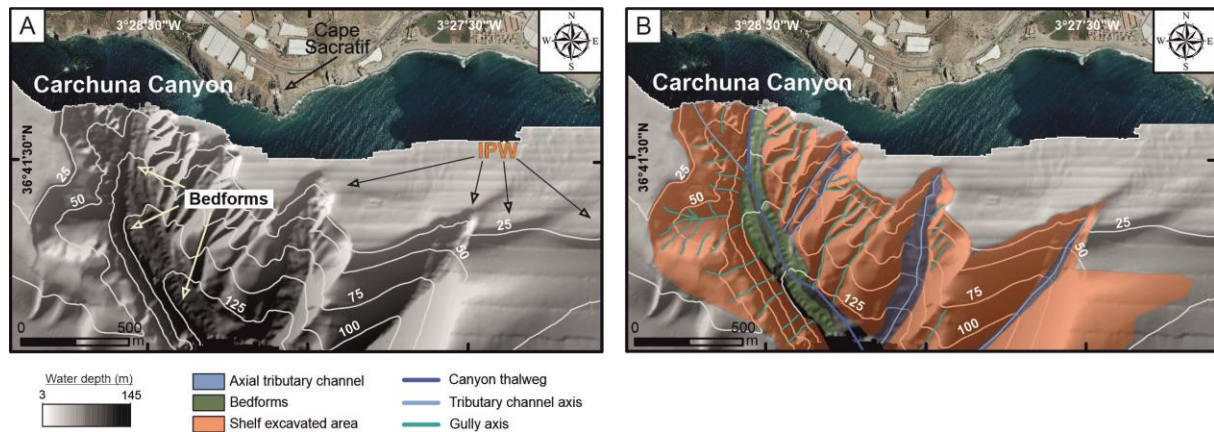


Figure 4.2. (A) Shaded relief from a 5 m resolution bathymetric grid (Ministerio de Pesca, Agricultura y Alimentación, 2002) of the Carchuna Canyon head incised in the shelf and cutting the Carchuna Infralittoral Prograding Wedge (IPW). (B) Geomorphological mapping of the Carchuna Canyon head. Bathymetric contours in meters.

Downslope, the eastern flank becomes steeper (ca. 35°), with short terraces (Figure 4.1B; Table 4.1). The western flank in the uppermost shelf-incised section is even steeper (ca. 40°) and contains several gullies, plus two tributary channels (Figure 4.2; Table 4.1). This flank becomes smoother downslope, having elongated and narrow terraces limited by steep walls (ca. 20°) (Figure 4.1B; Table 4.1). The transition between the upper and lower segments is marked by an abrupt change of orientation of the main valley from NNE-SSW to WNW-ESE (Figure 4.1). The lower segment is characterized by a straight and wide valley with a main N-S orientation until 740 m water depth. The axial channel is limited by two large lateral levees (Table 4.1). At 620 m water depth, the orientation of the axial channel shifts to the NNE-SSW. Superimposed undulations are identified over the eastern levee (Figure 4.1A; Table 4.1). The axial channel exhibits a sinuous path between 645 and 730 m water depth (Table 4.1). Downward from the channel mouth, a lobe, merged with the equivalent feature of the Motril Canyon, extends to 900 m water depth (Figure 4.1A).

4.1.1.2. Morphometric parameters

The longitudinal profile of the Intercanyon area is slightly convex; its slope gradient ranges from 11° close to the shelf edge to 2° downslope. The main knickpoints are located on the shelf edge and at 14 km from the coastline in the lower reaches of the intercanion (Fig. 4.3).

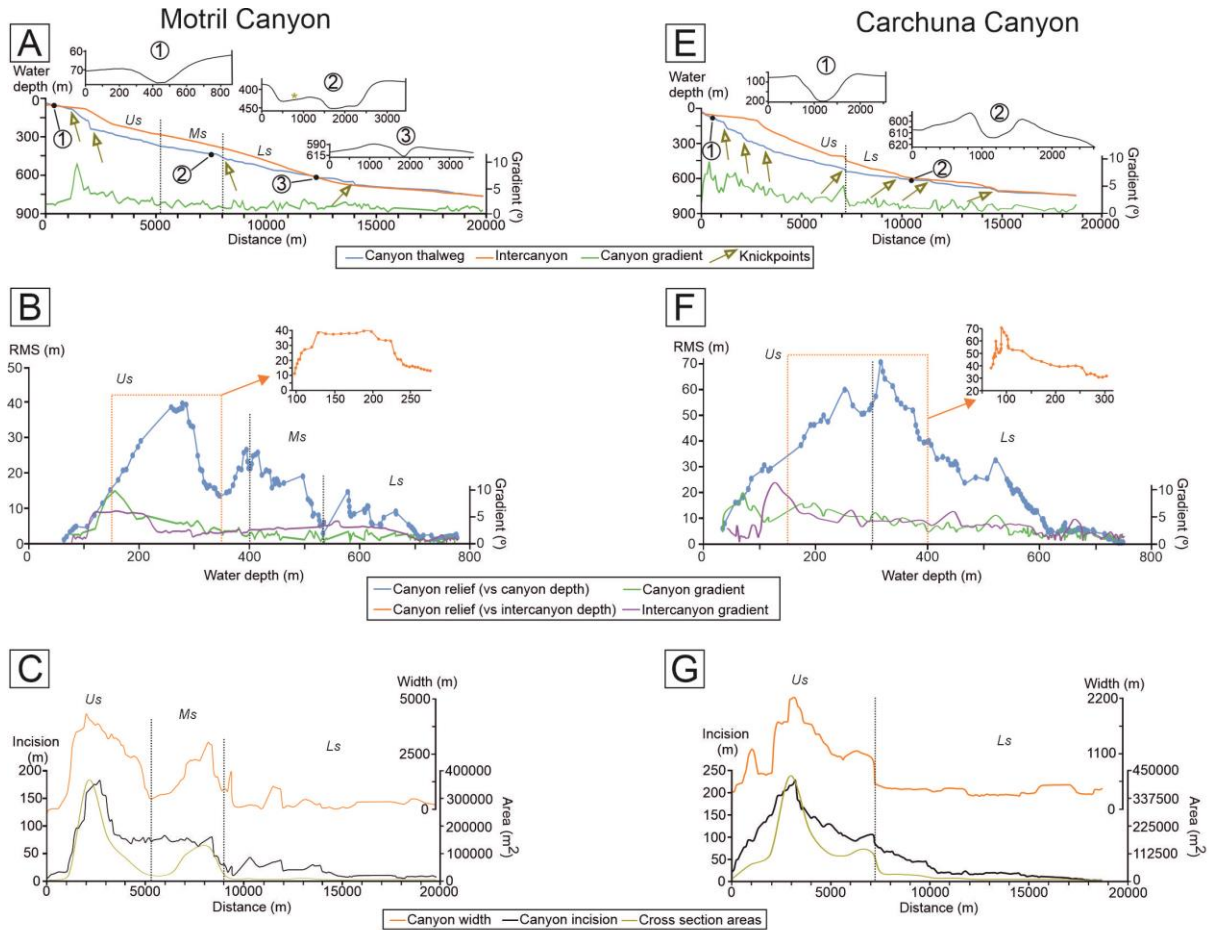


Figure 4.3. Bathymetric profiles of the Motril and Carchuna canyons, showing the relationships between selected morphologic parameters. (A, D) Depth profiles along the Motril and Carchuna canyons' thalweg (blue line), with indications of knickpoints, and along the intercanion slope (orange line). The canyon gradient is measured along the canyon thalweg (green line). Transverse profiles of each segment of the both canyons are also shown. The yellow asterisk indicates terraced features dipping outward from the axial channel of the Motril Canyon. (B, E) Downslope variation of canyon relief (vs. canyon depth) (blue line), canyon relief (vs. intercanion depth) in the canyon head (orange line), canyon gradient along the Motril and Carchuna canyons (green line), and slope gradient of the intercanion area (purple line). (C, F) Downslope changes in canyon width (orange line), incision (black line) and cross-sectional area (yellow line) along the Motril and Carchuna canyons.

Motril Canyon

The Motril Canyon is almost 27 km long and has a sinuosity index of 1.28, an average width of 1.5 km, and a maximum width of 4.6 km. The maximum width of the axial channel is 1560 m and its maximum incision is 179 m. The maximum gradient of the canyon walls is ca. 17°. Motril Canyon is fed by 17 gullies (12 in the western and 5 in the eastern flank) mainly located in the upper segment (Table 4.2).

The longitudinal profile of the Motril Canyon thalweg is slightly concave shape (Figure 4.3A). The thalweg profile exhibits four knickpoints located at 110, 210, 450, and 670 m water depths (Figure 4.3A). The axial channel is U-shaped, and the flanks locally exhibit terraced features dipping outward from the axial channel (Figure 4.3A). In the lower segment, the narrow channel is limited by wide levees (Figure 4.3A).

In terms of canyon depth, the relief grows progressively, reaching its highest value (ca. 40 m) at 250 m water depth in the upper segment; after which the relief decreases downslope, showing two peaks in the middle segment, ca. 25 m at 400 m water depth and ca. 20 m at 500 m water depth; and one peak in the lower segment, ca. 15 m at 580 m water depth (Figure 4.3B). The relief in the canyon head regarding intercanyon depth exhibits high values between 130 and 225 m water depth (Figure 4.3B). The canyon gradient has a maximum value of 10° at the shelf edge (Figure 4.3B).

Altogether, the values of canyon width, incision, and area decrease from the upper to the lower segment, although canyon width and incision have high values at ca. 2100, 8000, and 11800 m from the canyon head that correspond to 260, 460, and 610 m water depths, respectively (Figure 4.3C). The canyon cross-section area decreases downcanyon, yet exhibits a peak value at 460 m water depth (8 km off the canyon head) that coincides with the change from the middle to the lower segment (Figure 4.3C).

Table 4.2.

Summary of the main metric characteristics of the submarine canyons in the study area.

| C | Longitude (W) | Latitude (N) | L (m) | SL (m) | S | mD (m) | MD (m) | MW (m) | AvW (m) | FIW (m) | I (m) | CGr (°) | GrW (°) | GrE (°) | MGrW (°) | MGrE (°) | G | Az |
|----------|------------------|-----------------|----------|-----------|------|-----------|-----------|-----------|------------|------------|----------|------------|------------|------------|-------------|-------------|----|--------|
| Motril | 3°31'15.51" | 36°42'1.32" | 26944 | 20945 | 1.28 | 66.49 | 763.84 | 4660 | 1560 | 1090 | 179 | 2.22 | 6.65 | 6.08 | 16.73 | 16.35 | 17 | 175.75 |
| Carchuna | 3°28'34.34" | 36°41'41.02" | 20366 | 17677 | 1.15 | 18.42 | 749.33 | 4020 | 1230 | 2160 | 226 | 2.39 | 9.67 | 8.06 | 33.88 | 24.55 | 55 | 182.38 |

C: canyon; L: total length (distance between the shallowest part of the canyon head and the deepest part of the canyon mouth measured along the canyon thalweg); SL: straight length (shortest distance between the shallowest part of the canyon head and the deepest part of the canyon mouth); S: sinuosity (relationship between the total and straight length); mD: minimum depth (depths at which canyon commences); MD: maximum depth (depth at which canyon ends); MW: maximum width (maximum horizontal distance perpendicular to the canyon valley between the highest part of the interfluves); AvW: average width (average value of canyon width measured along the axis channel); FIW: maximum floor width (maximum distance across the canyon floor measured perpendicular to the axial channel); I: maximum canyon incision (depth difference between the axis channel and the adjacent interfluves); CGr: average canyon gradient (average angle measured between two points along the canyon thalweg relative to horizontal); GrW: average gradient of the western canyon wall (average angle measured between the shallowest and deepest points along the western canyon wall relative to horizontal); GrE: average gradient of the eastern canyon wall (average angle measured between the shallowest and deepest points along the eastern canyon wall relative to horizontal); MGrW: maximum gradient of the western canyon wall; MGrE: maximum gradient of the eastern canyon wall; G: number of gullies; Az: azimuth (orientation relative to north between the starting and ending points).

Carchuna Canyon

The Carchuna Canyon, some 20 km long, has a sinuosity index of 1.15, an average width of 1.2 km, and a maximum width of 4020 m. The maximum incision is 226 m, the maximum axial channel width is 2160 m, and the maximum gradient of the canyon walls is ca. 34°. Fifty-five gullies are excavated in the flanks, mainly in the upper segment (Table 4.2).

The longitudinal profile of the Carchuna Canyon thalweg is characterized by a concave up shape (Figure 4.3D). Several knickpoints are found in the upper segment. One knickpoint is located in the transition from the upper to the lower segment, at 520 m water depth. Two additional knickpoints lie along the lower segment at 650 and 690 m water depths (Figure 4.3D). Transversal depth profiles of the Carchuna Canyon show V shapes in the upper segment and U shapes along the lower segment, having narrower levees (Figure 4.3D).

Canyon relief values progressively increase up to 70 m in the middle part of the upper segment at 320 m water depth; downslope, canyon relief decreases towards the lower segment, with a peak value of 32 m at the abrupt transition between the upper and lower segments (Figure 4.3E). The relief in the canyon head with respect to intercanyon depth exhibits a high value at 90 m water depth and then a downcanyon decrease (Figure 4.3F). High canyon gradient values are situated along the Carchuna Canyon head (up to 100 m water depth). Although gradient values decrease steadily towards the lower segment, several knickpoints run into high values of canyon gradients along the Carchuna Canyon: e.g., 7° at 180 m water depth, 5° at 300 and 520 m water depths, 2.5° at 650 m water depth, and 2.2° at 690 m water depth (Figure 4.3E).

Overall, canyon width, incision, and cross-section values for the Carchuna Canyon decrease with parallel trends from the upper to the lower segment (Figure 4.3F). High values of canyon width, incision, and area occur at 300 and 490 m water depths. The latter water depth coincides with the upper-lower segment transition. Furthermore, the canyon width exhibits peak values at 100 m water depth in the Carchuna Canyon head (Figure 4.3F).

4.1.2. Surficial sediments

4.1.2.1. Sedimentary facies from seafloor imaging and grain size

The seafloor of the upper segment of the Motril Canyon comprises four sedimentary facies (Figure 4.4; Table 4.1). In the shallowest upper segment, the axial channel is characterized by

very fine sands that evolve toward the shelf edge to sandy mud including scarce gravel and pebble bioclasts (Figure 4.4B). Downcanyon, the axial channel has a homogeneous muddy floor with medium silts and scarce bioturbation (Figure 4.4B). Coarser sediments with sandy mud floors showing bioturbation and bioclasts would characterize the western flank of the tributaries (Figure 4.4B).

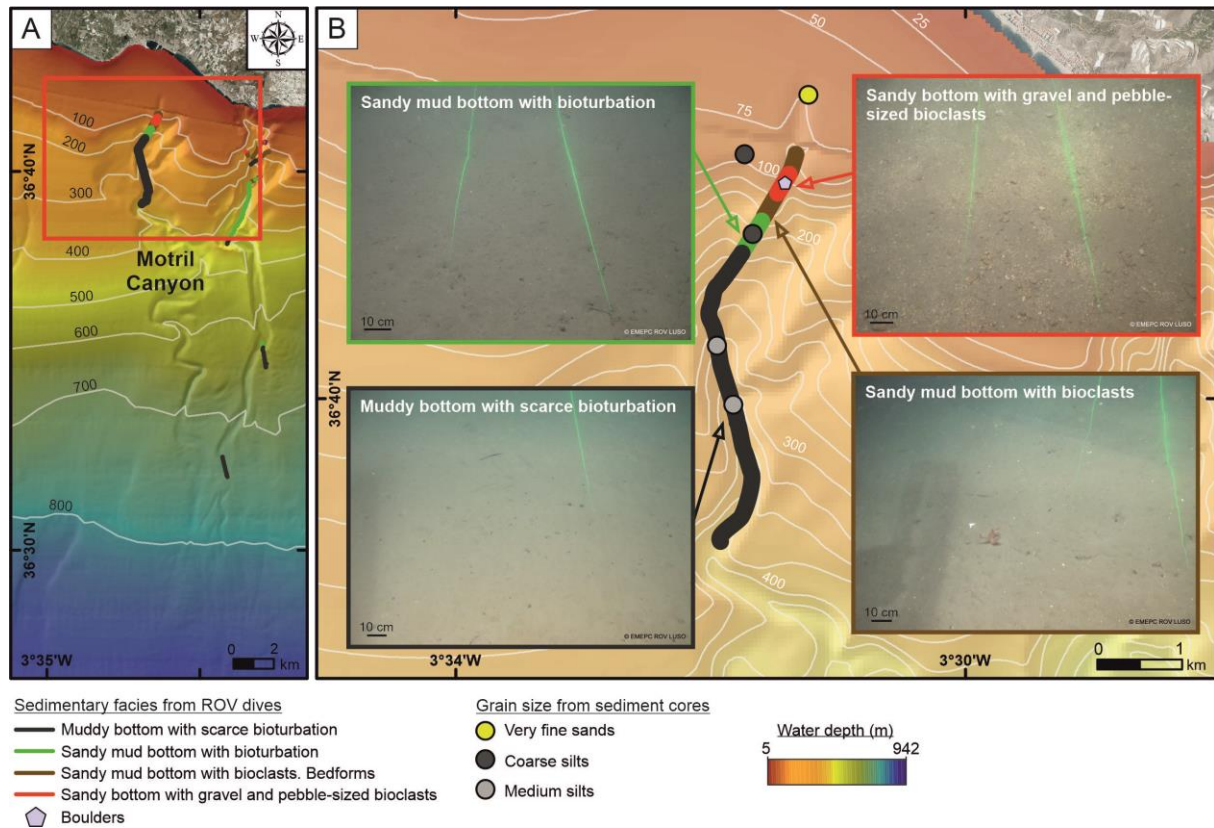


Figure 4.4. Sedimentary facies along ROV dives and texture of surficial sediment samples in the Motril Canyon (A) and zoom of specific dive sites with photographic images of representative seafloor sedimentary facies (B). Laser beam spacing of 62 cm. Bathymetric contours in meters.

Carchuna Canyon displays six sedimentary facies along its entire length (Figure 4.5; Table 4.1). In the shallowest part of the upper segment, the axial channel exhibits sandy mud floors with bioclasts that evolve downcanyon to sandy muds with coarse silts and bioturbation (Figure 4.5B). The eastern flank is characterized by very fine sands with pebble-sized bioclasts and granules, along with cobble clasts, poorly sorted and colonized by bivalves (Figure 4.5B). The bioclasts comprise coralline red algae and disarticulated fragmented bivalves. The western flank is characterized by well-sorted fine sands with gravel and pebble-sized coralline red algae (Figure 4.5B). The axial channel is characterized by muddy sediments in the transition between the upper and the lower segments (Figure 4.5B). In the

lower one, the axial channel has sandy mud floors: very fine sands and bioturbation (Figure 4.5A). Yet lateral levees in the lower segment can be characterized as homogeneous muddy floors with coarse silts and bioturbation (Figure 4.5A). The axial channel is characterized by muddy sediments in the transition between the upper and the lower segments (Figure 4.5B). In the lower one, the axial channel has sandy mud bottoms: very fine sands and bioturbation (Figure 4.5A). Yet lateral levees in the lower segment can be characterized as homogeneous muddy bottoms with coarse silts and bioturbation (Figure 4.5A).

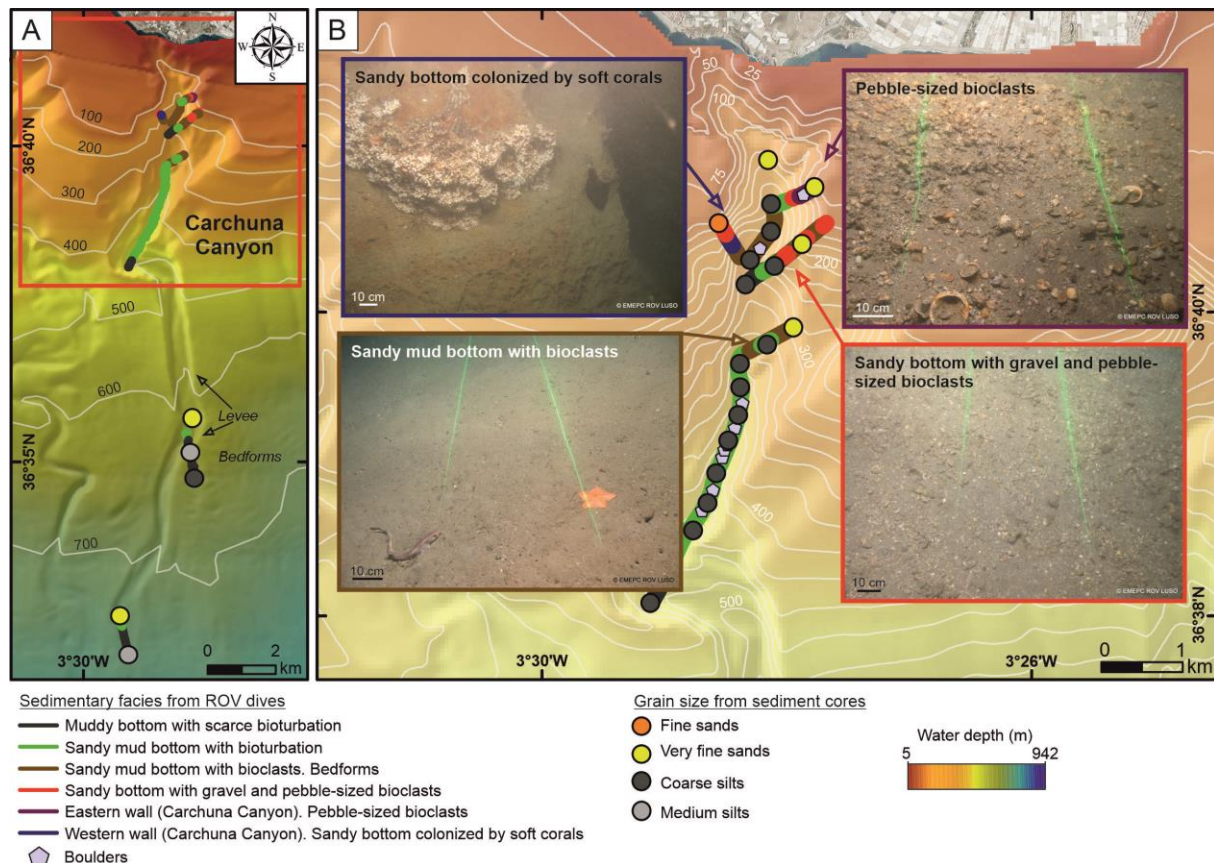


Figure 4.5. Sedimentary facies along ROV dives and texture of surficial sediment samples in the Carchuna Canyon (A) and zoom of specific upper segment dive sites with photographic images of representative seafloor sedimentary facies (B). Laser beam spacing of 62 cm. Bathymetric contours in meters.

4.1.2.2. Organic matter and carbonate contents

The seafloor sediments in the shallowest part of the upper segment of the Motril Canyon have low organic matter (5%) and carbonate (6%) contents (Figure 4.6A and B). Downcanyon, the axial channel exhibits the highest values of organic matter (ca. 8%), while carbonate content varies between 5% and 8% (Figure 4.6A and B; Table 4.1).

In the upper segment of the Carchuna Canyon, the axial channel reflects a downcanyon increase of organic matter content (from ca. 5% to 12%), whereas carbonate content increases slightly, from ca. 5% to 8% (Figure 4.6A and B; Table 4.1). The flanks of the upper segment exhibit the lowest content in organic matter (ca. 4%). Carbonate percentages range between 12% in the eastern flank to ca. 20% in the western flank.

In the lower segment of the Carchuna Canyon, organic matter content increases from ca. 7% to 9% downcanyon, from the axial channel to the lobe, though carbonate percentages are homogeneous along the axial channel, their values (7-8%) being similar to those of the upper segment (Figure 4.6A and B; Table 4.1). The highest organic matter and carbonate percentages (up to 10%) in this segment are found in the eastern levee.

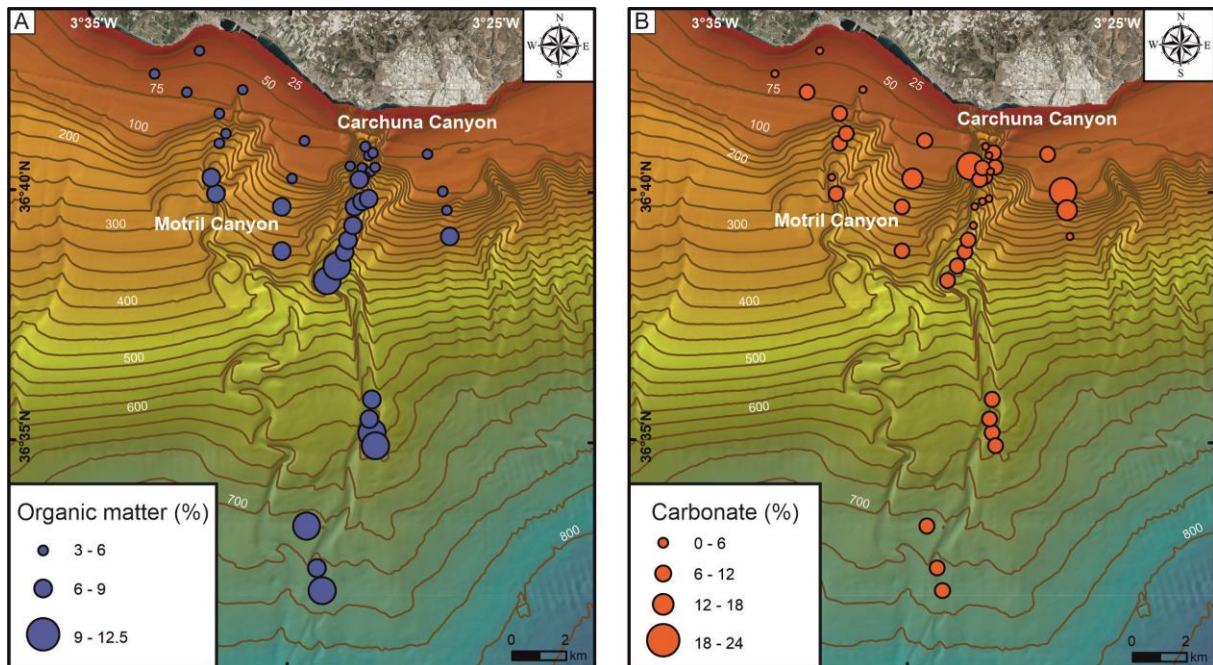


Figure 4.6. Percentages of organic matter (A) and carbonate (B) in surficial sediment samples of the study area. Bathymetric contours in meters.

4.1.3. Sub-surface sediments

4.1.3.1. Sediment cores

Sediment cores near the Guadalfeo River mouth —at about 50 m water depth— are characterized by sandy mud containing clasts and bioclasts with interbedded fine sands, alongside homogenous mud with organic matter clasts (Figure 4.7). The bioclasts are mostly abraded fragmented bivalve shells, whereas the lithoclasts are sub-angular pebbles. Sub-surface sediments along the upper segment of the Motril Canyon are quite homogeneous. They show massive homogeneous mud with negligible percentages of very fine sands. (Figure 4.7; Table 4.1). A fining-upward trend, from coarse and medium sands with sub-rounded bioclasts to sandy muds with a few bioclastic remains, is found in the shallowest sector of the upper segment. These cores are capped by very thin beds with matrix-supported gravels.

Sediment cores along the Carchuna Canyon exhibit a more heterogeneous composition (Figure 4.7; Table 4.1). Sandy muds with bioclasts and interbedded very fine sands are found in the canyon head. Downcanyon, homogenous sandy mud lie over medium and fine sand. The distal part of the upper segment is characterized by massive and homogeneous mud. In both flanks of the upper segment, coarsening-upward trends with sub-rounded very coarse sands, and gravel and pebble-sized bioclasts formed by sub-angular disarticulated shells, can be observed (Figure 4.7). Homogeneous sandy muds with very thin interbedded well-sorted fine sands as well as sub-rounded very coarse bioclastic sand and gravel occur along the lower segment axial channel (Figure 4.7). Finally, fining-upward trends —from basal sands to homogeneous sandy muds with thin interbedded sands— are discerned in the lateral levees and the distal lobe (Figure 4.7).

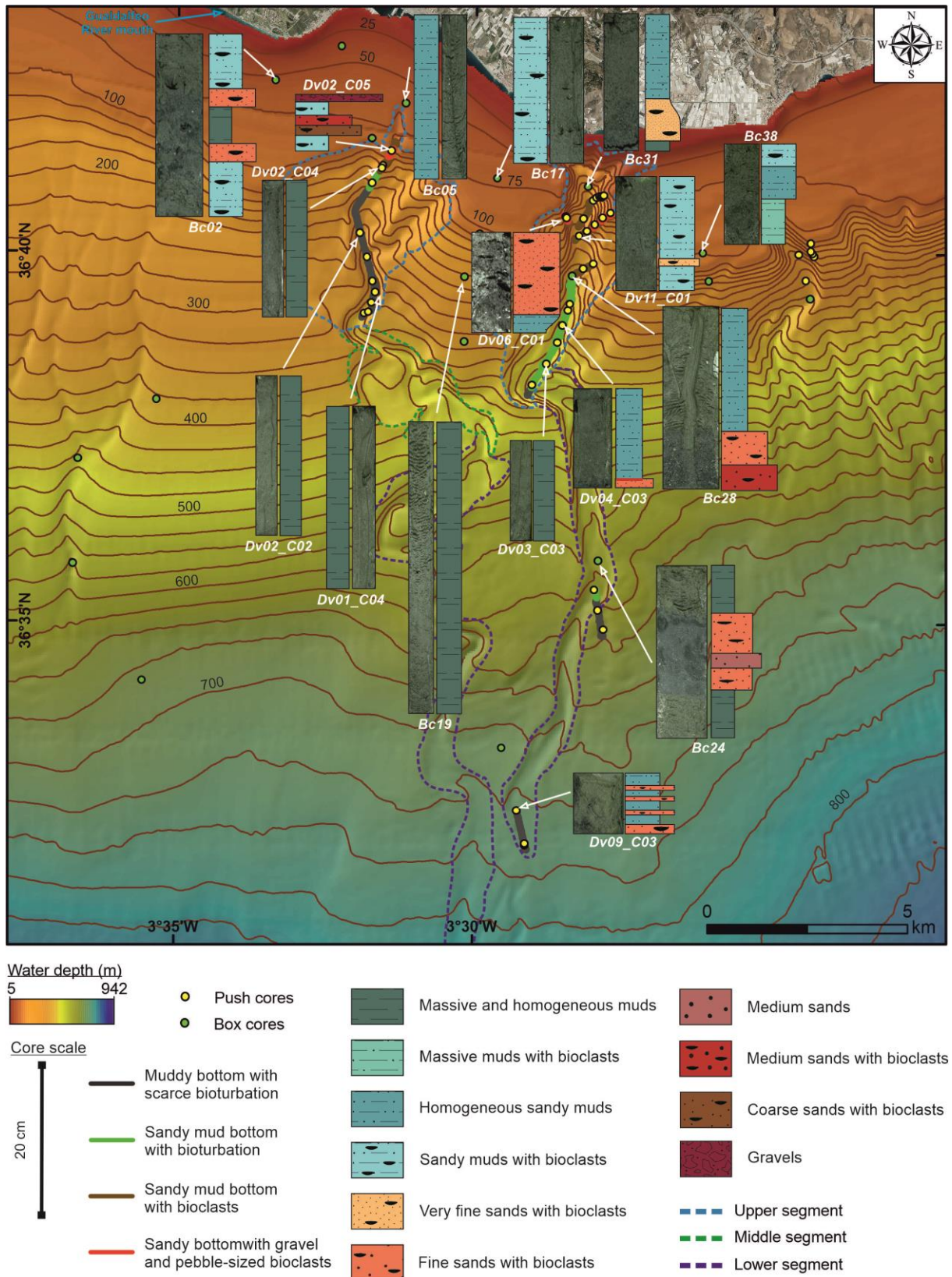


Figure 4.7. Sedimentary logs of main short sediment cores (collected with push and box corers) along the studied canyons, the intercanyon area, and the shelf around the study area. The segment distribution within each canyon and surficial sedimentary facies along ROV dives are also indicated. Bathymetric contours in meters.

4.1.3.2. Mass accumulation rates

The highest mass accumulation rate measured in the study area resides in the axial channel of the Motril Canyon (312 m water depth; Figure 4.8A and B; Table 4.1): an average value of $15.21 \text{ kg} \cdot \text{m}^{-2} \cdot \text{yr}^{-1}$, where the sedimentation rate is $1.45 \text{ cm} \cdot \text{yr}^{-1}$. In contrast, the lowest mass accumulation rate ($5.40 \text{ kg} \cdot \text{m}^{-2} \cdot \text{yr}^{-1}$) occurs in the axial channel of the Carchuna canyon (370 m water depth; Figure 4.8A and C; Table 4.1), at a sedimentation rate of $0.49 \text{ cm} \cdot \text{yr}^{-1}$. The intercanyon area (230 m water depth; Figure 4.8A and D) can be characterized by a mass accumulation rate of $11.13 \text{ kg} \cdot \text{m}^{-2} \cdot \text{yr}^{-1}$ and a sedimentation rate of $0.96 \text{ cm} \cdot \text{yr}^{-1}$.

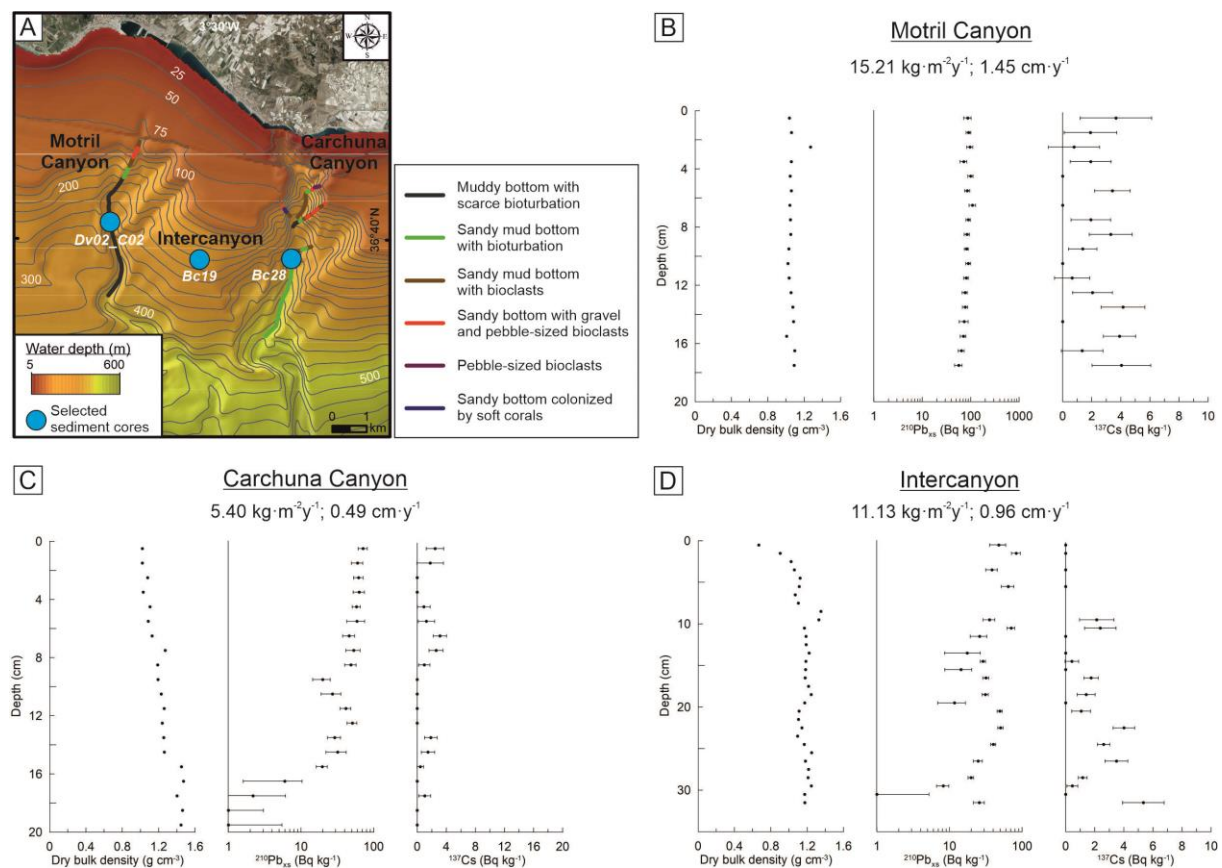


Figure 4.8. Dry bulk density and ^{210}Pb and ^{137}Cs activities in three short sediment cores located in the study area (A): Motril Canyon (B), Carchuna Canyon (C) and intercanyon site (D).

4.1.3.3. Surficial foraminifera

The percentage of benthic foraminifera in the shallowest part of the upper segment of the Motril Canyon ranges from 61% to 70%. These values decrease downcanyon, to 59% in the upper segment axial channel (Figure 4.9). Meanwhile, planktonic foraminifera increase

significantly downcanyon from 13% to 28% along the axial channel (Figure 4.9). The values of foraminiferal fragments are constant (~12%) along the upper segment of the Motril Canyon (Figure 4.9). There is a sharp downslope decrease in the number of reworked foraminifera — from 14% to 0% — in the upper segment (Figure 4.9; Table 4.1).

In the Carchuna Canyon, benthic foraminiferal content increases downcanyon in the upper segment, from 66% to 72%. However, they become less frequent in the lower segment (31%) (Figure 4.9). Planktonic foraminifera are constant throughout the upper segment (~20%) and increase toward the lower segment (62%). The values of foraminiferal fragments decrease downcanyon in both the upper and lower segments — from 9% to 6% and from 5% to 4%, respectively (Figure 4.9). The values of reworked foraminifera decrease downcanyon from 3% in the canyon head to 1% in the deeper sector of the upper segment. In the lower segment, the values remain constant, ~3% (Figure 4.9; Table 4.1).

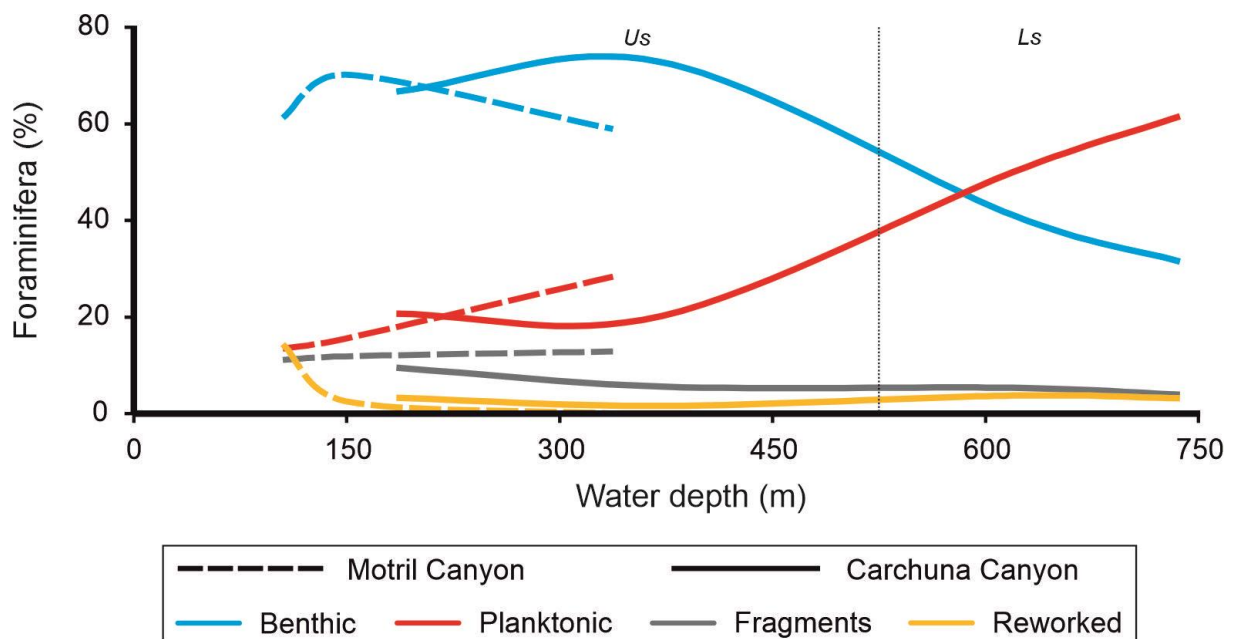


Figure 4.9. (A) Percentage of benthic and planktonic foraminifera along the upper segment of the Motril Canyon (dashed lines) and Carchuna Canyon (continuous lines) showing fragments and reworked foraminifera. The black dotted line marks the boundary between the upper (Us) and the lower segments (Ls) of the Carchuna Canyon.

The lower segment of the Carchuna Canyon has the highest values of transported shelf taxa, which include *Elphidium crispum*, *Ammonia beccarii*, *Elphidium complanatum*, *Quinqueloculina berthelotiana*, *Quinqueloculina pseudobuchiana*, *Elphidium advenum*,

Pseudotriloculina limbata, *Neoconorbina terquemi* and *Asterigerinata* spp. (Murray, 1991, 2006; Pérez-Asensio and Aguirre, 2010) (Table 4.3). The flanks of the upper segment exhibit lower values of transported shelf taxa. In turn, the percentage of planktonic foraminifera (%P) exhibits higher percentages in the lower segment (54.3% and 72.3%) than in the upper segment (6.7% and 37%) (Tables 4.1 and 4.3).

Table 4.3.

Benthic foraminiferal assemblages of the studied ROV samples located in the Carchuna Canyon showing the percentage of each species (numbers in brackets) and transported shelf taxa in bold. The total percentage of transported shelf taxa, the percentage of planktonic foraminifera (%P), and the sampling water depth for each sample are also indicated. See Fig. 1D for location of the surficial samples.

| S01 | S02 | S03 | S04 |
|---|--|--|--|
| <i>Lobatula lobatula</i> (34.8) | <i>Elphidium crispum</i> (11.2) | <i>Elphidium crispum</i> (18.8) | <i>Lobatula lobatula</i> (11.2) |
| <i>Cibicides refulgens</i> (16.3) | <i>Cassidulina laevigata</i> (10.6) | <i>Quinqueloculina seminulum</i> (13.1) | <i>Cibicides refulgens</i> (10.3) |
| <i>Elphidium complanatum</i> (15.7) | <i>Quinqueloculina seminulum</i> (7.1) | <i>Quinqueloculina berthelotiana</i> (5.4) | <i>Cassidulina laevigata</i> (10.0) |
| <i>Elphidium crispum</i> (4.4) | <i>Ammonia beccarii</i> (6.1) | <i>Ammonia beccarii</i> (5.1) | <i>Elphidium complanatum</i> (10.0) |
| <i>Cibicides</i> spp. (3.1) | <i>Elphidium complanatum</i> (6.1) | <i>Hyalinea balthica</i> (5.1) | <i>Elphidium crispum</i> (5.9) |
| <i>Ammonia beccarii</i> (2.2) | <i>Quinqueloculina berthelotiana</i> (5.4) | <i>Cibicidoides mundulus</i> (4.8) | <i>Quinqueloculina seminulum</i> (5.6) |
| <i>Quinqueloculina seminulum</i> (1.9) | <i>Cibicides refulgens</i> (5.1) | <i>Quinqueloculina pseudobuchiana</i> (4.8) | <i>Uvigerina peregrina</i> (5.0) |
| <i>Lachlanella</i> spp. (1.6) | <i>Lobatula lobatula</i> (4.5) | <i>Cassidulina laevigata</i> (4.1) | <i>Nonion faba</i> (4.4) |
| <i>Quinqueloculina berthelotiana</i> (1.6) | <i>Bolivina spathulata</i> (3.8) | <i>Melonis affinis</i> (2.9) | <i>Quinqueloculina berthelotiana</i> (3.7) |
| | <i>Quinqueloculina</i> spp. (3.5) | <i>Uvigerina peregrina</i> (2.9) | <i>Trifarina angulosa</i> (3.4) |
| | <i>Elphidium advenum</i> (3.2) | <i>Bulimina marginata</i> (2.5) | <i>Ammonia beccarii</i> (2.8) |
| | <i>Bulimina gibba</i> (2.2) | <i>Cibicides refulgens</i> (2.5) | <i>Bulimina elongata</i> (2.8) |
| | <i>Cibicidoides mundulus</i> (1.9) | <i>Elphidium complanatum</i> (2.5) | <i>Bolivina spathulata</i> (2.5) |
| | <i>Hyalinea balthica</i> (1.9) | <i>Lobatula lobatula</i> (2.2) | <i>Spiroplectinella wrighti</i> (2.2) |
| | <i>Melonis affinis</i> (1.9) | <i>Pseudotriloculina limbata</i> (2.2) | <i>Asterigerinata mamilla</i> (1.9) |
| | <i>Neoconorbina terquemi</i> (1.9) | <i>Hoeglundina elegans</i> (1.9) | |
| | <i>Triloculina tricarinata</i> (1.6) | <i>Asterigerinata</i> spp. (1.6) | |
| | | <i>Cibicidoides wuellerstorfi</i> (1.6) | |
| | | <i>Triloculina tricarinata</i> (1.6) | |
| Total transported shelf taxa (%): 5.0 %P: 6.7 | Total transported shelf taxa (%): 48.7 %P: 54.3 | Total transported shelf taxa (%): 45.5 %P: 72.3 | Total transported shelf taxa (%): 39.3 %P: 37.0 |
| Sampling depth (m): 149 | Sampling depth (m): 741 | Sampling depth (m): 633 | Sampling depth (m): 261 |

4.2. Discussion

The first detailed mapping of the Motril and Carchuna canyons reveals substantial geomorphological and sedimentary differences between the two, despite their close proximity. We discuss the relationships between sedimentary processes and canyon morphology, in addition to the implications regarding recent canyon activity.

4.2.1. Relation between sedimentary processes and canyon morphology

4.2.1.1. Comparison with other shelf-incised canyons

The studied canyons show spatial patterns and dimensions that differ from the average population of Mediterranean canyons. The Motril and Carchuna canyons are slightly shorter, narrower, less incised, and less steep than Mediterranean canyons (Table 4.4). These differences point to a lower development of the studied canyons that may be linked to sediment discharges toward the coast and the capture of longshore sediment transport by the canyon heads (Bernhardt and Schwanghart, 2021) considering that the occurrence of shelf-incised Mediterranean canyons correlates with regionally averaged sediment discharge to the coast (Harris and Macmillan-Lawler, 2015). In the study area, the sediment discharged from the rivers is vastly smaller than Mediterranean canyons (Table 4.4). Modern canyon head connectivity with the coast has been proposed for the Carchuna Canyon, which likely captures littoral drift cells (Ortega-Sánchez et al., 2014). In the case of the Motril Canyon, its head incised in the shelf could eventually constitute a limited collector of south-eastward derived sediment plumes emanating from the Guadalfeo River mouth (Lobo et al., 2006; Bárcenas et al., 2011).

Table 4.4.
Differences in the spatial patterns and dimensions between the studied canyons and the Mediterranean canyons.

| Characteristics | Motril and Carchuna canyons | Mediterranean canyons |
|----------------------|---|--|
| Length | 27 and 20 km | ca. 30 km (Harris et al., 2014) |
| Width | 4.6 and 4 km | ca. 8 km (Harris and Macmillan-Lawler, 2015) |
| Incision | 792 and 741 m | ca. 1100 m (Harris et al., 2014) |
| Slope gradient | ca. 2.3° | ca. 6.5° (Harris and Whiteway, 2011) |
| Rivers associated | Guadalfeo River, ca. 24 m ³ ·s ⁻¹ (Bárcenas et al., 2015) | Gulf of Lion, ca. 2000 m ³ ·s ⁻¹ (e.g., Palanques et al., 2012); Catalan Coast, ca. 400 m ³ ·s ⁻¹ (e.g., Tubau et al., 2015) |
| Channel levee length | ca. 11 km | Alboran canyons, ca. 4 km e.g., Ercilla et al., 2019; Rest of canyons, >15 km (e.g., Gamberi et al., 2013) |

In addition, shelf-sourced canyons have a range of sedimentary features and processes that reflect downslope changes in canyon geometry, signaling a transition from proximal erosive to distal depositional settings (e.g., Lastras et al., 2009; Brothers et al., 2013). The studied canyons generally meet these observations, both exhibiting proximal incisions flanked by tributary channels and gullies. Distally, the lower segments of both canyons show U-shaped axial channels with lateral levees and superimposed bedforms, as evidenced in other Mediterranean canyons (e.g., Cap de Creus Canyon, Lastras et al., 2007; Neto-Lipuda Canyon, Rebesco et al., 2009). The depositional features of the Motril and Carchuna canyons are similar to those of other shelf-incised canyons systems around the Alboran Sea (e.g., the Guadiaro Canyon, Alonso and Ercilla, 2002a), but their channel-levee systems are longer than other Alboran Sea canyons and shorter than other Mediterranean canyons (Table 4.4). Shorter channel-levee systems in the Mediterranean Sea can be attributed either to the absence of connection between canyon heads and river mouths, or to the presence of short rivers near canyon heads that mainly supply coarse-grained sediment; this appears to be the case along the northern Alboran Sea and the Catalan Coast.

Despite general similarities, the Motril and Carchuna canyons also exhibit distinctive features not often found in canyon populations. One outstanding trait is the occurrence of straight segments of variable orientations, which is generally associated with fault control on canyon geometry (e.g., Popescu et al., 2004; García et al., 2006; Gaudin et al., 2006). The Motril and Carchuna canyons share an abrupt change (ca. 90°) in the orientation of the axial channel in the upper segment termination (Figure 4.1). This most likely indicates tectonic control in the WNW-ESE orientation of the Motril and Carchuna axial channels, due to a normal fault that crosses both sectors (Figure 2.1B) (Comas et al., 1999; Pérez-Belzuz, 1999; Rodríguez et al., 2017) that may also condition the variations observed in canyon relief, incision, and area (Figure 4.3), suggesting that erosional and/or depositional processes are enhanced in segment transitions. The termination of the segments, related to abrupt orientation changes of the axial channels, would favor the deposition of muddy sediments and wider canyon sections as observed in both canyons (Figures 4.3, 4.4, 4.5, and 4.7). In the segment of the axial channel having WNW-ESE orientation, associated with tectonic control (Figure 1B), the values of canyon relief and incision are high (Figure 4.3B, C, E, and F), suggesting a dominance of erosional processes along both canyons. The abrupt change of the axial channel from WNW-ESE to N-S in both canyons accompanies canyon widening (Figure 4.3C and F) and subsequent sediment deposition in the lateral levees (Figure 4.1A).

Overall, shelf-incised canyons tend to exhibit downslope increases in canyon width (e.g., Chiang and Yu, 2006; Lastras et al., 2007, 2009; Gamboa et al., 2012; Wiles et al., 2019), while canyon relief decreases downcanyon (e.g., Goff, 2001; Baztan et al., 2005; Green et al., 2007; Puga-Bernabéu et al., 2013; Micallef et al., 2014; Wiles et al., 2019). Such general trends are attributed to the dominance of erosional processes upslope, including retrogressive failures (Goff, 2001; Green et al., 2007; Li et al., 2021; Li et al., 2023). In other cases, heightened downcanyon relief may result from greater erosion or the convergence of abundant canyon tributaries (Goff, 2001). Although the relief, width, incision, and cross-section area values of the Motril and Carchuna canyons are concordant among themselves and decrease downcanyon (Figure 4.3), the variation of one parameter with respect to the others may evidence erosive or depositional sectors controlled by local factors. Specifically, abrupt orientation changes of the axial channel in both submarine canyons condition variations in canyon relief, incision, and area along their traces. Noteworthy on the one hand are the shelf incision of the Carchuna Canyon and its proximity to the coast, showing a high width value at 120 m water depth (Figure 4.3F). In turn, the Motril Canyon exhibits low relief (Figure 4.3B) and high width at 350 m water depth in the upper segment (Figure 4.3C), suggesting a depositional area; and high relief (Figure 4.3B) and low width and incision (Figure 4.3C) at 500 m water depth, in coincidence with an abrupt change of the axial channel, in the middle to lower segment transition.

4.2.1.2. Geomorphological differences between Motril and Carchuna canyons

In spite of their close proximity and the fact that they share some common geomorphological attributes, the Motril and Carchuna canyons also exhibit striking differences that could hold implications for the distinct dominance of sedimentary processes in each canyon setting.

The shapes of longitudinal depth profiles along submarine canyons provide information about the balance between sediment supply and transport (Gerber et al., 2009; Covault et al., 2011). A concave thalweg downslope profile is interpreted to signal the modification of the original slope shape by erosional processes in the canyon head and the deposit of transported material at the termination of the channel (Mitchell, 2005; Gerber et al., 2009; Kertznus and Kneller, 2009; Covault et al., 2011; Amblas et al., 2012). Very concave profiles are linked to canyons that are relatively steep in their proximal reaches having coarse-grained sediments and being incised in narrow shelves (Covault et al., 2011). In contrast, the slightly concave shape of

submarine canyons is associated with fine-grained sediments and wide, mature passive continental margins (Covault et al., 2011). Although the Motril and Carchuna canyons are located in a narrow margin nearby high topography hinterlands, they exhibit different grades of concave longitudinal profiles, hence indicative of different equilibrium states (Figure 4.3). In addition, the longitudinal profile of the Motril Canyon is also slightly divergent from concave profiles of other canyons (Covault et al., 2011) (Figure 4.10). Thus, the tectonic setting or the individual physiographic parameters of each canyon do not suffice to explain the evolution of the submarine canyon; several factors intervene, meaning a detailed study is needed.

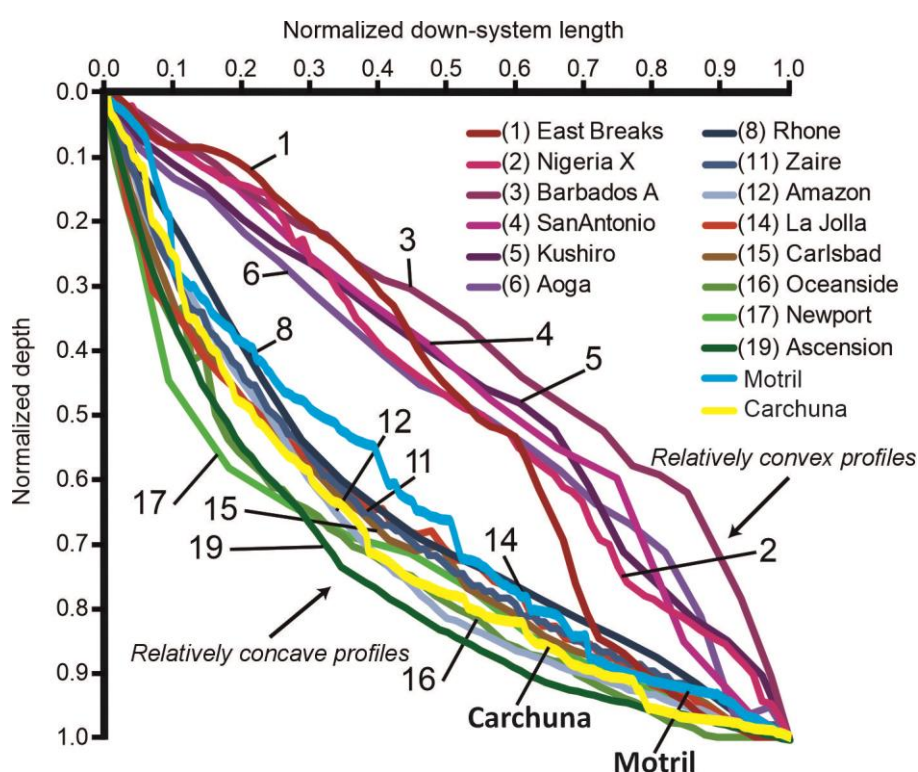


Figure 4.10. Canyon longitudinal profiles normalized on the basis of profile lengths (from canyon head to the end of the confined portion of the system) of nineteen submarine canyons and the two studied canyons (after Covault et al., 2011).

The very concave shape and occurrence of sandy muds along the Carchuna Canyon axial channel (Figures 4.3, 4.5, and 4.7) point to a continuous supply of sandy sediments, regardless of the sea-level stand (Covault et al., 2011). Such profiles are indicative of significant bypass of the canyon head as it distally feeds downslope turbidity currents (Gerber et al., 2009). The Carchuna Canyon furthermore shows conspicuous evidence of erosional activity (Lastras et

al., 2011a), such as higher incision depths and the occurrence of knickpoints (Figure 4.3). In contrast, the dominance of muddy sediments along the axial channel of the Motril Canyon (Figures 4.4 and 4.7), and the sigmoidal shape of the intercanyon area (Figure 4.3A) could be attributed to an excess of sediment supplied by the Guadalfeo River mouth in the upper reaches of the Motril Canyon and shelf, as evidenced elsewhere, where submarine canyons may serve as mud traps collecting sediments exchanged between river mouths and offshore (e.g., Prins et al., 2000; Liu et al., 2002; Walsh and Nittrouer, 2003; Hill et al., 2009; Clift et al., 2014; Warrick, 2014). In fact, upper slope sigmoidal profiles have been linked to sediment supply exceeding the capacity of subaqueous currents to transport sediments downslope (e.g., Gerber et al., 2009; Amblas et al., 2012; Puga-Bernabéu et al., 2013; Soutter et al., 2021). Differences between the recent erosional/depositional behavior of the two canyons studied are also seen in the canyon relief values (Figure 4.3): low for the Motril Canyon, likely due to a more recent depositional setting; high for the Carchuna Canyon, indicating significant erosional processes.

The two canyons exhibit different sinuosity values as well (Table 4.2). The Motril Canyon shows a meandering path downslope and distal axial channel narrowing (Figure 4.1), an overall pattern accompanied by a low gradient (Figure 4.3) and mantling with fine-grained sediments (Figure 4.4). In contrast, the Carchuna Canyon is straighter, steeper and floored by coarser sediments (Figures 4.1, 4.3, and 4.5). Yet both overlie similar features of the gradient slope. Therefore, the sinuosity differences point to different phases of maturity (Clark et al., 1992; Kane et al., 2008; Babonneau et al., 2010; Janocko et al., 2013; Wiles et al., 2019), even if both studied canyons exhibit contrasting recent activities, as it will be discussed in the following section.

The greater sinuosity of the Motril Canyon would indicate a more mature state, an interpretation supported by the wide terraces along the upper and middle segments (Figure 4.1) indicative of lateral canyon migrations (Clark et al., 1992, Mayall et al., 2006; Arzola et al., 2008) and interpreted as generated through progressive erosion, channel migration, and meander development, as documented in other canyon systems (e.g., Babonneau et al., 2010; Hubbard et al., 2014; Jobe et al., 2015). At some sites the terraces dip away from the axial channel (Figure 4.3A), a morphological configuration indicative of sediment aggradation in the boundary of the channel by sediment overflows (Babonneau et al., 2004). In addition, the dominance of fine-grained sediments that mantle the axial channel is also related to low gradient, highly sinuous canyons (e.g., Abreu et al., 2003). In line with this interpretation, the

less sinuous, steeper, and coarser-grained Carchuna Canyon would be related to a youthful development, possibly associated with the erosive behavior of coarse-grained turbidity currents (Clark et al., 1992; Clark and Pickering, 1996). In addition, its narrow, elongated terraces at various depths (Figure 4.1) may evidence multiple axial incisions (Baztan et al., 2005; Arzola et al., 2008; Micallef et al., 2014), or even recent canyon excavation (Tubau et al., 2013).

Finally, another distinctive or contrasting feature is that the two canyons have very different canyon heads, in terms of morphology and sediment composition. Canyon heads contribute to the erosion and deepening of upper canyons that bypass the slope via canyon valleys, reshaping canyon walls through widening and shelf incision and increasing material delivery into the axial channel (Pratson and Coackley, 1996; Popescu et al., 2004; Puga-Bernabéu et al., 2011; Micallef et al., 2014; Li et al., 2021; Li et al., 2023). The deep shelf incision of the Carchuna Canyon can be attributed to canyon head widening along the shelf edge, and penetration farther into the shelf towards the coastline over time. Headward erosion is also evidenced by the high values of canyon relief (vs intercanyon depth) upslope from the shelf edge (Figure 4.3E), indicating retrogression of the canyon head (Green et al., 2007). The strong entrenchment of the thalweg of the Carchuna Canyon head limits its lateral migration, impeding the creation of terraces, while producing the erosion of the walls and terraces, as evidenced by the occurrence of gullies and steep flanks (Figures 4.1 and 4.2). Besides, the abundance of bioclasts and coarse-grained sizes are compatible with widespread sediment failures distally evolving into turbidity flows. Indeed, the V-shaped canyon head is characteristic of turbidity-flow dominated canyons (Babonneau et al., 2004; Rebesco et al., 2009; Li et al., 2021; Li et al., 2023).

In marked contrast, in the Motril Canyon, the high values of canyon relief (vs intercanyon depth) are recorded downcanyon of the shelf edge (Figure 4.3B), meaning that the canyon head widened mostly along the shelf edge over time (Green et al., 2007). The lack of entrenchment of the thalweg is evidenced by the cross-profiles that exhibit U shapes in the upper reaches of the canyon (Figure 4.3A), and the finer-grained sediment composition. Therefore, the above would indicate minor mass movements from the canyon head to the axial channel (Babonneau et al., 2004; Rebesco et al., 2009), and only partial mantling by hemipelagic deposition.

4.2.2. Implications for canyon activity

Many canyons presently active, and capable of maintaining their levels of activity during sea-level highstands, do not directly depend on sediment input from a river or river mouth (e.g., the Cap de Creus Canyon, Canals et al., 2006; the Monterey Canyon, Xu et al., 2008; Heijnen et al., 2022). In fact, the volume of sediment deposited in shallow water that might be captured by canyons relies on two factors (Mullenbach and Nittrouer, 2000; Puig et al., 2014, 2017; Sweet and Blum, 2016): the degree of canyon shelf incision and the location of the canyon head with respect to the main sedimentary source (Herzer and Lewis, 1979; Mullenbach et al., 2004; Green, 2009; Bernhardt et al., 2015; Bernhardt and Schwanghart, 2021).

The distance between the canyon head and the shoreline strongly conditions sediment transport. Shelf-incised canyons are able to capture either transported shelf sediments, water masses potentially transporting sediments, or deep-sea currents (e.g., Canals et al., 2006; Marchès et al., 2007; Xu et al., 2008). Shelf-incised canyons can additionally be distinguished according to the principal sedimentary source supplying the canyon heads: longshore-drift-fed systems, river-fed systems, or delta-fed systems (Sweet and Blum, 2016). The fact that the Motril and Carchuna canyons exhibit significant geomorphological and sedimentary differences suggests they played distinct roles in recent patterns of sediment transport and accumulation, hence displaying diverse degrees of canyon shelf incision. The Motril Canyon head lies ca. 2 km from the coastline and close to the Guadalfeo River mouth; whereas the Carchuna Canyon head is 200 m offshore and cuts infralittoral prograding wedges (Figures 4.1 and 4.2).

Although the Motril Canyon exhibits a mature state, there are strong indications that at present the Motril Canyon accumulates sediment along the axial channel and acts as a sediment trap. The dominance of muddy sediments (Figures 4.4 and 4.7) and high values of organic matter (Figure 4.6A) point to fine sediment settling with low sediment remobilization in submarine canyons (Cronin et al., 2005; Oliveira et al., 2007) where the heads are remote to the shoreline and show low activity (Harris and Whiteway, 2001; Sweet and Blum, 2016; Mascle et al., 2015). The lack of sediment transport through the Motril Canyon axial channel is further supported by a lack of shelf benthic foraminifera transported along the channel (Figure 4.9). In addition, sedimentation and mass accumulation rates ($1.45 \text{ cm}\cdot\text{yr}^{-1}$ and $15.21 \text{ kg}\cdot\text{m}^{-2}\text{yr}^{-1}$; Figure 4.8B) are higher than in other western Mediterranean submarine canyons, where accumulation rates do not exceed $0.47 \text{ cm}\cdot\text{yr}^{-1}$ (Miralles et al., 2005; Martín et al.,

2008; Puig et al., 2008; Zúñiga et al., 2009). Low densities of marine litter buried and scattered along the Motril Canyon also agrees with its recent behavior as a sediment sink (Cerrillo-Escoriza et al., 2023).

Contrariwise, the Carchuna Canyon is envisaged as an active system whose canyon head is able to capture littoral cell sediments, eventually leading to sediment transport along the axial channel toward the channel termination owing to turbidity flows. Longshore sheltering and wave focusing in canyon heads are known to lead to increased shear stress that can mobilize coarse-grained sediments (Smith et al., 2018). This interpretation is supported by several lines of evidence. In the upper segment, the bedforms superposed over the tributary channels located in the eastern flank and the axial channel of the Carchuna Canyon head (Figures 4.1B and 4.2) evidence downcanyon sediment transport from the tributary channels to the axial channel, and from the axial channel of the canyon head to the downcanyon. In addition, active canyon heads tend to be located in the vicinity of shorelines, and are mantled by coarse-grained sediments (e.g., Lewis and Barnes, 1999; Mullenbach and Nittrouer, 2000; Normandeau et al., 2015; Sweet and Blum, 2016). In the Carchuna Canyon, the coarse composition of surficial sediments located in the axial channel (Figures 4.5 and 4.7), the lower mass sediment accumulation rates in comparison with the Motril Canyon and the intercanyon area (Figure 4.8), and the high values of organic matter found in the termination of the upper segment (Figure 4.6A), are indicative of transport by turbidity flows, as in other canyons (e.g., Biscara et al., 2011). Further support of the occurrence of deep transport by turbidity flows along the Carchuna Canyon is provided by the accumulations of marine litter in the upper segment, in turn favored by the irregular morphology dictated by rocky seafloor areas and smooth depressions along the thalweg (Cerrillo-Escoriza et al., 2023).

Within the lower segment of the Carchuna Canyon, the coarser surficial sediment samples (Figure 4.5) and the high values of organic matter (Figure 4.6A) found along the axial channel suggest sediment transport, whereas the sediment waves superimposed over the eastern levee (Figure 4.12) signal overflow. Similar values for carbonate contents along the Carchuna Canyon (Figure 4.6B) support that the sediment along the axial channel is uniform and predominantly terrigenous, without significant variations due to shelf bioclastic or pelagic contributions (Puga-Bernabéu et al., 2011). Coarse-grained sediment transport most likely reached the distal termination of the channel, as evidenced by the occurrence of sub-surface interbedded sands (Figure 4.7), high values of organic matter (Figure 4.6A), and high values

of transported shelf benthic foraminifera (Table 4.4); all these evidences are indicative of transported material (Schmiedl et al., 2000; Bolliet et al., 2014; Duros et al., 2014).

The differences in sediment trapping and downcanyon transport efficiency highlighted above can be explained by the physiographic configuration of each canyon, plus their interaction with wind-driven regional oceanographic conditions. Two basic situations are envisaged, given the seasonal alternance of wind regimes. Under westerlies dominance, shelf currents trend towards the E-SE (Bárcenas et al., 2011; Figure 4.11A), when the Motril Canyon head can capture laterally redistributed fine-grained sediments supplied by the Guadalfeo River (Figure 4.11A and C). In the Carchuna Canyon head, energetic western waves mainly influence the eastern flank (Ortega-Sánchez et al., 2014); this process is reflected in the submarine geomorphology of the head, as the eastern flank shows widespread erosional features. Enhanced erosion of the eastern flank may resuspend sediments by the canyon head, ultimately favoring the formation of sediment transport pulses driven by downcanyon bottom flows, as described in the bottom layer (Serrano et al., 2020; Figure 4.11C).

Canyon activity would be more limited under easterlies dominance. For one, sediment erosion and remobilization would have been reduced in the Carchuna canyon head, as eastern waves are less energetic (Ortega-Sánchez et al., 2014). Yet canyon activity cannot be discarded during such conditions: W-NW directed shelf currents exhibit velocities above $0.1 \text{ m}\cdot\text{s}^{-1}$ (Bárcenas et al., 2011; Figure 4.11B), conditions that could trigger the input of moderate amounts of sediments in the canyon, subsequently redistributed downslope by downwelling flows, likewise active during easterlies dominance (Serrano et al., 2020; Figure 4.11D). In contrast, the Motril Canyon would essentially be inactive under easterlies dominance, because of the trapping effect of the Carchuna Canyon —impeding westward-directed sediment flows— and the minor influence of Guadalfeo River inputs.

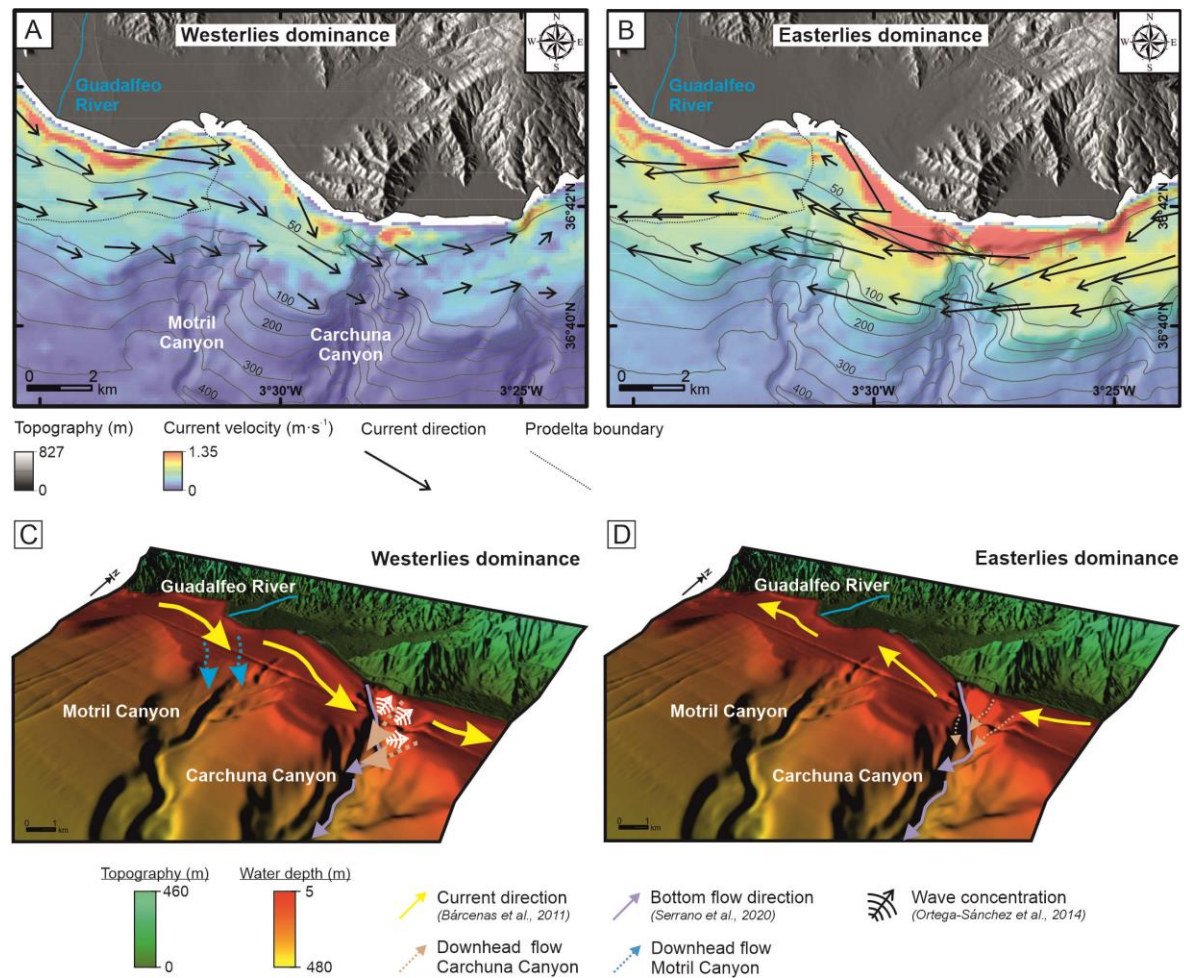


Figure 4.11. Mapping of direction and depth-averaged current speed ($\text{m}\cdot\text{s}^{-1}$) under westerlies dominance (A) and easterlies dominance (B) (modified from Bárcenas et al., 2011). The black dotted line indicates the prodelta boundary (extracted from Lobo et al., 2015). Bathymetric contours in meters. Model of recent sedimentary activity in the upper segments of the Motril and Carchuna canyons based on the current direction (Bárcenas et al., 2011), bottom flow direction (Serrano et al., 2020), and wave concentration in the Carchuna Canyon head (Ortega-Sánchez et al., 2014). Under westerlies dominance (C), the Motril Canyon head receives fine sediments supplied by the lateral redistribution of the Guadalfeo River input, whereas energetic western waves erode the eastern flank of the Carchuna Canyon head, feeding downcanyon sediment transport pulses. Under easterlies dominance (D), wave activity is reduced in the Carchuna Canyon head, although the canyon may intercept limited sediment transport by relatively intense shelf currents; in contrast, the Motril Canyon head remains essentially inactive.

4.3. Conclusions

Although the Motril and Carchuna canyons share morphologic features typical of Mediterranean canyons, they also exhibit a number of distinctive features. They have segments characterized by downslope variations of geomorphological parameters attributed to enhanced erosional/depositional processes and promoted by tectonically controlled abrupt changes of the axial channel orientation.

Significant geomorphological differences between the two studied canyons reflect different balances between canyon maturity and recent activity of sedimentary processes. The U-shaped Motril Canyon head suggests the imprint of minor mass movements in the canyon head that jointly with the greater sinuosity, the occurrence of wide terraces, the low slope gradients, and the slightly concave shape point to a relatively mature system. In contrast, the steeper Carchuna Canyon with the deep V-shaped incision of the canyon head, the less sinuosity, the coarser-grained sediments along the axial channel, and the narrow and elongated terraces would be related to a youthful canyon development.

The degree of shelf incision, the location of the Motril and Carchuna canyon heads in relation with the local sediment sources, and the seasonally variable hydrodynamic regimes determine the amount of sediment potentially captured by both canyons and hence, the recent sedimentary activity. In the recent past, the Motril Canyon has mainly acted as a sediment trap accumulating hemipelagic sediments, where the distant location of the canyon head from the coastline (ca. 2 km) favors fine-grained sediment accumulation from the major regional fluvial source, mainly under wind-driven westerlies dominance. In contrast, the proximity of the Carchuna Canyon to the coastline (<200 m) favors littoral cell sediment trapping, under both wind-driven westerlies and easterlies dominance, downslope coarse-grained sediment transport and continuous thalweg erosion driven by turbidity flows along the axial channel toward the channel termination.

Chapter 5

Bedform development in confined and unconfined settings of the Carchuna Canyon: An example of cyclic steps in shelf-incised canyons

This chapter is entitled as Bedform development in confined and unconfined settings of the Carchuna Canyon (Alboran Sea, western Mediterranean Sea): An example of cyclic steps in shelf-incised canyons, in *Marine Geology*. Received 2 December 2023. Under review.

^{1,2*}Cerrillo-Escoriza, J., ³Micallef, A., ¹Lobo, F.J., ²Puga-Bernabéu, Á., ⁴Bárcenas, P., ^{5,6}Schulten, I., ⁷Durán, R., ^{1,2}Carrión-Torrente, Á., ²López-Quirós, A., ⁸Luján, M., ⁴Sánchez-Guillamón, O. ⁹Sánchez, M.J

¹Department of Marine Geosciences, Instituto Andaluz de Ciencias de la Tierra (CSIC-UGR), Armilla, Granada Spain, ²Departamento de Estratigrafía y Paleontología, Facultad de Ciencias, Universidad de Granada, Granada, Spain, ³Monterey Bay Aquarium Research Institute, California, USA, ⁴Instituto Español de Oceanografía, Centro Oceanográfico de Málaga (IEO-CSIC), Fuengirola, Málaga, Spain, ⁵Marine Geology and Seafloor Surveying, Department of Geosciences, University of Malta, Msida, Malta, ⁶Department of Earth and Environmental Sciences, Dalhousie University, 1355 Oxford Street, B3H 4R2 Halifax, Nova Scotia, Canada, ⁷Institute of Marine Sciences (CSIC), Barcelona, Spain, ⁸Department of Earth Sciences, CASEM – Facultad de Ciencias del Mar y Ambientales, Universidad de Cádiz, Puerto Real, Spain, ⁹Instituto de Oceanografía y Cambio Global (IOCG), Universidad de Las Palmas de Gran Canaria, Las Palmas de Gran Canaria, Spain

Abstract

Newly acquired high-resolution multibeam bathymetry in combination with sub-bottom acoustic profiles, surficial sediment samples, and a three-dimensional flow simulation made possible the characterization of bedforms along the axial channel and depositional lobe of the shelf-incised Carchuna Canyon (Alboran Sea, western Mediterranean Sea). This chapter aims to describe the erosional and depositional bedforms in confined and unconfined settings of the Carchuna Canyon in order to determine the genetic constraints on sedimentary processes leading to bedform development along the canyon in recent times.

The straight Carchuna Canyon hosts crescentic-shaped bedforms (CSBs) that exhibit distinctive crest concavities, asymmetries, and lengths along the axial channel. The Carchuna Canyon features continuous lateral levees and a channel bend with three depressed stretches of the levee crest. A set of concentric sediment waves and two scour trails were identified proximal to the channel bend on the open slope east of the Carchuna Canyon. Two distinct acoustic groups consisting of four acoustic units with distinct acoustic patterns were defined along the sediment wave field. The sediment transport simulation shows the highest flow velocities along the Carchuna Canyon thalweg, while along the overbank deposition the highest velocity values occur along the top of the bedform crests, with the higher Froude values being found over the bedform lee sides.

The occurrence of CSBs suggests the imprint of confined sediment-laden gravity flows descending from the canyon head and exhibiting a flow variability along the canyon induced by local variations of slope gradient and/or sediment concentration. A spatial relationship is identified between the development of sediment waves over the overbank deposit and lowered levee crest heights at the channel bend. In contrast, more energetic downstream turbiditic flows would exceed the levee crest at the channel bend, focusing the overflow and promoting erosion of the overbank deposit, thereby generating the scour trains. Based on the recent history of overbank deposition, two alternating scenarios of flow behavior can be interpreted. In a high-density turbidity current setting, erosion would prevail along the axial channel. Widespread spillover flows of coarse-grained sediments would occur in both levees, forming heterogeneous sedimentary patterns that change downslope along the depositional lobe. In contrast, in a low-density turbidity current setting, turbidity currents flowing along the Carchuna Canyon would form depositional bedforms, while spillover processes would be localized at the channel bend, forming either depositional or erosional bedforms over the depositional lobe according to the frequency, magnitude and focusing of turbiditic flows.

5.1. Results

5.1.1. Geomorphology and sedimentology of the Carchuna Canyon

The Carchuna Canyon has a length of 20.3 km from the canyon head to the mouth and displays an axis with a sinuosity of 1.15. It has a maximum width of 4 km and a maximum relief of 226 m (Table 5.1; Figure 5.1). Its longitudinal profile is concave (Figure 5.2). Two geomorphological segments can be identified in the Carchuna Canyon (Figure 5.1). In the upper segment (30-500 m water depths), the canyon is deeply incised in the shelf (Figures 5.1 and 5.2B); its head, located just 200 m off the coastline, features a 100 m wide axial channel delimited by very steep flanks (68°). The canyon is straight in this segment, where the axial channel widens up to 300 m from 370 m to 430 m water depth and is limited by a narrow and steep eastern flank and large terraces on the western flank (Figure 5.3A). Sediments on the axial channel comprise very fine sands in the canyon head, changing downcanyon to coarse silts (Figure 5.1). The transition between the upper and lower segments is marked by an abrupt change in orientation of the main valley from NNE-SSW to WNW-ESE (Figure 5.1).

Table 5.1.
Morphological parameters of Carchuna Canyon crescentic-shaped bedforms.

| | | | | | | | | | | | | | | | |
|-----------------------------------|----------------------|----------------|------------|------------|-------------|-------------|------------|------------|------------|------------|------------|----------|-------------|-------------|--|
| Carchuna Canyon | Longitude (W) | 3° 28' 34.34" | | | | | | | | | | | | | |
| | Latitude (N) | 36° 41' 41.02" | | | | | | | | | | | | | |
| | Total length (m) | 19320 | | | | | | | | | | | | | |
| | Sinuosity | 1.15 | | | | | | | | | | | | | |
| | Maximum width (m) | 4020 | | | | | | | | | | | | | |
| | Maximum incision (m) | 226 | | | | | | | | | | | | | |
| Sets of CSBs of the upper segment | a | b | c | d | e | f | g | h | i | j | k | l | Total | a' | |
| Length of the set (m) | 310 | 510 | 510 | 410 | 490 | 590 | 540 | 600 | 570 | 730 | 530 | 720 | | 610 | |
| Number | 7 | 9 | 8 | 11 | 11 | 11 | 8 | 5 | 5 | 17 | 7 | 12 | 111 | 8 | |
| Wavelength (m) | 20 to 60 | 30 to 90 | 30 to 90 | 10 to 60 | 20 to 60 | 20 to 70 | 30 to 80 | 90 to 120 | 40 to 100 | 20 to 80 | 40 to 80 | 30 to 80 | 10 to 120 | 40 to 100 | |
| Amplitude (m) | 1 to 5 | 1 to 4 | 2 to 9 | 1 to 4 | 1 to 4 | 1 to 6 | 2 to 4 | 4 to 9 | 2 to 4 | 1 to 5 | 1 to 3 | 1 to 4 | 1 to 9 | 7 to 12 | |
| Lee side (°) | 5.2 to 10.4 | 4.1 to 7.3 | 5.1 to 8.8 | 4.2 to 8.5 | 3.2 to 11.3 | 2.5 to 10.2 | 4.7 to 8.8 | 6.1 to 8.8 | 2.7 to 5.3 | 3.4 to 6.4 | 2.7 to 7.1 | 3 to 6.5 | 2.5 to 11.3 | 9.6 to 13.8 | |
| Stoss side (°) | 1.2 to 3.9 | 1.7 to 4 | 3.8 to 5.9 | 2.5 to 4.5 | 0.5 to 4.4 | 0.8 to 4.2 | 0.6 to 3.3 | 0.3 to 4.1 | 0.4 to 1 | 0.9 to 4.5 | 0.7 to 1.7 | 0.2 to 3 | 0.2 to 5.9 | 4 to 9.5 | |
| Concavity mean | 0.37 | 0.61 | 0.64 | 0.43 | 0.68 | 0.62 | 0.29 | 0.64 | 0.57 | 0.43 | 0.75 | 0.25 | | 0.58 | |
| Gradient mean | 4.9 | 5.2 | 7.2 | 4.6 | 5 | 4.6 | 3.9 | 3.6 | 2.6 | 3.6 | 3.2 | 2.7 | | 9.5 | |
| Sets of CSBs of the lower segment | q | r | s | t | u | v | w | x | y | z | Total | | | | |
| Length of the set (m) | 1230 | 840 | 1340 | 780 | 960 | 490 | 760 | 510 | 890 | 430 | | | | | |
| Number | 17 | 12 | 14 | 11 | 12 | 7 | 10 | 4 | 4 | 5 | 96 | | | | |
| Wavelength (m) | 30 to 120 | 30 to 120 | 30 to 140 | 30 to 90 | 30 to 100 | 30 to 100 | 20 to 120 | 100 to 120 | 50 to 130 | 70 to 100 | 20 to 140 | | | | |
| Amplitude (m) | 1 to 4 | 1 to 3 | 1 to 5 | 1 to 2 | 1 to 3 | 1 to 2 | 1 to 3 | 1 to 3 | 1 to 5 | 1 | 1 to 5 | | | | |
| Lee side (°) | 3.2 to 8.4 | 2.5 to 5.7 | 2 to 6 | 2.1 to 4 | 3 to 4.6 | 2.4 to 4.2 | 2.8 to 7.5 | 3.4 to 5.6 | 3.2 to 7.5 | 3.4 to 4.2 | 2.1 to 8.4 | | | | |
| Stoss side (°) | 0.1 to 2.9 | 0.2 to 2.4 | 0.1 to 1.6 | 0.1 to 1.6 | 0.2 to 1.7 | 0.2 to 1.3 | 0.1 to 1.7 | 0.1 to 1.2 | 0.5 to 1.5 | 0.2 to 1 | 0.1 to 2.4 | | | | |
| Concavity mean | 0.50 | 0.67 | 0.53 | 0.40 | 0.86 | 0.60 | 0.86 | 0.70 | 0.44 | 0.96 | | | | | |
| Gradient mean | 2.9 | 2.6 | 2.1 | 1.7 | 2 | 2 | 3.1 | 2.3 | 2 | 2.1 | | | | | |

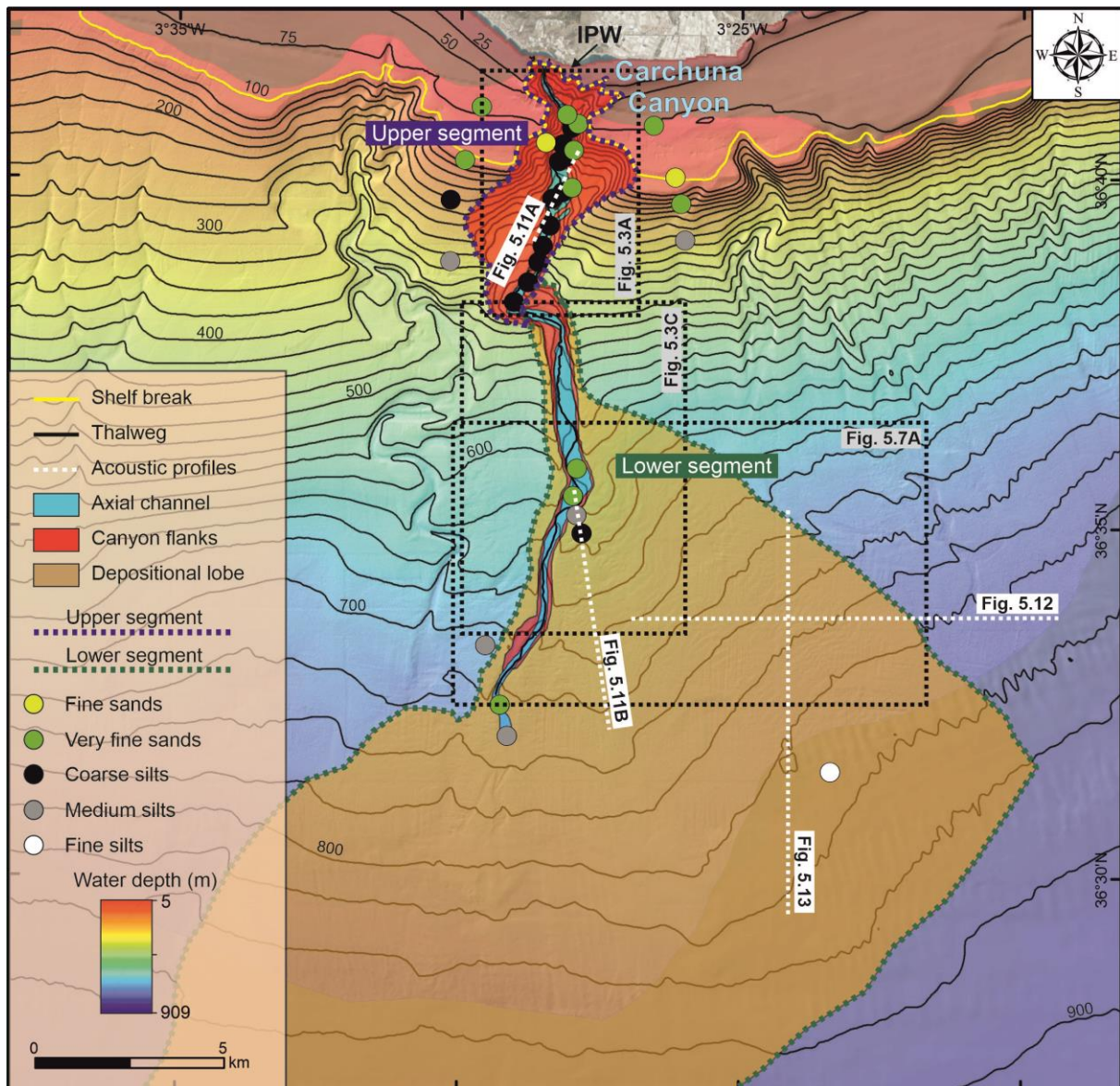


Figure 5.1. Geomorphological map of the Carchuna Canyon showing the segment distribution and the texture of surficial sediment samples. The location of interpreted acoustic profiles is also shown. Note the change in orientation of the valley in the transition from the upper to lower segment. IPW: Infralittoral Prograding Wedge. Bathymetric contours in meters

The lower segment (500-730 m water depths) is characterized by a straight and wide valley (up to 550 m wide) with a main N-S orientation, an axial channel bounded by steep walls (ca. 20°) and continuous lateral levees (Figures 5.1, 5.2B and 5.3B). The axial channel is straight but exhibits a bend at 620 m water depth that shifts from NNW-SSE to NNE-SSW orientation (Figures 5.1 and 5.4). Overall, the height between the eastern levee crest and the thalweg decreases from 90.6 m in the upper reaches of the lower segment (ca. 500 m water depth) to 3.5 m at the termination of the channel (ca. 730 m water depth) (Figure 5.4A). However, three

stretches (upper, middle and lower) along the channel bend between 585 and 645 m water depths in the levee crest exhibit levee heights below 20 m that are separated by heights up to 28 m (Figure 5.4B, C). Upslope of the channel bend, the levee height is 18.7 m between 591 to 600 m water depths (Figure 5.4B, C). The levee is 19.9 m high where the axial channel changes its orientation between 611 to 621 m water depths. This middle stretch is separated from the upper and lower stretches by 26-28 m high levees (Figure 5.4B, C). Downslope, the lower stretch of the channel bend between 631 to 642 m water depths exhibits a 17.6 m high levee (Figure 5.4B, C). The eastern levee evolves downslope to an overbank deposit having superimposed features that extend up to 900 m water depth, forming a depositional lobe (Figure 5.1). Sediments in the lower segment vary from very fine sands in the axial channel to fine silts in the depositional lobe (Figure 5.1).

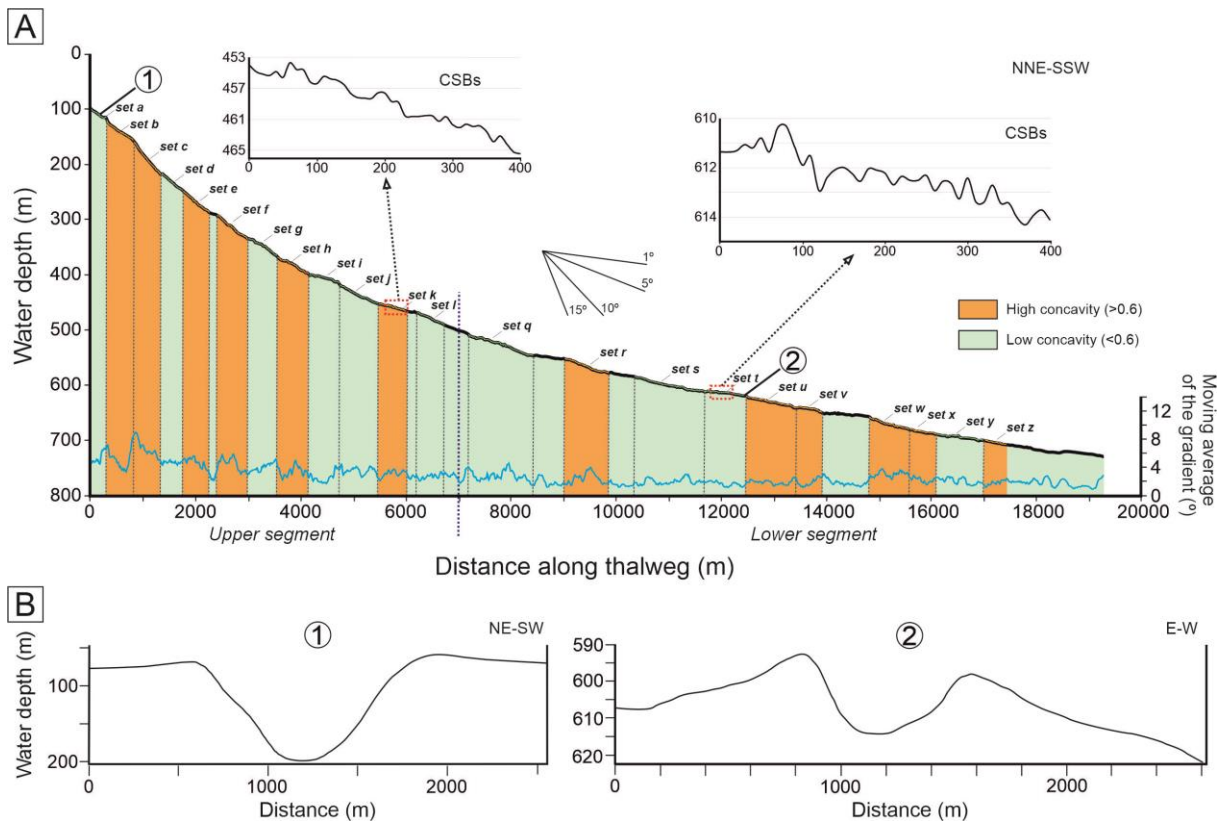


Figure 5.2. (A) Bathymetric longitudinal profile and moving average (10 points) of the Carchuna Canyon thalweg gradient with indication of each CSB set according to its concavity. Zoom-ins of two sectors located in the upper and lower segments are provided. (B) Transverse profiles showing the shelf incision of the Carchuna Canyon in the upper segment (1) and the lateral levees in the lower segment (2). Location of transverse profiles indicated in A. Note that the eastern levee exhibits lower values of height than the western levee, forming an asymmetric cross section.

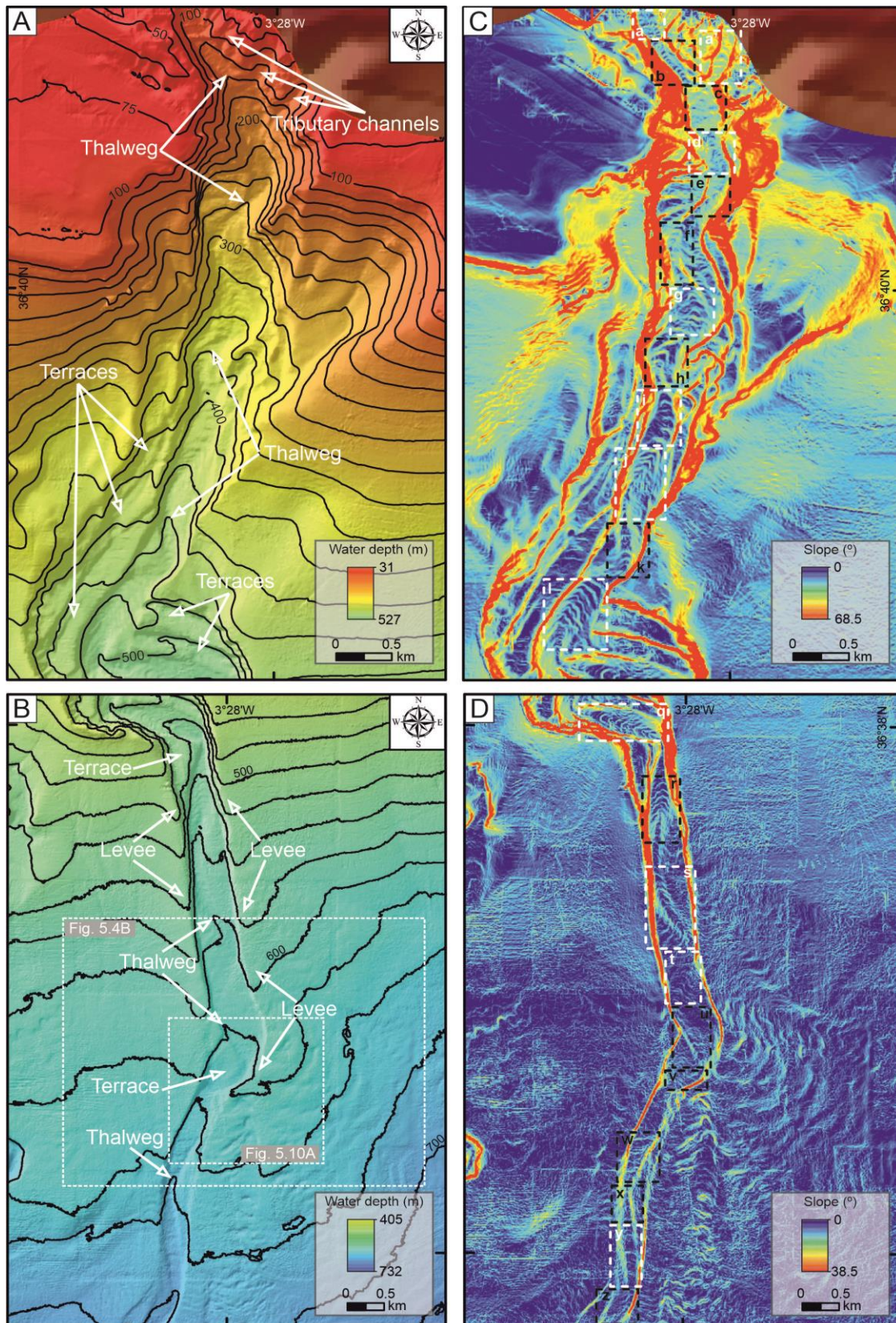


Figure 5.3. High-resolution bathymetric maps of the upper (A) and lower segments (B) in the Carchuna Canyon. Slope gradient maps of the upper (C) and lower segments (D) in the Carchuna Canyon show the location of CSB sets according to their concavity (white rectangle: low concavity; black rectangle: high concavity). Bathymetric contours in meters. Location shown in Figure 5.1.

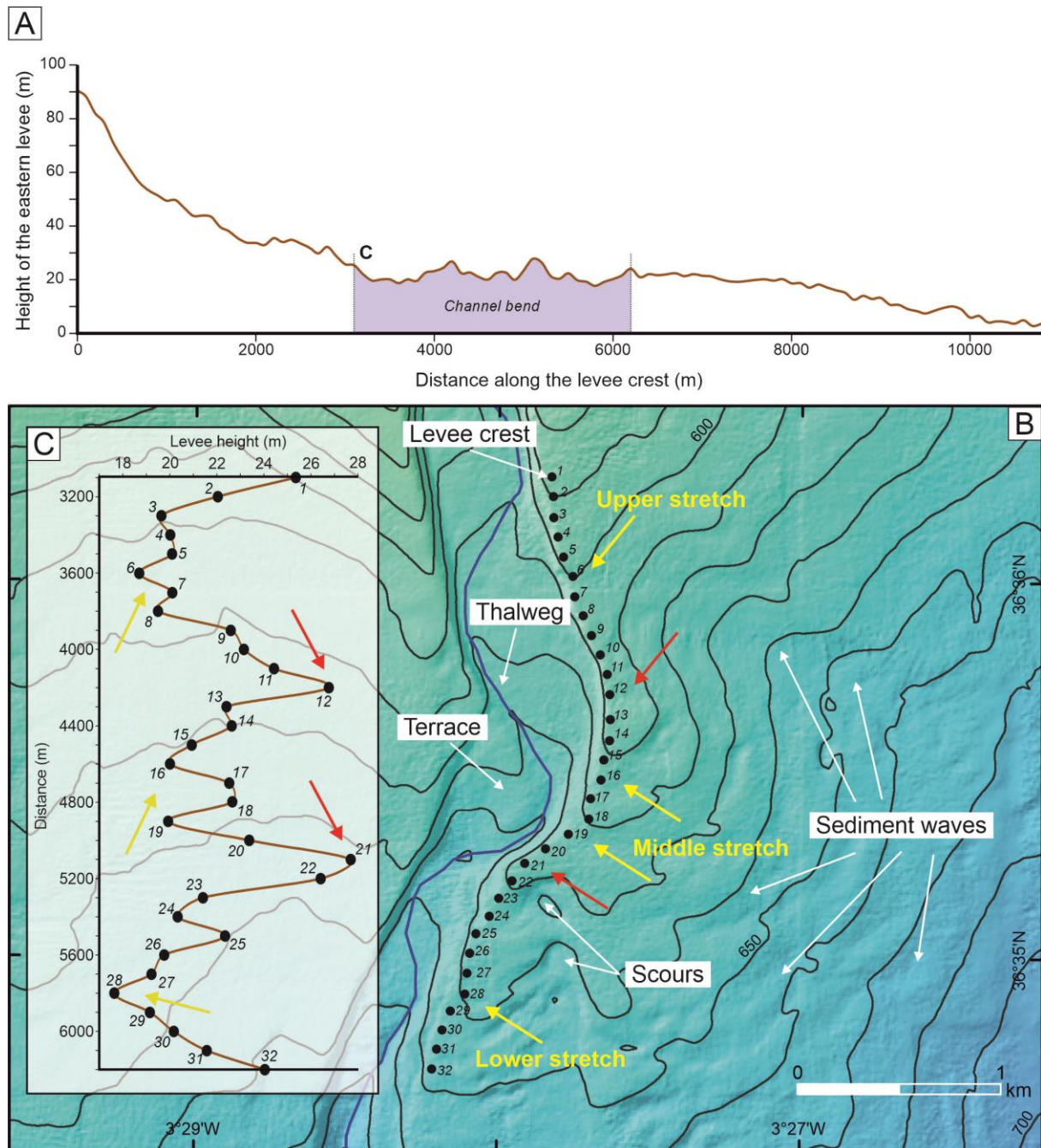


Figure 5.4. (A) Height of the eastern levee crest along the channel bend in the lower segment of the Carchuna Canyon. (B) Zoomed-in high-resolution bathymetric map of the channel bend in the lower segment, showing the points along the levee crest where the levee height was calculated (C). Red arrows mark the highest height values along the levee. Yellow arrows mark the upper, middle and lower stretches along the channel bend with the lowest height values in the levee. Bathymetric contours in meters.

5.1.2. Fine-scale morphology of the Carchuna Canyon

A total of 111 crescentic-shaped bedforms (CSBs) were observed along the axial channel of the upper segment from 96 to 496 m water depths. These CSBs have wavelengths from 10 to 120 m and amplitudes between 1 and 9 m. The lee sides of the CSBs exhibit gradients between 2.5 and 11.3°, while the stoss sides dip between 0.2 and 5.9° (Table 5.1). CSBs are grouped in 12 sets of 7 to 17 CSBs, ranging in length from 310 m to 730 m (Figures 5.2 and 5.3; Table 5.1). CSB sets have distinctive crest concavities, asymmetries and lengths. Overall, the CSB sets with high concavity (length/width >0.6) associated with high seafloor slope gradients (sets *b*, *c*, *e*, *f*, *h*, and *k*; Figures 5.2, 5.3 and 5.5A; Table 5.1) alternate with CSB sets of low concavity downcanyon (length/width <0.6) associated with lower slope gradients (sets *a*, *d*, *g*, *i*, *j*, and *l*; Figures 5.3 and 5.5A; Table 5.1). In the upper segment, most CSBs show a preferred downcanyon-directed asymmetry (Figure 5.6A, B).

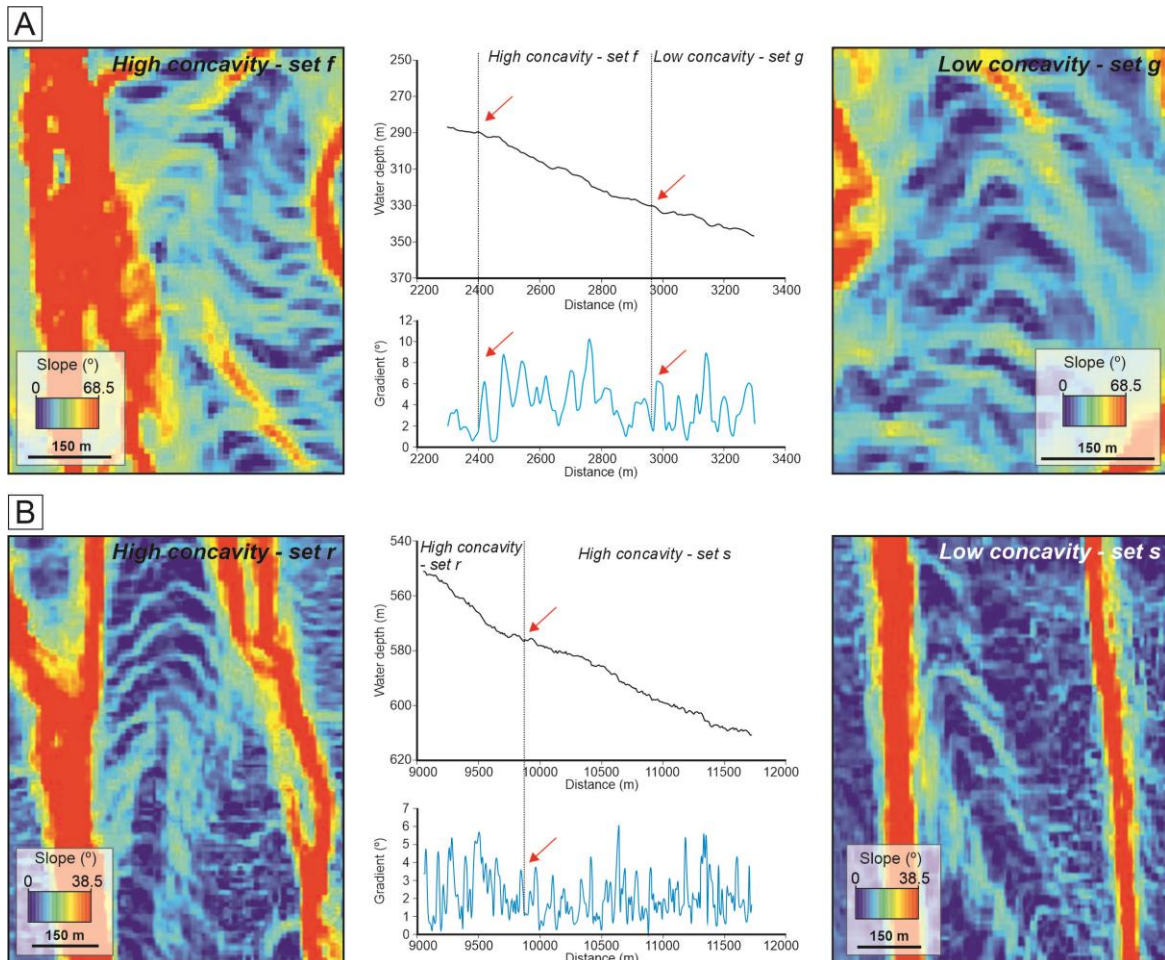


Figure 5.5. Zoomed-in high-resolution bathymetric maps of the study area showing several examples of CSB sets with high concavity in the upper (A) and lower (B) segments. The variation from high to low concavity linked to slope gradient changes of the CSB sets is also shown. See Figure 5.3C and D for location.

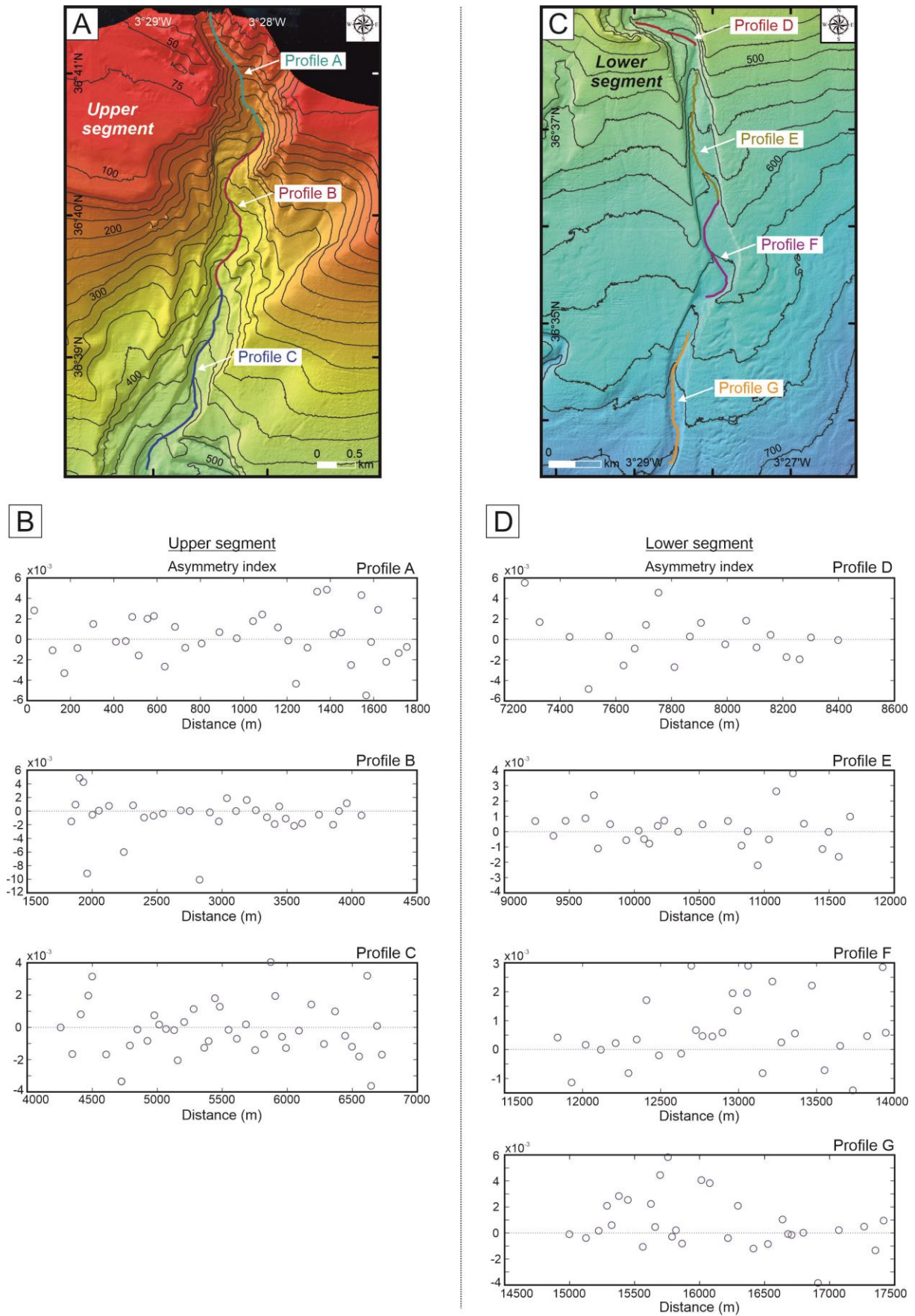


Figure 5.6. Asymmetry index variability of CSBs along three longitudinal profiles (A) in the upper segment thalweg (B) and along four longitudinal profiles (C) in the lower segment thalweg (D).

A total of 96 CSBs with wavelengths between 20 and 140 m and amplitudes from 1 to 5 m were identified along the axial channel of the lower segment from 502 to 704 m water depths. There, CSBs lee side gradients vary between 2.1° to 8.4° , while stoss sides are longer and their gradients vary between 0.1 to 2.4° (Table 5.1). In the lower segment, CSBs are grouped in 10 sets (Figures 5.2 and 5.3; Table 5.1) of 4 to 17 CSBs that extend between 430 and 1340 m (Figure 5.3). As in the upper segment, there is an alternation between CSB sets that exhibit high concavity (length/width >0.6) associated to high seafloor gradients (sets *r*, *u*, *v*, *w*, *x*, and *z*; Figures 5.3 and 5.5B) and CSB sets with low concavity (length/width <0.6) associated with lower slope gradients (sets *q*, *s*, *t*, and *y*; Figures 5.3 and 5.5B; Table 5.1). In this lower segment, most of the CSBs show a preferred upcanyon-directed asymmetry (Figure 5.6C, D).

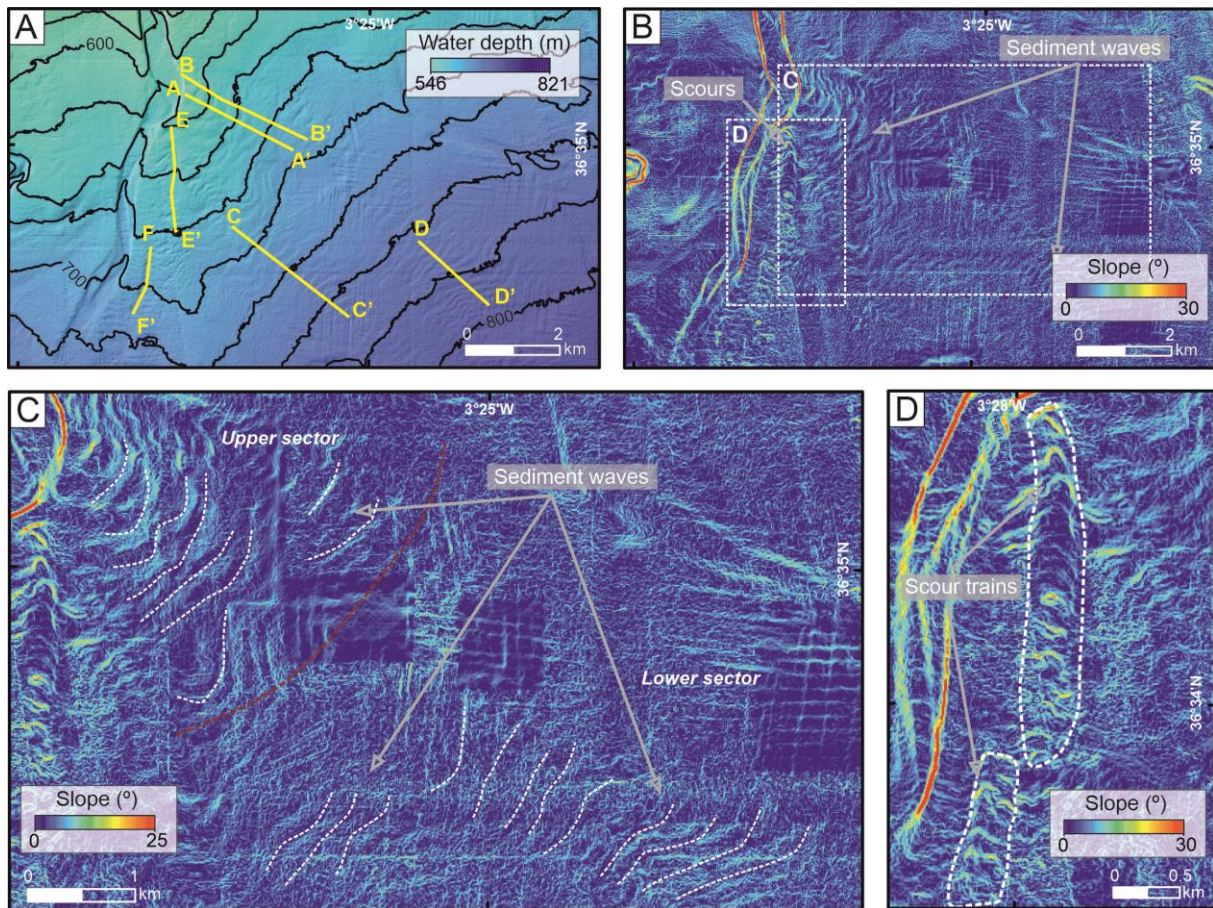


Figure 5.7. (A) High-resolution bathymetric map and (B) slope map of the eastern sector of the depositional lobe of the Carchuna Canyon, with the location of bathymetric profiles shown in Figure 5.8. (C) Zoom-in of the field of sediment waves with indication of the upper and lower sectors. (D) Zoom-in of two trains of scours identified along the depositional lobe of the Carchuna Canyon. Bathymetric contours in meters. See Figure 5.1 for location.

Two types of bedforms were identified on the open slope east of the lower canyon segment: sediment waves and scours (Figure 5.7). A sediment wave field was mapped over an area of 57 km² between 555 and 805 m water depths, with a mean seafloor gradient of 2°. The main orientation of the sediment wave crests is NW-SE (Figure 5.7B, C). Two sectors (upper and lower) were identified in the sediment wave field according to differences in wavelength and amplitude (Figures 5.7C and 5.8). In the upper sector, between 625 and 700 m water depths, the average wavelength of the sediment waves is 106 m, with a maximum wavelength of 350 m. They have average and maximum amplitudes of 6.2 m and 15 m, respectively (Figures 5.7C and 5.8A, B). Additionally, sediment waves in this sector exhibit a downcanyon asymmetric trend (Figure 5.9A, B). In the lower sector (between 700 and 800 m water depths), the average wavelength of the sediment waves is 146 m, with a maximum wavelength of 380 m. Here, sediment waves have an average amplitude of 4.9 m and a maximum amplitude of 9 m (Figures 5.7C and 5.8C, D) and an upcanyon asymmetric trend (Figure 5.9A, C).

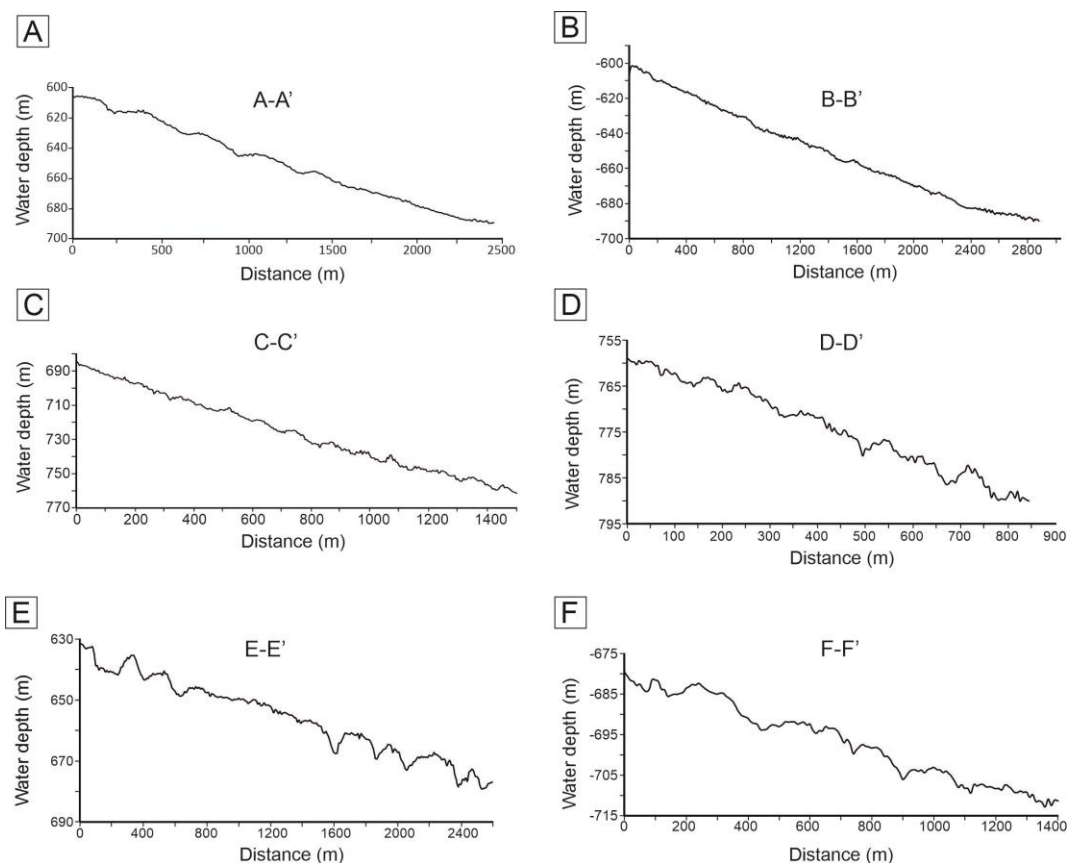


Figure 5.8. Bathymetric profiles of the upper sector (A and B) and the lower sector (C and D) of the sediment wave field, and the trains of scours (E and F) identified along the depositional lobe of the Carchuna Canyon. See Figure 5.7A for location.

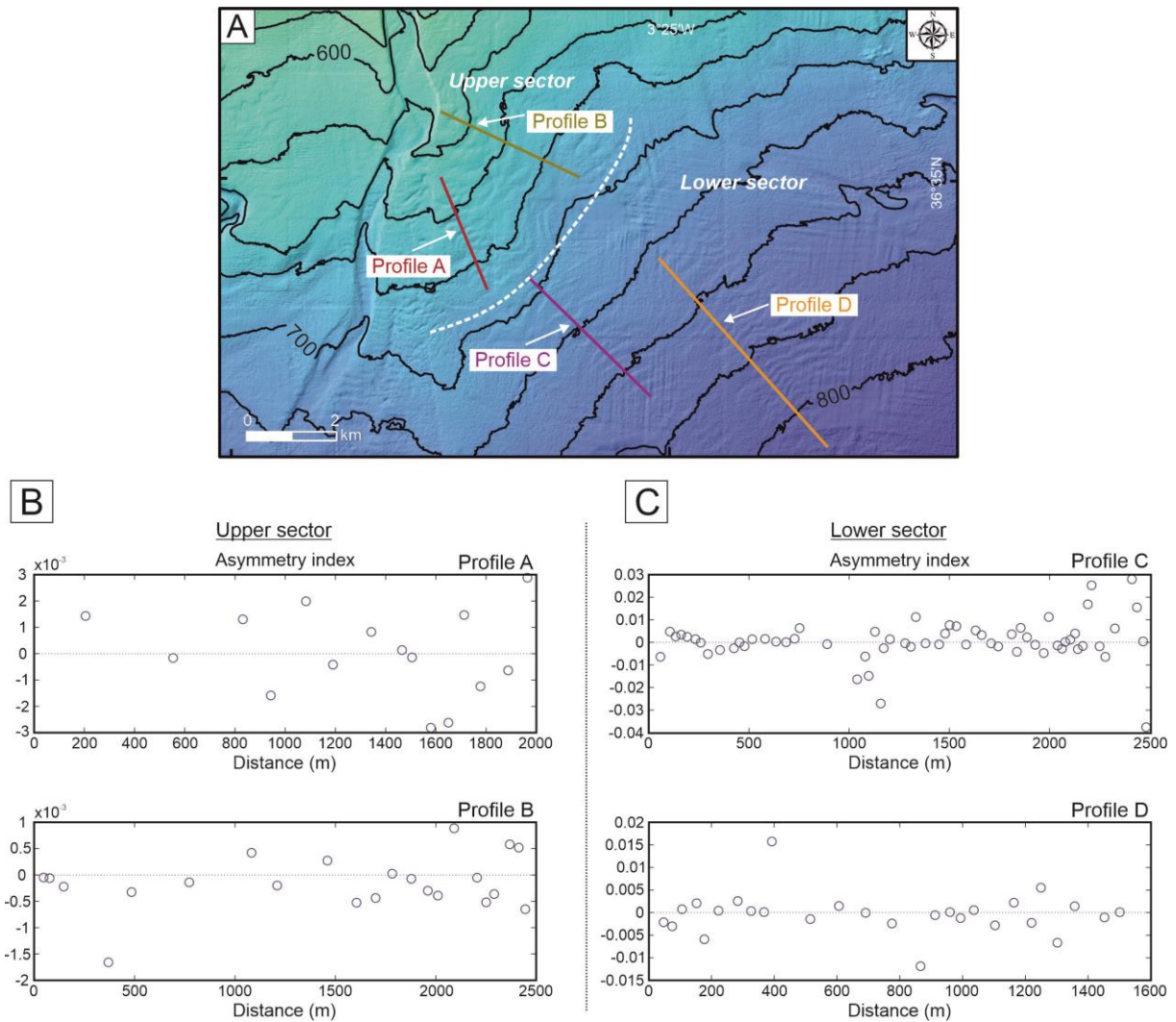


Figure 5.9. Asymmetry index variability of sediment waves from two longitudinal profiles along the upper sector (A) and two longitudinal profiles along the lower sector (B) of the depositional lobe of the Carchuna Canyon.

Two trains of N-S oriented scours are located over the eastern overbank deposit between the upper sector of the sediment wave field and the Carchuna axial channel at 623 to 711 m water depths (Figure 5.7). In plan view, these scours display parallel to divergent limbs and crescentic depressions at the base of headwall scarps (Figure 5.7B, D). The shallowest train of scours occurs between 623 and 678 m water depths and comprises 13 scours extending along 2600 m (Figure 5.7D and 5.8E). Individual scours range from 130 to 280 m in width, from 70 to 180 m in length, and from 2 to 8 m in headwall height (Figure 5.10A). The sidewalls and the depressions display slopes of 1° to 5° ; sub-surface sediments are characterized by homogeneous sandy muds with thin interbedded fine sands (Figure 5.10A, C). In contrast, the steepest gradients (6° to 12.6°) occur on the headwalls, which are characterized by strong

changes in the slope gradients and erosional features such as furrows, while the sub-surface sediments exhibit homogeneous sandy muds with very dispersed clasts of very coarse sands (Figure 5.10). The deepest train occurs between 681 and 711 m water depths and is formed by 8 scours, extending 1420 m (Figure 5.7D and 5.8F). Individual scours range from 60 to 190 m in width, from 15 to 80 m in length, and from 1 to 8 m in headwall height. The sidewalls and the depressions have slopes of 1° to 4° , while the steepest gradients (5° to 9°) occur on the headwalls.

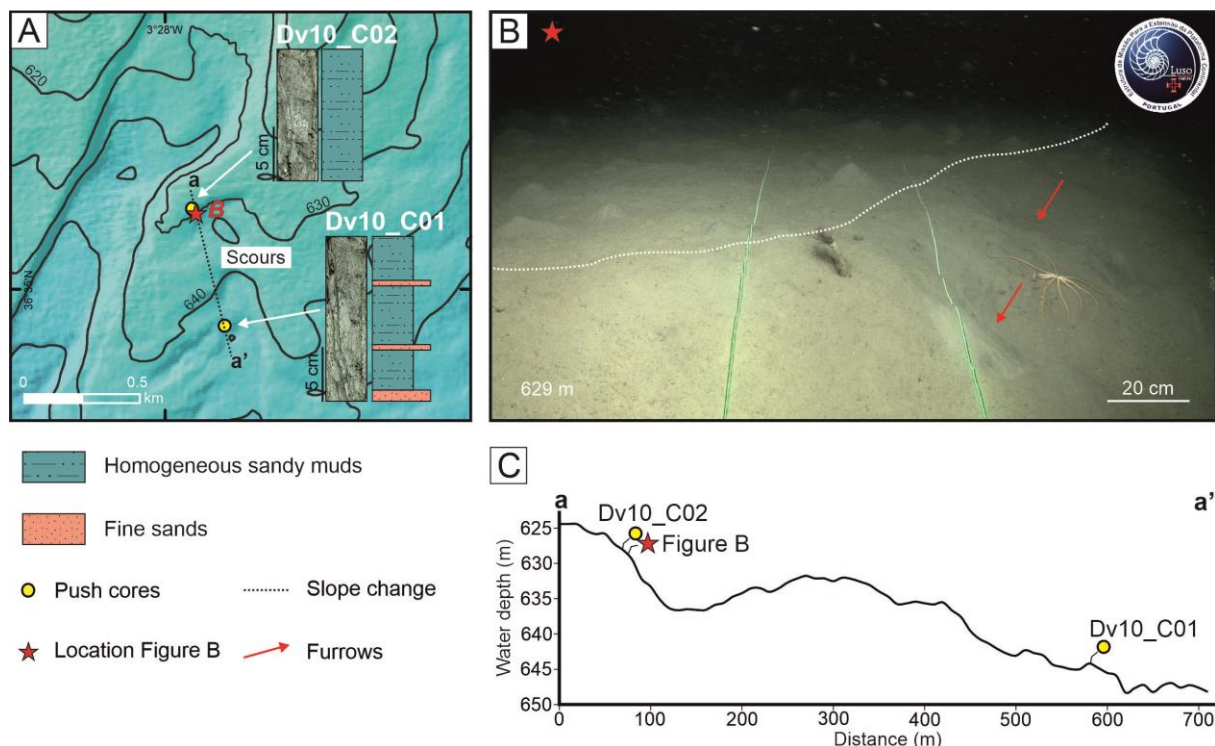


Figure 5.10. (A) Zoomed-in high-resolution bathymetric map of the upper reaches of the scour train showing the sedimentary logs of two push cores collected with the ROV. Location is shown in Figure 5.3B. Bathymetric contours in meters. (B) Photographic image collected by the ROV in the abrupt change of slope gradient (white dotted line) and the furrows over the wall of the scour (red arrows). Laser beam spacing of 62 cm indicated by green lines. (C) Longitudinal bathymetric profile along the scour train. The location of both sediment cores and the photographic image are indicated. Location of bathymetric profile indicated in A.

5.1.3. Sub-surface acoustic facies and architecture of Carchuna Canyon bedforms

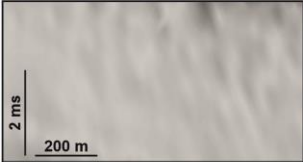
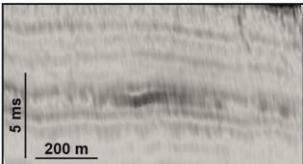
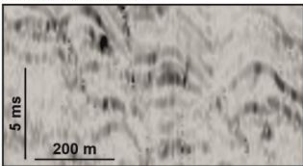
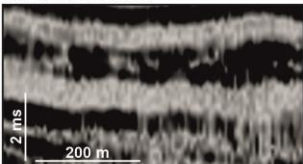
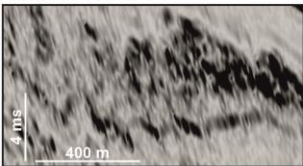
5.1.3.1. Description of acoustic facies

Five acoustic facies were distinguished along the Carchuna Canyon (Table 5.2). *Acoustic facies a* is characterized by a transparent configuration. *Acoustic facies b* exhibits low- to moderate-amplitude continuous and parallel reflections. *Acoustic facies c* features by

moderate- to high-amplitude discontinuous undulating reflections; internal reflections stack vertically with asymmetric shapes. *Acoustic facies d* exhibits high-amplitude parallel to gently undulating reflections. *Acoustic facies e* is characterized by diffractive reflections with lateral continuity and by prominent transparent and/or chaotic layers bounded at the base by a relatively high acoustic amplitude and irregular surface.

The superficial reflections of CSBs in the axial channel are characterized by high-amplitude *acoustic facies c* (Figure 5.11A, B), but they exhibit a lack of internal structure downward in the acoustic profiles (Figure 5.11). In the unconfined environment located close to the bend in the lower segment of the Carchuna Canyon, scours up to 8 ms high as well as downslope sediment waves are characterized by *acoustic facies c* (Figure 5.11B). Both unconfined bedforms also display a lack of internal structures downsection (Figure 5.11B).

Table 5.2.
Acoustic facies defined in the acoustic profiles.

| Acoustic facies | Description |
|--|--|
| <p>Acoustic facies a</p>  | Transparent reflections. |
| <p>Acoustic facies b</p>  | Continuous and parallel reflections with low to moderate amplitude. |
| <p>Acoustic facies c</p>  | Undulating, discontinuous medium to high amplitude reflections. |
| <p>Acoustic facies d</p>  | Parallel and gently undulating reflections with high amplitude. |
| <p>Acoustic facies e</p>  | Diffractive reflections with lateral continuity and by prominent transparent and/or chaotic layers |

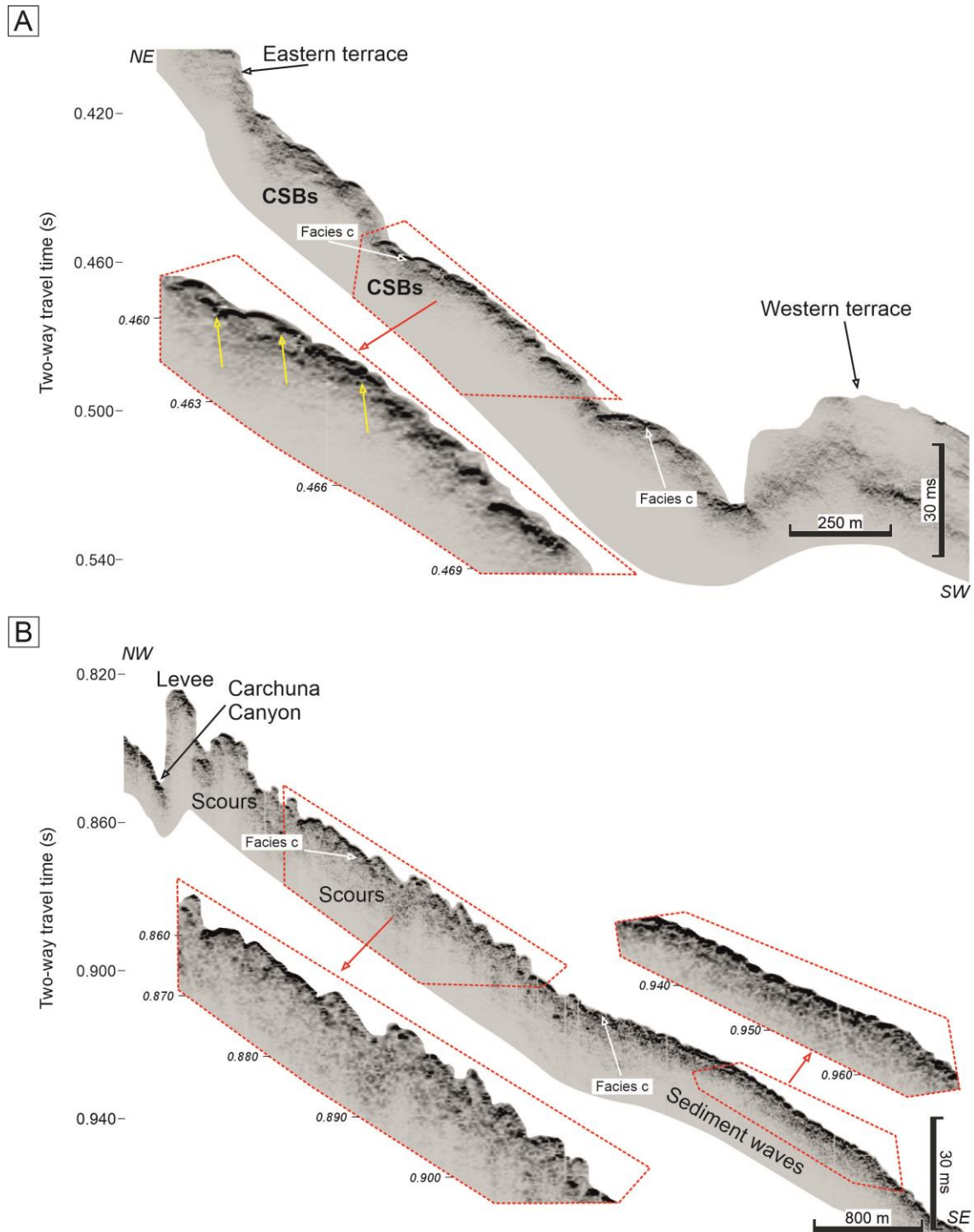


Figure 5.11. (A) Acoustic profile located in the upper segment of the Carchuna Canyon, illustrating CSBs *acoustic facies c* and the lateral terraces. Zoom-in of a sector of the axial channel showing the backsets of CSBs on the downstream end of stoss sides truncated by upstream-advancing lee sides indicated by yellow arrows. (B) Acoustic profile located in the transition from the Carchuna Canyon towards the depositional lobe illustrating the scour *acoustic facies c*. Note the downslope change to sediment waves. Zoom-ins of a sector of scours and sediment waves, respectively. See Figure 5.1C for location

Four acoustic units were defined along the sediment wave field identified over the depositional lobe (Figures 5.12 and 5.13). The deeper Acoustic Unit 4 exhibits *acoustic facies c* (Figure 5.12) in the upper sector of the sediment wave field. Downslope in the lower sector, a lenticular-shaped body 1100 m long and with laterally variable thickness—from 14 ms to 10 ms—is identified (Figure 5.13). This lenticular body is characterized by *acoustic facies c* that evolve downslope to *acoustic facies b* up to 7 ms thick (Figure 5.13). Acoustic Unit 3 is characterized by *acoustic facies a* up to 5 ms thick (Figures 5.12 and 5.13) that change downslope to *acoustic facies b* (Figure 5.12).

Acoustic Unit 2 is characterized by *acoustic facies c* in the upper sector of the sediment wave field, changing to *acoustic facies d* towards the east (Figure 5.12). Downslope in the lower sector, a 2-10 ms thick lenticular body is characterized by *acoustic facies c* that change downslope to *acoustic facies e* (Figure 5.13). Further downslope, *acoustic facies c* up to 1 ms thick evolve seaward to *acoustic facies d*. The uppermost Acoustic Unit 1 is characterized by *acoustic facies a* up to 4 ms thick (Figures 5.12 and 5.13), generating a wavy seafloor topography. This acoustic unit exhibits *acoustic facies c* up to 1 ms thick in the upper and lower sectors of the sediment wave field (Figures 5.12 and 5.13).

5.1.3.2. Interpretation of acoustic facies

The acoustic facies identified in the study area are thought to result from distinct sedimentary processes in the unconfined setting of the Carchuna Canyon. We suggest that transparent reflections (*acoustic facies a*) are linked to low-density turbidity currents characterized by fine-grained sediments (e.g., Scacchia et al., 2022). On the other hand, high-density turbidity currents can generate either high-amplitude parallel reflections (i.e., *acoustic facies d*) (e.g., Droz et al., 2003; García et al., 2006; Sylvester et al., 2012; Li et al., 2017) or cyclic steps characterized by *acoustic facies c* (e.g., Schattner and Lazar, 2016; Wunsch et al., 2017). Downslope, parallel reflections (i.e., *acoustic facies b*) are thought to be formed by decreased flow velocities (e.g., von Lom-Keil et al., 2002). High-amplitude chaotic reflections of *acoustic facies e* are typically linked to mass-transport deposits, as suggested in numerous deep-water studies (e.g., Rogers et al., 2015; Li et al., 2017; Wang et al., 2017; Normandeau et al., 2019; Wan et al., 2022).

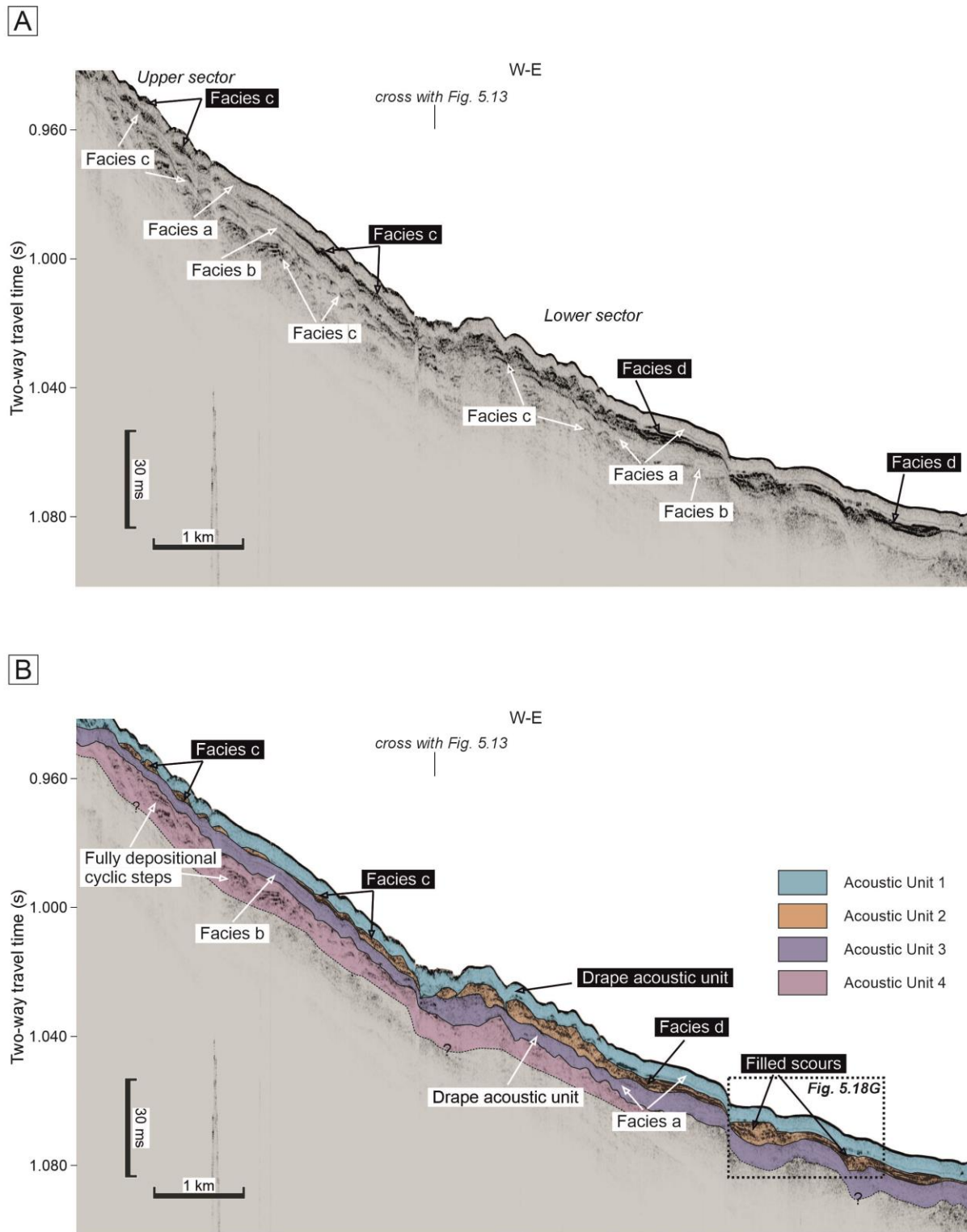


Figure 5.12. (A) East-West oriented acoustic profile located in the eastern overbank deposit of the Carchuna depositional lobe with indication of acoustic facies, and (B) the interpretation of four acoustic units. Location of Figure 5.18G is also indicated. See Figure 5.1 for profile location.

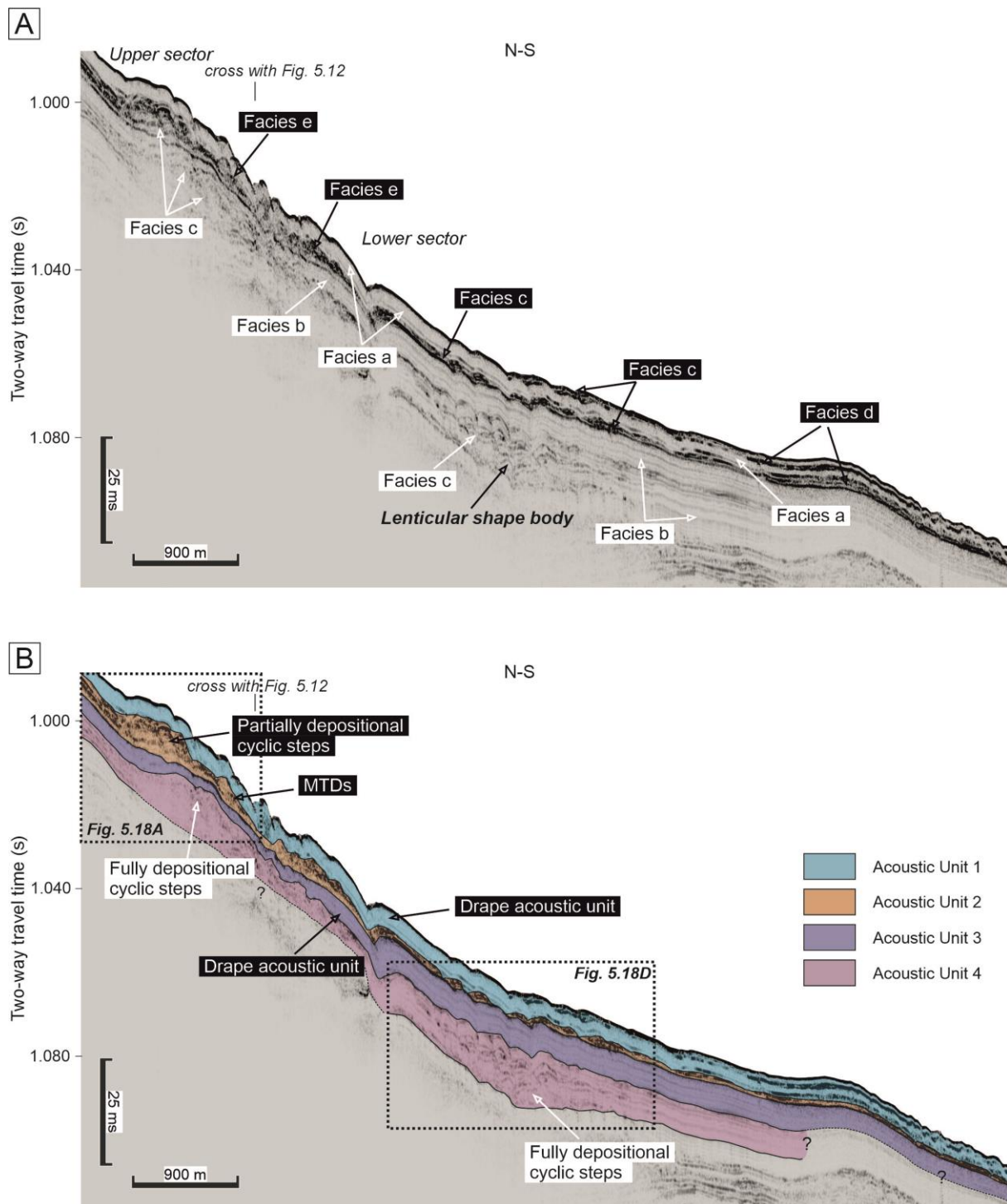


Figure 5.13. (A) North-South oriented acoustic profile located in the eastern overbank deposit of the Carchuna depositional lobe with indication of acoustic facies, and (B) the interpretation of four acoustic units. Location of Figure 5.18A and D is also indicated. See Figure 5.1 for location.

5.1.4. Sediment transport simulation

The highest simulated flow velocities are found along the Carchuna Canyon thalweg (Figure 16A). In the upper segment, the flow follows the sinuous path of the thalweg, with the highest flow velocities between 210 and 335 m water depths. At 250 m water depth, the simulation shows maximum flow velocities. Downslope from 335 m water depth, the flow velocity decreases up to the termination of the upper segment at 500 m water depth. The lowest values of flow velocity in the upper segment correspond to in the lateral terraces. The highest Froude values of the flow model occur in the walls adjacent to the lateral terraces of the upper segment, whereas the lowest values occur over the terraces. The sinuous path of the thalweg is characterized by intermediate values of the Froude number (Figure 16B).

In the lower segment, the flow follows the sinuous path of the thalweg with the highest flow velocities between 500 and 595 m water depths (Figure 16A). Downcanyon, the flow velocity decreases along the thalweg. Along the sinuous path of the thalweg, the simulated flow shows intermediate values of the Froude number. A spillover extending over the depositional lobe was identified at the bend in the lower segment. The simulation shows three overflow orientations: a western flow with NE-SW orientation, parallel to the main channel; an eastern flow with N-S orientation, along the main train of scours defined in the eastern overbank deposit; and an eastern flow with NW-SE orientation along the sediment wave fields (Figure 16B). Average velocity values in the eastern overbank deposit are higher on top of the bedform crests, whereas the higher values of Froude number are located in the bedform lee sides.

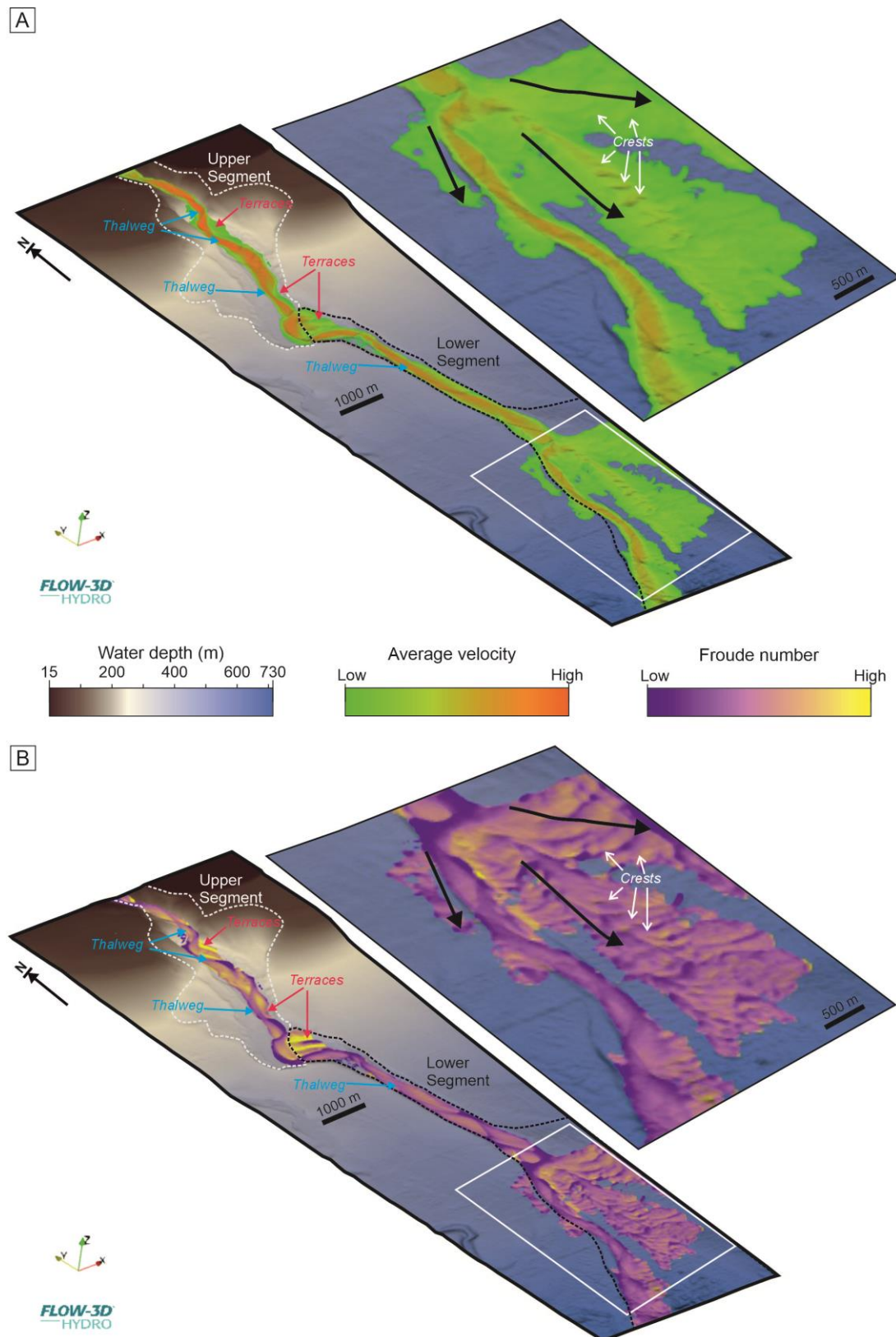


Figure 5.14. Variation of the average velocity (A) and the Froude number (B) of the three-dimensional flow simulation executed along the axial channel of the Carchuna Canyon. The most significant feature is a flow spillover at the channel bend over the depositional lobe in the lower segment.

5.2. Discussion

5.2.1. Development of cyclic steps along the confined setting of the Carchuna Canyon

5.2.1.1. The role of turbidity currents in CSB development

CSBs are common features in confined submarine settings mantled by coarse-grained sediments (Paull et al., 2010; Hage et al., 2018), such as the thalweg of active submarine canyons. There, CSBs are interpreted as the result of the combined effects of erosional and depositional processes during relatively short, high-energy turbidity flow events (Smith et al., 2005; Xu et al., 2008; Paull et al., 2010; Babonneau et al., 2013) that produce rhythmic seafloor bedforms known as cyclic steps (Cartigny et al., 2011; Kostic, 2011). In the Carchuna Canyon, several evidences point to the activity of confined sediment-laden gravity flows descending along the axial channel. Most notably, the presence of CSBs in the axial channel of the canyon between 95 and 706 m water depths signals the likely occurrence of flows that maintain these bedforms. This inference is supported by flow simulations that exhibit higher flow velocities along the thalweg (Figure 5.14A). Additionally, very concave profiles are linked to steep and coarse-grained shelf-incised canyons in narrow shelves adjacent to mountainous reliefs that supply coarse-grained sediments to canyon heads (Covault et al., 2011). The very concave shape and the occurrence of sandy muds and sands along the axial channel of the Carchuna Canyon (Figures 5.1 and 5.2) would indicate a continuous supply of sandy sediments regardless of the sea-level stand and turbidity current activity throughout the channel, as documented in other canyon settings (Mitchell, 2005; Gerber et al., 2009; Kertznus and Kneller, 2009; Covault et al., 2011; Ambblas et al., 2012).

Turbidity current activity is also evidenced by the CSB dimensions. CSBs in submarine canyons can be defined as *small sediment waves* (Symons et al., 2016) (Figure 5.15A). These sediment waves are restricted to medium-scale canyons (<50 km) in confined settings, characterized by wavelengths from 20 to 300 m and amplitudes between 0.5 and 8 m (Symons et al., 2016), and are composed primarily of coarse-grained sediments (Paull et al., 2010). CSB dimensions in the Carchuna Canyon are consistent with their classification as *small sediment waves* (Figure 5.15A), supporting CSB formation by coarse-grained turbidity current activity along the axial channel. Besides, CSBs along the axial channel of the Carchuna Canyon mostly exhibit upstream migration (Figure 5.11A); in fact, they can be classified as partially erosional cyclic steps (Slootman and Cartigny, 2020) due to the fact that net erosion is not limited to lee sides, but also affects the region beyond the trough on the upstream part

of stoss sides. Indeed, the backsets of the CSBs at the downstream end of stoss sides are truncated by upstream-advancing lee sides (Figure 5.11A) evidencing that the canyon floor is in an overall degradational state. The fact that CSBs in confined settings do not have a well-defined internal stratigraphy is linked to the erosive behavior of turbiditic flows (e.g., Paull et al., 2010; Zhong et al., 2015), which are formed by very dense, coarse-grained layers (Cartigny et al., 2013; Symons et al., 2016). In this sense, the lack of stratification within the cyclic steps along the axial channel of the Carchuna Canyon (Figure 5.11) provides additional evidence of the dominance of erosion over deposition along the canyon seafloor, as documented in other canyon settings (Zhong et al., 2015).

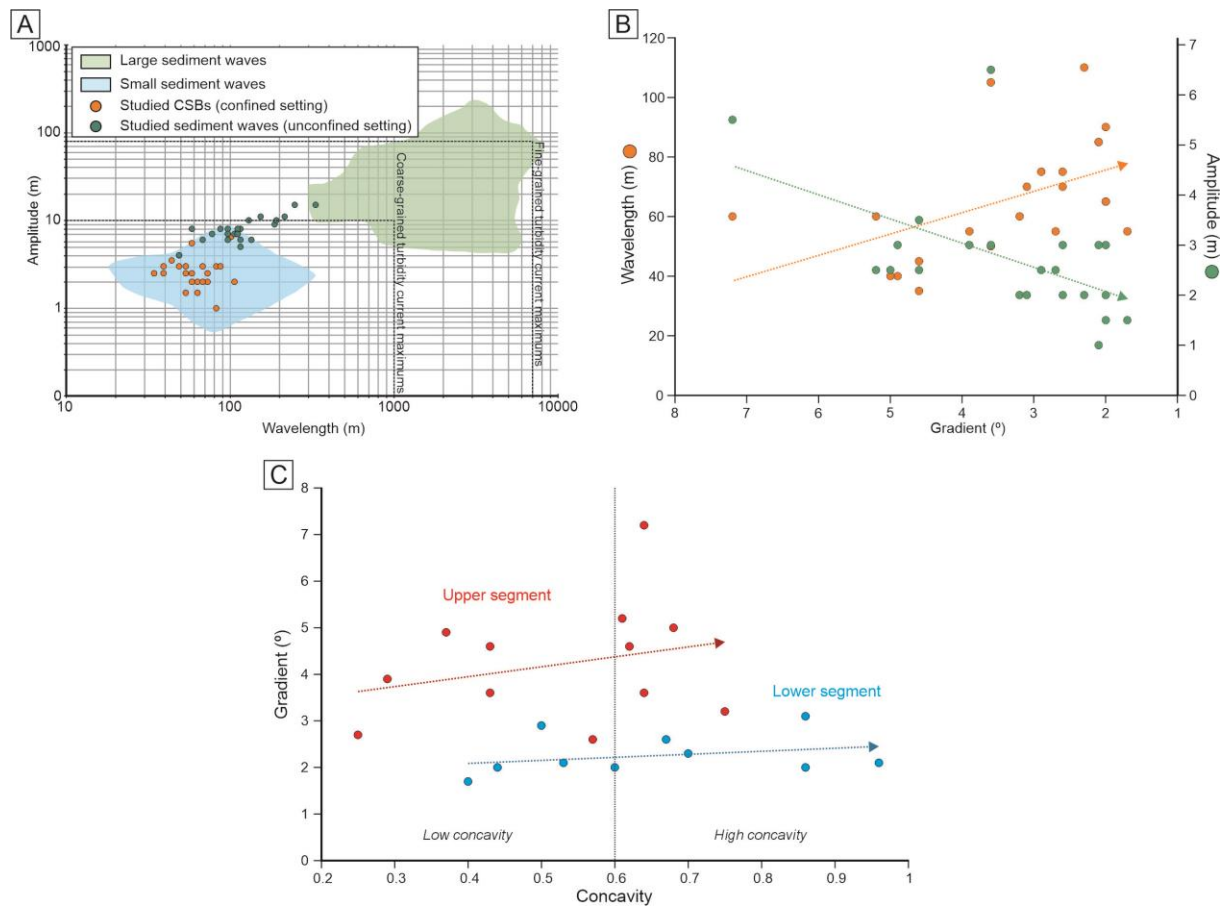


Figure 5.15. (A) Logarithmic plot of wavelength versus amplitude for global bedform examples highlighting groups based on bedform scale and relief according to Symons et al. (2016). Average amplitude and wavelength values of the studied confined (orange circles) and unconfined (green circles) bedforms are plotted. The maximum wavelength and amplitude values that define the coarse- and fine-grained turbidity current boundaries are shown as dotted lines after Wynn et al. (2002b). (B) Bi-variate relationships between CSB wavelengths (orange) and amplitudes (green) and the slope gradient along the Carchuna Canyon indicating the trend of each parameter with dotted arrows. (C) Bi-variate relationships between slope gradients and CSB concavity along the upper (red) and lower (blue) segments of the Carchuna Canyon, indicating the trend of each segment with dotted arrows

The inferred gravity flows in Carchuna Canyon could be traced to a combination of factors, involving increased shear stresses that frequently mobilize coarse-grained sediments, as in canyon heads similarly close to coastlines (Smith et al., 2018). Thus, the Carchuna Canyon head could act as a sediment trap due to its proximity to the coastline, enabling the capture of littoral cell sediments, then sediment transport along the axial channel toward the channel termination owing to gravity flows (Cerrillo-Escoriza et al., 2024). Additionally, the proximity of the Carchuna Canyon to the coast would favor an energy concentration of coastal and storm waves, focusing in the canyon head (Ortega-Sánchez et al., 2014; Cerrillo-Escoriza et al., 2024). These processes could erode proximal sandy infralittoral prograding wedges, providing a coarse-grained sediment source for the development of gravity flows. Besides, downcanyon sediment transport pulses generating the confined cyclic steps along the axial channel can be driven by downcanyon bottom flows —postulated to occur in the Carchuna Canyon head (Serrano et al., 2020). The occurrence of such sediment transport trends is supported by the identification of marine litter at the distal termination of the channel (Cerrillo-Escoriza et al., 2023).

5.2.1.2. Variability in CSB geometries along the axial channel

The geometric characteristics of bedforms gradually change as the slope gradients of submarine canyon axial channels decrease downslope (Zhou et al., 2021). In axial channels, downslope-decreasing gradients tend to cause flow deceleration, leading to greater wavelengths (Cartigny et al., 2011; Slootman and Cartigny, 2020) and lesser amplitudes of the cyclic steps (Normark et al., 1980; Carter et al., 1990; Migeon et al., 2000). This general trend is also observed in the CSBs along the Carchuna Canyon axial channel, where the overall downslope decrease in slope gradient along the axial channel coincides with a downslope increase in cyclic step wavelength and a decrease in their amplitude (Figure 5.15B; Table 5.1). Hence, steeper slope gradients and coarser sediments in the upper segment of the Carchuna Canyon would favor the formation of shorter and higher CSBs with steeper stoss sides, in contrast to the lower segment.

Downslope asymmetries appear to characterize coarse-grained cyclic steps in confined settings (Migeon et al., 2000; Symons et al., 2016), as reported in the Monterey Canyon (Smith et al., 2005, 2007; Xu et al., 2008) and the Var Canyon (Piper and Savoye, 1993; Khripounoff et al., 2012). CSBs recognized along the upper segment of the Carchuna Canyon

axial channel mostly exhibit downcanyon-directed asymmetries (Figure 5.6A, B) that can be related to a high amount of sediment available for entrainment by overrunning turbidity currents (Kostic, 2011). High slope gradients in the canyon's upper segment (Figure 5.2) would moreover favor the preferential development of downslope asymmetries, as is evidenced in other coarse-grained cyclic steps in confined settings (Migeon et al., 2000; Symons et al., 2016; Sun et al., 2023). In contrast, most of the CSBs in the lower segment of the Carchuna Canyon exhibit upcanyon-directed asymmetry (Figure 5.6C, D) pointing to an environmental energy decrease (Cartigny et al., 2011), likely due to lower slope gradients (Figure 5.2). This trend can furthermore be interpreted because the distances required for flow acceleration towards flow supercritical conditions on the stoss sides increase (Normandeau et al., 2016).

5.2.1.3. Implications of local variability in the slope gradient

Differences in asymmetry, wavelength, amplitude, and concavity between CSB sets observed along the axial channel (Figure 5.2; Table 5.1) could be indicative of variable flow behavior along the Carchuna Canyon path. Local variations of slope gradient affect both velocities and concentrations of bottom sediment flows; this phenomenon is consistent with variation in the behavior of turbidity currents flowing downcanyon (Kostic, 2011; Covault et al., 2017; Casalbore et al., 2018; Maselli et al., 2019; Zhou et al., 2021; Pohl et al., 2022). The increase in slope gradient promotes the formation of hydraulic jumps (Kostic, 2011), which increase flow velocities (Wilkin et al., 2023) and support sediment erosion and bypass (Kneller and McCaffrey, 1995); as a consequence, shorter and higher cyclic steps tend to be formed (Covault et al., 2017). In contrast, decreased slope gradients facilitate a decrease in flow velocities and sediment deposition (Kneller and McCaffrey, 1995; Kubo and Nakajima, 2002).

In the axial channel of the Carchuna Canyon, we propose that bedform set dimensions and concavity are determined to a large extent by gradient changes observed along the canyon thalweg. Highly concave CSB sets have higher amplitudes and lower wavelengths (e.g., sets *b*, *c*, *e*, *f*, *r*, *u*, *v*, *w*, *x*, and *z*; Figure 5.2; Table 5.1) that are usually related to locally increased seafloor gradients (Figure 5.5 and 5.15C). Such local increases in slope gradients would induce flow accelerations and erosive behavior, leading to the formation of highly concave CSB sets, where the erosion rate on steeper lee sides would increase bedform amplitude

(Casalbore et al., 2014; Covault et al., 2017) and decrease bedform wavelength (Covault et al., 2017; Slooman and Cartigny, 2020; Sun et al., 2023). The formation of these highly concave CSB sets may also be favored by the prevalence of coarse-grained sediments in the axial channel (Figure 5.1), considering that coarse-grained cyclic steps tend to show increased heights and decreased wavelengths (Dietrich et al., 2016; Slooman and Cartigny, 2020). Following this interpretation, we infer that CSB sets with low concavity can be linked to flow decelerations leading to enhanced deposition and/or suppressed incision.

There are a few exceptions where highly concave CSB sets are not located in areas with increased seafloor gradients, but instead, occur along meanders of the Carchuna thalweg (e.g., sets *h* and *k*; Figure 5.2; Table 5.1). We infer that these CSB sets are influenced by increases in flow density resulting in either more sediment entrainment or more erosion (Cartigny et al., 2011) along these thalweg bends. Downcanyon, these high concavity CSB sets change to low concavity sets (Figure 5.2) driven by decreasing slope gradients, favoring a decrease of flow velocities. Therefore, we infer that downslope variations of CSB set concavity mainly reflect spatially variable, discontinuous axial channel flows that remobilize and concentrate sediment in a step-like fashion, triggering sediment transport pulses downstream.

5.2.2. Development of cyclic steps along the unconfined setting of the Carchuna Canyon

5.2.2.1. Factors that control the overflows in the Carchuna Canyon

Flow stripping can occur by spillover of the upper parts of the flows at submarine canyon meanders if the flow is thicker than the confinement height, whereas the lower part of the flow would continue moving downcanyon (Piper and Normark, 1983; Peakall et al., 2000; Fildani et al., 2006; Sumner et al., 2013; Hansen et al., 2015; Tubau et al., 2015a; Covault et al., 2017). Spillover processes and increased turbulence can also be triggered by the action of centrifugal force at channel bends, which gives rise to increased flow velocity (Migeon et al., 2004; Scacchia et al., 2022; Tek et al., 2022). In the Carchuna Canyon, spillover flows can be envisaged at the bend located in the lower canyon segment. Indeed, silty sediments characterize overbank deposits at the canyon bend, while sandy sediments can be found at the distal termination of the channel (Figure 5.1). It is therefore inferred that fine-grained sediments are continuously deposited on the lateral canyon levees, whereas coarse-grained sediments are concentrated in the lower part of the flows and remain confined within the canyon, allowing the deposition of coarse sediments farther downstream.

The slope gradients of the lower segment of the Carchuna Canyon ($>2^\circ$; Figure 5.2) are high in comparison with other lower reaches of axial channels in shelf-incised submarine canyons ($<1^\circ$; e.g., Fildani et al., 2006; Lamb et al., 2008; Zhong et al., 2015; Zhou et al., 2021). Evidences found in the Carchuna Canyon supports that these relatively high gradients could favor high flow velocities leading to downcanyon increases in sediment entrainment and flow turbulence. For example, a set of straight, high-concavity CSBs is located in the channel bend (Figure 5.3). Additionally, surficial sediments over the Carchuna Channel inner bend terrace are characterized by coarse-grained sediments (Figure 5.1), suggesting that the flow is very substantial and engulfs the entire channel bend, favoring both downstream sediment transport and spillover over the levee in the channel bend, as reported elsewhere (Hansen et al., 2015).

In proximal levee areas, local flow directions of overflows are highly variable, owing to the irregular heights along the levees (Normark et al., 2002; Migeon et al., 2004; Hansen et al., 2015; Tek et al., 2022). Although the studied bedforms are essentially concentric around the channel bend of the Carchuna Canyon, a spatial relationship is established between the development of bedform fields over the overbank deposit and lowered levee heights in the proximal areas of the bedform fields (i.e., upper, middle, and lower levee stretches; Figure 5.4). We infer that these depressed levee stretches are genetically linked with overflow paths that generate sediment waves (Figure 5.16A). Considering that the minimum levee height in the channel bend is 17.5 m, we speculate that turbidity currents descending along the axial channel and approaching the channel bend most likely exhibit thickness around that value or just slightly less, given that channel bends induce flow acceleration as a result of centrifugal force, and favor flow stripping (Migeon et al., 2004).

In contrast to the relationship found between sediment wave fields and lowered levee stretches, the scour trains found in the overbank deposit of the Carchuna Canyon are not related proximally with low levee heights (Figure 5.4). In this case, we surmise that the drastic change of orientation of the axial channel in the lower segment (NNW-SSE to NNE-SSW; Figure 5.1 and 5.4) would be a key factor in the formation of the scours. In other sharp bends of submarine canyons, turbidity currents tend to flow downslope of orientation changes by overflowing the levee crests (e.g., Fildani et al., 2006). We infer that the studied scour trains formed by means of a mechanism similarly described at channel bends (e.g., Fildani et al., 2006; Covault et al., 2014); accordingly, the overflow of turbidity currents that descend along the axial channel and exceed the high levee crest at the channel bend would trigger an abrupt change in the turbidity current behavior (Figure 5.16B).

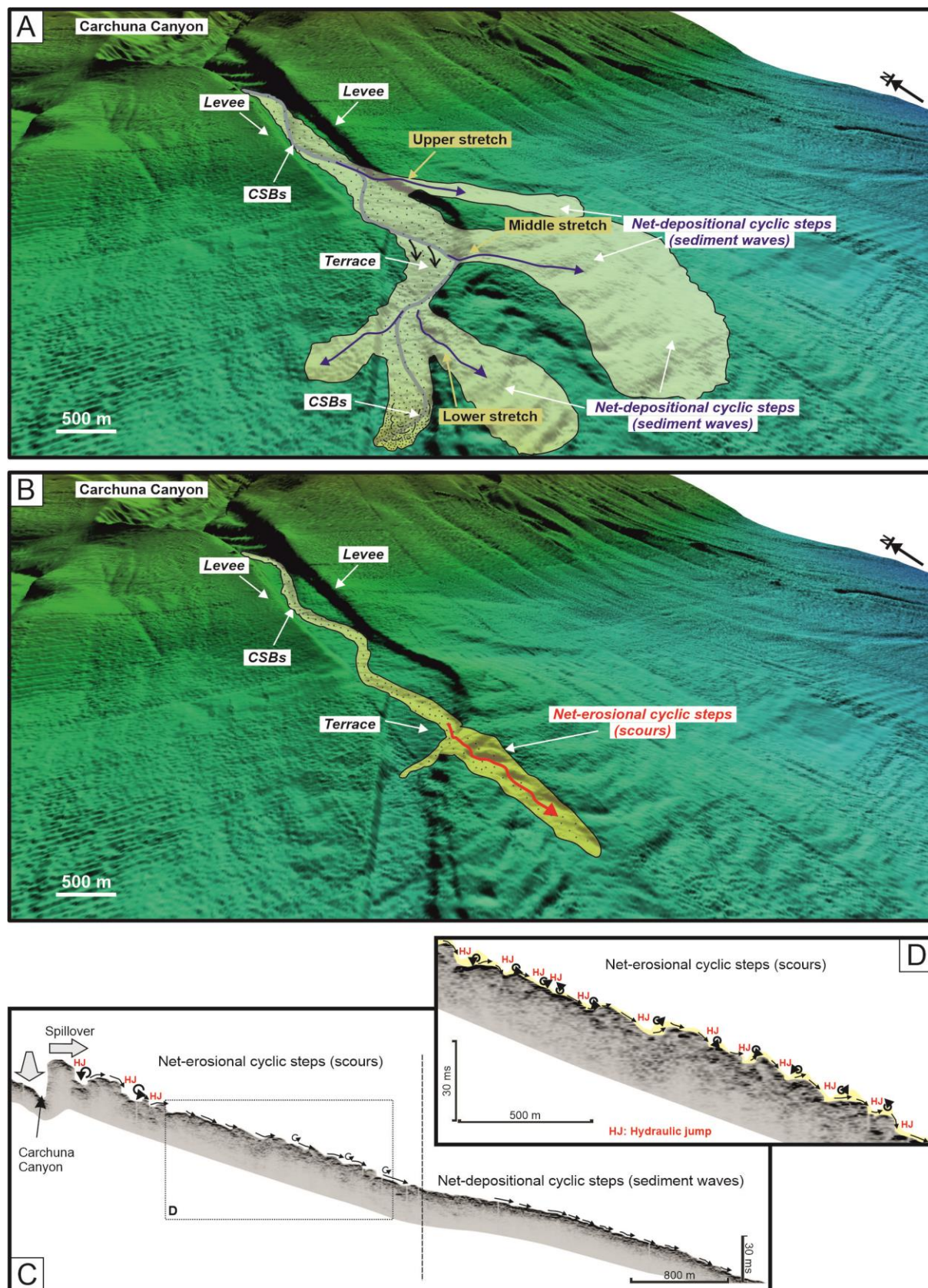


Figure 5.16. 3D reconstruction of the study area illustrating two different settings according to the development of the bedforms along the overbank deposit at the channel bend of the Carchuna Canyon. (A) Three main overflows (in blue) transiting along three depressed levee crests (upper, middle, and lower levee stretches) and contributing to development of sediment waves. (B) An energetic and casual turbidity flow exceeding the levee crest at the channel bend (in red) favors the erosion of the overbank deposit forming scour trains. (C) Interpretation of the acoustic profile of Figure 5.11B, illustrating the erosional stripped flow over the scour train that evolves downslope to sediment waves. (D) Zoom-in of the upper sector of the depositional lobe illustrating the hydraulic jumps of the flow along the scour train (net-erosional cyclic steps).

5.2.2.2. Sediment waves formed in the overbank deposit of the Carchuna Canyon

In unconfined settings, sediment waves have been interpreted as supercritical flow bedforms, that is, net-depositional cyclic steps (Fildani et al., 2006; Cartigny et al., 2011, 2014; Kostic, 2011, 2014; Zhong et al., 2015) mantled by fine-grained sediments (Symons et al., 2016) particularly covering the overbank areas of submarine canyons and channels (Fildani et al., 2006, 2013; Kostic and Parker, 2006; Maier et al., 2011, 2013; Armitage et al., 2012; Zhong et al., 2015). The unconfined setting makes these cyclic steps more prone to form positive reliefs due to preferential sediment deposition on the upstream side (Flood and Giosan, 2002), in contrast to confined CSBs, where erosion is thought to play a larger role (Symons et al., 2016).

Because sediment waves in unconfined settings exhibit higher amplitudes and wavelengths than those found in confined canyon settings, they are categorized as *large sediment waves* (Symons et al., 2016) (Figure 5.15A). Amplitude and wavelength values of the unconfined sediment waves in the depositional lobe of Carchuna Canyon are larger than the CSB dimension values; hence they lie between *small* and *large sediment waves* (Figure 5.15A). This fact supports a sediment wave genesis of the Carchuna depositional lobe related to the activity of fine-grained turbidity currents, in view of the genetic conditions behind *small* and *large sediment waves* put forth by Symons et al. (2016).

The crests of these unconfined sediment waves are not aligned parallel to the canyon axis (ca. NW-SE orientation of the crests vs ca. N-S orientation of the canyon axis; Figures 5.7 and 5.16A). In addition, the flow simulation shows that the Froude number is higher on the bedform lee sides (Figure 5.15B), indicating supercritical flow conditions (Cartigny et al., 2011). Both evidences point to the development of the studied sediment waves in a context of recurring stripped turbidity currents spilling out of the axial channel (Figure 5.16A), as

evidenced in similar environments (e.g., Lewis and Pantin, 2002; Normark et al., 2002; Wynn and Stow, 2002; Fildani et al., 2006; Kostic et al., 2010; Covault et al., 2017). As in axial channels, decreasing slope gradients in overbank deposits cause a streamwise flow deceleration (e.g., Cartigny et al., 2011). In the overbank deposit of the Carchuna Canyon, this is evidenced by a downslope wavelength increase and amplitude decrease of the sediment waves, accompanied by a downslope decrease in flow velocities (Figure 5.14A).

Upslope-directed asymmetries of cyclic steps are characteristic of fine-grained sediment waves in unconfined, low-energy environments, as at the Monterey Fan (Normark et al., 1980, 2002; Fildani et al., 2006), the Var Sedimentary Ridge (Migeon et al., 2000, 2001), the overbank deposits of the Eel Canyon (Lamb et al., 2008), or the overbank deposits in the Gioia Basin (Gamberi et al., 2013). However, downslope-directed asymmetries or symmetric trends of sediment waves are related to aggradational building of levees that tend to be covered by coarse-grained sediments (Kostic, 2011). Such evidence is seen in the upper sector of the overbank deposit of the Carchuna Canyon, where the coarsest-grained sediments of the overbank deposit are located close to the levee crest (Figure 5.1), with sediment waves showing dominantly downslope-directed asymmetries (Figure 5.9B). In contrast, the sediment waves in the lower sector over the overbank deposit exhibit an upslope asymmetry trend (Figure 5.9C), suggesting that up-slope migration dominates over vertical aggradation (Figures 5.11B, 5.12, and 5.13) in relation to the distal decrease in slope gradients.

5.2.2.3. Scours formed in the overbank deposit of the Carchuna Canyon

Turbidity currents that mostly carry coarse-grained sediments can create large-scale scours nearby internal hydraulic jumps (Hiscott et al., 2013; Sumner et al., 2013; Covault et al., 2017). Linear trains of scours can be interpreted as a result of net-erosional cyclic steps in supercritical flows (Fildani et al., 2006; Kostic, 2011; Covault et al., 2017), where repeated hydraulic jumps along the scour trains form due to lee side erosion rates by Froude-supercritical flows —exceeding stoss side erosion rates by Froude-subcritical flows— ultimately causing an upstream migration (Sumner et al., 2013; Hiscott et al., 2013). Alternatively, scour trains may signal an excavation of initial bed defects by a subcritical flow with enough shear stress (Symons et al., 2016).

According to the flow model, the highest velocity values occur along the scour trains in the overbank deposit of the Carchuna Canyon (Figure 5.14A). In addition, there are high

estimated values of Froude number on the lee side of scours (Figure 5.14B), evidencing supercritical flows with high velocities that favor erosion on both lee and stoss sides (Slootman and Cartigny, 2020) and lead to upstream migration (Figure 5.16C, D). Downslope of the scour trains, net-erosional cyclic steps evolve to net-depositional cyclic steps (Figures 5.11A and 5.16C), thus indicating a progressive downslope decrease in sediment transport capacity and erosive flow behavior, reflected by decreasing velocities in the flow model (Figure 5.14A); this pattern has been observed elsewhere (e.g., Li and Gong, 2018). Therefore, we interpret the scours located close to the bend of the Carchuna Canyon as net-erosional cyclic steps carved by flow-stripped turbidity currents that have incised the overbank deposit of the canyon (Figure 5.16B, C).

The noteworthy location of the scours in the overbank deposit of the Carchuna Canyon agrees with a scenario of turbidity currents focused (e.g., Izumi, 2004) (Figure 5.16B) where erosion rates are intensified in places of flow concentration, leading to channel formation in topographic lows of outer levees (Fildani et al., 2006; Normandeau et al., 2019; Maier et al., 2020). Accordingly, the scour trains studied here could mark an early phase of the Carchuna Canyon channel evolution due to an ongoing avulsion process. The flow concentration is evidenced by the distribution of surficial sediments along the scours generated in the overbank deposit of the Carchuna Canyon, the coarser sediments being found on stoss sides (Figure 5.10A). This pattern may be attributed to coarse-grained sediment preferentially bypassed on the lee sides —favored by the concentration and high velocities of the overspilling flow— and deposited on the stoss sides of the following scour downslope. The erosive behavior of the flow is further evidenced over the lee side as erosive features (Figure 5.10B). In contrast, finer-grained sediments are deposited upstream over the lee sides (Figure 5.10A) in response to low velocities of the tails of overspilling flows, as seen in other cyclic steps on overbank deposits (e.g., Tek et al., 2022). We infer that the flow concentration in the channel bend is due to episodic, energetic sediment transport pulses that exceed the levee crest where the channel bend changes its orientation.

5.2.3. Recent evolution of the Carchuna Canyon

The flow density and turbulence of overspilling confined flows control the grain size partitioning between in-channel flow and levee deposits (Hiscott et al., 1997; Peakall et al., 2000; Posamentier and Walker, 2006; Scacchia et al., 2022), defining two end-member situations: low- and high-density turbidity currents (Lowe, 1982; Kneller and Buckee, 2000; Shanmugam, 2019). In low-density turbidity currents, partial inertia-driven flow spillover may occur on outer channel bends, where fine-grained sediments in the upper part of the current escape the channel, yet the denser lower part remains within the channel (Piper and Normark, 1983; Leeder, 1999; Peakall et al., 2000; Hansen et al., 2015). In contrast, high-density turbidity currents feature heights greater than the channel confinement depth, meaning widespread coarse-grained spillover on both outer and inner channel bends (Hesse, 1995; Peakall et al., 2000; Hansen et al., 2015).

The acoustic units that define the overbank deposit of the Carchuna Canyon suggest the occurrence of recurrent spillovers in the recent past. However, the vertical alternation of acoustic units suggests that overflows over the depositional lobe reflect different characteristics and energy conditions. Depending on the development of high- or low-density turbidity currents descending along the axial channel and approaching the sharp bend in the Carchuna Canyon (Figure 5.17A), spillover processes along the channel bend and subsequent deposition in the overbank area would have been different, ultimately leading to the construction of the Carchuna depositional lobe (Figure 5.17).

5.2.3.1. High-density turbidity current scenario

High-reflectivity acoustic facies in overbank deposits usually indicate coarse-grained sediments derived from high-density turbidity currents that generate an overall positive topography (e.g., Scacchia et al., 2022). The depositional lobe of the Carchuna Canyon contains two acoustic units (4 and 2) mainly characterized by high-reflectivity acoustic facies (Figures 5.12 and 5.13), a likely result of high-density turbidity currents. Ample evidence supports this inference. High-amplitude reflectors that separate acoustic units have been identified in overbank deposits as abrupt sedimentological changes traced to an erosive flow behavior (Heiniö and Davies, 2009; Gong et al., 2012; Schattner and Lazar, 2016). In the Carchuna depositional lobe, the high-amplitude reflectors that limit the bases of acoustic units 4 and 2 (Figures 5.12 and 5.13) exhibit irregular shapes that can be related to bypass

processes generating local unconformities, and favoring hydraulic jumps, with the subsequent downslope increase in overflow turbulence (Figure 5.18), as evidenced in other canyon depositional lobes (e.g., Li and Gong, 2018). Deposits resulting from high-density turbidity currents exhibit a spatial variability from upper to lower reaches of depositional lobes as the turbidity currents become less energetic with distance. In this sense, the imprint of high-density turbidity currents is also evidenced by the downslope increase in the deposit thickness (Figure 5.12) suggesting an efficient downslope sediment transfer along the depositional lobe.

Sediment wave fields exhibit different dimensions, geometries and sediment distribution, depending on the interaction between overspilling turbidity currents and slope topography (Migeon et al., 2000; Kubo and Nakajima, 2002; Cartigny et al., 2011; Maselli et al., 2019; Scacchia et al., 2022). The upper sector of the Carchuna depositional lobe hosts partially depositional sediment waves (Figures 5.13 and 5.18B) that are interpreted as low-aggradational cyclic steps indicative of coarse grained-sediments and high seafloor shear stresses (Normark et al., 2002; Kostic, 2014; Slooman and Cartigny, 2020). These bedforms can be related with highly turbulent flows capable of eroding lee sides while depositing on stoss sides. The accumulation of these sediment waves conforms a lenticular-shaped body truncated downslope (Figure 5.13) that change to a MTD (Figure 5.18C). This variation downslope represents a localized instability of this lenticular body as a consequence of the high accumulation of the overlapping sediment waves and the high slope gradient exhibited by the proximal sector of Carchuna Canyon's sediment wave field triggering the formation of the MTD. Instability during channel-levee building has been identified in the upper reaches of other overbank deposits in submarine canyon environments (e.g., Marsset et al., 2022).

The middle reaches of the Carchuna depositional lobe are characterized by fully depositional sediment waves (Figures 5.13 and 5.18E), which signal a loss of erosional capacity, an aggradational state, and high deposition rates (Migeon et al., 2000; Nakajima and Satoh, 2001; Gong et al., 2012; Morris et al., 2014). The accumulation of such sediment waves in the studied depositional lobe, plus their lateral change to sub-parallel lenticular bodies, would suggest the activity of recurring turbidity currents that decrease in flow velocity downslope (Figure 5.18E, F). The absence of sediment waves and the occurrence of an aggradational infilling in the lower reaches of the Carchuna depositional lobe (Figure 5.18H, I) is most likely a consequence of low slope gradients and low turbulence values of turbidity currents, common in such environments (e.g., Stacey et al., 2019).

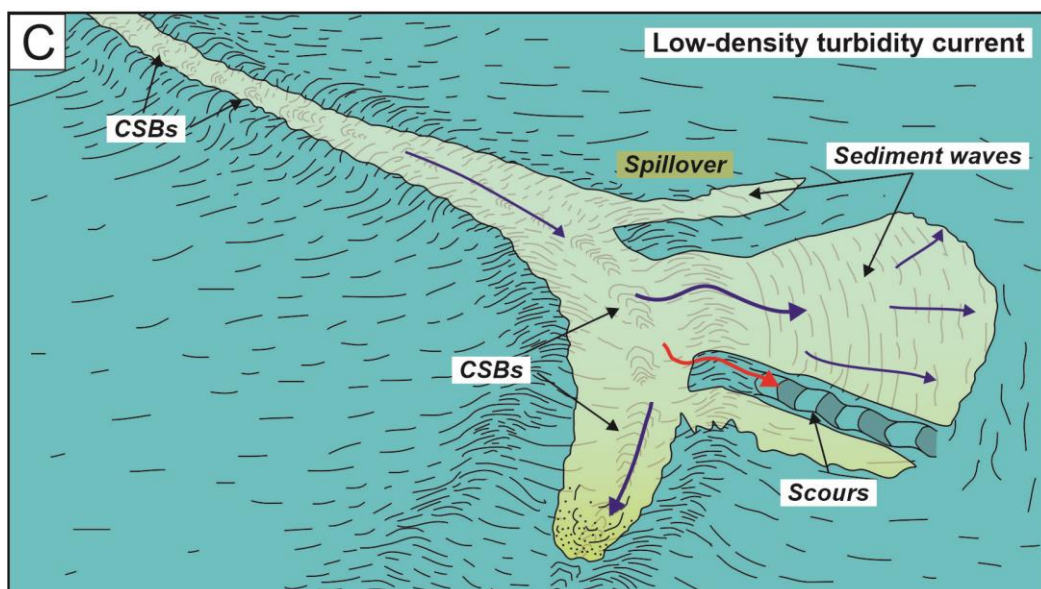
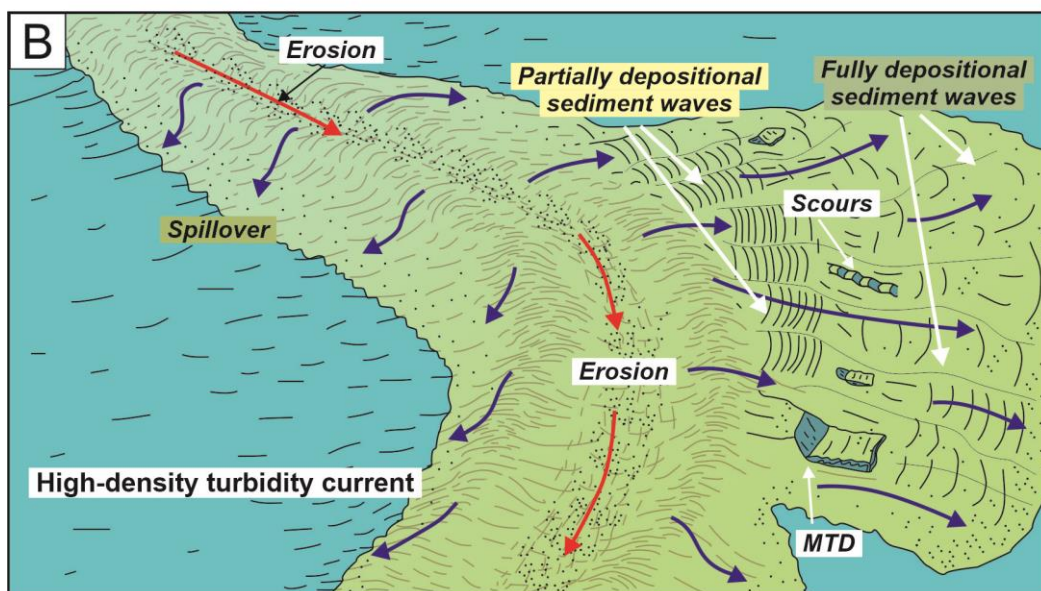
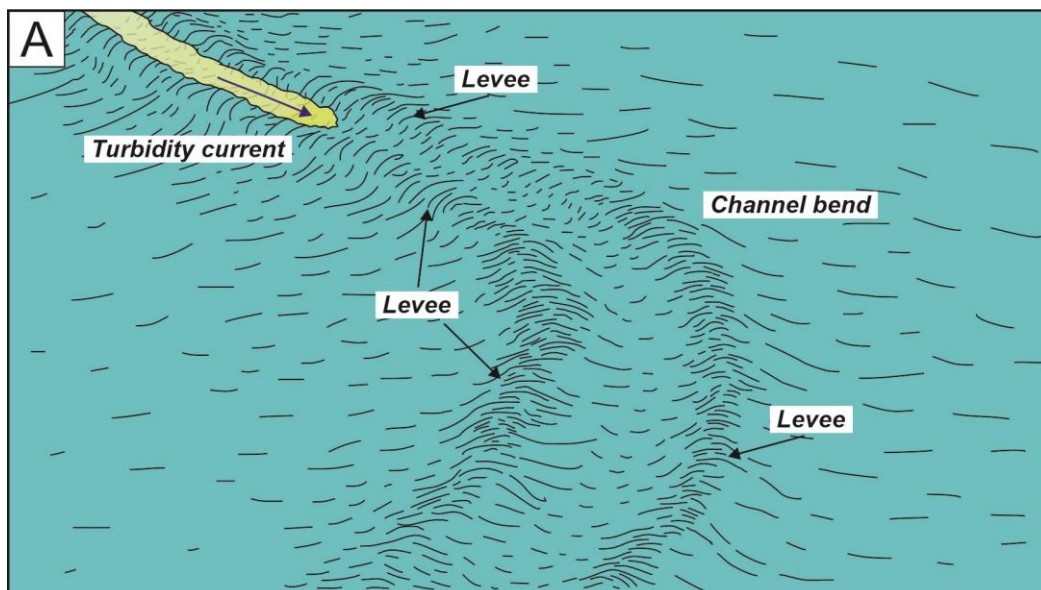


Figure 5.17. Illustration of two different scenarios of downcanyon channelized turbiditic flows descending along the axial channel and approaching the sharp bend in the Carchuna Canyon (A). (B) High-density turbidity currents flowing along the Carchuna Canyon eroding the axial channel, while widespread spillover flows would form along both levees. At the channel bend, heterogeneous deposits resulting from the high-density turbidity currents. (C) Low-density turbidity currents flow along the Carchuna Canyon forming bedforms along the axial channel while spillover processes are localized at the channel bend, forming either depositional or erosional bedforms.

We suggest that acoustic units 4 and 2 are indicative of high-density turbidity current scenarios in the Carchuna Canyon (Figure 5.17B). Under such conditions, the axial channel would be mainly characterized by erosion due to the entrainment of coarse-grained sediments by high-velocity flows, enabling the formation of widespread spillovers along both levees. At the channel bend, abundant overflows would generate an irregular seafloor forming an overbank deposit characterized by heterogeneous deposition and high sedimentation rates. These conditions would lead to a widespread occurrence of sediment waves evolving seaward, from low- to high-aggradational system, in response to the velocity decrease of overflows (Figure 5.17B). The formation of scour trains cannot be discarded (Figure 5.17B), considering that at likely seafloor variability in the overbank deposit could trigger hydraulic jumps. In addition, the irregular slope topography and high depositional rates would be conducive to mass movements eventually forming MTDs (Figure 5.17B).

5.2.3.2. Low-density turbidity current scenario

Sediment drapes in submarine canyon settings can be linked to hemipelagic sediments that exhibit transparent acoustic facies (e.g., Paull et al., 2013; Tubau et al., 2015a; Covault et al., 2017) or high-amplitude continuous reflections atop acoustic units that define the overbank deposits (e.g., Lewis and Pantin, 2002; Zhu et al., 2010). Alternatively, drape units can be the sedimentary product of fine-grained turbidity currents (Covault et al., 2014), which tend to develop sediment waves in overbank deposits (e.g., von Lom-Keil et al., 2002; Migeon et al., 2006; Scacchia et al., 2022). In this sense, the depositional lobe of Carchuna Canyon exhibits two acoustic units (3 and 1) mainly characterized by transparent acoustic facies (Figures 5.12 and 5.13) with undulating tops interpreted as sediment waves (Figure 5.12 and 5.13). Considering such an arrangement, we infer that both transparent acoustic units are linked to low-density turbidity currents depositing fairly homogeneous fine-grained sediments.

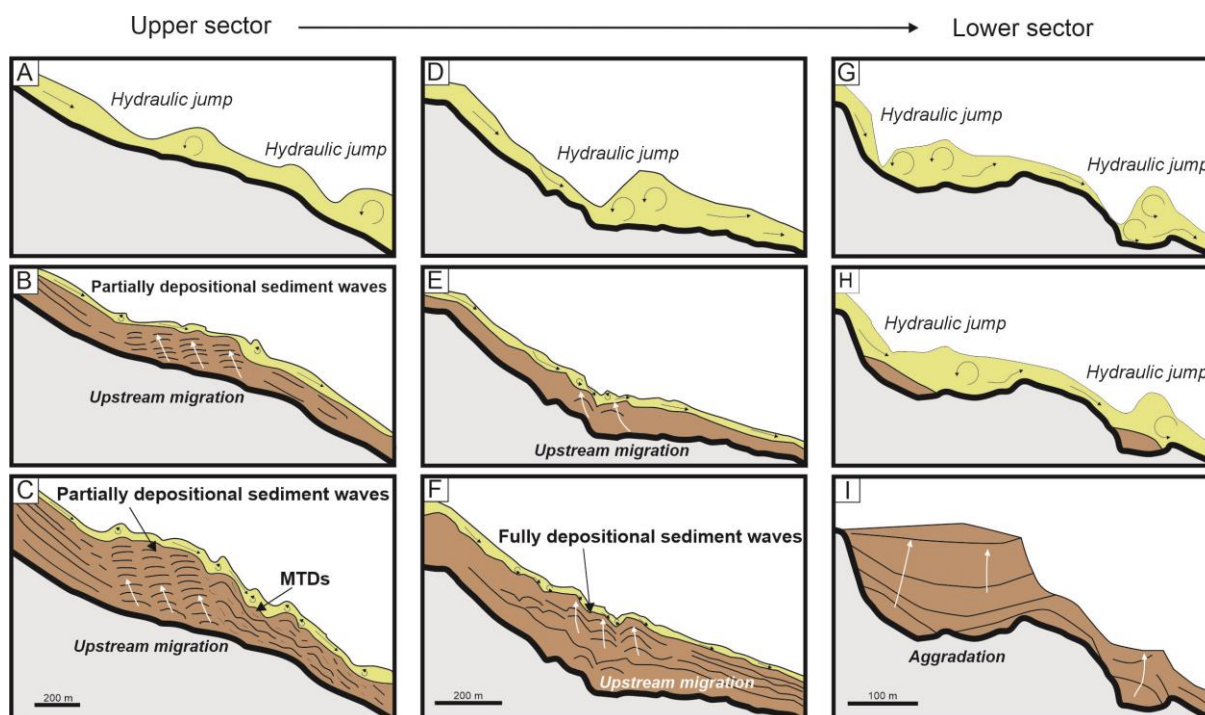


Figure 5.18. Downslope deposit evolution resulting from high-density turbidity currents moving from the upper to lower sector of the Carchuna depositional lobe over pre-existing irregular surfaces (A, D, and G). (A-C) Evolution model of the fill of the ancient seafloor in the upper sector characterized by partially depositional sediment waves truncated downstream by MTDs likely due to the steep slope gradient. (D-F) Evolution model of the fill of the ancient seafloor in the middle reaches of the depositional lobe characterized by fully depositional sediment waves; distally, sub-parallel bodies indicate the decrease in flow velocities of turbidity currents. (G-I) Evolution model of the fill of the ancient seafloor in the lower sector, where aggradational deposits evidence the low velocities of turbidity currents in this sector of the depositional lobe.

In low-density turbidity current scenarios in the Carchuna Canyon setting (Figure 5.17C), coarse-grained sediments would be mainly limited to the axial channel and would contribute to the generation of confined CSBs. The finer sediment fractions, in contrast, could be transferred along localized depressed stretches of the levee by top spillover currents, subsequently contributing to growth of the overbank deposit. Energetic and episodic transport pulses would exceed the levee crest in the channel bend, forming scour trains. A low-density turbidity current scenario could be active at present, considering that: (1) both CSBs and sediment waves developed in the overbank deposit are migrating today, suggesting the occurrence of repetitive turbidites along the Carchuna Canyon; (2) hemipelagic drapes have been not identified over the overbank deposits.

5.3. Conclusions

Detailed analysis of bedform distribution and morphology along the Carchuna Canyon, on the northern margin of the Alboran Sea, stands as a contribution to cataloguing bedform genesis in submarine canyons worldwide and to understanding the role of sedimentary activity of submarine canyons in bedform generation. The main conclusions of this study are:

1. The shelf-incised Carchuna Canyon exhibits recent sedimentary activity, evidenced by net-erosional and net-depositional cyclic steps, depending on the confined/unconfined nature of the flows. The occurrence of crescentic-shaped bedforms (CSBs) (confined cyclic steps) in the axial channel of the Carchuna Canyon suggests the influence of confined sediment-laden gravity flows characterized by coarse-grained sediments descending along the channel. The variation in morphometric parameters of CSB sets along the axial channel is indicative of flow behavior variability, in turn dependent on local slope gradients that induce flow accelerations and local increases in sediment concentration.
2. Unconfined spillover flows may be generated in a sharp channel bend in the lower canyon segment, eventually triggering the formation of two types of bedforms over the depositional lobe. The occurrence of depressed stretches of the levee crest favor a spillover along the channel bend and the formation of sediment waves, likely indicating recurring stripping by fine-grained turbidity currents. In contrast, more energetic and occasional downstream turbidity flows would exceed the levee crest at the channel bend to focus the overflow and favor the erosion of the overbank deposit in terms of scour trains.
3. The overbank deposits grew by means of the alternance of turbidity currents, which exhibit two contrasting patterns —likely suggesting a periodic temporal change in the behavior of the canyon as a sediment transport system. High-density turbidity currents flowing downstream would favor erosion along the axial channel and a widespread spillover flow of coarse-grained sediments, giving rise to the formation of a complex arrangement of deposits and morphologies having a marked bathymetric zonation. MTDs, low-aggradational sediment waves and erosive features preferentially occur in the upper reaches, evolving downslope to fully depositional sediment waves and distal aggradation. In contrast, under the dominance of low-density turbidity currents, limited coarse-grained sediment deposition would occur along the Carchuna Canyon axial channel, whereas spillover processes would be localized along the channel bend.

Chapter 6

Origin and driving mechanisms of marine litter in the shelf-incised Motril, Carchuna, and Calahonda canyons

This chapter have been published in *Frontiers* as:

^{1,2}Cerrillo-Escoriza, J., ¹Lobo, F.J., ²Puga-Bernabéu, Á., ³Rueda, J.L., ³Bárcenas, P., ³Sánchez-Guillamón, O., ³Serna Quintero, J.M., ³Pérez Gil, J.L., ²Murillo, Y., ³Caballero-Herrera, J.A., ²López-Quirós, A., ⁴Mendes, I., ²Pérez-Asensio, J.N. Origin and driving mechanisms of marine litter in the shelf- incised Motril, Carchuna, and Calahonda canyons (northern Alboran Sea). *Front. Mar. Sci.* 10, 1–24. <https://doi.org/10.3389/fmars.2023.1098927>

¹Department of Marine Geosciences, Instituto Andaluz de Ciencias de la Tierra (CSIC-UGR), Armilla, Granada Spain, ²Departamento de Estratigrafía y Paleontología, Facultad de Ciencias, Universidad de Granada, Granada, Spain, ³Instituto Español de Oceanografía, Centro Oceanográfico de Málaga (IEO-CSIC), Fuengirola, Málaga, Spain, ⁴Department of Geoscience, Aarhus University, Aarhus, Denmark, ⁴Centro de Investigação Marinha e Ambiental (CIMA), Universidade do Algarve, Faro, Portugal,

Abstract

Marine litter density, distribution and potential sources, and the impact on canyon seafloor habitats were investigated in the Motril, Carchuna and Calahonda canyons. Canyon floor imagery was collected by a Remotely Operated Vehicle along 5 km in the Motril Canyon, 10 km in the Carchuna Canyon, and 3 km in Calahonda Canyon, together with 41 surficial sediment samples. Additionally, coastal uses, maritime traffic and fishing activity data were analyzed. A 50 m resolution multibeam bathymetry served as base map.

In the Motril and Calahonda canyons, the density of marine litter was low and the material was dispersed, very degraded and partially buried. In contrast, the Carchuna Canyon contained a greater amount and variety of litter. The Carchuna Canyon thalweg exhibited a density of marine litter up to $8.66 \text{ items} \cdot 100 \text{ m}^{-1}$, and litter hotspots with a density of up to $42 \text{ items} \cdot \text{m}^2$ are found along the upper reaches of the canyon thalweg.

Low litter abundances found in the studied canyons most likely reflect low population densities and the absence of direct connections with streams in the nearby coasts. The high shelf incision of the Carchuna Canyon and its proximity to the coastline favor littoral sediment remobilization and capture as well as the formation of gravity flows that transport the marine litter along the thalweg toward the distal termination of the channel. Litter hotspots are favored by the canyon morphology and the occurrence of rocky outcrops. Most debris is of coastal origin and related to beach occupation and agricultural practices in the adjacent coastal plain. A third origin was represented by fishing gear in the study area. Fishing activity may be producing an impact through physical damage to the skeletons of the colonial scleractinians located in the walls of the Carchuna Canyon. In contrast, the Motril and Calahonda canyons can be considered passive systems that have mainly acted as depositional sinks in the recent past, as evidenced by buried marine litter.

6.1. Results

6.1.1. Overall geomorphology and sedimentology of submarine canyons

The shelf in the study area is up to 3 km wide, narrowing due to the occurrence of shelf-incised canyon heads (Figure 6.1). Shelf surface sediments vary from coarse silts close to fine sands on the shelf edge (Figure 6.1).

Three geomorphological segments were identified in the Motril Canyon. The upper segment is defined by a 4.3 km wide amphitheater-like canyon head incised in the outer shelf and upper slope. The canyon head is located 2 km off the coastline and connects to a 950 m long and 140 m wide short and straight shelf channel (Figure 6.1). The canyon valley is bounded by gentle flanks (ca. 3°), and it widens and increases in sinuosity downward to 400 m water depth. Surface sediment grain size decreases down the canyon thalweg, from very fine sands to medium silts (Figure 6.1). The middle segment is characterized by an abrupt change in the direction of the valley from N-S to NW-SE down to 500 m water depth. The canyon valley shows a sinuous path with a gentle south-western flank (ca. 2°), whereas the north-eastern flank is steeper (ca. 8°) (Figure 6.1). The lower segment is characterized by a meandering channel limited by steep walls with continuous adjacent deposits over the slope.

Two geomorphological segments were identified in the Carchuna Canyon. In the upper segment, the canyon is deeply incised in the shelf, as its head is located just 200 m off the coastline. It is characterized by a 100 m wide narrow axial channel with large steep flanks (Figure 6.1). The straight canyon increases its width up to 430 m water depth and it is bounded by a narrow and steep eastern flank and large terraces in the western flank. The axial channel in the upper segment is characterized by fine sands in the canyon head that change downslope to coarse silts, while the flanks are characterized by fine sands (Figure 6.1). The landward tip of the lower segment is marked by an abrupt change of orientation of the canyon from NE-SW to WNW-ESE. This lower segment has a straight and wide valley (up to 550 m) bounded by steep walls (ca. 20°) and continuous lateral slope deposits. Grain sizes in the lower segment range from very fine sands in the axial channel to medium silts in lateral deposits (Figure 6.1).

Two geomorphological segments were identified in the Calahonda Canyon. In the upper segment, the canyon incises the shelf edge, where the canyon head is located 2.5 km off the coastline (Figure 6.1). The canyon head is 150 m wide at the shelf edge and has steep flanks. In the lower segment, the canyon exhibits a meandering pattern and is bounded by smooth

flanks. The axial channel is characterized by fine sands in the canyon head that change downslope to medium silts, while the eastern flank is characterized by fine sands (Figure 6.1).

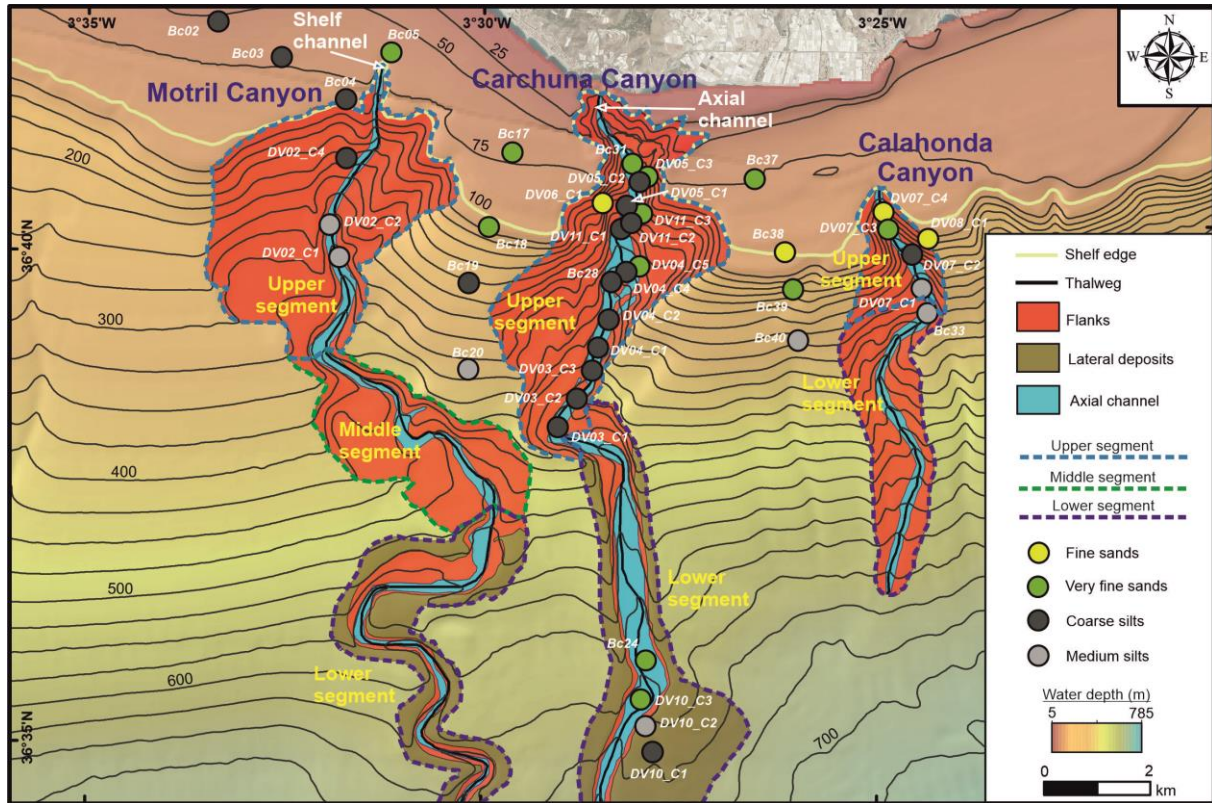


Figure 6.1. Geomorphologic map of the Motril, Carchuna and Calahonda submarine canyons showing the segment distribution within each canyon and the texture of surficial sediment samples. Bathymetric contours in meters. See Supplementary Table S1 in which location and depth of the sediment cores sampled for grain size analysis are included.

6.1.2. Marine litter distribution

A total of 454 litter items were observed in the 11 ROV video dives (Figure 6.2; Table 6.1). Plastics predominate (almost 75% of occurrences), and they include bottles, bags, fishing nets, sheets, seedbeds and other objects with sizes from centimeters to meters. Other minor components of marine litter in the studied canyons include metal items, building material, and rubber items (Figures 6.2A and 6.3). Overall, the marine litter is partially buried, covered by a thin layer of mud and in a degraded state.

Table 6.1.

Summary of ROV dives used in this study including their water depth range, length, the amount of litter detected, litter density and the percentage of plastic litter recorded in each dive. (T: canyon thalweg; F: canyon flank; D: lateral deposit).

| Dive | Submarine canyon | Date | Coordinates | | | | Water depth range (m) | | Transect length (m) | Litter items | Litter density (items·100 m ⁻¹) |
|--------|------------------|--------------------------|--------------|---------------|--------------|---------------|-----------------------|-----|---------------------|--------------|---|
| | | | Start | | End | | Min | Max | | | |
| | | | Latitude (N) | Longitude (W) | Latitude (N) | Longitude (W) | | | | | |
| 01-02a | Motril (T) | 08/30/2019 08/31/2019 | 36°39'6.17" | 3°31'53.53" | 36°40'22.14" | 3°31'57.78" | 294 | 388 | 2534 | 3 | 0.12 |
| 02b | Motril (F) | 08/31/2019 | 36°40'22.14" | 3°31'57.78" | 36°41'30.35" | 3°31'21.2" | 106 | 294 | 2520 | 13 | 0.52 |
| 07 | Calahonda (T) | 09/04/2019 | 36°39'36.69" | 3°24'26.64" | 36°40'26.82" | 3°24'57.28" | 152 | 324 | 1860 | 21 | 1.13 |
| 08 | Calahonda (F) | 09/04/2019 | 36°39'42.71" | 3°24'24.27" | 36°40'9.34" | 3°24'22.55" | 127 | 316 | 1055 | 2 | 0.19 |
| 03-04 | Carchuna (T) | 09/01/2019 09/02/2019 | 36°38'5.05" | 3°29'6.63" | 36°39'51.57" | 3°28'1.48" | 313 | 480 | 4407 | 382 | 8.66 |
| 05a | Carchuna (T) | 09/03/2019 | 36°40'21.57" | 3°28'16.59" | 36°40'42.01" | 3°28'5.25" | 227 | 283 | 715 | 3 | 0.42 |
| 05b | Carchuna (F) | 09/03/2019 | 36°40'42.01" | 3°28'5.25" | 36°40'47.01" | 3°27'50.76" | 120 | 150 | 552 | 12 | 2.3 |
| 11 | Carchuna (F) | 09/06/2019 | 36°40'10.58" | 3°28'20.52" | 36°40'33.27" | 3°27'44.15" | 107 | 307 | 1420 | 5 | 0.35 |
| 6 | Carchuna (F) | 09/03/2019 | 36°40'24.31" | 3°28'25.14" | 36°40'31.15" | 3°28'31.31" | 140 | 260 | 374 | 7 | 1.87 |
| 10a | Carchuna (D) | 09/05/2019 | 36°34'49.56" | 3°27'50.61" | 36°35'12.73" | 3°27'55.28" | 624 | 649 | 878 | 1 | 0.11 |
| 10b | Carchuna (T) | 09/05/2019 | 36°35'20.02" | 3°27'56.12" | 36°35'27.96" | 3°27'57.24" | 631 | 636 | 510 | 2 | 0.40 |
| 09 | Carchuna (T) | 09/05/2019 | 36°31'56.02" | 3°29'6.19" | 36°32'28.39" | 3°29'15.70" | 730 | 740 | 1016 | 3 | 0.30 |

The lowest average abundances of litter were found in the Motril and Calahonda canyons (Figures 6.1B, and 6.2; Table 6.1). In the Motril Canyon, the litter density along the thalweg was 0.12 items·100 m⁻¹. A higher litter density (0.52 items·100 m⁻¹) was observed along the western flank of the canyon (Figure 6.3). Marine litter in the upper segment of the Motril Canyon included plastics (60%), metals (6.67%), and unspecified items (33.33%) (Figures 6.2B and 6.3). The litter appeared dispersed, degraded and frequently broken, both in the thalweg (Figure 6.4A) and the western flank.

In the Calahonda Canyon, litter density was higher along the thalweg (1.13 items·100 m⁻¹) than in the eastern flank (0.19 items·100 m⁻¹) (Figure 6.3; Table 6.1). Marine litter in the Calahonda Canyon was composed of plastics (almost 70%), metals, building material, and unspecified items in the upper segment of the canyon (Figures 6.2C and 6.3). Marine litter generally occurred as 2-5 item accumulations (Figure 6.4B) or dispersed along the thalweg and eastern canyon flank. Marine litter on the seafloor was found degraded and partially buried.

The highest litter abundance was detected in the Carchuna Canyon (Figures 6.2D and 6.3; Table 6.1). Litter densities along the flanks of the upper segment varied between 0.35 and 2.3 items·100 m⁻¹. The highest litter density was detected along the thalweg in the upper canyon with 8.66 items·100 m⁻¹. In contrast, the lowest densities of marine litter occurred in the lower canyon up to 0.35 items·100 m⁻¹ in the thalweg and the lateral deposits (Figure 6.3). In the Carchuna Canyon, marine litter was made up of plastics (almost 76%), metals, building

material, rubber, and unspecified items (Figures 6.2D and 6.3). Plastic items mainly included bottles, fishing nets, bags, sheets, and seedbeds (Figures 6.2D and 6.3). Marine litter on the flanks was composed of plastics such as fishing nets (Figure 6.4C), and dispersed and degraded building items (Figure 6.4D). In the lower canyon, marine litter was largely composed of very degraded and buried plastic items.

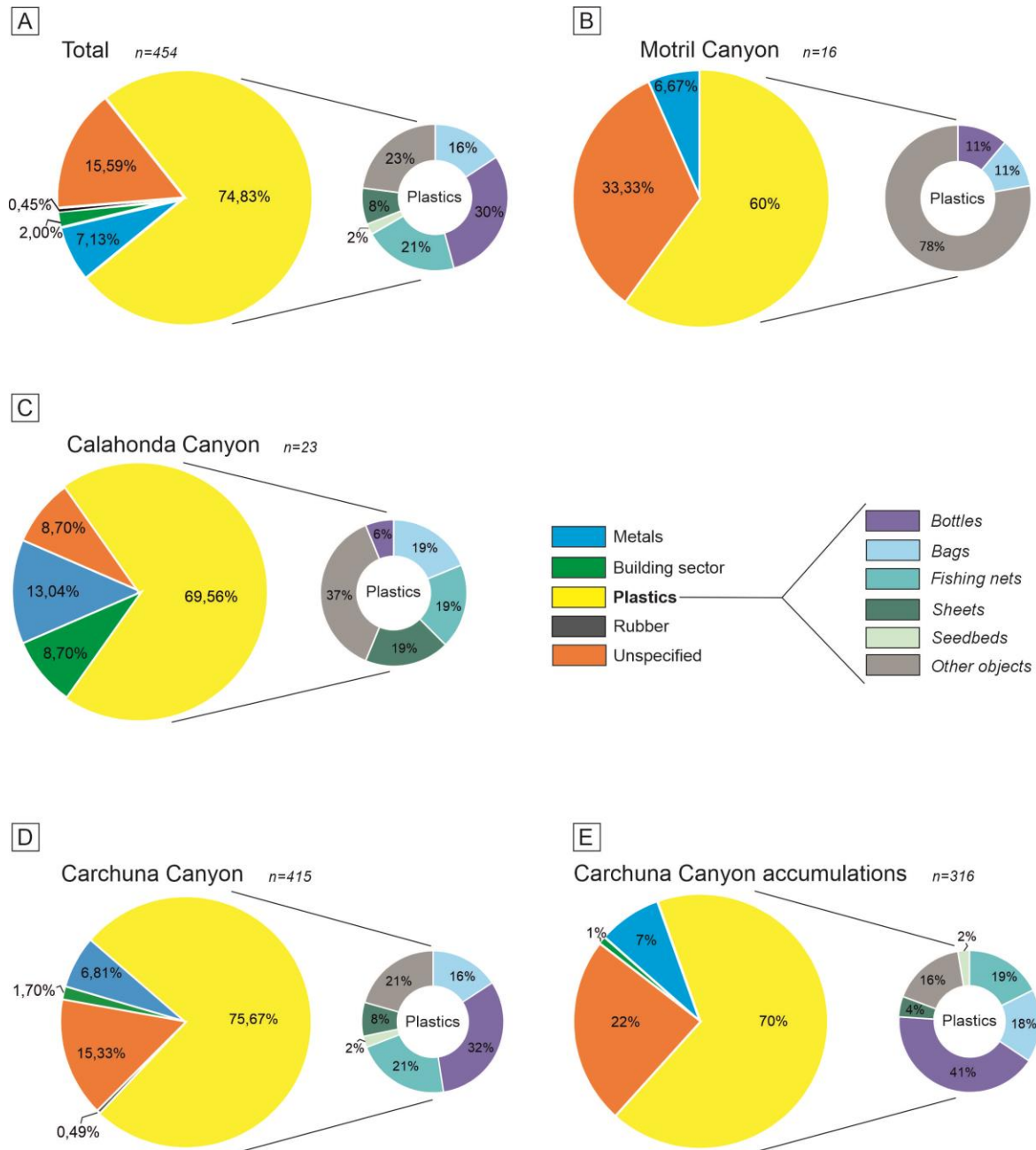


Figure 6.2. Litter composition in the three studied submarine canyons. Percentages of litter items are divided into five litter categories and six plastic subcategories as defined by the Guidance on Monitoring of the Marine Litter in the Mediterranean Sea (European Commission of the European Union, 2013): (A) studied submarine canyons; (B) upper segment of Motril Canyon; (C) upper segment of Calahonda Canyon; (D) Carchuna Canyon; and (E) Carchuna Canyon accumulations. n: total number of litter items counted.

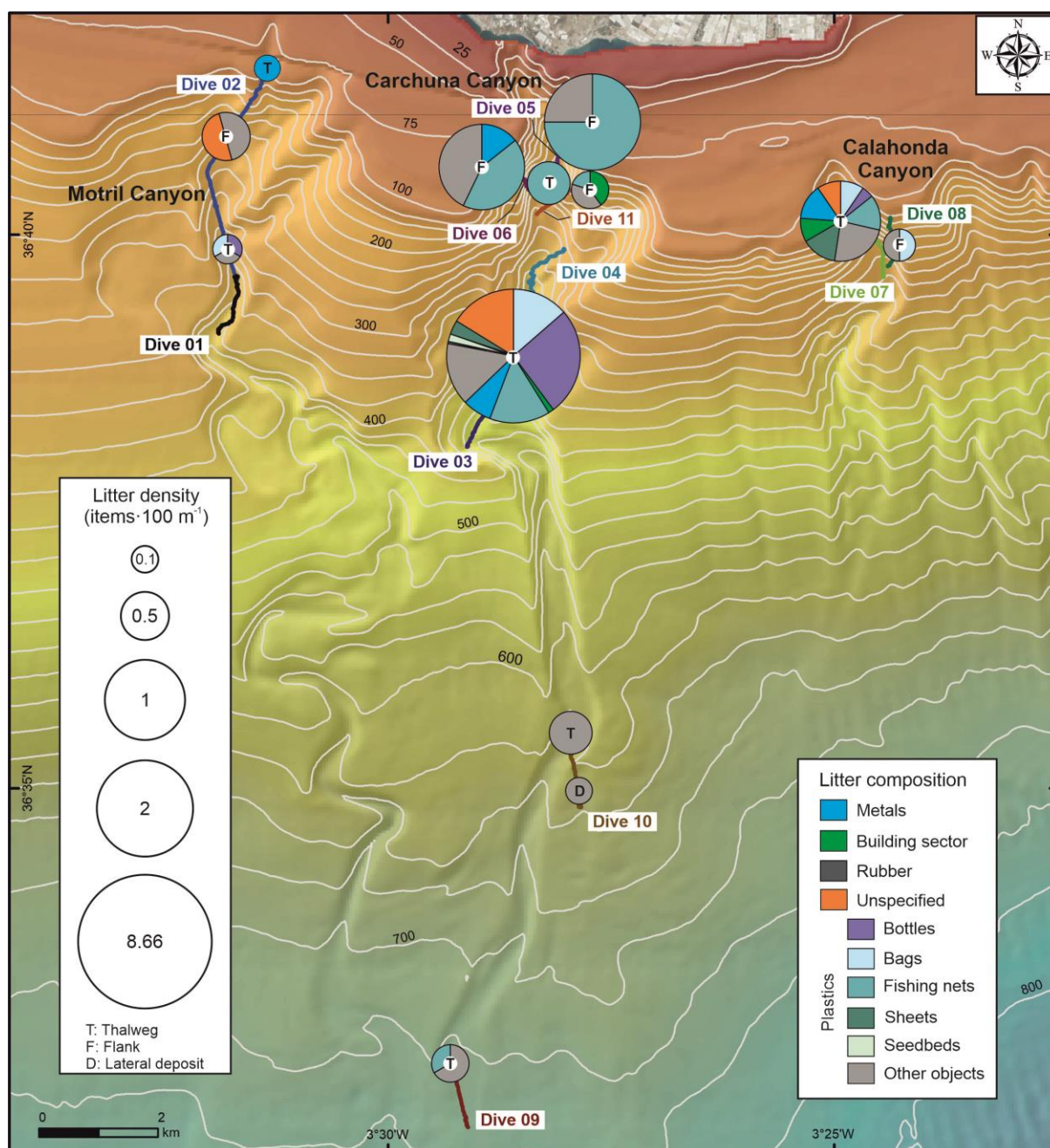


Figure 6.3. Spatial distribution and composition of marine litter along the canyon thalwegs and flanks of the three studied submarine canyons. The size of the pie charts is proportional to the abundance of litter (expressed as number of items·100 m⁻¹). The maximum litter density (8.66 items·100 m⁻¹) was found in the thalweg of the Carchuna Canyon. Bathymetric contours in meters.

In the Carchuna Canyon, marine litter mainly occurred as large accumulations or litter hotspots of up to 6 m² (Accumulations 17, 18, and 20) in extent or containing up to 42 items·m⁻² (Accumulation 19) (Table 6.2) that alternate with isolated items (Figure 6.4E). Three different types of accumulations were observed along the canyon thalweg: (1) marine litter accumulated in smooth canyon floor depressions (Figure 6.4F); (2) marine litter

accumulated by rocky floor blocking (Figure 6.4G); (3) marine litter accumulated by tangling of fishing nets (Figure 6.4H). These accumulations were composed of plastics (70%), metals, building material, and unspecified items (Figure 6.2E) and they were detected along the canyon thalweg between 339-493 m water depths (Figure 6.5). Overall, the marine litter accumulations appeared degraded and partially buried.

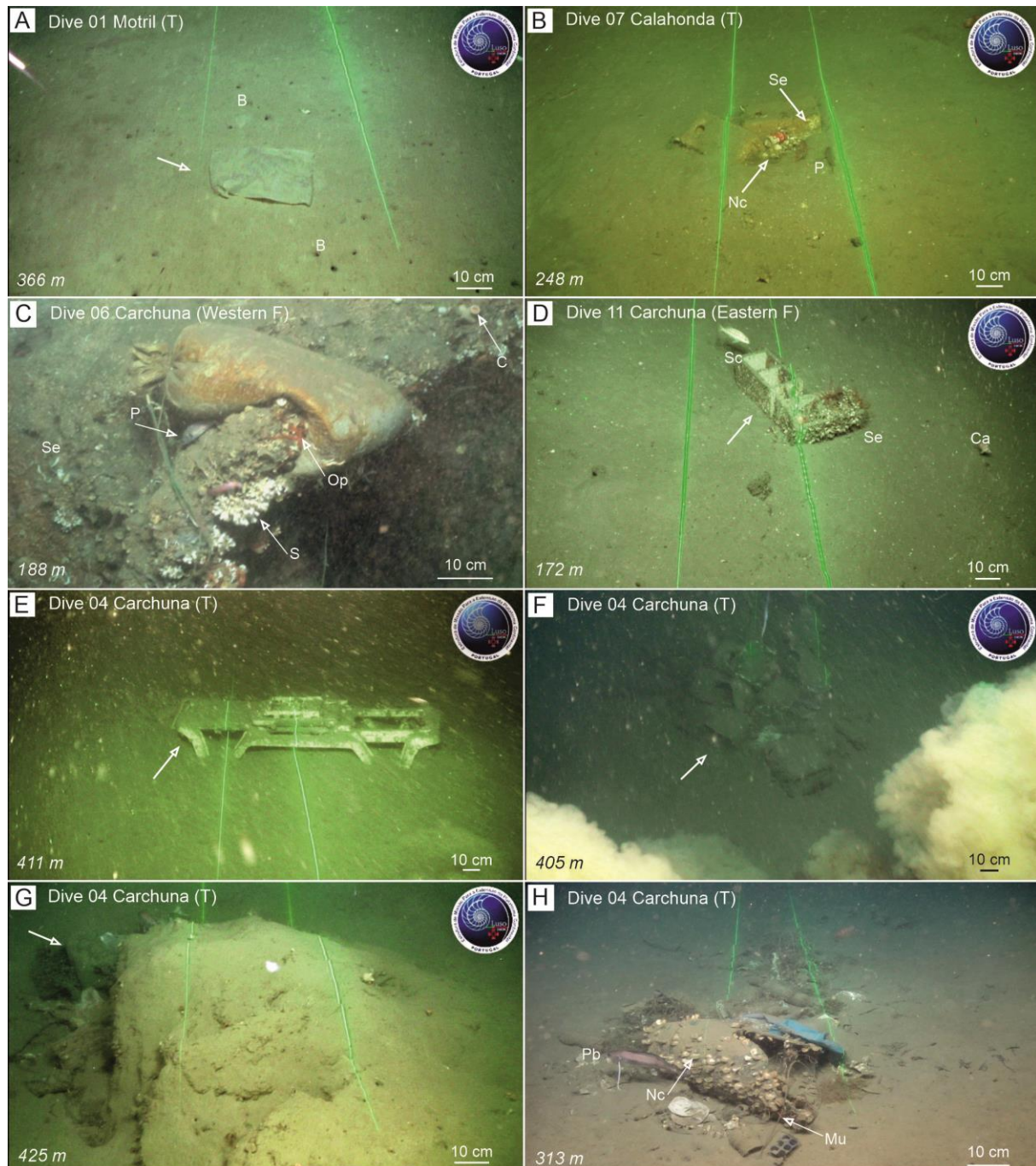


Figure 6.4. Examples of litter items observed during ROV dives in the Motril, Calahonda, and Carchuna canyons, and litter accumulations found in Dive 04 along the thalweg of the Carchuna Canyon. Dive number, water depth and relative location within the canyons (T: canyon thalweg; F: canyon flank) are indicated. (A) Plastic bag (arrow) on the thalweg of the Motril Canyon. (B) Two concrete blocks used in longline fishing as weights, colonized by serpulid polychaetes and *N. cochlear* aggregations, together with two *P. bogaraveo* individuals as well as a soda can and small plastic fragments on the thalweg of the Calahonda Canyon. (C) A filled plastic bag (used as weight in longline fishing) on rocks colonized by unidentified colonial scleractinians, serpulid polychaetes and *Ophiotrix* sp., together with individuals of the black-spot seabream *Pagellus bogaraveo* (one of the target species of longline fishing). (D) Two bricks colonized by serpulids on the eastern flank of the Carchuna Canyon, with some fishes (*Serranus cabrilla* and *Capros aper*). (E) Sunbed over the seafloor on the thalweg of the Carchuna Canyon. (F) Accumulation characterized by a large number of bottles. (G) Accumulation composed of bottles, bags and fishing nets blocked behind a seafloor rocky outcrop. (H) Accumulation with bricks, a broken sheet, various bags and bottles, fishing nets, a metal tube and diverse plastic items, some of them colonized by *N. cochlear*, but also providing shelter to the greater forkbeard *Phycis blennoides* and *Munida* sp. B: Burrows made by decapods; C: *Caryophyllia* sp.; Ca: *Capros aper*; Mu: *Munida* sp.; Nc: *Neopycnodonte cochlear*; Op: *Ophiothrix* sp.; P: *Pagellus bogaraveo*; S: Scleractinians; Sc: *Serranus cabrilla*; Se: Serpulid polychaetes.

Table 6.2.

Characterization of litter accumulations found in the Carchuna Canyon in terms of extent, item density and number of items.

| Accumulation number | Size (m ²) | Density (items·m ⁻²) | Items |
|---------------------|------------------------|----------------------------------|-------|
| 1 | 0.8 | 15 | 12 |
| 2 | 0.72 | 2.78 | 2 |
| 3 | 0.96 | 7.29 | 7 |
| 4 | 0.64 | 4.68 | 3 |
| 5 | 0.72 | 27.7 | 20 |
| 6 | 0.24 | 33.3 | 8 |
| 7 | 4 | 9.5 | 38 |
| 8 | 3 | 7.67 | 23 |
| 9 | 3 | 3.33 | 10 |
| 10 | 2.5 | 3.2 | 8 |
| 11 | 0.3 | 20 | 6 |
| 12 | 4.5 | 2.89 | 13 |
| 13 | 3.6 | 5 | 18 |
| 14 | 1 | 30 | 30 |
| 15 | 0.4 | 5 | 2 |
| 16 | 4 | 4.75 | 19 |
| 17 | 6 | 2.17 | 13 |
| 18 | 6 | 3.83 | 23 |
| 19 | 0.5 | 42 | 21 |
| 20 | 6 | 6.67 | 40 |

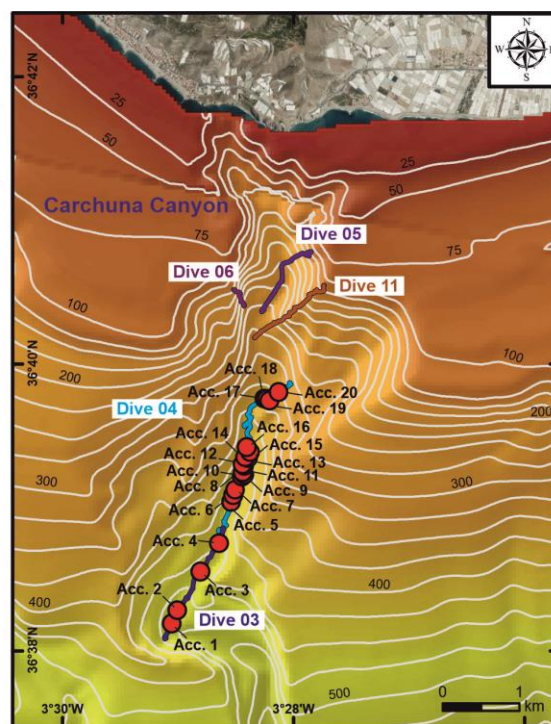


Figure 6.5. Zoomed-in bathymetric map of the study area ("Ministerio de Pesca, Agricultura y Alimentación", Spanish government) showing the location of the litter accumulations found in the Carchuna Canyon, Bathymetric contours in meters.

6.1.3. Other seafloor bottom anthropogenic marks

Ten straight, regular, and continuous bottom trawling marks were detected on the seafloor of the studied canyons: six in the Motril Canyon (370-180 m water depths), two in the Carchuna Canyon (450-400 m water depths), and two in the Calahonda Canyon (290 m water depth) (Supplementary Table S2). These marks were more frequent in the thalweg and the western flank of the Motril Canyon, but they were also detected in the thalwegs of Calahonda and Carchuna canyons (Figure 6.6A, B). Some bottom trawling marks exhibited a well-defined groove having straight marks with an extensive and lateral continuous mound (Figure 6.6A). In some places, irregular broken fragments of organisms were observed over the muddy seafloor of the grooves (Figure 6.6A). Other mark types were smoother, comprising various parallel lines with straight margins, which may correspond to marks of the weights attached to the bottom part of the opening of bottom trawling nets (Figure 6.6B).

6.1.4. Anthropogenic activity regarding the main seafloor habitats

A total of 13 habitat types have been detected in the 11 ROV video dives, however, 6 of those habitats may represent facies of the detected habitats but occur at different depths (e.g., Circalittoral and bathyal detritic bottom vs. Bathyal detritic bottom with bivalve and cold-water coral remains) and sediment types (e.g., Bathyal muddy sand and sandy mud bottom with burrowing megafauna vs. Bathyal sandy silt bottom with burrowing megafauna). The detected habitats ranged from highly complex ones with a high biogenic component (e.g., Bathyal rocky bottom with scleractinians) to habitats with low complexity and low biogenic component (e.g., Bathyal sandy mud bottom with burrowing megafauna) (Figures 6.6 and 6.7). Regarding the main habitats detected, the most common ones in the explored canyons (based on their length along the analysed video transects) were: (1) bathyal muddy sand and sandy mud bottom with burrowing megafauna (including the different facies) (Total Length = 8420 m, %Length of all habitats = 50.4%); (2) circalittoral and bathyal sandy silt bottoms with alcyonaceans (mainly dominated by *Alcyonum palmatum*) (2964 m, 17.7%) (Figure 6.6C); (3) bathyal sandy silt bottoms with ceriantharians (1739 m, 10.4%) (Figure 6.6D); (4) bathyal sandy mud and muddy sand with ceriantharians and *Funiculina quadrangularis* (mainly dominated by *Cerianthus* spp.) (1279 m, 7.7%) (Figure 6.6E); and (5) circalittoral and bathyal detritic bottom (1154 m, 6.9%). Data on the length of the different habitats and their facies as well as the percentage of the habitat length within each dive and submarine

canyon are given in Figure 6.7, together with annotations of the main dominant taxa of each habitat.

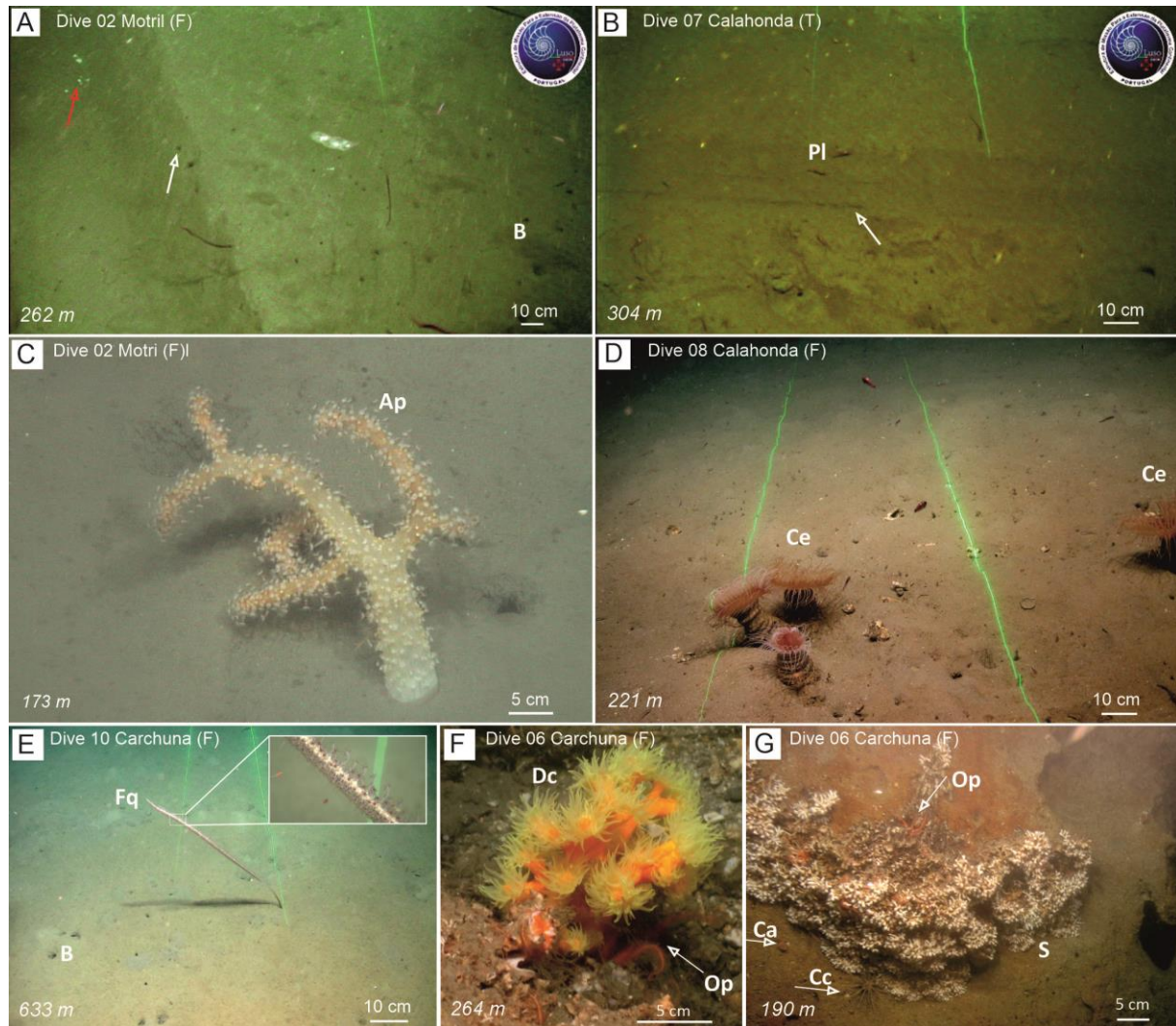


Figure 6.6. Examples of seafloor trawling marks observed during ROV dives along the flank of the Motril Canyon (A) and the thalweg of the Calahonda Canyon (B), and benthic and demersal fauna detected in the Motril (C), Calahonda (D) and Carchuna (E-G) canyons. (A) Seafloor groove made by the otter board of a bottom trawling gear with broken fragments (red arrow) and a lateral mound (white arrow) on the western flank of the Motril Canyon. (B) Seafloor groove made by the otter board of a bottom trawling gear on the thalweg of the Calahonda Canyon. The bottom trawling marks seen on video footage collected by the ROV in the three submarine canyons is shown in Figure 6.9D. (C) The soft octocoral *Alcyonium palmatum*. (D) Aggregation of the cerianthiid *Cerianthus* sp. (E) Muddy bottoms with decapod burrows and the sea-pen *Funiculina quadrangularis*, with a detail of its polyps. (F) The colonial scleractinian *Dendrophyllia cornigera* providing shelter to the ophiurid *Ophiothrix* sp. (G) Aggregation of unidentified colonial scleractinians, together with solitary *Caryophyllia* sp. and individuals of the echinoid *Cidaris cidaris* and the ophiuroid *Ophiothrix* sp. Legend: Ap: *Alcyonium palmatum*; B: Burrows made by decapods; Ca: *Caryophyllia* sp.; Cc: *Cidaris cidaris*; Ce: *Cerianthus* sp.; Dc: *Dendrophyllia cornigera*; Fq: *Funiculina quadrangularis*; Op: *Ophiothrix* sp.; Pl: *Plesionika* sp.; S: unidentified colonial scleractinians.

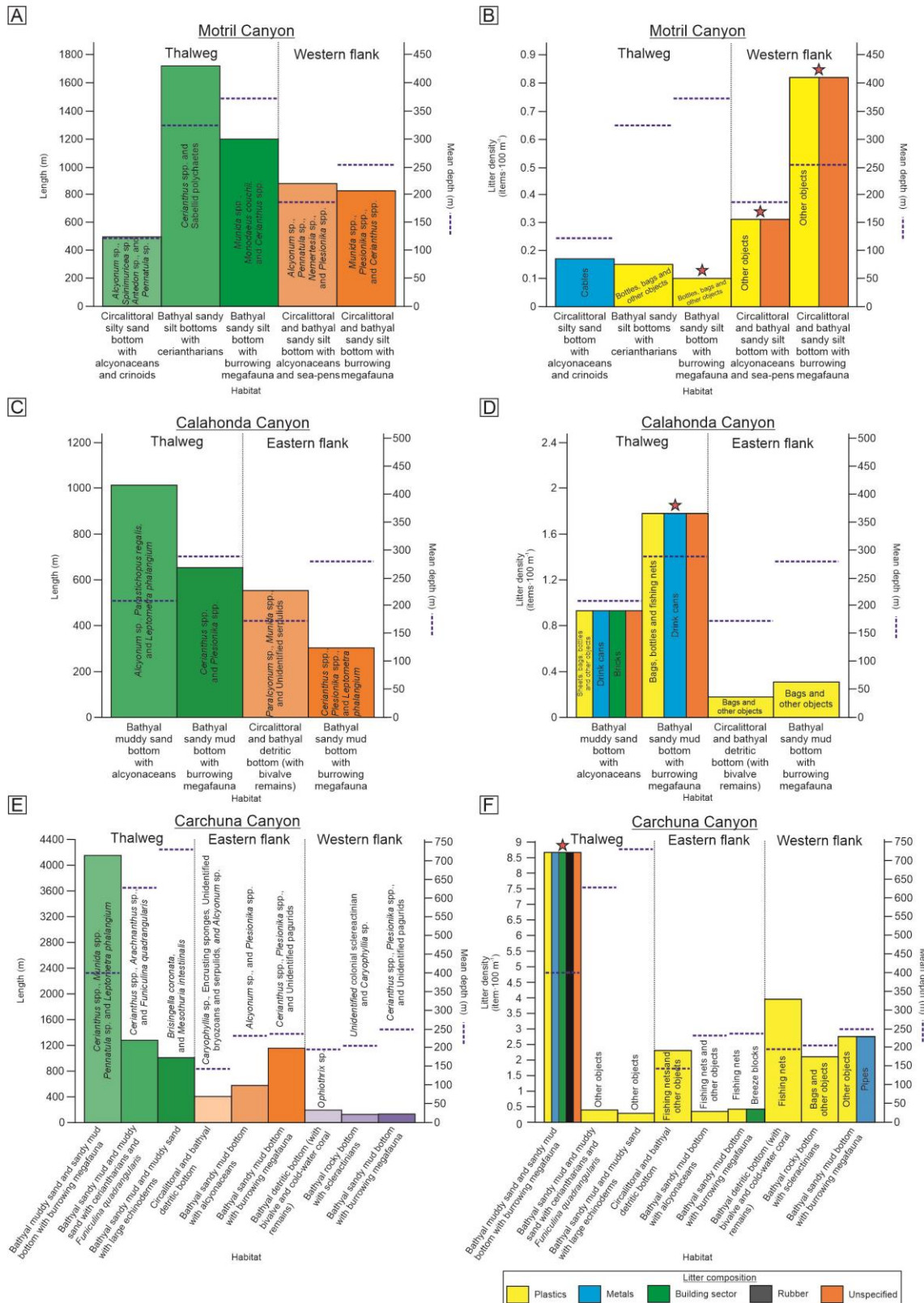


Figure 6.7. Types and length (in ROV underwater image transects) of habitats detected along the Motril (A), Calahonda (C), and Carchuna (E) canyons, with annotations of the dominant taxa and mean water depth (blue dotted line) of each habitat. Litter density and types of litter and other anthropogenic activity indicators along the Motril (B), Calahonda (D), and Carchuna (F) canyons is also shown. Stars indicate the presence of seafloor marks from bottom trawling in a particular habitat.

The habitats that displayed the highest average densities of anthropogenic activity indicators when combining all density values obtained in the same habitat at different canyons and sectors of the canyon (i.e., the 18 km of survey track) were (Figure 6.7): (1) bathyal detritic bottoms (occurring at the head of the three canyons, ca. 100-200 m water depths) (average $2.14 \text{ items} \cdot 100 \text{ m}^{-1}$), which mainly contained plastics and fishing nets; (2) bathyal sandy mud and muddy sand bottoms with burrowing megafauna (generally in the thalwegs of the studied canyons, ca. 200-500 m water depths) ($2.13 \text{ items} \cdot 100 \text{ m}^{-1}$) affected by plastics, bottom trawling marks and fishing nets, among others; and (3) bathyal rocky bottoms with scleractinians (western flank of the Carchuna Canyon head, 193-222 m water depths) ($2.1 \text{ items} \cdot 100 \text{ m}^{-1}$) that mainly contained bags (Figures 6.4C, 6.6F, G, and 6.7). In contrast, the habitats that displayed the lowest average densities of anthropogenic activity indicators were (Figure 6.7): (1) bathyal muddy sand and sandy mud bottoms with alcyonaceans (at the flanks of the three canyons, 100-250 m water depths) (average $0.44 \text{ items} \cdot 100 \text{ m}^{-1}$), mostly containing plastics, bottom trawling marks, cables, and fishing nets; (2) bathyal sandy mud and muddy sand bottoms with large echinoderms as well as bathyal sandy mud and muddy sand bottoms with ceriantharians and *Funiculina quadrangularis* (deep part of the Carchuna thalweg, 630-730 m water depths) ($0.34 \text{ items} \cdot 100 \text{ m}^{-1}$) mainly containing plastics; and (3) bathyal sandy mud bottoms with ceriantharians (Motril and Calahonda canyon thalwegs, 273-377 m water depths) ($0.15 \text{ items} \cdot 100 \text{ m}^{-1}$) with plastics and bottom trawling marks (Figures 6.4, 6.6, and 6.7).

6.1.5. Mapping of the coastal domain

Prevailing land uses along the coasts adjacent to the study area (approximate area of 8706 ha) are agricultural (ca. 48%); farming (ca. 34%) and greenhouses (ca. 13%); scrubs and pastures (ca. 25%); and urban (ca. 8%) (Figure 6.8A). Motril Town is located 2 km north of the coastline, with a population density of $567.68 \text{ people} \cdot \text{km}^{-2}$ (“Instituto de Estadística y Cartografía de Andalucía, Junta de Andalucía”, regional government) and at least 83% of the population residing in the town. Motril Town is surrounded by pastures, industrial infrastructures and greenhouses and crops that extend up to the coastline.

The Motril Canyon head is located 2 km offshore the Port of Motril. The Carchuna Canyon head is located off a small bay limited laterally by beaches, greenhouses and Torrenueva and Carchuna towns. The Calahonda Canyon head is located 2.5 km off the beach of Calahonda Town. The coastline close to the studied canyons is mainly composed of gravel beaches

interrupted by the Port of Motril (200,000 m²) and its surrounding industrial area, some greenhouses (mostly concentrated between Calahonda and Carchuna towns) and urban land uses (Torrenueva, Carchuna and Calahonda towns). The population density in Torrenueva Town is 432 people·km⁻² while Carchuna and Calahonda towns have lower densities (72 and 53 people·km⁻², respectively) (“Instituto de Estadística y Cartografía de Andalucía, Junta de Andalucía”, regional government). Urban land uses on the coastline are typical of a touristic area, with summerhouses and various commercial uses, absorbing a duplication in population during summer that causes a triplication of urban litter (Ayuntamiento de Motril. Medio Ambiente Urbano, 2021).

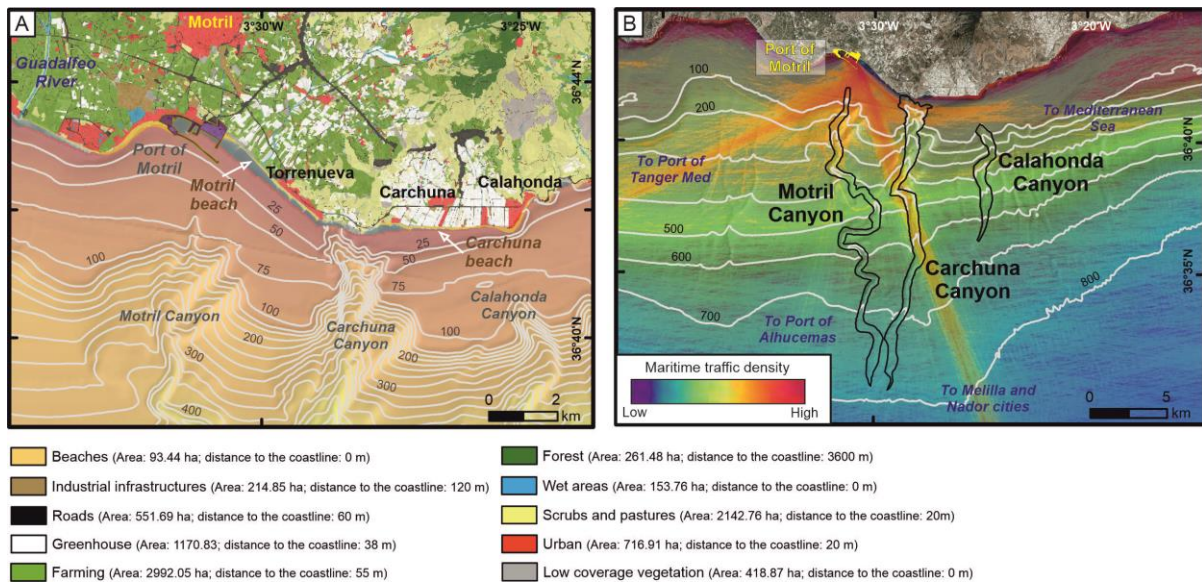


Figure 6.8. Depiction of coastal uses and maritime traffic in the study area. (A) Mapping of main land uses in the adjacencies of the three studied submarine canyons (“Consejería de Agricultura, Ganadería, Pesca y Desarrollo Sostenible, Junta de Andalucía”, regional government). The area and the minimum distance to the coastline of each land use are shown in the legend. (B) Density (number of routes·0.08 km⁻²·y⁻¹) of maritime traffic in 2018 (www.marinetraffic.com) with the drawing axial channel of the three studied submarine canyons. Bathymetric contours in meters.

6.1.6. Maritime traffic routes

The Port of Motril is an important commercial and fishing infrastructure offering freight and passenger traffic between Spain and northern Africa. The port has four maritime connections crossing the Alboran Sea (Figure 6.8B): (1) a south-southeast route that crosses the Carchuna Canyon towards Melilla and Nador cities; (2) a south-west route that crosses the Motril Canyon head towards the Port of Tanger Med; (3) a south-southwest route that crosses the upper segment of the Motril Canyon towards the Port of Alhucemas; and (4) an east route that

crosses the Carchuna Canyon head towards the Mediterranean Sea. Additional straight and short routes with north-south and west-east orientations along the slope can be identified in the study area.

6.1.7. Mapping of the fishing activity

The fishing fleet of Motril Port comprised ca. 53 fishing boats in 2019 (from the 640 fishing boats operating in GSA1- Northern Alboran Sea fishing area). The main fishing fleets were artisanal fishing boats (ca. 50%) using set gillnets, trammel nets and traps, followed by bottom otter trawling (ca. 26%), purse seine (ca. 22%), and set longline (ca. 2%) fishing boats. The spatial distribution of purse seine fishing, bottom trawling, and longline fishing displayed contrasting patterns (Figure 6.9). Purse seine fishing was mainly detected on the shelf outside the canyons (Figure 6.9A, B). Bottom trawling was higher in the shelf areas affected by the submarine canyons and in the upper slope of the Motril and Calahonda canyons (Figure 6.9C, D), where bottom trawling marks were identified (Figure 6.9D; Supplementary Table S2). Longline fishing showed a very low number of records due to a low number of boats and their highly seasonal trend (mainly in summer and autumn), but the highest activity was detected on the shelf close to the Motril Canyon head (Figure 6.9E, F).

Gillnet fishing boats operated at 0-100 m water depths. Cadufo fishing boats generally operated at ca. 50 m depth. Crab pot fishing boats operated in upper and middle slope areas are different from those used by bottom trawling boats. Some of these areas could be located within the submarine canyons, where large numbers of individuals of the main target species—the deep-water pandalid shrimp *Plesionika edwardsii*— were detected in the underwater images.

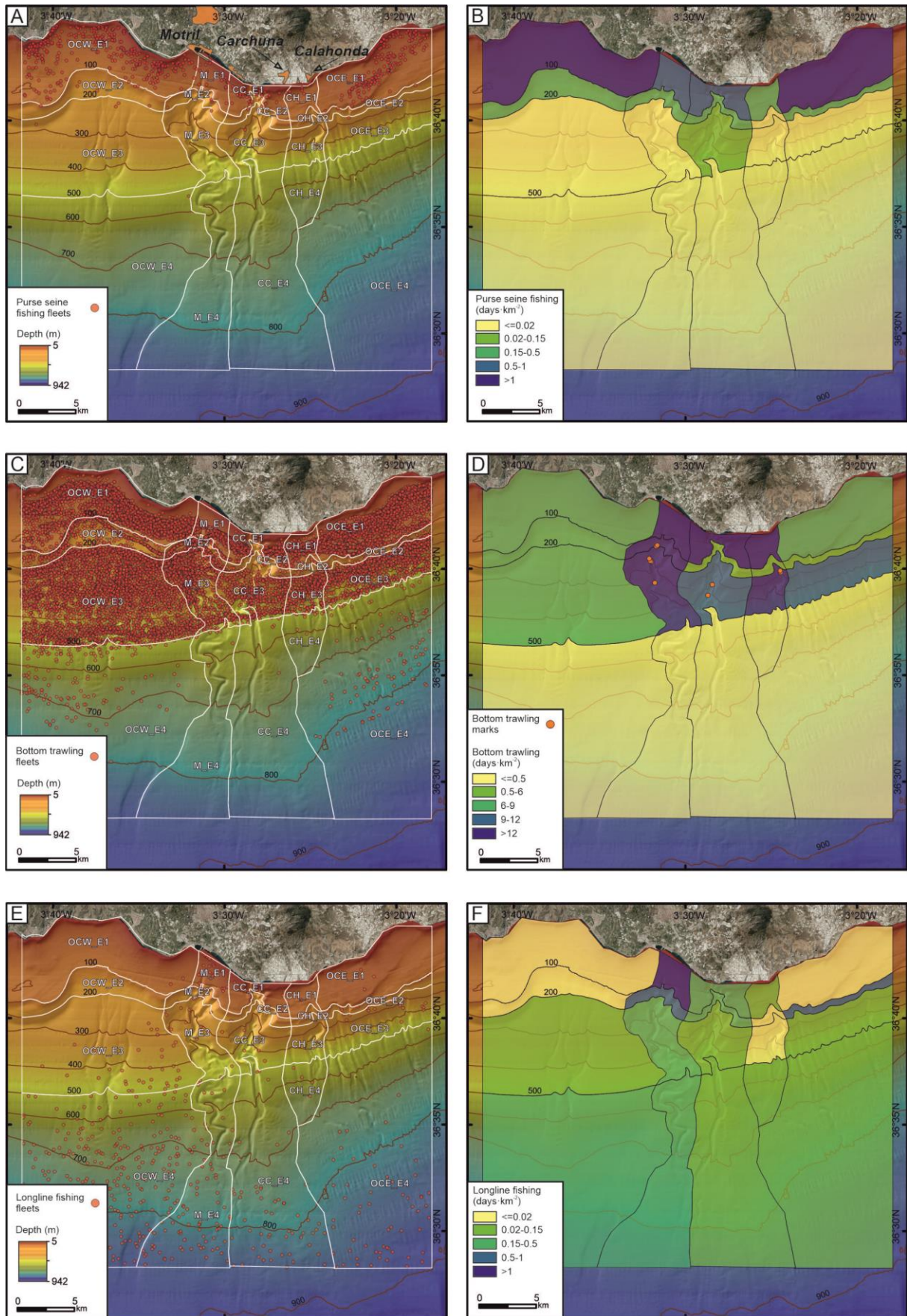
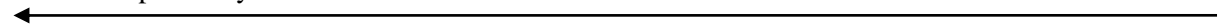


Figure 6.9. Data from Vessel Monitoring System during 2018-2019 (“Ministerio de Pesca, Agricultura y Alimentación”, Spanish government). Spatial distribution of purse seine fishing fleets (A), bottom trawling (C) and longline fishing (E). Fishing effort (in days·km⁻²) for purse seine fishing (B), bottom trawling (D) and longline fishing (F). The bottom trawling marks seen on video footage collected by the ROV in the three submarine canyons is shown (D). See Supplementary S2 to location and depth of the bottom trawling marks and Figure 6.5A and B for examples of seafloor trawling marks along the flank of the Motril Canyon and the thalweg of the Calahonda Canyon. OCW: Western sector of the study area; M: Motril Canyon; CC: Carchuna Canyon; CH: Calahonda Canyon; OCE: Eastern sector of the study area; E1: Shelf; E2: Outer shelf-uppermost slope; E3: Upper slope; E4: Middle slope. Bathymetric contours in meters.



6.2. Discussion

6.2.1. Drivers of the litter abundance

In the study area of the Northern Alboran Sea, average values of marine litter density in the Motril, Calahonda and Carchuna canyons (0.32, 0.66, and 1.8 items·100 m⁻¹, respectively) are lower than most of the values found in Mediterranean canyons (Table 6.3), where noteworthy amounts of marine litter have been reported, particularly as large accumulations or litter hotspots along the thalwegs (e.g., Pham et al., 2014b; Tubau et al., 2015b; Pierdomenico et al., 2020). The values of marine litter found in Italian, Calabrian and Sardinian canyons are much higher than values found in Spanish and French canyons. Litter density values in the studied canyons are in the range of the values found in the Portuguese canyons (0.083-3.31 items·100 m⁻¹; Mordecai et al., 2011; Oliveira et al., 2015), French Atlantic canyons (0.32-0.86 items·100 m⁻¹; van den Beld et al., 2017), and French Mediterranean canyons (0.5-1.3 items·100 m⁻¹; Fabri et al., 2014) (Table 6.3). Within the study area, the upper segment of the Carchuna Canyon displayed a relatively high litter density (8.6 items·100 m⁻¹), which is similar to the values registered in the Cap de Creus Canyon off the Catalan coast (up to 8.6 items·100 m⁻¹; Tubau et al., 2015b; Table 6.3).

The study area has a population density of up to 567 inhabitants·km⁻², and over 80% of the population around the study area is located 2 km inshore from the coastline. Such population density is low in comparison with other areas featuring submarine canyons close to the coastline which exhibit higher densities of marine litter. For example, the heads of the Blanes, La Fonera and Cap de Creus canyons are located on the Catalan margin with a coastal population density of up to 1091 inhabitants·km⁻², and exhibit marine litter densities of up to 18 items·100 m⁻¹ (Tubau et al., 2015b). As an extreme case, the Messina Strait and Gioia

canyons have the highest densities of marine litter in the Mediterranean Sea (up to 56.3 items·100 m⁻¹; Pierdomenico et al., 2020; Table 6.3), and exhibit a coastal population density of up to 800 inhabitants·km⁻². As high densities of marine litter generally display a strong correlation with the proximity of canyon heads to densely populated coasts (Hernandez et al., 2022; Taviani et al., 2023), we interpret that in the study area the relatively low amounts of litter found in the studied canyons are primarily determined by low coastal population densities.

Table 6.3.

Values of density of marine litter reported in linear measurements in different submarine canyons of the Atlantic Ocean and the Mediterranean Sea.

| Region | Submarine canyon | Items·100m ⁻¹ | Plastic (%) | Fishing related (%) ^a | Mean water depth (m) | Reference |
|----------------|------------------|--------------------------|-------------|----------------------------------|----------------------|---------------------------|
| Study area | Motril | 0.12-0.52 | 60 | 0 | 200 | This study |
| | Calahonda | 0.19-1.13 | 69.6 | 13.2 | 238 | This study |
| | Carchuna | 0.11-8.66 | 75.7 | 15.9 | 396 | This study |
| Portugal coast | Lisbon | 1.32 | 86 | 9 | 1602 | Mordecai et al., 2011 |
| | Setúbal | 0.49 | 30 | 8.6 | 2194 | Mordecai et al., 2011 |
| | Cascais | 0.21 | 54 | 9 | 4574 | Mordecai et al., 2011 |
| | Nazaré | 0.083 | 25 | 37 | 3144 | Mordecai et al., 2011 |
| | São Vicente | 0.58-3.31 | 15.9 | 80.5 | 230 | Oliveira et al., 2015 |
| Gulf of Lion | Grand Rhône | 0.5 | 25 | 20 | 345 | Fabri et al., 2014 |
| Ligurian Sea | Toulon | 1.3 | 10 | 5 | 412 | Fabri et al., 2014 |
| Catalan coast | Cap de Creus | 0.7-8.6 | 72.7 | 11.1 | 1210 | Tubau et al., 2015b |
| | La Fonera | 0.3-18 | 71.1 | 24 | 701 | Tubau et al., 2015b |
| | Blanes | 0.2-1.6 | 78.1 | 3.1 | 1509 | Tubau et al., 2015b |
| Bay of Biscay | Cap Ferret | 0.69 ^b | 65 | 25 | 1392 | van den Beld et al., 2017 |
| | Guilvec | 0.32 ^b | 72 | 12 | 877 | van den Beld et al., 2017 |
| | Belle-Île | 0.86 ^b | 55 | 25 | 682 | van den Beld et al., 2017 |
| Calabria | Gioia | 0.77-56.3 | 88 | 3 | 581 | Pierdomenico et al., 2020 |
| | Petrace | 3.94-41.9 | 80 | 0 | 612 | Pierdomenico et al., 2020 |
| Sardinia | Sardinia canyons | 1.01-3.06 | 88 | 42 | 302 | Cau et al., 2017a |

^aPercentage of litter related to fishing

^bAbundance reported as linear measurement (items·100 m⁻¹) by Cau et al., 2017a

Another factor that needs to be considered in explaining marine litter densities is the connectivity of submarine canyons to fluvial streams. The studied canyons are not directly connected to fluvial systems, and the nearby creeks exhibit very reduced dimensions and seasonal patterns (Liquete et al., 2005, 2009). In contrast, very high litter densities have been registered in shelf- incised submarine canyons with heads connected to fluvial systems or with subaerial streams, for example, up to 130 items·100 m⁻¹ in the Messina Strait canyons (Pierdomenico et al., 2019a, b). Therefore, the relatively low litter densities detected in the studied canyons are interpreted as the result of a combination of the low coastal population densities and the lack of connection of canyon heads with major streams (Figure 6.2). These regional conditions broadly resemble those of canyons located off the Catalan coast (Table

6.3), which incise narrow shelves and generally have heads near the coast, where population densities are relatively low and seasonally variable (Tubau et al., 2015b).

The proximity of the Carchuna Canyon head to the coastline (<200 m) implies that the litter density in this canyon is considerably higher than in the Motril and Calahonda canyons, located >2 km from the coastline. This observation agrees with reports from other Mediterranean canyons, where the highest marine litter densities occur in shelf-incised submarine canyons with canyons dissecting the entire shelf (e.g., Calabria coast; Pierdomenico et al., 2020), or in shelf-incised canyons located in very narrow shelves (e.g., Sardinia western coast; Cau et al., 2017a). In contrast, the lowest values of marine litter density occur in canyons incised in wide shelves and distant from the coastline (e.g., Gulf of Lion; Fabri et al., 2014). Therefore, we also suggest that differences in marine litter densities observed among the three studied submarine canyons should mainly reflect the distance between canyon heads and the coastline.

6.2.2. Drivers of the litter distribution

The transport and/or accumulation of litter along submarine canyons is considered to be determined by two major factors, downcanyon gravity flows (Dominguez-Carrió et al., 2020; Angiolillo et al., 2021; Zhong and Peng, 2021), and canyon geomorphological settings (Gerigny et al., 2019; Mecho et al., 2020; Pierdomenico et al., 2020).

The identification of litter hotspots along the upper segment of the Carchuna Canyon, the identification of marine litter along the thalweg in the lowest segment, even at the termination of the canyon (740 m water depth), and the occurrence of very fine sands in the lower segment canyon floor, are regarded as compelling evidences of the occurrence of deep transport by gravity flows along the Carchuna Canyon thalweg. Such sediment transport pulses in this canyon may be driven by downslope bottom flows, described during easterlies dominance (Serrano et al., 2020). Therefore, we consider that the Carchuna Canyon is an active system —it acts preferentially as a conduit, favouring the transport of marine litter from the deeply incised shelf (25 m water depth) to the termination of the channel in the transition towards a distal lobular deposit (740 m water depth) (Figure 6.1). In contrast to the Carchuna Canyon, evidences of gravity flow activity in the Motril and Calahonda canyons are lacking. Instead, the low densities of mainly buried litter by muddy sediments in those canyons can be interpreted as evidence that the canyons have behaved as sinks of marine litter

along their thalweg and flanks, possibly because of their relatively high distance from the coastline.

The geomorphological setting of the Carchuna Canyon seems also to have played a role in litter transport and/or accumulation in two ways, inducing the generation of (1) the above-mentioned gravity flows, and (2) litter accumulations along its course. On the one hand, the fact that the canyon head is located very close to the coast has been previously related to energy concentration in the canyon head due to coastal waves and storm focusing (Ortega-Sánchez et al., 2014). Those processes have been observed in other canyon heads close to coastlines, where they lead to increased shear stress that frequently mobilizes coarse-grained sediments (Smith et al., 2018). A similar situation is plausible in the Carchuna Canyon head, where energy concentration in the canyon head could erode proximal sandy infralittoral prograding wedges (IPW) defined along the coastline, providing a coarse-grained sediment source for the development of gravity flows.

On the other hand, litter hotspots are identified in the upper segment of the Carchuna Canyon favoured by geomorphological features such as smooth seafloor depressions and rocky outcrops blocking the thalweg (Figures 6.4F, H, and 6.5; Table 6.3). We consider that those evidences indicate the generation of litter sinks in the Carchuna Canyon, as evidenced elsewhere (Galgani et al., 1996, 2000; Watters et al., 2010; Miyake et al., 2011; Schlining et al., 2013). In canyon depressions, litter accumulations result from changes in the morphodynamic conditions of bottom currents (Carvajal et al., 2017; Zhong and Peng, 2021), whereas rocky bottoms may act as obstacles to litter items carried by gravity flows (Galgani et al., 2000; Watters et al., 2010; Schlining et al., 2013).

6.2.3. Litter origin: Coastal uses and marine activities

Coastal sources

Marine litter in the studied submarine canyons is overwhelmingly dominated by plastics, accounting for 75% of the total litter (Figures 6.2 and 6.3). This value is similar to the plastic percentages registered in most Mediterranean canyons (Table 6.3), and suggests a dominant coastal origin (at least 50%) in the studied canyons. Of the different coastal uses in the study area, the influence of coastal recreational uses linked to beaches and coastal urbanization would appear to be outstanding. In fact, most of the coastal fringe at both sides of the Carchuna Canyon head is delineated by several kilometers long beaches, such as Motril and

Carchuna beaches (Figure 6.8A). Although these beaches are periodically cleaned, because they are deemed suitable for tourism, abundant litter can be found on them (Godoy et al., 2020; Martín-Lara et al., 2021; MITECO-DGCM, 2021). Therefore, deficiencies in waste management in the beaches of the study area can increase the total amount of marine litter that can be eventually trapped by the canyons. The fact that 35% of marine litter in the studied canyons is made up of plastic bottles and bags constituted compelling evidence for coastal recreational origin. Several metal items, including beverage and food cans, can also be unequivocally attributed to beach occupation.

Almost 8% of marine litter in the study area consists of plastic sheets connected with remote pieces of greenhouses infrastructures, and seedbeds derived from agricultural practices. Both plastic types can be linked to the greenhouses and farming exploitations in the adjacent coastal plain, the main land use in the coastal domain surrounding the beaches (ca. 48%). Specifically, greenhouses are widespread in the backshore of Carchuna Beach, which is closer to the Carchuna Canyon head, whereas greenhouses in the backshore of Motril Beach are more scattered and they alternate with the farming land uses that are located backshore between the Guadalfeo River and Torrenueva town (Figure 6.8A). This interpretation is supported by several additional evidences that attest to the occurrence of litter derived from agricultural practices on the northern coast of the Alboran Sea. For example, microplastics found by Godoy et al. (2020) on the beaches of the coast of Granada are low-density polyethylene, high-density polyethylene, polypropylene, and high-strength polystyrene, all common plastic types used in agriculture. In addition, whales consuming greenhouse marine litter items have been found off Almeria and Granada coasts, which are severely occupied by the greenhouse industry (de Stephanis et al., 2013).

Finally, we consider that sporadic inputs of litter from creeks mainly draining farming areas (Figure 6.8A) would provide marine litter from both urban and agriculture uses due to the torrential behaviour of the ravines close to the Carchuna Canyon head (Liquete et al., 2005). The coast of the Carchuna Canyon head is moreover affected by long-term erosion associated with extreme events (Ortega-Sánchez et al., 2014) and by relatively high current velocity values, causing high values of shear stress (Bárcenas et al., 2011); both processes would favour the transport of marine litter to the Carchuna Canyon head. In contrast, fluvial influence should be minor in the Motril Canyon head, as this submarine feature is relatively far (i.e., several kilometers) from the Guadalfeo River mouth; in any case, the lateral redistribution of Guadalfeo River sediment plumes under westerlies dominance (Bárcenas et

al., 2011) could eventually lead to moderate amounts of marine litter from urban uses, considering the occurrence of several urban areas in the vicinity of the Port of Motril.

Marine activities

Submarine canyons can also locally receive human discards from ships if they are located along shipping routes (Stefatos et al., 1999; Wei et al., 2012; van den Beld et al., 2017; Morales-Caselles et al., 2021). In the study area, marine litter such as sunbeds and pipes found in the upper segment of the Carchuna Canyon can be attributed to shipping traffic because of the large size of these items and the fact that the canyon segment is crossed by a south-southeast shipping route (Figure 6.8B).

The high number of unspecified items found in the Motril Canyon makes it difficult to discern the origin of marine litter. However, the marine litter found in the upper segment of the Motril Canyon coincides with a high concentration of maritime traffic owing to the proximity of the Port of Motril and the junction of both south-west and south-southwest routes above the canyon (Figure 6.8B). Considering the distance between the Motril Canyon and the coastline (ca. 2 km), we infer that the marine litter in this canyon is mostly marine sourced.

Some evidence suggests the influence of fishing activities in the accumulation of marine litter in the studied canyons, considering that other types of marine debris, such as fishing gear, indicate an origin linked to marine extractive activities (Pham et al., 2014a; Vieira et al., 2015; Hernandez et al., 2022). Indeed, nearly 16% of marine litter is related to fishing activities in the study area, i.e., fishing nets and gear used by the artisanal fishing fleet. In addition, rubber items related to the floating defence of fishing boats and building items that are used as support for longline fishing can be found.

Fishing activity apparently produces a differential effect on the studied canyons, due to their distinctive geomorphological and sedimentological characteristics. The upper and middle segments of the Motril Canyon and the entire Calahonda Canyon contain smooth flanks and muddy bottoms that favour fishing activities; this is reflected by abundant evidence of high fishing efforts by bottom trawling, purse seine and longline fishing in those canyons (e.g., numerous marks by bottom trawling in the upper segment of the Motril Canyon; Figure 6.8A, B, and 9D). However, in the Motril and Calahonda canyons, no marine litter derived from fishing activities (e.g., fishing nets) was observed. This likely indicates an efficient sediment burial and subsequent alteration in muddy environments. In contrast, fishing effort, especially

bottom trawling, is lower in the Carchuna Canyon (Figure 6.9D) owing to the abrupt seafloor morphology, featuring very steep flanks and the local occurrence of rocky outcrops. These seafloor features might favour purse seine and longline fishing practices in the upper segment of the Carchuna Canyon. This is reflected by abundant evidence of high fishing efforts of purse seine and longline fishing (Figure 6.9B, F). In addition, it is evidenced by the high number of fishing nets, with several building and rubber items related to the fishing activities, found along both flanks and thalweg of the upper segment of the Carchuna Canyon (Figures 6.3 and 6.10). Indeed, the tangling of fishing nets along the canyon thalweg favours the formation of litter hotspots (Figure 6.4H).

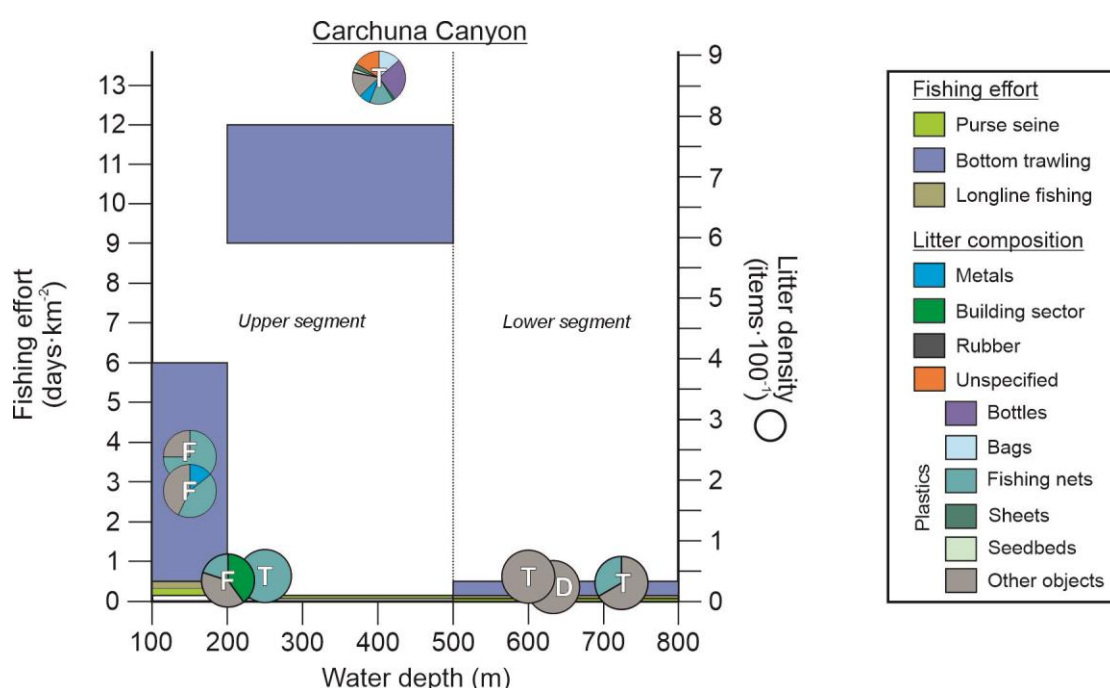


Figure 6.10. Chart showing the ranges of fishing effort (days·km⁻²) for each of the Carchuna Canyon sections (see Figure 6.8). Litter density (expressed as number of items·100 m⁻¹), and litter composition (as pie charts) are also shown. T: canyon thalweg; F: canyon flank; D: lateral deposit.

6.2.4. Interactions of anthropogenic activity indicators with marine habitats and species

The interaction of anthropogenic activities with marine habitats, and especially with certain species, may entail both positive and negative effects (Katsanevakis et al., 2007; Gregory, 2009; Browne et al., 2015; Deudero and Alomar, 2015). Such effects were identified in the study area. Among the positive ones, some litter items provide a hard substrate and refuge for specific sessile (e.g., the bivalve *Neopycnodonte cochlear*, hydrozoans) and mobile species (e.g., the decapod *Munida* sp., the greater forkbeard *Phycis blennoides*) on the sedimentary

bottoms of the studied canyons (Figure 6.3H). The role of some types of litter as artificial hard substrates for sessile species is widely known —particularly floating objects that may act as vectors of dispersion for some species, including indigenous invasive species (Thiel and Gutow, 2005). Among the species settling and growing on these artificial substrates (e.g., *N. cochlear*), some are generally considered ‘opportunistic’ and may represent pioneering species in the colonization of new natural substrates in circalittoral and bathyal bottoms (Sotomayor-García et al., 2019). The provision of refuge made by litter for mobile species has scarcely been investigated, although an increase in the total abundance and the number of species in soft bottoms with litter has been linked to litter that created refuge or reproduction sites for mobile species (Katsanevakis et al., 2007). In the submarine canyons studied here, some large pieces of litter served as refuge for squat lobsters *Munida* spp. or the greater forkbeard *Phycis blennoides* (Figure 6.4H). These species seem to benefit from the crevices and complexity provided by litter items, because they play a role similar to that of isolated rocks or coral rubble in sedimentary habitats (Uiblein et al., 2003; Poore et al., 2011; Rueda et al., 2021). The use of litter as a refuge by squat lobsters could be related to the fact that they commonly live in burrows or are associated with large sessile invertebrates, which would influence their resistance to physical pressures and their protection against predation and/or acquisition of food (Trenkel et al., 2007; Poore et al., 2011). In the case of the greater forkbeard, large litter affords cavities for these active station holders with an effective foraging strategy for capturing their main prey, such as epibenthic and benthopelagic crustaceans (Du Buit, 1978; Mauchline and Gordon, 1984; Uiblein et al., 2003).

Negative effects of anthropogenic activities on the seabed are widely known, and may include physical abrasion, damage, entanglement, and/or burial of sessile and mobile species, chemical transfer (including microplastics) to organisms and the food chain, as well as declines of important commercial stocks, among others (Gregory, 2009; Ramirez-Llodra et al., 2011; Browne et al., 2015; Clark et al., 2016; Trestrail et al., 2020). Fishing activity in submarine canyons was described as the main source of impacts on their seafloor and associated biota, whether habitat-forming species or those with important economic value (Puig et al., 2015; Cau et al., 2017b; Fernandez-Arcaya et al., 2017; Oberle et al., 2018; Giusti et al., 2019; Paradis et al., 2021). Some of the indirect impacts from bottom trawling are generally caused by the resuspension of shelf (and nearby) fine sediments during the trawling operations and their deposition in the seabed of the underlying canyons, which may cause siltation of some sessile habitat-forming species (Puig et al., 2012; Martín et al., 2014).

Indeed, in the analyzed underwater images, some of these benthic species seemed to be silted up in different parts of the canyon. In the present study, the largest average densities of anthropogenic activity indicators were detected in some of the shallowest habitats, including detritic bottoms and scleractinian aggregations (Figure 6.4C), considered vulnerable habitats with high ecological importance (Bellan-Santini et al., 2007; Rueda et al., 2021). Detritic bottoms host a biocoenosis of great diversity and abundance (Bellan-Santini et al., 2007; Rueda et al., 2021). The biocoenosis is favoured by the mixture of different substrate types, which enhances the substrate heterogeneity and the diversification of organisms and food sources. Despite their unquestionable species richness, detritic bottoms do not benefit from any kind of formal protection other than being included in marine protected areas designated for other components. Perspectives for specific protection are scant because these bottoms are a major target for trawling and because they can be very extensive (Figure 6.6A, B).

Meanwhile, scleractinian aggregations in hard substrates correspond to Habitat 1170 “Reefs” from the EU Habitat Directive (92/43/EEC), and this study detected them in the western wall of the Carchuna Canyon head, together with a high number of cloth bags and lines generally used in local longline fisheries (Figure 6.4C). Interaction of longline fishing with benthic fauna can be very localized to specific areas but still can cause a severe impact on slow-growing species that provide a high three-dimensional complexity (e.g., aggregations of colonial scleractinians) (Fabri et al., 2014; Tubau et al., 2015b; Ragnarsson et al., 2017). Longline fishing might alter the seabed to a lesser extent than bottom trawling, in view of its much narrower bottom mark (Pham et al., 2014a; Fabri et al., 2022). A negative impact may stem from the cloth bags filled with sediments or stones used as weights for the longline fisheries, and which, together with the lines, can easily break the skeletons of the scleractinians, inducing the decline and final loss of the habitat they conform (Fosså et al., 2002; Clark et al., 2016). In this sense, urgent protection measures are needed to preserve this vulnerable habitat structured by colonial scleractinians in the studied submarine canyons. Finally, it is important to mention that this study did not provide information on the potential ingestion of microplastics by the detected taxa. It is known that microplastic ingestion in some organisms (e.g., invertebrates) reduces somatic and reproductive growth (Trestrail et al., 2020). Considering this, further studies should provide information on those taxa that may contain high rates of microplastics in their bodies as well as on the potential negative effects on them.

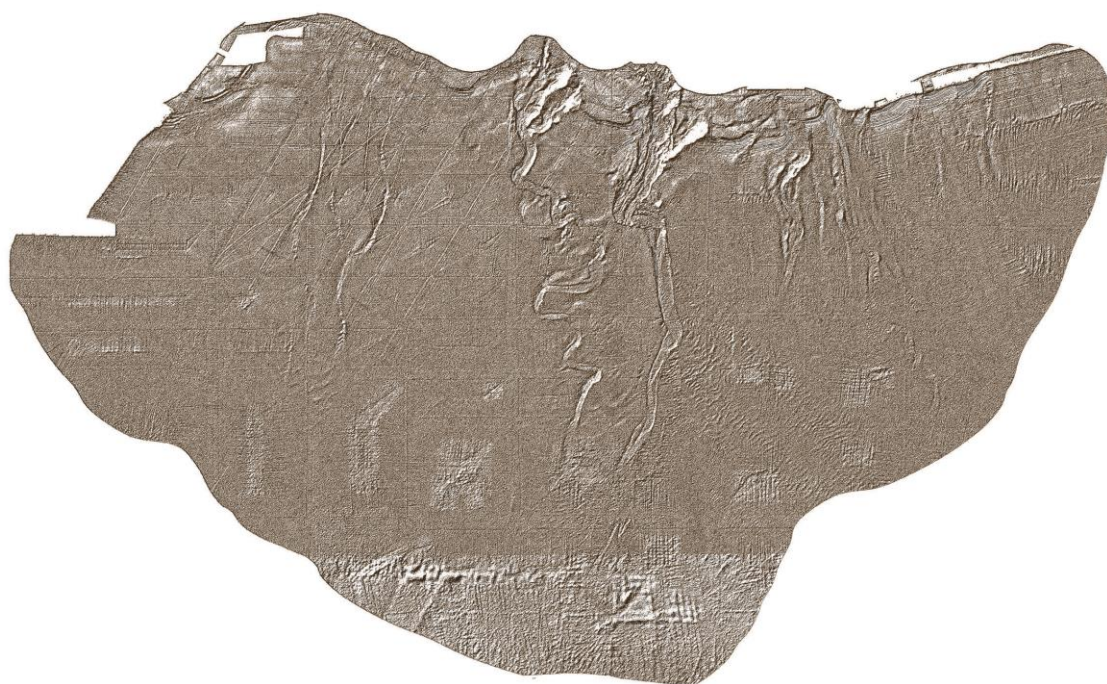
6.3. Conclusions

The detailed analysis of the origin and driving mechanisms of marine litter density and distribution and of the interactions between anthropogenic impacts and marine habitats and species, in this case in the Motril, Carchuna, and Calahonda canyons (northern margin of the Alboran Sea), stands as a contribution to cataloguing marine litter in submarine canyons worldwide, and to understanding the role of submarine canyons as conduits or sinks for litter, with its subsequent impact on benthic habitats. The main conclusions of this study are:

1. The Motril, Calahonda and Carchuna canyons exhibit low litter densities in comparison with other submarine canyons located in the Mediterranean Sea, due to the combination of relatively low coastal population densities and the lack of connection of canyon heads to major streams. The proximity of the Carchuna Canyon head (<200 m) to the coastline implies that the litter density in this canyon is considerably higher than in the Motril and Calahonda canyons, at longer distances from the coast.
2. The Motril and Calahonda canyons can be considered passive systems that have acted as mainly depositional sinks in the recent past, as evidenced by the occurrence of buried marine litter and mostly muddy sediments on the canyon floors. In contrast, the high shelf incision of the Carchuna Canyon and its proximity to the coastline favour the capture of littoral sediment transport, and the formation of gravity flows that transport the marine litter downslope, evidenced by marine litter along the thalweg (up to the termination of the canyon; 740 m water depth) and the occurrence of very fine sand in the lower segment; litter hotspots are favoured by the canyon morphology and the occurrence of rocky outcrops.
3. The main sources of marine litter in the study area (at least 35%) can be traced to coastal recreational uses, such as beaches and coastal urbanization as well as the pressure from tourism. Another coastal origin of the marine litter in the study area could be linked to agricultural practices (at least 8%) that is the main land use in the study area and characterized by greenhouse exploitation in the adjacent coastal plain. A third origin is related to fishing techniques and litter discards from ships. The Motril and Calahonda canyons have smooth flanks and muddy bottoms that favour fishing activities, as opposed to the Carchuna Canyon, having an abrupt seafloor morphology.
4. In the studied canyons, some large pieces of litter are used as refuges by some species against predation and/or for food acquisition. In contrast, fishing activity involving the use of cloth bags, gears, and lines may be producing an impact through entanglement and physical

damage to erect benthic fauna, including some aggregations of colonial scleractinians on the walls of the Carchuna Canyon.

Part 3



7. General discussion

8. Conclusions

9. Supplementary material

10. References

Chapter 7

General discussion

7.1. Sedimentary activity in shelf-incised versus blind submarine canyons

Sequence stratigraphic schemes were initially based on the assumption that canyons were preferentially active during sea-level lowstands, when the continental margins were subaerially exposed (Mitchum, 1985; Vail, 1987; Posamentier and Vail, 1988). In contrast, submarine canyons were considered largely inactive during sea-level highstands. However, contrary to sequence stratigraphy models, sediment gravity flows in canyon systems have been documented during sea-level highstands in various modern turbidite systems (Khripounoff et al., 2003; Carvajal and Steel, 2006; Covault et al., 2007; Normark et al., 2009a, b; Fisher et al., 2021; Chiang and Yu, 2022; Tarrés et al., 2022). Factors that control the different sedimentary activity in submarine canyons during highstands include the geodynamic setting, the location of canyon heads with regard to sediment entry points, and the margin width (Covault et al., 2007; Bernhardt et al., 2015; Fisher et al., 2021; Susanth et al., 2021). These factors are responsible for the significant differences in sedimentary activity between blind and shelf-incised canyons.

In blind canyons, margin oceanographic conditions play a key role in transferring fine-grained sediments to canyon heads; particularly, the interaction between longshore and cross-margin currents determines downslope sediment delivery and the degree of canyon activity during sea-level highstands (Figure 7.1A) (Boyd et al., 2008; Dalla Valle and Gamberi, 2011; Hansen et al., 2017; Yin et al., 2019; Gamberi, 2020; Fisher et al., 2021; Post et al., 2022). Blind canyons located distant from coastlines may also contain litter hotspots derived from human discards from ships (Wei et al., 2012; Quattrini et al., 2015; van den Beld et al., 2017; Mecho et al., 2020; Pierdomenico et al., 2023).

In shelf-incised canyons, key controls affecting sediment delivery to the deep basin are: (1) tectono-morphologic factors, such as continental margin width or the existence of direct connections between canyon heads and river systems; (2) climatic factors, such as inflow of subglacial meltwater or intense river floods; and (3) oceanographic regimes, such as the influence of longshore currents or dense water cascading (Figure 7.1) (Walsh and Nittrouer, 2003; Romans et al., 2009; Covault and Graham, 2010; Covault et al., 2010; Puig et al., 2014; Bernhardt et al., 2015; Sweet and Blum, 2016; Gamberi et al., 2017). These factors together with the density of coastal populations, fishing practices, and other maritime activities affect the amount of litter supplied to the heads of shelf-incised canyons (Figure 7.1) (Hernandez et al., 2022; Cerrillo-Escoriza et al., 2022; Pierdomenico et al., 2023).

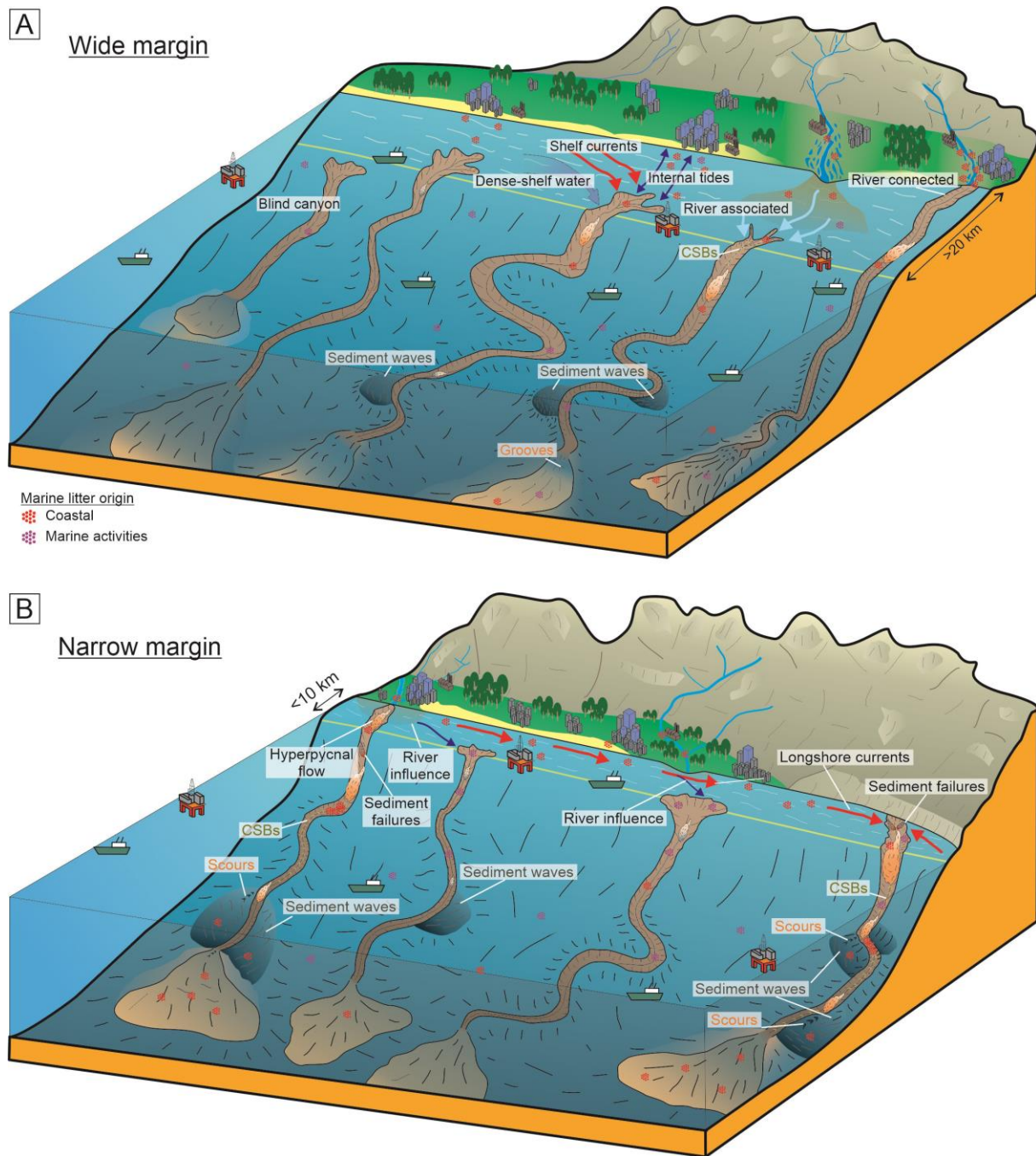


Figure 7.1. Sketches showing the relation between oceanographic and sedimentary transport processes in blind and shelf-incised canyons in wide (A) and narrow (B) margins. The major sources and sinks of marine litter are also shown. In wide margins (A), shelf-incised canyons are mantled by fine-grained sediments and exhibit low sedimentary activity. The main sediment transport processes that occur in shelf-incised canyons in wide margins are linked to river mouths and oceanographic processes, such as dense water cascading, margin currents, and internal tides. These sedimentary processes are reflected in bedform development (i.e., mainly sediment waves), and in a low abundance of transported marine litter. In contrast, in narrow margins (B), the grade of incision of canyon heads is a key factor controlling the sedimentary activity of shelf-incised canyons. Canyon heads deeply incised in the margin can channelize river-borne, coarse-grained hyperpycnal turbidity currents, or capture littoral drift driven by longshore currents, eventually triggering downcanyon turbidity currents.

Figure 7.1. (Continuation) These coarse-grained turbidity currents favor the formation of crescent-shaped bedforms (CSBs) along the axial channel and recurrent spillovers in the lower reaches. The erosion in the canyon head by turbidity currents triggers sediment failures in the canyon flanks and favors the headward erosion towards the coastline. Canyon heads deeply incised in the margin favor the capture of marine litter of coastal origin. In contrast, canyon heads incised in the shelf edge and located at remote locations show poor efficiency in capturing coarse-grained sediments, but they effectively trap fine-grained sediments. In addition, canyon heads incised in the shelf edge may contain marine litter derived from maritime activities.

7.2. Importance of margin physiography on sedimentary activity in shelf-incised submarine canyons

Several studies have demonstrated that shelf-incised canyons that show evidence of recent activity are characterized by coarse-grained sediments and remain connected to the shoreline if margins are steep and narrow (<10 km) (Gamberi, 2020; Bernhardt and Schwanghart, 2021). Canyons incised in narrow margins preferentially occur in tectonically active regions underlain by resistant bedrock (Figure 7.1B) (Covault et al., 2011; Bernhardt and Schwanghart, 2021; Soutter et al., 2021) and exhibit concave downslope profiles (Mitchell, 2005; Gerber et al., 2009; Kertznus and Kneller, 2009; Covault et al., 2011; Amblas et al., 2012; Soutter et al., 2021). The Motril and Carchuna canyons (Figure 4.3) can be considered as representative examples, characterized by the modification of original slope profiles by erosional processes in the canyon heads and deposition of transported material at the distal termination of the channels (Cerrillo-Escoriza et al., 2024).

In contrast, canyons incised in wide margins are generally inactive and characterized by muddy sediments due to the remote location of canyon heads in relation with sediment sources (Harris and Whiteway, 2011; Sweet and Blum, 2016). They occur preferentially on passive margins (Figure 7.1A) (Covault et al., 2011) and are characterized by concave downslope profiles (Covault et al., 2011; Soutter et al., 2021) due to sediment supply exceeding the capacity of subaqueous currents to transport sediments downslope, or to hemipelagic sedimentation exceeding the rates at which subaqueous currents can erode (Gerber et al., 2009; Amblas et al., 2012; Soutter et al., 2021). Although the distance from canyon heads to the shoreline primarily controls sediment caliber and fluxes transported to deep water, the sedimentary activity in shelf-incised canyons is mainly controlled by the relation between canyon heads and oceanographic and sedimentological processes.

7.2.1. Main sedimentary processes in canyons incised in narrow and wide margins

Sedimentary activity in shelf-incised canyons has been mainly observed along narrow margins due to the proximity of canyon heads to nearby coastlines, the interaction with main sedimentary sources, and the high gradients that exhibit those submarine systems. Oceanographic processes, including enhanced bottom currents and sediment resuspension by storm waves (Canals et al., 2006; Xu et al., 2011; Mulder et al., 2012; Kane et al., 2020; Pearman et al., 2020), and sedimentary processes, including sediment gravity flows triggered by mass-failures along canyon walls (Paull et al., 2010) and hyperpycnal flows during pulses of river discharge or ice melting (Mulder et al., 2003; Khripounoff et al., 2012; Hizzett et al., 2018; Talling et al., 2022), favor downcanyon sediment remobilization toward deep-sea areas in narrow margins (Piper and Normark, 2009; Paull et al., 2010; Xu et al., 2010).

In contrast, canyons incised in wide margins may exhibit sedimentary activity depending on: (1) the existence of a connection between the canyon head and river mouths; and (2) the interaction between the canyon head and oceanographic processes (Figure 7.1A). There are a few canyons incised in wide margins that cross the margin and are connected to river mouths; these canyons show recent sedimentary activity from the canyon head to the deep basin (Figure 7.1A). For example, the Zaire Canyon in the Gulf of Guinea incises the margin for more than 200 km (Babonneau et al., 2002, 2004; Khripounoff et al., 2003; Migeon et al., 2004; Andrieux et al., 2013; Talling et al., 2022); the Setúbal and Lisbon canyons in the western Iberian margin, and the Monterey Canyon, offshore California, incise the margin for more than 30 km (Arzola et al., 2008; Lastras et al., 2009; de Stigter et al., 2011; Maier et al., 2018, 2019).

Other canyons that incise wide margins and are located remote to the coastline (ca. 10-60 km) exhibit recent sedimentary activity conditioned by fine-grained sediment supplied by river mouths (Figure 7.1A) (e.g., the Indus Canyon, Clift et al., 2014; the “Swatch of No Ground” Canyon, Rogers et al., 2015; the Eel Canyon, Paull et al., 2014). The rest of shelf-incised canyons occurring in wide margins remote to the coastline (70-300 km) are considered inactive systems with very low rates of clastic fluxes, even if located in front of relatively large fluvial systems (e.g., Danube Canyon, Popescu et al., 2015; Amazon Canyon, Normark et al., 1997).

Additionally, there are canyons incising wide margins that are influenced by oceanographic processes which are able to generate sediment resuspension which is ultimately conducive to

deep-sea sediment transfer (Figure 7.1A). These oceanographic processes include: (1) capture of surface currents that transport water masses by canyon heads, as in the Perth Canyon, southwestern Australian margin (Rennie et al., 2009a, b; Wijeratne et al., 2018); (2) dense-water cascading events, as in the Cap de Creus, Plainer, and Lacaze-Duthiers canyons in the Gulf of Lion (Palanques et al. 2006, 2008; Bonnín et al. 2008; Fabres et al. 2008; Puig et al., 2008; Ribó et al., 2011) or the Adriatic Pit and Bari Canyon in the Adriatic Sea (Trincardi et al. 2007; Turchetto et al. 2007); (3) internal tides, as in the Logan and Gully canyons in the Scotian Slope (Li et al., 2019; Normandeau et al., 2023), or in the Whittard Canyon in the Celtic Margin (Amaro et al., 2016; Heijnen et al., 2022); (4) storm events, as in the Logan Canyon (Mosher et al., 2004; Li et al., 2019; Normandeau et al., 2023), or in the Nazaré and Capreton canyons, deeply incised in the Iberian Atlantic margin (Vitorino et al., 2005; Oliveira et al., 2007; Martín et al., 2011; Masson et al., 2011; Mazières et al., 2014; Allin et al., 2016; Gómez-Ballesteros et al., 2022); (5) capture of littoral cells, as in the Monterey Canyon, deeply incised in the margin offshore California (Xu et al., 2014; Maier et al., 2019).

7.2.2. Development of bedforms in shelf-incised canyons along narrow versus wide margins

The development of bedforms along shelf-incised canyons reflects the recurrent passage of turbidity currents and is indicative of recent canyon sedimentary activity (Peakall et al., 2000; Fildani et al., 2006; Kostic, 2011; Covault et al., 2014, 2017). Bedform development may occur in canyons incising narrow and wide margins, but they exhibit sedimentary and geomorphic differences in the bedforms located in axial channels (confined bedforms) and overbank deposits (unconfined bedforms) (Figure 7.1).

7.2.2.1. Confined bedforms in shelf-incised canyons in narrow versus wide margins

Bedforms hosted in canyons incised in narrow margins are coarse-grained, crescentic-shaped (CSBs) and usually confined along axial channels (Figure 7.1B) (e.g., Smith et al., 2005, 2007; Xu et al., 2008; Kostic, 2011; Paull et al., 2011, 2013; Babonneau et al., 2013; Covault et al., 2014; Mazières et al., 2014; Tubau et al., 2015a; Sun et al., 2023). The formation of CSBs as a result of the combined effects of erosional and depositional processes is due to short-lived, high-energy turbidity flow events (Smith et al., 2005; Xu et al., 2008; Paull et al., 2010; Babonneau et al., 2013). The proximity of canyon heads to adjacent coastlines favors

the capture of coarse-grained sediments derived from river mouths (e.g., Var Canyon, Mas et al., 2010; Migeon et al., 2001, 2006; Pointe-des-Monts Canyon, Normandeau et al., 2014, 2022), fjord-deltas (e.g., Squamish Delta, Hage et al., 2018; Stacey et al., 2019), or longshore drifts (e.g., Gioia Canyon, Bosman et al., 2017). Ultimately, those processes are able to generate downcanyon turbidity flows and the formation of CSBs.

In contrast, canyons incising wide margins usually exhibit fine-grained, small-scale (<5 m) sediment waves, especially in the axial channel of canyon heads (e.g., internal tide currents, Lo Iacono et al., 2020; Normandeau et al., 2014, 2023). Canyons incising wide margins do not usually exhibit confined CSBs because of their low gradients and fine-grained sediment composition (e.g., Lamb et al., 2008; Lastras et al., 2009). The development of confined CSBs in canyons incising wide margins is restricted to the upper reaches of narrow and steep canyons (Figure 7.1A) with canyon heads connected directly to river mouths (e.g., Biobío Canyon, Bernhardt et al., 2015) or associated with large rivers (e.g., South Taiwan Shoal and West Penghu canyons, Zhong et al., 2015; Zhang et al., 2022; Sun et al., 2023); canyon heads influenced by internal tides and sediment advection during storms (e.g., Scotian Slope, Wynn et al., 2002a; Normandeau et al., 2023); or canyon heads deeply incised in the shelf that capture coastal sediments which are transported downcanyon (e.g., Monterey Canyon, Smith et al., 2005, 2007; Paull et al., 2011).

7.2.2.2. Unconfined bedforms in shelf-incised canyons in narrow versus wide margins

The lower reaches of canyons incised in narrow margins exhibit numerous overbank sediment wave fields due to the recurrent passage of spillover flows (Figure 7.1B) (e.g., Kaikōura Canyon, Tek et al., 2022; Var Canyon, Mas et al., 2010). In addition, coarse-grained confined flows can spillover in channel bends due to high-flow velocities and are able to develop linear depressions or scour trains over overbank deposits, such as in the La Jolla Canyon (offshore California, Paull et al., 2013) or the studied Carchuna Canyon.

The development of sediment waves in unconfined settings of canyons incising wide margins is common, even where no bedforms occur in the confined setting (Figure 7.1A) (e.g., Nazaré, Setúbal, and Lisbon canyons, Arzola et al., 2008, Lastras et al., 2009; Zaire Canyon, Migeon et al., 2004; Vangriesheim et al., 2009). The occurrence of sediment waves evidence that channelized fine-grained turbidity currents can generate spillovers in the canyon lower reaches. In contrast, few canyons incised in wide margins exhibit net-erosional bedforms (e.g.

scours) over overbank deposits (e.g., Monterey Canyon, Fildani et al., 2006; or Eel Canyon, Lamb et al., 2008).

7.2.3. Abundance, origin, and distribution of marine litter in shelf-incised canyons in narrow versus wide margins

The comparison between studies of abundance, distribution, and origin of marine litter is hindered by the uneven geographical distribution of marine litter, sampling efforts and bathymetric ranges of studied canyons, and the general lack of standardization of data collection and reporting in the literature (Canals et al., 2021; Hernandez et al., 2022; Pierdomenico et al., 2023). The abundance, origin, and distribution of marine litter in shelf-incised canyons may differ due to the combined influence of anthropogenic, geomorphological and physical factors (Galgani et al., 2022), with spatial densities spanning several orders of magnitude between different shelf-incised canyons (Hernandez et al., 2022; Pierdomenico et al., 2023).

7.2.3.1. Abundance of marine litter in shelf-incised canyons in narrow versus wide margins

The abundance of marine litter is considerably higher in canyons incising narrow margins than in wide margins, as evidenced by recent abundance comparison studies (Hernandez et al., 2022; Pierdomenico et al., 2023; Taviani et al., 2023). Canyons incised in narrow margins, such as the North Pacific and Mediterranean canyons, contain >11 orders of litter density magnitude than North Atlantic shelf-incised canyons, which are mostly incised in wide margins (Hernandez et al., 2022). This difference in marine litter density is also evident within the North Pacific and Mediterranean canyon populations; there, canyons incising wide margins exhibit lower densities of marine litter. For example, shelf-incised canyons of the middle Gulf of Lion located >50 km from the coastline, contain up to $85 \text{ items}\cdot\text{km}^{-2}$; in contrast, the canyons located in the western part of the Gulf of Lion and the nearby Catalan canyons, located up to 3 km from the coastline, where densities up to $25,990 \text{ items}\cdot\text{km}^{-2}$ have been reported (Tubau et al., 2015b; Dominguez-Carrió, 2018; Gerigny et al., 2019; Hernandez et al., 2022; Pierdomenico et al., 2023; Taviani et al., 2023). Therefore, the proximity of canyon heads to coastlines is a key factor controlling the abundance of marine litter in shelf-incised canyons. Rarely, there are some canyons incising wide margins that exhibit large

densities of marine litter, such as the SY82 Canyon located ca. 150 km from the coastline in the southern China Sea with $>50,000$ items·km⁻² (Peng et al., 2019).

The proximity of shelf-incised canyons to densely populated areas can substantially increase the amount of marine litter, as evidenced in French canyons incised in the narrow margin of the Ligurian Sea (e.g., Paillon Canyon with ca. >8 items·100 m⁻¹, Galgani et al., 1996), the Catalan canyons incised in a wide margin (e.g., >8 items·100 m⁻¹, Tubau et al., 2015b), or the Messina Strait canyons, Tyrrhenian Sea, where up to 1.3 million items·km⁻² have been reported (Pierdomenico et al., 2019a), representing the most litter-affected deep-marine environment recorded worldwide. The impact of population density is clearly observed in the Lisbon Canyon, close to a large population center (1.32 items·100 m⁻¹, Mordecai et al., 2011), compared with the nearby Sétubal and Cascais canyons (0.49 items·100 m⁻¹, Mordecai et al., 2011).

7.2.3.2. Origins of marine litter along shelf-incised canyons in narrow versus wide margins

The main factors that can determine the connectivity of shelf-incised canyons to the sources of marine litter are mainly river systems and human activity in the marine realm (e.g., Pham et al., 2014a; Vieira et al., 2015; Alves et al., 2021; Morales-Caselles et al., 2021).

Coastal origins

Canyons incising narrow margins host marine litter from land due to the proximity of canyon heads to the coastlines (e.g., Gioia Canyon, Pierdomenico et al., 2020; Carchuna Canyon, Cerrillo-Escoriza et al., 2023), particularly in river-supplied canyon heads (Figure 7.1B) (e.g., Messina Strait canyons, Pierdomenico et al., 2019a; Ligurian Sea canyons, Galgani et al., 1996; Gisuti et al., 2019; Angiolillo et al., 2021). Plastics are the most common type of marine litter derived from land, mainly from river mouths, although other litter types such as metal items can also suggest a river source (Alves et al., 2021; Morales-Caselles et al., 2021). In addition, plastics from coastal recreational activities linked to beaches and coastal settlements, as well as to agricultural practices, can be supplied more easily to the coast and potentially be captured by canyon heads (Cerrillo-Escoriza et al., 2023).

In some canyons incised in wide margins, relatively large abundances of coastal litter may occur if canyon heads are connected to rivers. For example, high plastic concentrations have been found in the Setúbal, Cascais and Lisbon canyons, which cross the entire western Iberian

margin and are connected to the Tajo and Sado river mouths (Lastras et al., 2009; Mordecai et al., 2011). Other canyon heads located remotely from the coastline but influenced by large rivers exhibit high percentages of plastic items of coastal origin (van den Beld et al., 2017). For example, the Belle-île and Arcachon canyons in the Bay of Biscay with canyon heads located up to 180 km from the coastline and influenced by the Loire and Gironde rivers, respectively (Galgani et al., 1996). In the Gulf of Lion, the high amount of plastics found in the Rhône fan, at 2200 m water depth more than 150 km away from the river mouth, suggests a highly efficient seaward litter transfer (Galgani et al., 2000).

Marine origins

Marine litter linked to maritime activities is ancillary in canyons incising narrow margins (Figure 7.1B), such as the Ligurian Sea (Angiolillo et al., 2021), Alboran Sea (Cerrillo-Escoriza et al., 2023), and Tyrrhenian Sea canyons (Pierdomenico et al., 2020). In contrast, canyons incising wide margins mainly contain marine litter from maritime activities (Figure 7.1A), such as fishing-related items. This is the case of most of the canyons of the Bay of Biscay (van den Beld et al., 2017), the Bremer Canyon in southwestern Australia (Taviani et al., 2023), the São Vicente and Nazaré canyons in western Portugal (Mordecai et al., 2011; Oliveira et al., 2015), and the Norfolk and Baltimore canyons in the northwestern Atlantic margin (Quattrini et al., 2015; Jones et al., 2022). In addition, the fact that there is a high abundance of marine litter from fishing activities in canyons incising wide margins also suggests low sedimentary activities, considering that fishing-related marine litter in shelf-incised canyons has relatively lower mobility than plastic items (Pierdomenico et al., 2023).

Other sources of marine litter in wide margin canyons include items discarded from ships, such as glass, clinker, and large metal objects (e.g., Stefatos et al., 1999; Wei et al., 2012; Ramirez-Llodra et al., 2013; van den Beld et al., 2017; Morales-Caselles et al., 2021), and large metal objects derived from naval bases or accumulated in military dumping sites, e.g., in the Gulf of Lion canyons (Fabri et al., 2014; Gerigny et al., 2019) or in the Perth Canyon in southwestern Australia (Taviani et al., 2023).

7.2.3.3. Litter distribution within shelf-incised canyons in narrow versus wide margins

Marine litter can be remobilized and redistributed downcanyon toward deep-sea areas by a variety of oceanographic and sedimentary processes (Schluning et al., 2013; Tubau et al.,

2015b; Pierdomenico et al., 2019a, b, 2020; Dominguez-Carrió et al., 2020; Angiolillo et al., 2021; Zhong and Peng, 2021). In addition, geomorphological features along canyon courses can be responsible for the uneven distribution of litter among and within individual canyons (Galgani et al., 1996; Tubau et al., 2015b; Gerigny et al., 2019; Mecho et al., 2020; Pierdomenico et al., 2020).

Overall, canyons incised in narrow margins are characterized by high flow velocities and transport capacity, where turbidity currents are able to redistribute significant amounts of litter downcanyon (Pierdomenico et al., 2023). As a consequence, large marine litter accumulations have been found in several canyons (Figure 7.1B), such as the Messina Strait canyons (Pierdomenico et al., 2019a), the Monaco Canyon (Angiolillo et al., 2021), or the Carchuna Canyon (Cerrillo-Escoriza et al., 2023). In canyons incised in narrow margins, geomorphological features such as seafloor depressions and rocky outcrops can favor the accumulation of marine litter (Pierdomenico et al., 2019a, b; Angiolillo et al., 2021; Zhong and Peng, 2021; Cerrillo-Escoriza et al., 2023). This is due to their usually abrupt seafloor morphology, with very steep flanks and local occurrence of rocky outcrops (Galgani et al., 1996; Tubau et al., 2015b; Pierdomenico et al., 2019a, b, 2020; Angiolillo et al., 2021; Cerrillo-Escoriza et al., 2023). This geomorphological setting also favors the formation of marine litter hotspots along the thalwegs (e.g., Pierdomenico et al., 2019a; Angiolillo et al., 2021; Cerrillo-Escoriza et al., 2023) and the entanglement of fishing-related debris in canyon flanks (e.g., Watters et al., 2010; Oliveira et al., 2015; Cau et al., 2017a; Enrichetti et al., 2020; Cerrillo-Escoriza et al., 2023).

In contrast, marine litter is more scattered in canyons incising wide margins (Figure 7.1A), such as the canyons in the Bay of Biscay (van den Beld et al., 2017), the Gulf of Lion (Fabri et al., 2014), western Portugal (Mordecai et al., 2011; Oliveira et al., 2015), southwestern Australia (Taviani et al., 2023), and the northwestern Atlantic Ocean (Quattrini et al., 2015; Jones et al., 2022). Rarely, canyons incising wide margins exhibit high accumulations of marine litter in the middle and lower reaches of these systems, such as the SY82 Canyon (ca. 1900 m water depth, Zhong and Peng, 2021), the Rhône deep-sea fan (ca. 2200 m water depth, Galgani et al., 2000), or between 2000 and 4000 m water depths in the Monterey Canyon (Schluning et al., 2013), evidencing that marine litter is also remobilized downcanyon by turbidity flows (Pierdomenico et al., 2019a, b, 2023; Zhong and Peng, 2021).

7.3. Sedimentary processes of shelf-incised canyons in narrow margins

The high sedimentary activity of shelf-incised canyons in narrow margins is evidenced by the interaction of canyon heads with the main sedimentary sources, the development of CSBs in axial channels, and the high abundance of marine litter accumulated in hotspots. However, the different sedimentary activities between nearby canyons highlight the role played by the degree of incision and the connection of canyon heads with sediment sources in narrow margins (Mulder and Alexander, 2001; Parson et al., 2007; Piper and Normark, 2009; Talling et al., 2012, 2014) (Figure 7.1B), as shown in the studied Motril and Carchuna canyons (Cerrillo-Escoriza et al., 2024). The Carchuna Canyon, deeply incised in ca. 3.5 km wide margin, exhibits recent sedimentary activity, whereas the Motril Canyon, incising the shelf edge, acts as a passive system that accumulates sediments. These differences have also been observed in other narrow margins, mainly offshore California and in several places in the Mediterranean Sea (Figure 7.2; Table 7.1).

7.3.1. Relationship between the degree of canyon incision and turbidity current initiation

Turbidity currents tend to be initiated in canyon heads due to their proximity to sediment sources and high slope gradients (Normark and Piper, 1991, Talling, 2014). Different initiation processes can be envisaged: sediment failures, direct fluvial supplies, and resuspension of coastal sediments by oceanographic processes including longshore cells, storms, and internal waves (Parsons et al., 2001; Mulder and Alexander, 2001; Hesse et al., 2004; Parson et al., 2007; Piper and Normark, 2009; Puig et al., 2014; Talling, 2014). In canyon heads, several of these genetic processes may interact in a complex manner; for example, the joint capture by canyon heads of sediments supplied by river flows, longshore cells, or sediment resuspension by storms (e.g., Piper and Normark, 2009; Xu et al., 2010; Paull et al., 2013).

7.3.1.1. Shelf-incised canyons fed by river systems in narrow margins

There are two types of canyons influenced by river supplies: canyon heads deeply incised in the margin (shelf-cutting canyons) that are directly connected with river mouths and canyon heads incised in the shelf edge (shelf-edge canyons) that are indirectly influenced by river mouths. There are few examples of direct connection between shelf-cutting canyon heads and

river mouths in narrow margins, offshore California and the Mediterranean Sea (Figures 7.1B and 7.2; Table 7.1). These examples are characterized by continuous discharges and large volumes of coarse-grained sediments resulting in hyperpycnal turbidity currents (e.g., Var Canyon, Mas et al., 2010; Khripounoff et al., 2009, 2012; Migeon et al., 2012). In contrast, shelf-edge canyons are draped by recent muddy sediments (Figure 7.1B). This setting can be observed in the Motril Canyon, as well as in several other shelf-incised canyons located in the shelf edge offshore California, such as the Santa Monica, San Gabriel, Oceanside, and Carlsbad canyons (Covault et al., 2007; Normark et al., 2009a; Tubau et al., 2015a; Maier et al., 2018); in the Ligurian Sea, such as the Polcevera and Bisagno canyons (Carugati et al., 2019); and the Tyrrhenian Sea, such as the Mesima Canyon (Morelli et al., 2022). In some few cases, shelf-edge canyons exhibit recent sedimentary activity as they are influenced by river mouths able to discharge great amounts of sediments (e.g., the Guadiaro Canyon, Palanques et al., 2005; Ercilla et al., 2019; the San Mateo Canyon in offshore California, Covault et al., 2014).

The high abundance of shelf-edge canyons in front of river mouths with little sedimentary activity is related to physiographic and sediment supply constraints. The Californian and Mediterranean margins are characterized by the occurrence of short rivers with ephemeral or intermittent character in steep hinterlands that mainly supply coarse-grained sediments to the coastline (Normark et al., 2009a; Harris and Whiteway, 2011; Miramontes et al., 2023). There, coarse-grained sediments do not reach the canyon heads due to the remote distances between river mouths and canyon heads, favoring instead the hemipelagic drape of these canyon systems.

The formation and evolution of the shelf-cutting and shelf-edge canyons associated with river systems can provide key information to understand their recent sedimentary activity. Both canyon types were supposedly active during the Last Glacial Maximum when they were connected to river mouths (Mauffrey et al., 2015, 2017). The subsequent sea-level rise led to the landward migration of coastlines resulting in a significant decrease of river supplies that were not able to reach shelf-edge canyon heads. As a consequence, passive shelf-edge canyons were formed, as evidenced by paleo-heads detected between present-day shelf-edge canyon heads and river mouths (e.g., the Mesima Canyon in the Tyrrhenian Sea, Morelli et al., 2022). A similar setting can be proposed for the Motril Canyon, characterized by a shelf-edge head located at ca. 5 km from the Guadalfeo River mouth. The lowstand connection between the canyon head and the river mouth has not been observed in the margin. On the

other hand, active shelf-cutting canyons connected directly to river mouths maintained the connection of canyon heads with shorelines during highstands.

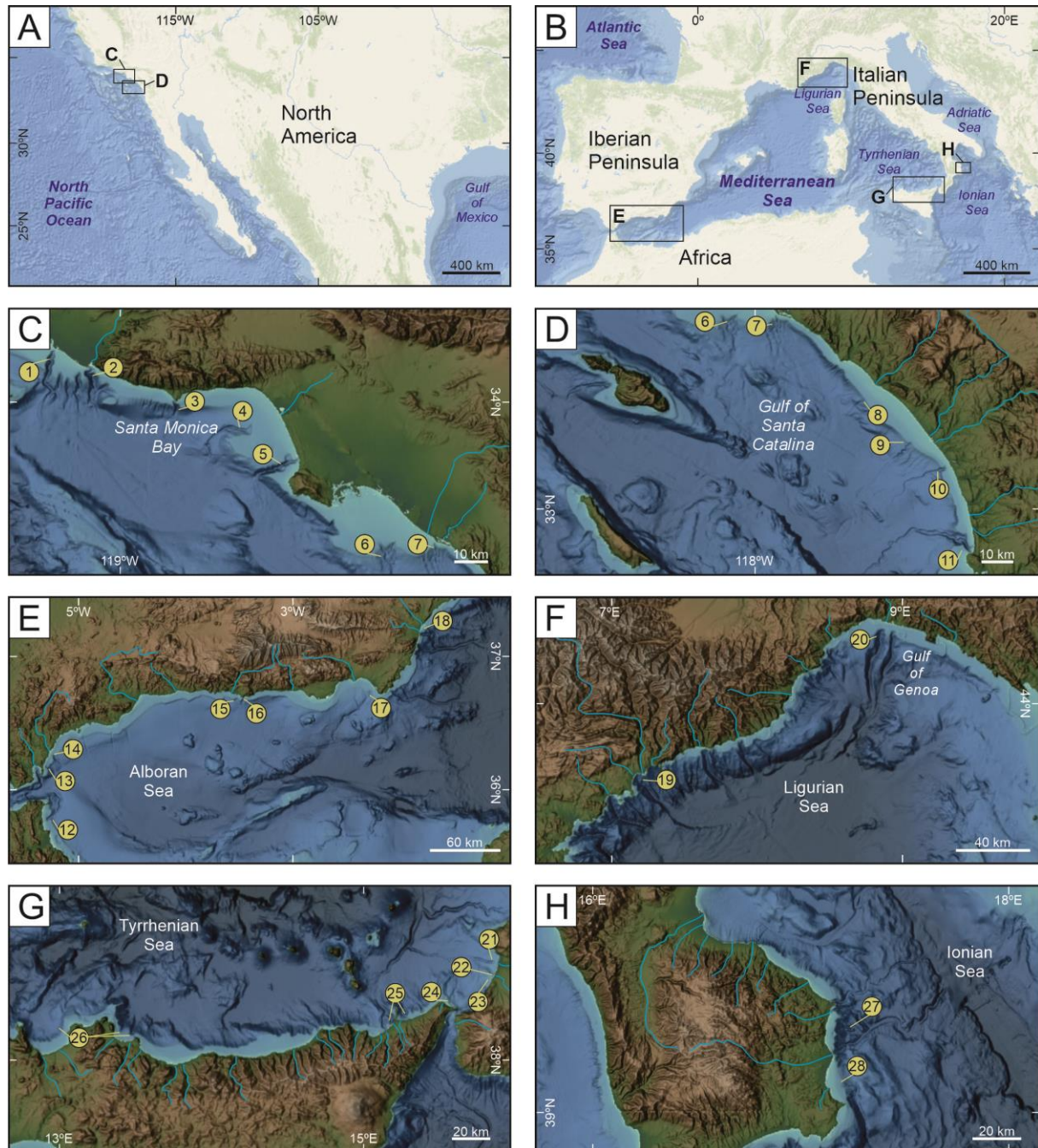


Figure 7.2. Location of shelf-incised canyons in narrow margins (A) offshore California and (B) in the Mediterranean Sea showing different sedimentary activities. Shelf-incised canyons offshore California from (C) Santa Monica Bay to the (D) Gulf of Santa Catalina. Mediterranean shelf-incised canyons are located in: (E) the northern margin of the Alboran Sea; (F) the northern margin of the Ligurian Sea; (G) the southern margin of the Tyrrhenian Sea; (H) and the northwestern Ionian Sea. See Table 7.1 for the nomenclature and main characteristics of shelf-incised canyons. Main river systems are also shown (in blue). Topobathymetric images were extracted from NOAA (2023).

7.3.1.2. *Shelf-incised canyons fed by longshore currents in narrow margins*

Shelf-cutting canyons with no direct connection with river systems are usually mantled by coarse-grained sediments and exhibit recent sedimentary activity (Figure 7.2; Table 7.1) because canyon heads are influenced by oceanographic processes that lead to the capture of littoral sediments. In sand-rich littoral-fed canyons, such as shelf-cutting canyons along the California Margin (e.g., La Jolla Canyon, Covault et al., 2007; Redondo Canyon, Normark et al., 2009a, b; Dume Canyon, Gardner et al., 2003; Hueneme Canyon, Xu et al., 2010), turbidity current activity preferentially occurs during winter storm seasons, when sediment transport to canyon heads is enhanced. Turbidity currents may also occur in other seasons, but are much less common (e.g., in the Tyrrhenian Sea, Gioia Canyon, Pierdomenico et al., 2016; Morelli et al., 2022). A similar oceanographic setting occurs in the studied Carchuna Canyon, which can capture the littoral drift under easterlies dominance (Cerrillo-Escoriza et al., 2024). Additionally, the increase of wave heights in the canyon head favors long-term coastal erosion owing to energy concentration (Ortega-Sánchez et al., 2014). Eventually, resuspended sediments are transported downcanyon by bottom flows.

Most shelf-edge canyons cannot trap littoral cells and are passive systems (e.g., Oceanside, Carlsbad, and Coronado canyons, Covault et al., 2007; Normark et al., 2009a) due to their distant location from nearby coastlines (Figure 7.1B). However, specific oceanographic conditions driven by increases in amplitudes of internal waves favored by the coastal physiography may transport littoral sediments toward canyon heads, such as the cases of Ceuta and La Linea canyons (Figures 7.1B and 7.2; Table 7.1) (Vázquez et al., 2015; Ercilla et al., 2019; Palomino et al., 2019). The present-day situation contrasts with the Last Glacial Maximum, during which many shelf-edge canyons were influenced by littoral drift processes; such influence declined during the post-glacial transgression, as the canyon heads were detached from longshore currents (Piper et al., 1999; Estrada et al., 2011).

Table 7.1.

Summary of the main characteristics of shelf-incised canyons offshore California and the Mediterranean Sea that include: shelf width, shelf canyon incision, major sediment source, canyon floor sediments and bedform development in each canyon. See Figure 7.2 for the location of the canyons. Continued on next page.

| | Shelf incised canyons | Shelf width (km) | Shelf incision (km) | Main sediment supply | Canyon floor sediments | Bedforms | References |
|-----------------------------|-------------------------------|------------------|---------------------|--------------------------|------------------------|-----------------|---|
| Offshore California | | | | | | | |
| 1 | Hueneme Canyon | ca. 8 | ca. 7 | Littoral drift | Gravel and sand | - | Normark et al. (2009a); Xu et al. (2010) |
| 2 | Mugu Canon | ca. 3.5 | ca. total | River and littoral drift | Sand | - | Normark et al. (2009a); Xu et al., (2010) |
| 3 | Santa Monica | 10 | 1.5 | River | Hemipelagic mud | No | Normark et al. (2009a); Tubau et al. (2015) |
| 4 | Dume Canyon | ca. 2.5 | ca. total | Littoral drift | Sand | No | Gardner et al. (2003); Normark et al. (2009a); Piper et al. (2009) |
| 5 | Redondo Canyon | ca. 7 | ca. total | Littoral drift | Sand | CSB and SW | Normark et al. (2009b); Tubau et al. (2015) |
| 6 | San Gabriel Canyon | ca. 9 | ca. 2 | River | - | No | Normark et al. (2009a); Maier et al. (2018) |
| 7 | Newport Canyon | 2.5 | ca. total | River and littoral drift | Sand | SW | Normark et al. (2009a); Covault et al. (2010) |
| 8 | San Mateo Canyon | 9 | 1 | River | Sand | CSBs | Covault et al. (2014) |
| 9 | Oceanside Canyon | ca. 7 | <1 | River | Hemipelagic mud | No | Covault et al. (2007); Normark et al. (2009a) |
| 10 | Carlsbad Canyon | 5 | 2.5 | River | Hemipelagic mud | No | Covault et al. (2007); Normark et al. (2009a) |
| 11 | La Jolla Canyon | 5 | ca. total | Littoral drift | Gravel and sand | CSB and SC | Covault et al. (2007); Normark et al. (2009a); Paull et al. (2013); Maier et al. (2020) |
| Mediterranean Sea | | | | | | | |
| <u>Alboran Sea</u> | | | | | | | |
| 12 | Ceuta Canyon | 8 | 4.5 | Littoral drift | Gravel | No | Ercilla et al. (2019) |
| 13 | La Linea Canyon | 5 | 3.5 | Littoral drift | Sand | CSB and SC | Vázquez et al. (2015); Ercilla et al. (2019); Palomino et al. (2019) |
| 14 | Guadiaro Canyon | 6.5 | 3.5 | River | Sand | - | Palanques et al. (2015); Ercilla et al. (2019) |
| 15 | Motril Canyon | 3.5 | 2 | River | Mud | SW | Cerrillo-Escoriza et al. (2024) |
| 16 | Carchuna Canyon | 3.5 | ca. total | Littoral drift | Sand | CSB, SW, and SC | Cerrillo-Escoriza et al. (2024) |
| 17 | Almeria Canyon | 7.5 | 3.5 | River | Mud | No | Alonso and Ercilla (2002); Vázquez et al. (2015) |
| <u>SE Iberian Peninsula</u> | | | | | | | |
| 18 | Garrucha Canyon | 4.5 | ca. total | River and littoral drift | Sand | CSB and SW | Puig et al. (2017); Tarrés et al. (2022) |
| <u>Ligurian Sea</u> | | | | | | | |
| 19 | Var Canyon | 2.5 | ca. total | River-connected | Gravel and sand | SW and SC | Khripounoff et al. (2012); Migeon et al. (2012) |
| 20 | Polcevera and Bisagno canyons | ca. 6 | ca. 2.5 | River | Silt | - | Carugati et al. (2019) |

CSB: Crescent-shaped bedforms linked to confined settings; SW: Sediment waves linked to unconfined settings; SC: scours linked to unconfined settings

Table 7.1. *Continuation*

| | Shelf incised canyons | Shelf width (km) | Shelf incision (km) | Main sediment supply | Canyon floor sediments | Bedforms | References |
|--------------------------|--|---------------------|------------------------|-----------------------------|--------------------------------|----------|---|
| Mediterranean Sea | | | | | | | |
| <u>Tyrrhenian Sea</u> | | | | | | | |
| 21 | Mesima Canyon | ca. 3.5 | 2 | River | Hemipelagic mud | No | Morelli et al. (2022) |
| 22 | Gioia Canyon | ca. 3.5 | ca. total | Littoral drift | Sand | CSB | Pierdomenico et al. (2016) Morelli et al. (2022) |
| 23 | Petrace Canyon | ca. 4 | ca. total | River and littoral drift | Sand | CSB | Pierdomenico et al. (2016) Morelli et al. (2022) |
| 24 | Acquarone Canyon | ca. 4.5 | 1.5 | River | Fine-grained sediment | SW | Scacchia et al. (2022) |
| 25 | Niceto and Milazzo canyons | ca. 4 | ca. total | River- connected | Coarse- grained sediment | SW | Gamberi et al. (2017); Gamberi (2020) |
| 26 | Eleutorio, Oreto, and Castellammare canyons | Ca. 8 | 2-4 | River, Littoral drift | Fine-grained sediment | No | Lo Iacono et al. (2011, 2014, 2015) |
| <u>Ionian Sea</u> | | | | | | | |
| 27 | Neto-Lipuda Canyon | ca. 8 | 3.5 | River | Muds and sands | - | Rebesco et al. (2009) Perri et al. (2012) |
| 28 | Esaro Canyon | ca. 9 | 2.5 | River | Muds and sands | - | Perri et al. (2012) |

CSB: Crescent-shaped bedforms linked to confined settings; SW: Sediment waves linked to unconfined settings; SC: scours linked to unconfined settings

7.3.1.3. Shelf-incised canyons fed by multiple processes in narrow margins

Multiple processes triggering turbidity currents may interact in canyon heads deeply incised in narrow margins. The more frequent interaction is given by lateral redistribution of fluvial supplies by longshore currents; this type of interaction is typical of stormy weathers where rivers can generate large floods, as evidenced in the Hueneme, Mugu, and Newport canyons, offshore California (Covault et al., 2010, Xu et al., 2010) or the Garrucha Canyon, southeastern Iberian Peninsula (Puig et al., 2017; Tarrés et al., 2022). Sediment resuspension increases during storm events, favoring the capture of sediment by canyon heads, even in shelf-edge canyon heads, such as the Guadiaro Canyon in the northwestern margin of the Alboran Sea (Puig et al., 2004; Palanques et al., 2005), and the Eleutorio, Oreto, and Castellammare canyons in the Tyrrhenian Sea (Lo Iacono et al., 2011, 2014, 2015).

Canyon heads deeply incised in narrow margins are usually considered as retrogradational features where erosional processes prevail and sediment failures can initiate turbidity currents, which further erode the canyon heads (Figure 7.1B) (Pratson and Coakley, 1996; Piper and Normark, 2009). As an example, a large sediment failure triggered an energetic turbidity current that reached >2000 m water depths in the Var Canyon (Gennessieux et al., 1980,

Piper and Savoye, 1993, Mulder et al., 1997). Turbidity currents initiated by sedimentary processes (i.e., littoral drift and hyperpycnal flows) can also promote canyon incision in shelf-cutting canyon heads, resulting in increased rates of canyon-floor downcutting. This process, in turn, favors oversteepening of canyon walls, resulting in retrogressive failures (Densmore et al., 1997; Pratson and Coakley, 1996; Guiastrennec-Faugas et al., 2020) that can initiate turbidity currents, which further erode the canyon head (Pratson and Coakley, 1996). This erosional setting has been observed in shelf-cutting canyons that interact with littoral cells.

The littoral-drift fed Carchuna Canyon exhibits geomorphological and sedimentary characteristics similar to the Dume, Redondo, and La Jolla canyons, offshore California, whose canyon heads are located close to capes or high-relief coasts. These characteristics include deep shelf incision and canyon floor mantling by coarse-grained sediments (Figure 7.2; Table 7.1). In those cases, the combination of littoral drift coarse sediment supplies and wave focusing in the canyon heads promotes canyon incision (Finnegan et al., 2017; Lamb et al., 2015; Sunamura, 2018). The effectiveness of this mechanism is ultimately related to the occurrence of tectonic uplift and durable bedrock lithologies (e.g., Delgada Canyon, Smith et al., 2017, 2018). Long-term coastal erosion owing to energy concentration is able to trigger retrogradational failures in the canyon head and headward erosion.

7.3.2. Bedform development in shelf-incised canyons carved in narrow margins

A lack of bedform development in shelf-edge canyons (Figures 7.1B and 7.2; Table 7.1) largely reflects their inactivity, such as the Motril Canyon (this study); the Santa Monica, Oceanside, and Carlsbad canyons, offshore California, (Covault et al., 2007; Tubau et al., 2015a); or the Mesima Canyon, Tyrrhenian Sea (Morelli et al., 2022). Only shelf-edge canyons linked to high discharges from river mouths or longshore currents that reach the canyon heads exhibit bedform development (Figure 7.2; Table 7.1) (e.g., San Mateo Canyon, Covault et al., 2014; Acquarone Canyon, Scacchia et al., 2022; La Linea Canyon, Palomino et al., 2019). In contrast, shelf-cutting canyons exhibit wide development of bedforms along axial channels and depositional lobes (Figure 7.2; Table 7.1). Bedform development differs depending on the sediment source (i.e., littoral cell versus river-fed canyons).

CSB maintenance requires the continuous influence of coarse-grained, high-energy turbidity flow events (Symons et al., 2016; Hage et al., 2018; Sun et al., 2023). Shelf-cutting canyons fed by littoral drift usually exhibit CSBs along the axial channel (Figure 7.1B), where high

seafloor gradients favor the erosion and ignition of dense sediment flows (Mulder and Alexander, 2001; Piper and Normark, 2009). These CSBs have been observed in littoral-fed canyons such as the Redondo and La Jolla canyons, offshore California (Normark et al., 2009b; Tubau et al., 2015a; Paull et al., 2013; Maier et al., 2020), the Carchuna Canyon, northern Alboran Sea (Cerrillo-Escoriza et al., 2024), and the Gioia Canyon, Tyrrhenian Sea (Morelli et al., 2022). In some cases, CSBs are recognized along the axial channel up to the termination of the channel (e.g., La Jolla Canyon or the studied Carchuna Canyon).

Shelf-cutting canyons connected with river mouths also tend to host CSBs in the upper reaches due to recurrent supply of coarse-grained sediments by hyperpycnal turbidity currents (Figures 7.1B and 7.2; Table 7.1), such as the cases of the Garrucha Canyon, southeastern Iberian Peninsula (Puig et al., 2017; Tarrés et al., 2022), the Var Canyon, Ligurian Sea (Migeon et al., 2012), or the Petrace Canyon, Tyrrhenian Sea (Morelli et al., 2022). The fact that CSB development is mainly restricted to upper reaches suggests that the hyperpycnal flows generated in canyon heads are energetically insufficient to transport coarse-grained sediments downcanyon. Other examples of CSB development in relation with continuous and powerful fluvial supplies include the channels formed in fjord deltas (e.g., Conway et al., 2012; Normandeau et al., 2016; Stacey et al., 2019), where high-density hyperpycnal flows can be formed even with low amounts of suspended sediments.

7.3.3. Relation between the degree of incision of margin canyons and marine litter in narrow margins

Overall, most shelf-incised canyons around the world have been poorly studied for the purposes of marine litter characterization (Hernandez et al., 2022; Pierdomenico et al., 2023); this is the case of California canyons. Most of the research on seafloor litter and microplastics has focused on Mediterranean canyons, accounting for more than 50% of the canyons where anthropogenic debris has been reported (Pierdomenico et al., 2023) (Table 7.2).

Table 7.2. Occurrence of marine litter in shelf-incised canyons in narrow margins along the Mediterranean Sea indicating the depth range, litter density, and the dominant marine litter type. Modified from Pierdomenico et al. (2023).

| Shelf-incised canyon | Depth range (m, min-max or mean) | Litter density | Dominant marine litter type | Reference |
|-------------------------|----------------------------------|--------------------------------|-----------------------------|---------------------------------|
| Shelf-edge canyons | | | | |
| East Sardinia canyons | | | | |
| Arbatax | 147-180 | 1.5 items·100 m ⁻¹ | Fishing gears | Cau et al. (2017a) |
| Caprera | 160-220 | | | |
| Cavoli | 170-190 | | | |
| Capo Coda Cavallo | 145 | | | |
| Tavolara | 170-290 | | | |
| Mortorio | 120-145 | | | |
| Nora | 420-463 | | | |
| Orosei | 120-186 | | | |
| East-Sardinia Canyon #1 | 93-142 | 40000 items·km ⁻² | Fishing gears | Cau et al. (2017b) |
| East-Sardinia Canyon #2 | 90-150 | 280000 items·km ⁻² | | |
| East-Sardinia Canyon #3 | 110-148 | 220000 items·km ⁻² | | |
| East-Sardinia Canyon #4 | 90-124 | 10000 items·km ⁻² | | |
| Corsic canyons | | | | |
| Galeria | 59-567 | 0.25 items·100 m ⁻¹ | Fishing gears | Gerigny et al. (2019) |
| Ile Rousee | 100-600 | 0.08 items·100 m ⁻¹ | Fishing gears/Plastic | |
| Calvi | 143-580 | 0.18 items·100 m ⁻¹ | Fishing gears/Plastic | |
| Saint Florent | 132-643 | 0.22 items·100 m ⁻¹ | Plastic | |
| Alboran Sea | | | | |
| Motril | 200 | 0.52 items·100 m ⁻¹ | Plastic | Cerrillo-Escoriza et al. (2022) |
| Calahonda | 238 | 1.13 items·100 m ⁻¹ | | |
| Shelf-cutting canyons | | | | |
| Corsic canyons | | | | |
| Ajaccio | 50-545 | 0.68 items·100 m ⁻¹ | Plastic | Gerigny et al. (2019) |
| Porto | 56-555 | 0.4 items·100 m ⁻¹ | Plastic/Fishing gears | |
| Valinco | 50-620 | 0.18 items·100 m ⁻¹ | Plastic | |
| Valinco | 1694-1950 | 6000 items·km ⁻² | Plastic | |
| Ligurian Sea | | | | |
| Arma di Taggia | 25-95 | 4418 items·km ⁻² | Plastic/Fishing gears | Giusti et al. (2019) |
| Bergeggi | 230-445 | 4539 items·km ⁻² | | |
| Bordighera | 20-300 | 12138 items·km ⁻² | | |
| Cannes | 945-1443 | 0.27 items·100 m ⁻¹ | Plastic | Angiolillo et al. (2021) |
| Dramont | 20-342 | 2564 items·km ⁻² | Fishing gears | Giusti et al. (2019) |
| Monaco | 1291-2194 | 3856 items·100 m ⁻¹ | Plastic | Angiolillo et al. (2021) |
| Paillon | 575-820 | 10.4 items·100 m ⁻¹ | Plastic | Galgani et al. (1996) |
| Saint Tropez | 66-665 | 0.51 items·100 m ⁻¹ | Plastic | Gerigny et al. (2019) |
| Stoechades | 180-720 | 0.3 items·100 m ⁻¹ | Fishing gears | Fabri et al. (2014) |
| Var | 370-1408 | 2.74 items·100 m ⁻¹ | Plastic | Galgani et al. (1996) |
| Messina Strait canyons | | | | |
| San Gregorio | 243-518 | 270 items·100 m ⁻¹ | Plastic | Pierdomenico et al. (2019a) |
| Sant'Agata | 275-524 | 14 items·100 m ⁻¹ | | |
| Tremestieri Ch1 | 384-581 | 132 items·100 m ⁻¹ | | |
| Tremestieri Ch2 | 337-381 | 56 items·100 m ⁻¹ | | |
| Tyrrhenian Sea | | | | |
| Gioia-Petrace | 17-541 | 5.6 items·100 m ⁻¹ | Plastic | Pierdomenico et al. (2020) |
| Ionian Sea | | | | |
| Caulonia | 145-526 | 2.9 items·100 m ⁻¹ | Plastic | Pierdomenico et al. (2019b) |
| Alboran Sea | | | | |
| Carchuna | 396 | 8.66 items·100 m ⁻¹ | Plastic | Cerrillo-Escoriza et al. (2022) |

7.3.3.1. Relation between the abundance of marine litter and the degree of canyon incision

A relation between the abundance of marine litter and the degree of canyon incision has been documented along the Mediterranean Sea. Shelf-edge canyon heads exhibit low marine litter densities (Figure 7.1B; Table 7.2). For example, eastern Sardinian shelf-edge canyons (ca. 1.5 items·100 m⁻¹, Cau et al., 2017a), North Corsican canyons (up to 0.25 items·100 m⁻¹, Gerigny et al., 2019), or the studied shelf-edge Motril and Calahonda canyons (up to 1.13 items·100 m⁻¹, Cerrillo-Escoriza et al., 2023). In contrast, shelf-cutting canyons exhibit higher densities of marine litter evidencing that coast proximity enhances sediment and litter capture (Table 7.2). For example, shelf-cutting canyons of eastern Corsica Island (up to ca. 7 items·100 m⁻¹, Grinyó et al., 2020); the Ligurian Sea canyons (up to 11 items·100 m⁻¹, Galgani et al., 1996; Giusti et al., 2019); canyons located in the Messina Strait (27 items·100 m⁻¹ in the San Gregorio Canyon, Pierdomenico et al., 2019a); or the studied Carchuna Canyon (8.66 items·100 m⁻¹, Cerrillo-Escoriza et al., 2023).

7.3.3.2. Relation between the origin of marine litter and the degree of canyon incision

The origin of marine litter found in Mediterranean shelf-incised canyons also seems to be related with the amount of canyon head incision. Shelf-cutting canyons mostly host plastic items (Figure 7.1B; Table 7.2), suggesting a dominant coastal origin, as evidenced elsewhere, such as in Ligurian canyons (e.g., Cannes Canyon, Angiolillo et al., 2021), Tyrrhenian canyons (e.g., Petrace Canyon, Pierdomenico et al., 2021), Ionian canyons (e.g., Caulonia Canyon, Pierdomenico et al., 2019b), West Corsica canyons (e.g., Porto Canyon, Gerigny et al., 2019), Messina Strait canyons (e.g., Sant'Agata, Pierdomenico et al., 2019a), and the studied Carchuna Canyon (Cerrillo-Escoriza et al., 2023).

In most of the cases, plastic abundance in shelf-cutting canyons is linked to the connection of canyon heads with river mouths (Fabri et al., 2014; Gerigny et al., 2019; Giusti et al., 2019; Pierdomenico et al., 2019a). Torrential rivers can transport large amounts of sediments that entrain marine litter through the generation of hyperpycnal flows during seasonal flash floods (Pierdomenico et al., 2022). Litter hotspots found in the deep reaches of some shelf-cutting canyons connected to river systems, such as the Cannes, Monaco, and Paillon canyons, would indicate that turbidity currents are able to remobilize marine litter up to ca. 2200 m water depth (Galgani et al., 1996; Angiolillo et al., 2021). The capture of marine litter remobilized by longshore currents by shelf-cutting canyon heads is an alternative mechanism to explain

the widespread occurrence of plastic debris in shelf-cutting canyons with not direct connection to rivers (e.g., Gioia Canyon in the Tyrrhenian Sea, Pierdomenico et al., 2020; Carchuna Canyon, Cerrillo-Escoriza et al., 2023).

In contrast, shelf-edge canyons are mostly characterized by fishing-derived debris (Figure 7.1B; Table 7.2), as evidenced in the eastern margin of Sardinia (Cau et al., 2017a, b) or the northern margin of Corsica (Gerigny et al., 2019). Fishing gear comprises between 84 to 100% of marine litter in these canyons (Cau et al., 2017a, b; Gerigny et al., 2019). Shelf-edge canyons are also affected by numerous marks of bottom trawling. This is observed in the Motril Canyon (Cerrillo-Escoriza et al., 2023), where fishing activity seems to be favored by smooth flanks and muddy canyon bottoms. There, sedimentological and geomorphological characteristics (Cerrillo-Escoriza et al., 2024) do not support the generation of turbidity currents triggered by bottom trawling. In contrast, in other steeper shelf-edge canyons characterized by coarse-grained sediments, turbidity currents triggered by bottom trawling have been documented (e.g., Guadiaro Canyon, Palanques et al., 2005).

Chapter 8

Conclusions

8.1. Conclusions

The results and discussions presented across the three main chapters of this PhD Thesis reveal a comprehensive understanding of the sedimentary activity of shelf-incised canyons in narrow margins highlighted from geomorphological and sedimentary differences between the nearby Motril and Carchuna canyons. This study elucidates their respective roles in recent patterns of sediment transport and accumulation, the formation and maintenance of bedforms in submarine canyons, and the controls on litter distribution, abundance, and origin in shelf-incised submarine canyons. In addition, a worldwide comparison of shelf-incised canyons located in both narrow and wide margins provides evidence of outstanding differences in degrees of sedimentary activity. In this way, the overarching aim of this PhD Thesis – to establish the factors that control the sedimentary activity in shelf-incised canyons - has been addressed with the following conclusions related to each specific objective:

1) Distance from canyon heads to coastlines exerts the primary control on the caliber and flux of sediment that is potentially captured by the shelf-incised canyons and eventually transported downcanyon.

- A. Steep shelf-incised canyons located in narrow shelves (<10 km) are located in active margins where canyon heads interact with oceanographic processes, littoral cells, or river systems, leading to highly active canyons which are mantled by coarse-grained sediments with frequent formation of CSBs along axial channels and sediment waves and scours in overbank deposits. The proximity of canyon heads to coastlines favors the capture of coastal-derived marine litter that flows downcanyon creating numerous hotspots.
- B. Smooth shelf-incised canyons located in wide shelves (>10 km) are mainly located in passive margins with low sedimentary activity due to the remote distance of coastlines to canyon heads. These canyons are characterized by fine-grained sediments, lack of CSBs along axial channels, and low densities of marine litter mainly derived from anthropogenic marine activities.
- C. Some shelf-incised canyons in wide margins exhibit recent sedimentary activity, which is restricted to steep and narrow canyon heads with a high grade of margin incision. Those canyon heads are either directly connected to river mouths or are able to capture sediments derived from large rivers, littoral cells, or resuspension by oceanographic processes, such as internal tides or dense shelf-water cascading.

2) The grade of canyon head incision is a key factor driving the recent sedimentary activity of canyons in narrow margins.

- A. Canyon heads incised in the shelf edge (i.e., shelf-edge canyons) exhibit low sedimentary activity, such as the studied Motril Canyon, as evidenced by fine-grained sediment mantling, low or absent development of sediment waves along the canyon and low densities of marine litter. Few shelf-edge canyons exhibit recent sedimentary activity; they are linked to high fluvial discharges or to extensive littoral cells able to reach canyon heads.
- B. Canyon heads deeply incised in the margin (shelf-cutting canyons) exhibit high sedimentary activity, such as the studied Carchuna Canyon, as evidenced by coarse-grained sediment mantling and high development of CSBs along axial channels. In addition, the development of sediment waves and scours in overbank deposits is indicative of recurrent and energetic coarse-grained turbidity currents that flow downcanyon and spillover in the lower reaches, transporting high amounts of marine litter along the canyon and depositing in the distal depositional lobes.
- C. Shelf-cutting canyon heads initiate turbidity currents by: (1) hyperpycnal flows favored by steep hinterlands that mainly supply coarse-grained sediments and potentially marine litter to the coastline; and (2) capture of extensive littoral cells offshore California and the Mediterranean Sea, such as the Carchuna Canyon.

3) The configuration of narrow margins, such as offshore California and the Mediterranean Sea, is a factor controlling the evolution and recent sedimentary activity in shelf-incised canyons.

- A) Shelf-edge canyons are mostly located in the front or close to river mouths, such as the Motril Canyon. Those canyons were possibly connected to river mouths during the LGM. During the Holocene highstand, the amount of sediment supplied by river mouths decreased significantly and most of the terrigenous sediment was stored in the continental shelf generating a separation between canyon heads and the coastline; coarse-grained sediments supplied by ephemeral short rivers is not able to reach canyon heads, which tend to be buried by hemipelagic drapes.
- B) Shelf-cutting canyons are mainly located close to high-relief promontories or capes, such as the Carchuna Canyon. Coarse sediment supplied by longshore currents and wave focusing by canyon-head morphology interact to promote canyon incision and maintain coast-canyon connectivity, due to headward erosion by retrogradational

failures. This setting favors canyon floor erosion and canyon flank failures, ultimately leading to the generation of turbidity flows.

- C) The role of rivers that cross densely populated areas along the Mediterranean margin affected by flashfloods can explain the high concentration of litter in several shelf-incised canyons.

8.2. Forthcoming research

The results of this PhD Thesis represent an important contribution to understand active sedimentary processes in submarine canyons. However, some issues remain open for future research that can be collected in the coming oceanographic survey SANIMED (March of 2024). Significant open issues and possible approaches to address them are as follows:

1. Take advantage of the location of the nearby Motril and Carchuna canyons to understand the influence of river supplies in the Motril Canyon head and longshore supplies in the Carchuna Canyon head, in order to discover the turbidity currents triggered in the canyon heads. The deployment of moorings in the upper reaches of both canyons and/or of benthic tripods in the nearby shelf would allow the collection of simultaneous measurements of currents and suspended-sediment concentrations, as have been done in other shelf-incised canyons (e.g., Xu et al., 2002; Puig et al., 2003; Bonnin et al., 2008; Symons et al., 2017; Maier et al., 2019; Tarrés et al., 2022).
2. To conduct repeated multibeam surveys over multi-month or multi-year periods and examine morphological changes undergone by the Carchuna CSBs along the axial channel and the sediment waves and scours over the overbank deposits, as executed in other bedform prolific environments (e.g., Smith et al., 2007; Paull et al., 2010; Hughes Clarke, 2016; Hage et al., 2018; Ribó et al., 2022). This research would help to understand the processes behind the formation, development and maintenance of canyon bedforms, including the influence of sandy supercritical flows formed by turbidity currents, and their preservation in the sedimentary record.
3. Several classifications have been proposed for submarine canyon littoral connectivity (Romans et al., 2016; Sweet and Blum, 2016). However, no single mechanism has been identified to explain why a select group of shelf-incised canyons has avoided disconnection during the post-LGM sea level rise between the canyon head and the coastline. The General Discussion section of this thesis can serve as a starting point for a future review based on the

sedimentological and geomorphological characteristics (focus on the degree of incision and the type of margin of the canyons), the development of the bedforms depending on the type of canyon, and the abundance, origin, and distribution of the marine litter along the shelf-incised canyons.

4. Finally, the comprehensive analysis of acoustic lines would help to decipher the role played by the canyons on the shelf-to-slope sediment transport during different sea-level cycles at glacial/interglacial scales (10s-100s kyr), and to discern the sedimentological differences according to the varying degree of shelf incision during such cycles.

Chapter 9

Supplementary material

Table Supplementary S1. Location and water depth of the sediment cores sampled for grain size analysis.

| | Physiographic feature | Sediment core | Coordinates | | Water depth (m) | Grain size |
|--------------------------------|-----------------------|---------------|----------------|---------------|-----------------|-----------------|
| | | | Latitude (N) | Longitude (W) | | |
| Motril Canyon | Thalweg | DV02_C1 | 36° 39' 56.29" | 3° 31' 49.23" | 336.4 | Medium silts |
| | | DV02_C2 | 36° 40' 15.96" | 3° 31' 56.31" | 307.2 | Medium silts |
| | Western flank | DV02_C4 | 36° 41' 8.57" | 3° 31' 34.76" | 153.5 | Coarse silts |
| Shelf | Western shelf | BC02 | 36° 42' 19.74" | 3° 33' 21.9" | 54.2 | Coarse silts |
| | | BC03 | 36° 41' 58.14" | 3° 32' 33.36" | 69.4 | Coarse silts |
| | | BC04 | 36° 41' 32.52" | 3° 31' 44.58" | 91.7 | Coarse silts |
| | | BC05 | 36° 42' 1.26" | 3° 31' 10.5" | 61.2 | Very fine sands |
| | Shelf | BC17 | 36° 41' 0.61" | 3° 29' 37.92" | 71.3 | Very fine sands |
| Intercanyon Motril-Carchuna | Shelf break | BC18 | 36° 40' 15" | 3° 29' 55.8" | 112.1 | Very fine sands |
| | Slope | BC19 | 36° 39' 40.8" | 3° 30' 10.8" | 229.5 | Coarse silts |
| | Slope | BC20 | 36° 38' 48" | 3° 30' 10.8" | 338.8 | Medium silts |
| | | | | | | |
| Carchuna Canyon | Levee | DV10_C1 | 36° 34' 54.9" | 3° 27' 49.64" | 646.6 | Coarse silts |
| | | DV10_C2 | 36° 35' 10.58" | 3° 27' 55.11" | 629.4 | Medium silts |
| | Thalweg | DV10_C3 | 36° 35' 26.86" | 3° 27' 58.75" | 633.8 | Very fine sands |
| | | BC24 | 36° 35' 50.61" | 3° 27' 55.1" | 619.2 | Very fine sands |
| | | DV03_C1 | 36° 38' 13.04" | 3° 29' 2.62" | 491.8 | Coarse silts |
| | | DV03_C2 | 36° 38' 30.33" | 3° 28' 48.14" | 466.7 | Coarse silts |
| | | DV03_C3 | 36° 38' 47.49" | 3° 28' 36.91" | 450.0 | Coarse silts |
| | | DV04_C1 | 36° 39' 1.61" | 3° 28' 32.19" | 425.9 | Coarse silts |
| | | DV04_C2 | 36° 39' 18.95" | 3° 28' 24.54" | 403.9 | Coarse silts |
| | | BC28 | 36° 39' 41.88" | 3° 28' 22.56" | 371.8 | Coarse silts |
| | | DV04_C4 | 36° 39' 47.88" | 3° 28' 11.29" | 350.4 | Coarse silts |
| | | DV05_C1 | 36° 40' 28.32" | 3° 28' 11.32" | 259.6 | Coarse silts |
| | | DV05_C2 | 36° 40' 42.96" | 3° 28' 1.63" | 209.5 | Coarse silts |
| | | BC31 | 36° 40' 54.11" | 3° 28' 6.93" | 185.3 | Very fine sands |
| | Eastern flank | DV04_C5 | 36° 39' 51.52" | 3° 28' 1.31" | 313.2 | Very fine sands |
| | | DV11_C1 | 36° 40' 14.17" | 3° 28' 15.42" | 295.8 | Coarse silts |
| | | DV11_C2 | 36° 40' 17.92" | 3° 28' 7.64" | 261.9 | Coarse silts |
| | | DV11_C3 | 36° 40' 23.59" | 3° 27' 59.60" | 202.8 | Very fine sands |
| | | DV05_C3 | 36° 40' 46.28" | 3° 27' 55.19" | 160.3 | Very fine sands |
| | Western flank | DV06_C1 | 36° 40' 30.06" | 3° 28' 29.29" | 171.4 | Fine sands |
| Intercanyon Carchuna-Calahonda | Shelf | BC37 | 36° 40' 45" | 3° 26' 34.2" | 74.7 | Very fine sands |
| | Shelf break | BC38 | 36° 40' 0.56" | 3° 26' 10.86" | 100.6 | Fine sands |
| | Slope | BC39 | 36° 39' 37.8" | 3° 26' 4.67" | 192.1 | Very fine sands |
| | | BC40 | 36° 39' 6.6" | 3° 26' 0.6" | 316.5 | Medium silts |
| Calahonda Canyon | Thalweg | BC33 | 36° 39' 23.79" | 3° 24' 22.65" | 352.8 | Medium silts |
| | | DV07_C1 | 36° 39' 38.67" | 3° 24' 27.24" | 319.7 | Medium silts |
| | | DV07_C2 | 36° 39' 59.44" | 3° 24' 34.25" | 255.4 | Coarse silts |
| | | DV07_C3 | 36° 40' 14.71" | 3° 24' 52.80" | 204.9 | Very fine sands |
| | | DV07_C4 | 36° 40' 25.09" | 3° 24' 56.44" | 158.1 | Fine sands |
| | Eastern flank | DV08_C1 | 36° 40' 8.92" | 3° 24' 22.29" | 127.9 | Fine sands |
| | | | | | | |

DV: Push core; BC: Box core

Supplementary Table S2. Location and water depth of the bottom trawling marks identified in the Motril, Calahonda and Carchuna canyons.

| Submarine canyon | Dive | Physiographic feature | Coordinates | | Water depth (m) |
|------------------|---------|-----------------------|----------------|---------------|-----------------|
| | | | Latitude (N) | Longitude (W) | |
| Motril | Dive 01 | Thalweg | 36° 39' 17.67" | 3° 31' 43.88" | 372.04 |
| | Dive 02 | Western flank | 36° 40' 23.45" | 3° 31' 57.72" | 289.22 |
| | | | 36° 40' 34.81" | 3° 32' 1.8" | 265.67 |
| | | | 36° 40' 27.52" | 3° 31' 59.35" | 276.46 |
| | | | 36° 41' 1.09" | 3° 31' 41.46" | 189.93 |
| | | | 36° 41' 4.11" | 3° 31' 38.81" | 179.63 |
| Calahonda | Dive07 | Thalweg | 36° 39' 49.91 | 3° 24' 27.02" | 293.77 |
| | | | 36° 39' 51.93" | 3° 24' 27.68" | 287.79 |
| Carchuna | Dive 03 | Thalweg | 36° 38' 45.84" | 3° 28' 38.19" | 451.46 |
| | Dive 04 | | 36° 39' 17.2" | 3° 28' 25.43" | 406.58 |

Chapter 10

References

- Abelló, P., Carbonell, A., Torres, P., 2002. Biogeography of epibenthic crustaceans on the shelf and upper slope off the Iberian Peninsula Mediterranean coasts: Implications for the establishment of natural management areas. *Sci. Mar.* 66, 183–198. <https://doi.org/10.3989/scimar.2002.66s2183>
- Abreu, V., Sullivan, M., Pirmez, C., Mohrig, D., 2003. Lateral accretion packages (LAPs): An important reservoir element in deep water sinuous channels. *Mar. Petrol. Geol.* 20, 631–648. <https://doi.org/10.1016/j.marpetgeo.2003.08.003>
- Adams, S.M., 2005. Assessing cause and effect of multiple stressors on marine systems. *Mar. Pollut. Bull.* 51, 649–657. <https://doi.org/10.1016/j.marpolbul.2004.11.040>
- Albérola, C., Rousseau, S., Millot, C., Astraldi, M., Font, J., Garcialafuente, J., Gasparini, Gp., Send, U., Vangriesheim, A., 1995. Tidal currents in the Western Mediterranean Sea. *Oceanol. Acta* 18, 273–284. <https://archimer.ifremer.fr/doc/00097/20777/>
- Aldaya, F., 1981. Mapa Geológico y Memoria Explicativa de la Hoja 1056 (Albuñol) del Mapa Geológico de España. IGME, Madrid.
- Aldaya, F., García-Dueñas, V., Navarro-Vilá, F., 1979. Los Mantos Alpujárrides del tercio central de las Cordilleras Béticas. Ensayo de la correlación tectónica de los Alpujárrides. *Acta Geol. Hisp.* 14, 154–166.
- Allin, J.R., Hunt, J.E., Talling, P.J., Clare, M.A., Pope, E., Masson, D.G., 2016. Different frequencies and triggers of canyon filling and flushing events in Nazaré Canyon, offshore Portugal. *Mar. Geol.* 371, 89–105. <https://doi.org/10.1016/j.margeo.2015.11.005>
- Alonso, B., Ercilla, G., 2002a. Architecture of modern turbidite systems in different geologic settings on the Spanish margins (NW and SW Mediterranean Sea). In: Briand, F. (Ed.), *Turbidite systems and deep-sea fans of the Mediterranean and the Black seas*. CIESM, Monaco, pp. 19–22.
- Alonso, B., Ercilla, G., 2002b. Small turbidite systems in a complex tectonic setting (SW Mediterranean Sea): Morphology and growth patterns. *Mar. Petrol. Geol.* 19, 1225–1240. [https://doi.org/10.1016/S0264-8172\(03\)00036-9](https://doi.org/10.1016/S0264-8172(03)00036-9)

- Alonso, B., Maldonado, A., 1992. Plio-Quaternary margin growth patterns in a complex tectonic setting: Northeastern Alboran Sea. *Geo-Mar. Lett.* 12, 137–143. <https://doi.org/10.1007/BF02084924>
- Alves, T.M., Kokinou, E., Ekström, M., Nikolaidis, A., Georgiou, G.C., Miliou, A., 2021. Scientific, societal and pedagogical approaches to tackle the impact of climate change on marine pollution. *Sci. Rep.* 11, 1–15. <https://doi.org/10.1038/s41598-021-82421-y>
- Amaro, T., Huvenne, V. A. I., Allcock, A. L., Aslam, T., Davies, J. S., Danovaro, R., de Stigter, H. C., Duineveld, G. C. A., Gambi, C., Gooday, A. J., Gunton, L. M., Hall, R., Howell, K. L., Ingels, J., Kiriakoulakis, K., Kershaw, C. E., Lavaleye, M. S. S., Robert, K., Stewart, H., Van Rooij, D., White, M., Wilson, A. M., 2016. The Whittard Canyon – A case study of submarine canyon processes. *Prog. Oceanogr.* 146, 38–57. <https://doi.org/10.1016/j.pocean.2016.06.003>
- Amblas, D., Gerber, T.P., De Mol, B., Urgeles, R., Garcia-Castellanos, D., Canals, M., Pratson, L.F., Robb, N., Canning, J., 2012. Survival of a submarine canyon during long-term outbuilding of a continental margin. *Geology* 40, 543–546. <https://doi.org/10.1130/G33178.1>
- Amblas, D., Ceramicola, S., Gerber, T.P., Canals, M., Chiocci, F.L., Dowdeswell, J.A., Harris, P.T., Huvenne, V.A.I., Lai, S.Y.J., Lastras, G., Iacono, C. Lo, Micallef, A., Mountjoy, J.J., Paull, C.K., Puig, P., Sanchez-Vidal, A., 2018. Submarine Canyons and Gullies. In: Micallef, A., Krastel, S., Savini, A. (Eds.), *Submarine Geomorphology*. Springer Geol. Springer, pp. 251–272. https://doi.org/10.1007/978-3-319-57852-1_14
- Amblas, D., Micallef, A., Ceramicola, S., Gerber, T.P., Canals, M., Casalbore, D., Chiocci, F.L., Duran, R., Harris, P.T., Huvenne, V.A.I., Lai, S.Y.J., Lastras, G., Lo Iacono, C., Matos, F.L., Mountjoy, J.J., Paull, C.K., Puig, P., Sanchez-Vidal, A., 2022. In: Shroder, J (Ed.), 8.30-Submarine Canyons. *Treatise on Geomorphology*, Elsevier, Academic Press, pp. 830–846. <https://doi.org/10.1016/B978-0-12-818234-5.00146-2>
- Andrieux, O., Cooper, C. K., Wood J., 2013. Turbidity Current Measurements in the Congo Canyon. Offshore Technology Conference, Houston, Texas, USA, OTC-23992-MS. <https://doi.org/10.4043/23992-MS>
- Angiolillo, M., 2019. Chapter 14 - Debris in Deep Water, World Seas. In: Sheppard, C., (Ed.), *World Seas: an EEnvironmental Evaluation (Second edition)*. Volumen III: Ecological

- Issues and Environmental Impacts, Elsevier, Academic Press, pp. 251–268.
<https://doi.org/10.1016/B978-0-12-805052-1.00015-2>
- Angiolillo, M., Lorenzo, B. di, Farcomeni, A., Bo, M., Bavestrello, G., Santangelo, G., Cau, Angelo, Mastascusa, V., Cau, Alessandro, Sacco, F., Canese, S., 2015. Distribution and assessment of marine debris in the deep Tyrrhenian Sea (NW Mediterranean Sea, Italy). *Mar. Pollut. Bull.* 92, 149–159. <https://doi.org/10.1016/j.marpolbul.2014.12.044>
- Angiolillo, M., G rigny, O., Valente, T., Fabri, M.C., Tambute, E., Rouanet, E., Claro, F., Tunesi, L., Vissio, A., Daniel, B., Galgani, F., 2021. Distribution of seafloor litter and its interaction with benthic organisms in deep waters of the Ligurian Sea (Northwestern Mediterranean). *Sci. Total Environ.* 788, 147745. <https://doi.org/10.1016/j.scitotenv.2021.147745>
- Andersen, T.J., 2017. Some practical considerations regarding the application of ^{210}Pb and ^{137}Cs dating to estuarine sediments. In: Weckstr m, K., Saunders, K., Gell, P., Skilbeck, C. (Eds.), *Applications of paleoenvironmental techniques in estuarine studies, developments in paleoenvironmental research*, Springer, pp. 121–140. https://doi.org/10.1007/978-94-024-0990-1_6
- Appleby, P.G., 2001. Chronostratigraphic techniques in recent sediments. In: Last, W. M., Smol, J. P. (Eds.), *Tracking environmental change using lake sediments. Developments in Paleoenvironmental Research*, Springer, 1, pp. 171–203. https://doi.org/10.1007/0-306-47669-X_9
- Appleby, P.G., Oldfield, F., 1978. The calculation of lead-210 dates assuming a constant rate of supply of unsupported ^{210}Pb to the sediment. *Catena* 5, 1–8. [https://doi.org/10.1016/S0341-8162\(78\)80002-2](https://doi.org/10.1016/S0341-8162(78)80002-2)
- Arabelos, D.N., Papazachariou, D.Z., Contadakis, M.E., Spatalas, S.D., 2011. A new tide model for the Mediterranean Sea based on altimetry and tide gauge assimilation. *Ocean. Sci.* 7, 429–444. <https://doi.org/10.5194/os-7-429-2011>
- Armitage, D.A., McHargue, T., Fildani, A., Graham, S.A., 2012. Postavulsion channel evolution: Niger Delta continental slope. *AAPG Bull.* 96, 823–843. <https://doi.org/10.1306/09131110189>

- Arzola, R.G., Wynn, R.B., Lastras, G., Masson, D.G., Weaver, P.P.E., 2008. Sedimentary features and processes in the Nazaré and Setúbal submarine canyons, west Iberian margin. *Mar. Geol.* 250, 64–88. <https://doi.org/10.1016/j.margeo.2007.12.006>
- Ayuntamiento de Motril. Medio Ambiente Urbano, 2021. Anexo 2: Residuos urbanos y asimilables a urbanos. *Motril Agenda 21*, 45-73.
- Azpiroz-Zabala, M., Cartigny, M.J.B., Talling, P.J., Parsons, D.R., Sumner, E.J., Clare, M.A., Simmons, S.M., Cooper, C., Pope, E.L., 2017. Newly recognized turbidity current structure can explain prolonged flushing of submarine canyons. *Sci. Adv.* 3, e1700200. <https://doi.org/10.1126/sciadv.1700200>
- Babonneau, N., Savoye, B., Cremer, M., Klein, B., 2002. Morphology and architecture of the present canyon and channel system of the Zaire deep-sea fan. *Mar. Petrol. Geol.* 19, 445–467. [https://doi.org/10.1016/S0264-8172\(02\)00009-0](https://doi.org/10.1016/S0264-8172(02)00009-0)
- Babonneau, N., Savoye, B., Cremer, M., Bez, M., 2004. Multiple terraces within the deep incised Zaire Valley (ZaïAngo Project): Are they confined levees? *Geol. Soc. Spec. Publ.* 222, 91–114. <https://doi.org/10.1144/GSL.SP.2004.222.01.06>
- Babonneau, N., Cremer, M., Bez, M., 2010. Sedimentary architecture in meanders of a submarine channel: Detailed study of the present Congo turbidite channel (zaïango project). *J. Sediment. Res.* 80, 852–866. <https://doi.org/10.2110/jsr.2010.078>
- Babonneau, N., Delacourt, C., Cancouët, R., Sisavath, E., Bachèlery, P., Mazuel, A., Jorry, S.J., Deschamps, A., Ammann, J., Villeneuve, N., 2013. Direct sediment transfer from land to deep-sea: Insights into shallow multibeam bathymetry at La Réunion Island. *Mar. Geol.* 346, 47–57. <https://doi.org/10.1016/j.margeo.2013.08.006>
- Babonneau, N., Cattaneo, A., Ratzov, G., Déverchère, J., Yelles-Chaouche, A., Lateb, T., Bachir, R.S., 2017. Turbidite chronostratigraphy off Algiers, central Algerian margin: A key for reconstructing Holocene paleo-earthquake cycles. *Mar. Geol.* 384, 63–80. <https://doi.org/10.1016/j.margeo.2016.10.017>
- Bache, F., Popescu, S.-M., Rabineau, M., Gorini, C., Suc, J.-P., Clauzon, G., Olivet, J.-L., Rubino, J.-L., Melinte-Dobrinescu, M.C., Estrada, F., Londeix, L., Armijo, R., Meyer, B., Jolivet, L., Jouannic, G., Leroux, E., Aslanian, D., Reis, A.T.D., Mocochain, L., Dumurdžanov, N., Zagorchev, I., Lesić, V., Tomić, D., Namık Çağatay, M., Brun, J.-P., Sokoutis, D., Csato, I., Uçarkus, G., Çakır, Z., 2012. A two-knickpoint process for

- the reflooding of the Mediterranean after the Messinian Salinity Crisis. *Basin Res.* 24, 125–153. <https://doi.org/10.1111/j.1365-2117.2011.00521.x>
- Bailey, L.P., Clare, M.A., Rosenberger, K.J., Cartigny, M.J.B., Talling, P.J., Paull, C.K., Gwiazda, R., Parsons, D.R., Simmons, S.M., Xu, J., Haigh, I.D., Maier, K.L., McGann, M., Lundsten, E., 2021. Preconditioning by sediment accumulation can produce powerful turbidity currents without major external triggers. *Earth Planet. Sci. Lett.* 562, 116845. <https://doi.org/10.1016/j.epsl.2021.116845>
- Ballesteros, M., Rivera, J., Muñoz, A., Muñoz-Martín, A., Acosta, J., Carbó, A., Uchupi, E., 2008. Alboran Basin, southern Spain-Part II: Neogene tectonic implications for the orogenic float model. *Mar. Petrol. Geol.* 25, 75–101. <https://doi.org/10.1016/j.marpetgeo.2007.05.004>
- Bárcenas, P., 2013. Procesos Morfogenéticos y Evolución Reciente de los Depósitos Prodeltaicos del Sureste de la Península Ibérica: aplicaciones de Modelos Matemáticos. Ph.D. Thesis Doctoral, University of Malaga. Malaga, Spain, 432 pp.
- Bárcenas, P., Lobo, F.J., Macías, J., Fernández-Salas, L.M., Díaz del Río, V., 2011. Spatial variability of surficial sediments on the northern shelf of the Alboran Sea: the effects of hydrodynamic forcing and supply of sediment by rivers. *J. Iber. Geol.* 37, 195–214. https://doi.org/10.5209/rev_JIGE.2011.v37.n2.8
- Bárcenas, P., Lobo, F.J., Macías, J., Fernández-Salas, L.M., López-González, N., Díaz del Río, V., 2015. Submarine deltaic geometries linked to steep, mountainous drainage basins in the northern shelf of the Alboran Sea: Filling the gaps in the spectrum of deltaic deposition. *Geomorphology* 232, 125–144. <https://doi.org/10.1016/j.geomorph.2014.11.028>
- Baro, J., García-Jiménez, T., Serna-Quintero J.M., 2021. Description of Artisanal Fisheries in Northern Alboran Sea, in Alboran Sea. In: J.C. Báez, J.T. Vázquez, J.A. Camiñas, M. Malouli Idrissi (Eds.), *Alboran Sea – Ecosystems and Marine Resources*. Springer, pp. 524–542. https://doi.org/10.1007/978-3-030-65516-7_14
- Baztan, J., Berné, S., Olivet, J.L., Rabineau, M., Aslanian, D., Gaudin, M., Réhault, J.P., Canals, M., 2005. Axial incision: The key to understand submarine canyon evolution (in the western Gulf of Lion). *Mar. Petrol. Geol.* 22, 805–826. <https://doi.org/10.1016/j.marpetgeo.2005.03.011>

- Bellan-Santini, D., Bellan, G., Bitar, G., Harmelin, J.G., Pergent, G., 2007. Handbook for interpreting types of marine habitat for the selection of sites to be included in the national inventories of natural sites of conservation interest. UNEP-MAP RAC/SPA, Tunisia, 168 pp.
- Bengtsson, L., Enell, M., 1986. Chemical analysis. In: Berglund, B.E. (Ed.), Handbook of Holocene palaeoecology and paleohydrology, vol 4. Wiley, New York, pp. 423–455. <https://doi.org/10.1002/gea.3340040208>
- Bergmann, M., Collard, F., Fabres, J., Gabrielsen, G.W., Provencher, J.F., Rochman, C.M., van Sebille, E., Tekman, M.B., 2022. Plastic pollution in the Arctic. *Nat. Rev. Earth Environ.* 3, 323–337. <https://doi.org/10.1038/s43017-022-00279-8>
- Bernhardt, A., Schwanghart, W., 2021. Where and why do submarine canyons remain connected to the shore during sea-level rise? Insights from global topographic analysis and Bayesian regression. *Geophys. Res. Lett.* 48, e2020GL092234. <https://doi.org/10.1029/2020GL092234>
- Bernhardt, A., Melnick, D., Jara-Muñoz, J., Argandoña, B., González, J., Strecker, M.R., 2015. Controls on submarine canyon activity during sea-level highstands: The Biobío canyon system offshore Chile. *Geosphere* 11, 1226–1255. <https://doi.org/10.1130/GES01063.1>
- Blum, M.D., Hattier-Womack, J., 2009. Climate change, sea-level change, and fluvial sediment supply to deepwater depositional systems. In: Kneller, B.C., McCaffrey, W.D., Martinsen, O.J. (Eds.), External controls on deep-water depositional systems. *SEPM Spec. Publ.* 92. <https://doi.org/10.2110/sepmssp.092.015>
- Biscara, L., Mulder, T., Martinez, P., Baudin, F., Etcheber, H., Jouanneau, J.M., Garlan, T., 2011. Transport of terrestrial organic matter in the Ogooué deep sea turbidite system (Gabon). *Mar. Petrol. Geol.* 28, 1061–1072. <https://doi.org/10.1016/j.marpetgeo.2010.12.002>
- Bolliet, T., Jorissen, F.J., Schmidt, S., Howa, H., 2014. Benthic foraminifera from Cap Breton Canyon revisited; faunal evolution after repetitive sediment disturbance. *Deep-Sea Res. II* 104, 319–334. <https://doi.org/10.1016/j.dsr2.2013.09.009>
- Bonnin, J., Heussner, S., Calafat, A., Fabres, J., Palanques, A., Durrieu de Madron, X., Canals, M., Puig, P., Avril, J., Delsaut, N., 2008. Comparison of horizontal and

- downward particle fluxes across canyons of the Gulf of Lions (NW Mediterranean): Meteorological and hydrodynamical forcing. *Cont. Shelf Res.* 28, 1957–1970. <https://doi.org/10.1016/j.csr.2008.06.004>
- Bosman, A., Casalbore, D., Dominici, R., 2017. Cyclic steps at the head of channelized features along the calabrian margin (Southern Tyrrhenian Sea, Italy). In: *Atlas of bedforms in the western Mediterranean*. Springer, pp. 229–233. https://doi.org/10.1007/978-3-319-33940-5_35
- Boyd, R., Ruming, K., Goodwin, I., Sandstrom, M., Schröder-Adams, C., 2008. Highstand transport of coastal sand to the deep ocean: A case study from Fraser Island, southeast Australia. *Geology* 36, 15–18. <https://doi.org/10.1130/G24211A.1>
- Bozzano, G., Alonso, B., Ercilla, G., Estrada, F., García, M., 2009. Late Pleistocene and Holocene Depositional Facies of the Almeria Channel (Alboran Sea, Western Mediterranean). *Extern. Control. Deep. Depos. Syst.* 92, 199–206. <https://doi.org/10.2110/sepmsp.092.199>
- Brankart, J.M., Pinardi, N., 2001. Abrupt cooling of the Mediterranean levantine intermediate water at the beginning of the 1980s: Observational evidence and model simulations. *J. Phys. Oceanogr.* 31, 2307–2320. [https://doi.org/10.1175/1520-0485\(2001\)031<2307:acotml>2.0.co;2](https://doi.org/10.1175/1520-0485(2001)031<2307:acotml>2.0.co;2)
- Brothers, D.S., Brink, U.S., Andrews, B.D., Chaytor, J.D., 2013. Geomorphic characterization of the U.S. Atlantic continental margin. *Mar. Geol.* 338, 46–63. <https://doi.org/10.1016/j.margeo.2012.12.008>
- Browne, M.A., Underwood, A.J., Chapman, M.G., Williams, R., Thompson, R.C., Van Franeker, J.A., 2015. Linking effects of anthropogenic debris to ecological impacts. *Proc. R. Soc. B Biol. Sci.* 282, 20142929. <https://doi.org/10.1098/rspb.2014.2929>
- Campos, J., Maldonado, A., Campillo, A.C., 1992. Post-Messinian evolutionary patterns of the Central Alboran Sea. *Geo-Mar. Lett.* 12, 173–178. <https://doi.org/10.1007/BF02084929>
- Canals, M., Casamor, J.L., Lastras, G., Monaco, A., Acosta, J., Berné, S., Loubrieu, B., Weaver, P.P.E., Grehan, A., Dennielou, B., 2004. The role of canyons in strata formation. *Oceanography* 17, 80–91. <https://doi.org/10.5670/oceanog.2004.06>

- Canals, M., Puig, P., De Madron, X.D., Heussner, S., Palanques, A., Fabres, J., 2006. Flushing submarine canyons. *Nature* 444, 354–357. <https://doi.org/10.1038/nature05271>
- Canals, M., Pham, C.K., Bergmann, M., Gutow, L., Hanke, G., van Sebille, E., Angiolillo, M., Buhl-Mortensen, L., Cau, A., Ioakeimidis, C., Kammann, U., Lundsten, L., Papatheodorou, G., Purser, A., Sanchez-Vidal, A., Schulz, M., Vinci, M., Chiba, S., Galgani, F., Langenkämper, D., Möller, T., Nattkemper, T.W., Ruiz, M., Suikkanen, S., Woodall, L., Fakiris, E., Molina Jack, M.E., Giorgetti, A., 2021. The quest for seafloor macrolitter: A critical review of background knowledge, current methods and future prospects. *Environ. Res. Lett.* 16, 023001. <https://doi.org/10.1088/1748-9326/abc6d4>
- Carter, L., Carter, R.M., Nelson, C.S., Fulthorpe, C.S., Neil, H.L., 1990. Evolution of Pliocene to Recent abyssal sediment waves on Bounty Channel levees, New Zealand. *Mar. Geol.* 95, 97–109. [https://doi.org/10.1016/0025-3227\(90\)90043-J](https://doi.org/10.1016/0025-3227(90)90043-J)
- Cartigny, M.J.B., Postma, G., van den Berg, J.H., Mastbergen, D.R., 2011. A comparative study of sediment waves and cyclic steps based on geometries, internal structures and numerical modeling. *Mar. Geol.* 280, 40–56. <http://dx.doi.org/10.1016/j.margeo.2010.11.006>
- Cartigny, M.J.B., Eggenhuisen, J.T., Hansen, E.W.M., Postma, G., 2013. Concentration-dependent flow stratification in experimental high-density turbidity currents and their relevance to turbidite facies models. *J. Sediment. Res.* 83, 1046–1064. <https://doi.org/10.2110/jsr.2013.71>
- Cartigny, M.J.B., Ventra, D., Postma, G., van Den Berg, J.H., 2014. Morphodynamics and sedimentary structures of bedforms under supercritical-flow conditions: New insights from flume experiments. *Sedimentology* 61, 712–748. <https://doi.org/10.1111/sed.12076>
- Carugati, L., Lo Martire, M., Danovaro, R., 2019. Patterns and drivers of meiofaunal assemblages in the canyons Polcevera and Bisagno of the Ligurian Sea (NW Mediterranean Sea). *Prog. Oceanogr.* 175, 81–91. <https://doi.org/10.1016/j.pocean.2019.03.010>
- Carvajal, C.R., Steel, R.J., 2006. Thick turbidite successions from supply-dominated shelves during sea-level highstand. *Geology* 34, 665–668. <https://doi.org/10.1130/G22505.1>

- Carvajal, C., Paull, C.K., Caress, D.W., Fildani, A., Lundsten, E., Anderson, K., Maier, K.L., McGann, M., Gwiazda, R., Herguera, J.C., 2017. Unraveling the channel-lobe transition zone with high-resolution AUV bathymetry: Navy Fan, offshore Baja California, Mexico. *J. Sediment. Res.* 87, 1049–1059. <https://doi.org/10.2110/jsr.2017.58>
- Casalbore, D., Romagnoli, C., Bosman, A., Chiocci, F.L., 2014. Large-scale seafloor waveforms on the flanks of insular volcanoes (Aeolian Archipelago, Italy), with inferences about their origin. *Mar. Geol.* 355, 318–329. <https://doi.org/10.1016/j.margeo.2014.06.007>
- Casalbore, D., Falcini, F., Martorelli, E., Morelli, E., Bosman, A., Calarco, M., Chiocci, F.L., 2018. Characterization of overbanking features on the lower reach of the Gioia-Mesima canyon-channel system (southern Tyrrhenian Sea) through integration of morpho-stratigraphic data and physical modelling. *Prog. Oceanogr.* 169, 66–78. <https://doi.org/10.1016/j.pocean.2018.02.020>
- Cau, A., Alvito, A., Moccia, D., Canese, S., Pusceddu, A., Rita, C., Angiolillo, M., Follesa, M.C., 2017a. Submarine canyons along the upper Sardinian slope (Central Western Mediterranean) as repositories for derelict fishing gears. *Mar. Pollut. Bull.* 123, 357–364. <https://doi.org/10.1016/j.marpolbul.2017.09.010>
- Cau, A., Moccia, D., Follesa, M.C., Alvito, A., Canese, S., Angiolillo, M., Cuccu, D., Bo, M., Cannas, R., 2017b. Coral forests diversity in the outer shelf of the south Sardinian continental margin. *Deep. Res. Part I Oceanogr. Res. Pap.* 122, 60–70. <https://doi.org/10.1016/j.dsr.2017.01.016>
- Cerrillo-Escoriza, J., Lobo, F.J., Puga-Bernabéu, Á., Rueda, J.L., Bárcenas, P., Sánchez-Guillamón O, Serna Quintero, J.M., Pérez Gil, J.L., Murillo, Y., Caballero-Herrera, J.A., López-Quirós, A., Mendes, I., Pérez Asensio, J.N., 2023. Origin and driving mechanisms of marine litter in the shelf- incised Motril, Carchuna, and Calahonda canyons (northern Alboran Sea). *Front. Mar. Sci.* 10, 1–24. <https://doi.org/10.3389/fmars.2023.1098927>
- Cerrillo-Escoriza, J., Lobo, F. J., Puga-Bernabéu, Bárcenas, P., Mendes, I., Pérez-Asensio, J. N., Durán, R., Andersen, T. J., Carrión-Torrente, García, M., López-Quirós, A., Luján, M., Mena, A., Sánchez-Guillamón, O., Sánchez, M. J., 2024. Variable downcanyon morphology controlling the recent activity of shelf-incised submarine canyons

- (Alboran Sea, western Mediterranean). *Geomorphology* 453, 109127. <https://doi.org/10.1016/j.geomorph.2024.109127>
- Chiang, C.S., Yu, H.S., 2006. Morphotectonics and incision of the Kaoping submarine canyon, SW Taiwan orogenic wedge. *Geomorphology* 80, 199–213. <https://doi.org/10.1016/j.geomorph.2006.02.008>
- Chiang, C.S., Yu, H.S., 2022. Controls of submarine canyons connected to shore during the LGM sea-level rise: examples from Taiwan. *J. Mar. Sci. Eng.* 10, 494. <https://doi.org/10.3390/jmse10040494>
- Ciércoles, C., García-Ruiz, C., González-Aguilar, M., Ortiz de Urbina Gutiérrez, J., López-González, N., Urra-Recuero, J., Rueda, J., 2018. Molluscs collected with otter trawl in the northern Alboran Sea: main assemblages, spatial distribution and environmental linkage. *Mediterr. Mar. Sci.* 19, 209–222. <https://doi.org/10.12681/mms.2124>
- Ciércoles, C., García-Ruiz, C., Abelló, P., Hidalgo, M., Torres, P., González, M., Mateo-Ramírez, Á., Rueda, J.L., 2022. Decapod crustacean assemblages on trawlable grounds in the northern Alboran Sea and Gulf of Vera. *Sci. Mar.* 86. <https://doi.org/10.3989/scimar.05265.039>
- Clare, M. A., Hughes Clarke, J. E., Talling, P. J., Cartigny, M. J. B., Pratomo, D. G., 2016. Preconditioning and triggering of offshore slope failures and turbidity currents revealed by most detailed monitoring yet at a fjord-head delta. *Earth Planet. Sc. Lett.* 450, 208–220. <https://doi.org/10.1016/j.epsl.2016.06.021>
- Clark, J.D., Pickering, K.T., 1996. Architectural elements and growth patterns of submarine channels: Application to hydrocarbon exploration. *AAPG Bull.* 80, 194–221. <https://doi.org/10.1306/64ed878c-1724-11d7-8645000102c1865d>
- Clark, J., Kenyon, N., Pickering, K., 1992. Quantitative analysis of the geometry of submarine levees. *Geology* 20, 633–636. [https://doi.org/10.1130/0091-7613\(1992\)020<0633](https://doi.org/10.1130/0091-7613(1992)020<0633)
- Clark, M.R., Althaus, F., Schlacher, T.A., Williams, A., Bowden, D.A., Rowden, A.A., 2016. The impacts of deep-sea fisheries on benthic communities: A review. *ICES J. Mar. Sci.* 73, i51–i69. <https://doi.org/10.1093/icesjms/fsv123>

- Clift, P.D., Giosan, L., Henstock, T.J., Tabrez, A.R., 2014. Sediment storage and reworking on the shelf and in the Canyon of the Indus River-Fan System since the last glacial maximum. *Basin Res.* 26, 183–202. <https://doi.org/10.1111/bre.12041>
- Comas, M.C., García-Dueñas, V., Jurado, M.J., 1992. Neogene tectonic evolution of the Alboran Sea from MCS data. *Geo-Mar. Lett.* 12, 157–164. <https://doi.org/10.1007%2FBF02084927>
- Comas, M.C., Platt, J.P., Soto, J.I., Watts, A.B., 1999. The origin and tectonic history of the Alboran Basin: Insights from Leg 161 results. *Proc. Ocean Drill. Progr. Sci. Results* 161, 555–580. <https://doi.org/10.2973/odp.proc.sr.161.262.1999>
- Conway, K.W., Barrie, J.V., Picard, K., Bornhold, B.D., 2012. Submarine channel evolution: Active channels in fjords, British Columbia, Canada. *Geo-Marine Lett.* 32, 301–312. <https://doi.org/10.1007/s00367-012-0280-4>
- Covault, J.A., Graham, S.A., 2010. Submarine fans at all sea-level stands: Tectono-morphologic and climatic controls on terrigenous sediment delivery to the deep sea. *Geology* 38, 939–942. <https://doi.org/10.1130/G31081.1>
- Covault, J.A., Normark, W.R., Romans, B.W., Graham, S.A., 2007. Highstand fans in the California borderland: The overlooked deep-water depositional systems. *Geology* 35, 783–786. <https://doi.org/10.1130/G23800A.1>
- Covault, J.A., Romans, B.W., Fildani, A., McGann, M., Graham, S.A., 2010. Rapid climatic signal propagation from source to sink in a southern California sediment-routing system. *J. Geol.* 118, 247–259. <https://doi.org/10.1086/651539>
- Covault, J.A., Fildani, A., Romans, B.W., McHargue, T., 2011. The natural range of submarine canyon-and-channel longitudinal profiles. *Geosphere* 7, 313–332. <https://doi.org/10.1130/GES00610.1>
- Covault, J.A., Kostic, S., Paull, C.K., Ryan, H., Fildani, A., 2014. Submarine channel initiation, filling, and maintenance from sea-floor geomorphology and morphodynamic modelling of cyclic steps. *Sedimentology* 61, 1031–1054. <http://dx.doi.org/10.1111/sed.12084>
- Covault, J.A., Kostic, S., Paull, C.K., Sylvester, Z., Fildani, A., 2017. Cyclic steps and related supercritical bedforms: Building blocks of deep-water depositional systems, western

- North America. Mar. Geol. 393, 4–20.
<https://doi.org/10.1016/J.MARGE0.2016.12.009>
- Cronin, B.T., Akhmetzhanov, A.M., Mazzini, A., Akhmanov, G., Ivanov, M., Kenyon, N.H., 2005. Morphology, evolution and fill: Implications for sand and mud distribution in filling deep-water canyons and slope channel complexes. *Sediment. Geol.* 179, 71–97.
<https://doi.org/10.1016/j.sedgeo.2005.04.013>
- Dalla Valle, G., Gamberi, F., 2011. Slope channel formation, evolution and backfilling in a wide shelf, passive continental margin (northeastern sardinia slope, central tyrrhenian sea). *Mar. Geol.* 286, 95–105. <https://doi.org/10.1016/j.margeo.2011.06.005>
- Daly, R.A., 1936. Origin of submarine “canyons”. *Am. J. Sci.* 31, 401–420.
<https://doi.org/10.2475/ajs.s5-31.186.401>
- De Stephanis, R., Giménez, J., Carpinelli, E., Gutierrez-Exposito, C., Cañadas, A., 2013. As main meal for sperm whales: Plastics debris. *Mar. Pollut. Bull.* 69, 206–214.
<https://doi.org/10.1016/j.marpolbul.2013.01.033>
- de Stigter, H.C., Boer, W., de Jesus Mendes, P.A., Jesus, C.C., Thomsen, L., van den Bergh, G.D., van Weering, T.C.E., 2007. Recent sediment transport and deposition in the Nazaré Canyon, Portuguese continental margin. *Mar. Geol.* 246, 144–164.
<https://doi.org/10.1016/j.margeo.2007.04.011>
- de Stigter, H.C., Jesus, C.C., Boer, W., Richter, T.O., Costa, A., van Weering, T.C.E., 2011. Recent sediment transport and deposition in the Lisbon-Setúbal and Cascais submarine canyons, Portuguese continental margin. *Deep. Res. Part II Top. Stud. Oceanogr.* 58, 2321–2344. <https://doi.org/10.1016/j.dsr2.2011.04.001>
- Dean, W.E.Jr., 1974. Determination of carbonate and organic matter in calcareous sediments and sedimentary rocks by loss on ignition: Comparison with other methods. *J. Sediment. Petrol.* 44, 242–248. <https://doi.org/10.1306/74D729D2-2B21-11D7-8648000102C1865D>
- DeGeest, A.L., Mullenbach, B.L., Puig, P., Nittrouer, C.A., Drexler, T.M., Durrieu de Madron, X., Orange, D.L., 2008. Sediment accumulation in the western Gulf of Lions, France: The role of Cap de Creus Canyon in linking shelf and slope sediment dispersal systems. *Cont. Shelf Res.* 28, 2031–2047. <https://doi.org/10.1016/j.csr.2008.02.008>

- Densmore, A.L., Anderson, R.S., McAdoo, B.G., Ellis, M.A., 1997. Hillslope evolution by bedrock landslides. *Science* 275, 369–372. <https://doi.org/10.1126/science.275.5298.369>
- Deptuck, M.E., Sylvester, Z., 2018. Submarine Fans and Their Channels, Levees, and Lobes. In: Micallef, A., Krastel, S., Savini, A. (Eds.), *Submarine Geomorphology*. Springer, pp. 273–299. https://doi.org/10.1007/978-3-319-57852-1_15
- Deudero, S., Alomar, C., 2015. Mediterranean marine biodiversity under threat: Reviewing influence of marine litter on species. *Mar. Pollut. Bull.* 98, 58–68. <https://doi.org/10.1016/j.marpolbul.2015.07.012>
- Dietrich, P., Ghienne, J.F., Normandeau, A., Lajeunesse, P., 2016. Upslope-migrating bedforms in a proglacial sandur delta: Cyclic steps from river-derived underflows? *J. Sediment. Res.* 86, 113–123. <https://doi.org/10.2110/jsr.2016.4>
- Dissanayake, A., Davies, J.S., Kiriakoulakis, K., Huvenne, V.A.I., 2023. Editorial: Submarine canyons: human connections to the deep sea. *Front. Mar. Sci.* 10, 9–11. <https://doi.org/10.3389/fmars.2023.1304429>
- Dobbs, S.C., Paull, C.K., Lundsten, E.M., Gwiazda, R., Caress, D.W., McGann, M., Coholich, M.M., Walton, M.A.L., Nieminski, N.M., McHargue, T., Graham, S.A., 2023. Sediment gravity flow frequency offshore central California diminished significantly following the Last Glacial Maximum. *Front. Mar. Sci.* 10, 1–12. <https://doi.org/10.3389/fmars.2023.1099472>
- Dominguez-Carrió, C., 2018. ROV-based ecological study and management proposals for the offshore Marine Protected Area of Cap de Creus (NW Mediterranean). Ph.D. Thesis Doctoral, University of Barcelona. Barcelona, Spain, 345 pp.
- Dominguez-Carrió, C., Sanchez-Vidal, A., Estournel, C., Corbera, G., Riera, J.L., Orejas, C., Canals, M., Gili, J.M., 2020. Seafloor litter sorting in different domains of Cap de Creus continental shelf and submarine canyon (NW Mediterranean Sea). *Mar. Pollut. Bull.* 161, 111744. <https://doi.org/10.1016/j.marpolbul.2020.111744>
- Drexler, T.M., Nittrouer, C.A., Mullenbach, B.L., 2006. Impact for local morphology on sedimentation in a submarine canyon, ROV studies in Eel Canyon, Northern California, U.S.A. *J. Sediment. Res.* 76, 839–853. <https://doi.org/10.2110/jsr.2006.064>

- Droghei, R., Falcini, F., Casalbore, D., Martorelli, E., Mosetti, R., Sannino, G., Santoleri, R., Chiocci, F.L., 2016. The role of Internal Solitary Waves on deep-water sedimentary processes: The case of up-slope migrating sediment waves off the Messina Strait. *Sci. Rep.* 6, 1–8. <https://doi.org/10.1038/srep36376>
- Droz, L., Marsset, T., Ondréas, H., Lopez, M., Savoye, B., Spy-Anderson, F.L., 2003. Architecture of an active mud-rich turbidite system: The Zaire Fan (Congo–Angola margin southeast Atlantic) Results from ZaïAngo 1 and 2 cruises. *AAPG Bull.* 87, 1145–1168. <https://doi.org/10.1306/03070300013>
- Du Buit, M., 1978. Alimentation de quelques poissons téléostéens de profondeur dans la zone du seuil de Wyville Thomson. *Oceanol. Acta* 1, 129–134.
- Duros, P., Jorissen, F.J., Cesbron, F., Zaragosi, S., Schmidt, S., Metzger, E., Fontanier, C., 2014. Benthic foraminiferal thanatocoenoses from the Cap-Ferret Canyon area (NE Atlantic): A complex interplay between hydro-sedimentary and biological processes. *Deep. Res. Part II Top. Stud. Oceanogr.* 104, 145–163. <https://doi.org/10.1016/j.dsr2.2013.09.024>
- Enrichetti, F., Dominguez-Carrió, C., Toma, M., Bavestrello, G., Canese, S., Bo, M., 2020. Assessment and distribution of seafloor litter on the deep Ligurian continental shelf and shelf break (NW Mediterranean Sea). *Mar. Pollut. Bull.* 151, 110872. <https://doi.org/10.1016/j.marpolbul.2019.110872>
- Ercilla, G., Alonso, B., Baraza, J., 1992. Sedimentary evolution of the northwestern Alboran Sea during the Quaternary. *Geo-Mar. Lett.* 12, 144–149. <https://doi.org/10.1007/BF02084925>
- Ercilla, G., Alonso, B., Baraza, J., 1994. Post-Calabrian sequence stratigraphy of the northwestern Alboran Sea (southwestern Mediterranean). *Mar. Geol.* 120, 249–265. [https://doi.org/10.1016/0025-3227\(94\)90061-2](https://doi.org/10.1016/0025-3227(94)90061-2)
- Ercilla, G., Juan, C., Hernández-Molina, F.J., Bruno, M., Estrada, F., Alonso, B., Casas, D., Farran, M. lí, Llave, E., García, M., Vázquez, J.T., D'Acremont, E., Gorini, C., Palomino, D., Valencia, J., El Moumni, B., Ammar, A., 2016. Significance of bottom currents in deep-sea morphodynamics: An example from the Alboran Sea. *Mar. Geol.* 378, 157–170. <https://doi.org/10.1016/j.margeo.2015.09.007>

- Ercilla, G., Juan, C., Periañez, R., Alonso, B., Abril, J.M., Estrada, F., Casas, D., Vázquez, J.T., d'Acremont, E., Gorini, C., El Moumni, B., Do Couto, D., Valencia, J., 2019. Influence of along slope processes on modern turbidite systems and canyons in the Alboran Sea (southwestern Mediterranean). *Deep. Res. Part I Oceanogr. Res. Pap.* 144, 1–16. <https://doi.org/10.1016/j.dsr.2018.12.002>
- Ercilla, G., Vázquez, J.T., Alonso, B., Bárcenas, Pa., Casas, D., d'Acremont, E., Estrada, F., Fernández-Salas, L.M., Galindo-Zaldívar, J., Juan, C., Lobo, F., López-González, N., Palomino, D., Sánchez-Guillamón, O., Chourak, M., Gil, A., Gómez-Ballesteros, M., El Moumni, B., Peláez, J.A., Valencia, J., Gorini, C., 2021. Seafloor Morphology and Processes in the Alboran Sea. In: J.C. Báez, J.T. Vázquez, J.A. Camiñas, M. Malouli Idrissi (Eds.), *Alboran Sea – Ecosystems and Marine Resources*. Springer, 6, pp. 157–205.
- Estrada, F., Ercilla, G., Alonso, B., 1997. Pliocene-Quaternary tectonic-sedimentary evolution of the NE Alboran Sea (SW Mediterranean Sea). *Tectonophysics* 282, 423–442. [https://doi.org/10.1016/S0040-1951\(97\)00227-8](https://doi.org/10.1016/S0040-1951(97)00227-8)
- Estrada, F., Ercilla, G., Gorini, C., Alonso, B., Vázquez, J.T., García-Castellanos, D., Juan, C., Maldonado, A., Ammar, A., Elabbassi, M., 2011. Impact of pulsed Atlantic water inflow into the Alboran Basin at the time of the Zanclean flooding. *Geo-Marine Lett.* 31, 361–376. <https://doi.org/10.1007/s00367-011-0249-8>
- European Commission of the European Union, 2013. *MSDF Guidance on Monitoring Marine Litter*. Luxembourg: Publications Office of the European Union. <https://doi.org/10.2788/99475>
- Fabres, J., Calafat, A., Sanchez-Vidal, A., Canals, M., Heussner, S., 2002. Composition and spatio-temporal variability of particle fluxes in the Western Alboran Gyre, Mediterranean Sea. *J. Mar. Syst.* 33–34, 431–456. [https://doi.org/10.1016/S0924-7963\(02\)00070-2](https://doi.org/10.1016/S0924-7963(02)00070-2)
- Fabres, J., Tesi, T., Velez, J., Batista, F., Lee, C., Calafat, A., Heussner, S., Palanques, A., Miserocchi, S., 2008. Seasonal and event-controlled export of organic matter from the shelf towards the Gulf of Lions continental slope. *Cont. Shelf Res.* 28, 1971–1983. <https://doi.org/10.1016/j.csr.2008.04.010>
- Fabri, M.C., Pedel, L., Beuck, L., Galgani, F., Hebbeln, D., Freiwald, A., 2014. Megafauna of vulnerable marine ecosystems in French mediterranean submarine canyons: Spatial

- distribution and anthropogenic impacts. *Deep. Res. Part II Top. Stud. Oceanogr.* 104, 184–207. <https://doi.org/10.1016/j.dsr2.2013.06.016>
- Fabri, M.C., Bargain, A., Pairaud, I., Pedel, L., Taupier-Letage, I., 2017. Cold-water coral ecosystems in Cassidaigne Canyon: An assessment of their environmental living conditions. *Deep. Res. Part II Top. Stud. Oceanogr.* 137, 436–453. <https://doi.org/10.1016/j.dsr2.2016.06.006>
- Fabri, M.C., Dugornay, O., de la Bernardie, X., Guerin, C., Sanchez, P., Arnaubec, A., Autin, T., Piasco, R., Puig, P., 2022. 3D-Representations for studying deep-sea coral habitats in the Lacaze-Duthiers Canyon, from geological settings to individual specimens. *Deep. Res. Part I Oceanogr. Res. Pap.* 187, 103831. <https://doi.org/10.1016/j.dsr.2022.103831>
- Fernandez-Arcaya, U., Ramirez-Llodra, E., Aguzzi, J., Allcock, A.L., Davies, J.S., Dissanayake, A., Harris, P., Howell, K., Huvenne, V.A.I., Macmillan-Lawler, M., Martín, J., Menot, L., Nizinski, M., Puig, P., Rowden, A.A., Sanchez, F., Van den Beld, I.M.J., 2017. Ecological role of submarine canyons and need for canyon conservation: A review. *Front. Mar. Sci.* 4, 1–26. <https://doi.org/10.3389/fmars.2017.00005>
- Fernández-Salas, L.M., Dabrio, C.J., Goy, J.L., Díaz del Río, V., Zazo, C., Lobo, F.J., Sanz, J.L., Lario, J., 2009. Land-sea correlation between Late Holocene coastal and infralittoral deposits in the SE Iberian Peninsula (Western Mediterranean). *Geomorphology* 104, 4–11. <https://doi.org/10.1016/j.geomorph.2008.05.013>
- Fildani, A., Normark, W.R., Kostic, S., Parker, G., 2006. Channel formation by flow stripping: Large-scale scour features along the Monterey East Channel and their relation to sediment waves. *Sedimentology* 53, 1265–1287. <https://doi.org/10.1111/j.1365-3091.2006.00812.x>
- Fildani, A., Hubbard, S.M., Covault, J.A., Maier, K.L., Romans, B.W., Traer, M., Rowland, J.C., 2013. Erosion at inception of deep-sea channels. *Mar. Petrol. Geol.* 41, 48–61. <https://doi.org/10.1016/j.marpetgeo.2012.03.006>
- Fildani, A., 2017. Submarine Canyons: A brief review looking forward. *Geology* 45, 383–384. <https://doi.org/10.1130/focus042017.1>

- Finnegan, N.J., Klier, R.A., Johnstone, S., Pfeiffer, A.M., Johnson, K., 2017. Field evidence for the control of grain size and sediment supply on steady-state bedrock river channel slopes in a tectonically active setting. *Earth Surf. Proc. Land.* 42, 2338–2349. <https://doi.org/10.1002/esp.4187>
- Fisher, W.L., Galloway, W.E., Steel, R.J., Olariu, C., Kerans, C., Mohrig, D., 2021. Deep-water depositional systems supplied by shelf-incising submarine canyons: Recognition and significance in the geologic record. *Earth-sci. Rev.* 214, 103531. <https://doi.org/10.1016/j.earscirev.2021.103531>
- Flood, R.D., Giosan, L., 2002. Migration history of a fine-grained abyssal sediment wave on the Bahama Outer Ridge. *Mar. Geol.* 192, 259–273. [https://doi.org/10.1016/S0025-3227\(02\)00558-3](https://doi.org/10.1016/S0025-3227(02)00558-3)
- FLOW-3D® Version 2022R1 [FLOW-3D HYDRO], 2022. Santa Fe, NM: Flow Science, Inc. <https://www.flow3d.com>
- Folk, R.L., 1954. The distinction between grain size and mineral composition in sedimentary rock nomenclature. *J. Geol.* 62, 344–359. <https://doi.org/10.1086/626171>
- Folk, R.L., Ward, W.C., 1957. Brazos River bar: A study in the significance of grain size parameters. *J. Sediment. Petrol.* 27, 3–26. <https://doi.org/10.1306/74D70646-2B21-11D7-8648000102C1865D>
- Fosså, J.H., Mortensen, P.B., Furevik, D.M., 2002. The deep-water coral *Lophelia pertusa* in Norwegian waters: Distribution and fishery impacts. *Hydrobiologia* 471, 1–12. <https://doi.org/10.1023/A:1016504430684>
- Frey-Martinez, J., Cartwright, J.A., Burgess, P.M., Bravo, J.V., 2004. 3D seismic interpretation of the Messinian unconformity in the Valencia, Spain. In: Davies, R.J., Cartwright, J.A., Stewart, S.A., Lappin, M., Underhill, R. (Eds.), 3D seismic technology: application to the exploration of sedimentary basins. *Geol Soc. Mem.*, pp. 91–100. <https://doi.org/10.1144/GSL.MEM.2004.029.01.10>
- Friedrichs, C.T., Wright, L.D., 2004. Gravity-driven sediment transport on the continental shelf: Implications for equilibrium profiles near river mouths. *Coast. Eng.* 51, 795–811. <https://doi.org/10.1016/j.coastaleng.2004.07.010>

- Galgani, F., Souplet, A., Cadiou, Y., 1996. Accumulation of debris on the deep sea floor off the French Mediterranean coast. *Mar. Ecol. Prog. Ser.* 142, 225–234. <https://doi.org/10.3354/meps142225>
- Galgani, F., Leaute, J.P., Moguedet, P., Souplet, A., Verin, Y., Carpentier, A., Goraguer, H., Latrouite, D., Andral, B., Cadiou, Y., Mahe, J.C., Poulard, J.C., Nerisson, P., 2000. Litter on the sea floor along European coasts. *Mar. Pollut. Bull.* 40, 516–527. [https://doi.org/10.1016/S0025-326X\(99\)00234-9](https://doi.org/10.1016/S0025-326X(99)00234-9)
- Galgani, F., Michela, A., G rigny, O., Maes, T., Tambutt , E., and Harris, P. T., 2022. Marine litter, plastic, and microplastics on the seafloor. In: *Plastics and the ocean: origin, characterization, fate, and impacts*. Andrady A.L (Ed). John Wiley & Sons, 151–197. <https://doi.org/10.1002/9781119768432.ch6>
- Gamberi, F., 2020. Systems supplying sediment to canyon heads (SSSCHs) in the Tyrrhenian Sea: The past and the present as a key to understanding deep-sea stratigraphy. *Mar. Petrol. Geol.* 119, 104470. <https://doi.org/10.1016/j.marpetgeo.2020.104470>
- Gamberi, F., Rovere, M., Dykstra, M., Kane, I.A., Kneller, B.C., 2013. Integrating modern seafloor and outcrop data in the analysis of slope channel architecture and fill. *Mar. Petrol. Geol.* 41, 83–103. <https://doi.org/10.1016/j.marpetgeo.2012.04.002>
- Gamberi, F., Breda, A., Mellere, D., 2017. Depositional canyon heads at the edge of narrow and tectonically steepened continental shelves: Comparing geomorphic elements, processes and facies in modern and outcrop examples. *Mar. Petrol. Geol.* 87, 157–170. <http://dx.doi.org/10.1016/j.marpetgeo.2017.06.007>
- Gamboa, D., Alves, T.M., Cartwright, J., 2012. A submarine channel confluence classification for topographically confined slopes. *Mar. Petrol. Geol.* 35, 176–189. <https://doi.org/10.1016/j.marpetgeo.2012.02.011>
- Garc a, M., Alonso, B., Ercilla, G., Gr cia, E., 2006. The tributary valley systems of the Almeria Canyon (Alboran Sea, SW Mediterranean): Sedimentary architecture. *Mar. Geol.* 226, 207–223. <https://doi.org/10.1016/j.margeo.2005.10.002>
- Garc a-Due as, V., Balany , J.C., Mart nez-Mart nez, J.M., 1992. Miocene extensional detachments in the outcropping basement of the northern Alboran Basin (Betics) and their tectonic implications. *Geo-Mar. Lett.* 12, 88–95. <https://doi.org/10.1007/BF02084917>

- García-Lafuente, J., Cano, N., Vargas, M., Rubín, J.P., Hernández-Guerra, A., 1998. Evolution of the Alboran Sea hydrographic structures during July 1993. *Deep Sea Res Part I: Oceanograp. Res. Papers.* 45, 39–65. [https://doi.org/10.1016/S0967-0637\(97\)00216-1](https://doi.org/10.1016/S0967-0637(97)00216-1)
- García-Rivera, S., Lizaso, J.L.S., Millán, J.M.B., 2018. Spatial and temporal trends of marine litter in the Spanish Mediterranean seafloor. *Mar. Pollut. Bull.* 137, 252–261. <https://doi.org/10.1016/j.marpolbul.2018.09.051>
- García-Ruiz, C., Lloris, D., Rueda, J.L., García-Martínez, M.C., Gil de Sola, L., 2015. Spatial distribution of ichthyofauna in the northern Alboran Sea (western Mediterranean). *J. Nat. Hist.* 49, 1191–1224. <https://doi.org/10.1080/00222933.2014.1001457>
- García Raso, J.E., Marina, P., Baro, J., 2011. *Bythocaris cosmetops* (Decapoda: Caridea: Hippolytidae) in the western Mediterranean Sea. *Mar. Biodivers. Rec.* 4, 1–4. <https://doi.org/10.1017/S1755267211000467>
- García Raso, J.E., Salmerón, F., Baro, J., Marina, P., Abelló, P., 2014. The tropical african hermit crab *Pagurus mbizi* (Crustacea, Decapoda, Paguridae) in the western Mediterranean Sea: A new alien species or filling gaps in the knowledge of the distribution? *Mediterr. Mar. Sci.* 15, 172–178. <https://doi.org/10.12681/mms.530>
- Gardner, J. V., Dartnell, P., Mayer, L.A., Hughes Clarke, J.E., 2003. Geomorphology, acoustic backscatter, and processes in Santa Monica Bay from multibeam mapping. *Mar. Environ. Res.* 56, 15–46. [https://doi.org/10.1016/S0141-1136\(02\)00323-9](https://doi.org/10.1016/S0141-1136(02)00323-9)
- Gaudin, M., Berné, S., Jouanneau, J.M., Palanques, A., Puig, P., Mulder, T., Cirac, P., Rabineau, M., Imbert, P., 2006. Massive sand beds attributed to deposition by dense water cascades in the Bourcart canyon head, Gulf of Lions (northwestern Mediterranean Sea). *Mar. Geol.* 234, 111–128. <https://doi.org/10.1016/j.margeo.2006.09.020>
- Ge, Z., Nemec, W., Gawthorpe, R.L., Hansen, E.W.M., 2017. Response of unconfined turbidity current to normal-fault topography. *Sedimentology* 64, 932–959. <https://doi.org/10.1111/sed.12333>
- GEBCO Compilation Group, 2023. GEBCO 2023 Grid. <https://doi.org/10.5285/f98b053b-0cbc-6c23-e053-6c86abc0af7b>

- Gennesseaux, M., Mauffret, A., Pautot, G., 1980. Les glissements sous-marins de la pente continentale niçoise et la rupture de câbles en mer Ligure (Méditerranée Occidentale). CR Acad. Sci. Paris 290, 959–962.
- Gerber, T.P., Amblas, D., Wolinsky, M.A., Pratson, L.F., Canals, M., 2009. A model for the long-profile shape of submarine canyons. J. Geophys. Res. Earth Surf. 114, 1–24. <https://doi.org/10.1029/2008JF001190>
- Gerigny, O., Brun, M., Fabri, M.C., Tomasino, C., Le Moigne, M., Jadaud, A., Galgani, F., 2019. Seafloor litter from the continental shelf and canyons in French Mediterranean Water: Distribution, typologies and trends. Mar. Pollut. Bull. 146, 653–666. <https://doi.org/10.1016/j.marpolbul.2019.07.030>
- Giusti, M., Canese, S., Fourt, M., Bo, M., Innocenti, C., Goujard, A., Daniel, B., Angeletti, L., Taviani, M., Aquilina, L., Tunesi, L., 2019. Coral forests and Derelict Fishing Gears in submarine canyon systems of the Ligurian Sea. Prog. Oceanogr. 178, 102186. <https://doi.org/10.1016/j.pocean.2019.102186>
- Godoy, V., Prata, J.C., Blázquez, G., Almendros, A.I., Duarte, A.C., Rocha-Santos, T., Calero, M., Martín-Lara, M.Á., 2020. Effects of distance to the sea and geomorphological characteristics on the quantity and distribution of microplastics in beach sediments of Granada (Spain). Sci. Total Environ. 746, 142023. <https://doi.org/10.1016/j.scitotenv.2020.142023>
- Goff, J.A., 2001. Quantitative classification of canyon systems on continental slopes and possible relationship to slope curvature. Geophys. Res. Lett. 28, 4359–4362. <https://doi.org/10.1029/2001GL013300>
- Goldberg, E.D., 1997. Plasticizing the seafloor: An overview. Environ. Technol. 18, 195–201. <https://doi.org/10.1080/09593331808616527>
- Gómez-Ballesteros, M., Arrese, B., Díez, I.P., Galparsoro, I., Sánchez-Guillamón, O., Martínez-Carreño, N., Sayago, M., López-Rodríguez, C., Rodríguez, A., Sánchez, F., 2022. Morphosedimentary characterization of the Capbreton submarine canyon system, Bay of Biscay (Cantabrian Sea). Estuar. Coast. Shelf Sci. 274, 107955. <https://doi.org/10.1016/j.ecss.2022.107955>

- Gómez de la Peña, L., R. Ranero, C., Gràcia, E., Booth-Rea, G., 2021. The evolution of the westernmost Mediterranean basins. *Earth-sci. Rev.* 214, 103445. <https://doi.org/10.1016/j.earscirev.2020.103445>
- Gordon, R.L., Marshall, N.F., 1976. Submarine canyons: Internal wave traps? *Geophys. Res. Lett.* 3, 622-624. <https://doi.org/10.1029/GL003i010p00622>
- Gong, C., Wang, Y., Peng, X., Li, W., Qiu, Y., Xu, S., 2012. Sediment waves on the South China Sea Slope off southwestern Taiwan: Implications for the intrusion of the Northern Pacific Deep Water into the South China Sea. *Mar. Petrol. Geol.* 32, 95–109. <https://doi.org/10.1016/j.marpetgeo.2011.12.00>
- Goy, J.L., Zazo, C., Dabrio, C.J., 2003. A beach-ridge progradation complex reflecting periodical sea-level and climate variability during the Holocene (Gulf of Almería, Western Mediterranean). *Geomorphology* 50, 251–268. [https://doi.org/10.1016/S0169-555X\(02\)00217-9](https://doi.org/10.1016/S0169-555X(02)00217-9)
- Green, A., 2009. Sediment dynamics on the narrow, canyon-incised and current-swept shelf of the northern KwaZulu-Natal continental shelf, South Africa. *Geo-Mar. Lett.* 29, 201–219. <https://doi.org/10.1007/s00367-009-0135-9>
- Green, A.N., Goff, J.A., Uken, R., 2007. Geomorphological evidence for upslope canyon forming processes on the northern KwaZulu-Natal shelf, SW Indian Ocean, South Africa. *Geo-Mar. Lett.* 27, 399–409. <https://doi.org/10.1007/s00367-007-0082-2>
- Gregory, M.R., 2009. Environmental implications of plastic debris in marine settings-entanglement, ingestion, smothering, hangers-on, hitch-hiking and alien invasions. *Philos. Trans. R. Soc. B Biol. Sci.* 364, 2013–2025. <https://doi.org/10.1098/rstb.2008.0265>
- Grinyó, J., Lo Iacono, C., Pierdomenico, M., Conlon, S., Corbera, G., Gràcia, E., 2020. Evidences of human impact on megabenthic assemblages of bathyal sediments in the Alboran Sea (western Mediterranean). *Deep. Res. Part I Oceanogr. Res. Pap.* 165. <https://doi.org/10.1016/j.dsr.2020.103369>
- Guiastrennec-Faugas, L., Gillet, H., Silva Jacinto, R., Dennielou, B., Hanquiez, V., Schmidt, S., Simplet, L., Rousset, A., 2020. Upstream migrating knickpoints and related sedimentary processes in a submarine canyon from a rare 20-year morphobathymetric

- time-lapse (Capbreton submarine canyon, Bay of Biscay, France). *Mar. Geol.* 423, 106143. <https://doi.org/10.1016/j.margeo.2020.106143>
- Haalboom, S., de Stigter, H., Duineveld, G., van Haren, H., Reichart, G.J., Mienis, F., 2021. Suspended particulate matter in a submarine canyon (Whittard Canyon, Bay of Biscay, NE Atlantic Ocean): Assessment of commonly used instruments to record turbidity. *Mar. Geol.* 434, 106439. <https://doi.org/10.1016/j.margeo.2021.106439>
- Hage, S., Cartigny, M.J.B., Clare, M.A., Sumner, E.J., Vendettuoli, D., Clarke, J.E.H., Hubbard, S.M., Talling, P.J., Gwyn Lintern, D., Stacey, C.D., Englert, R.G., Vardy, M.E., Hunt, J.E., Yokokawa, M., Parsons, D.R., Hizzett, J.L., Azpiroz-Zabala, M., Vellinga, A.J., 2018. How to recognize crescentic bedforms formed by supercritical turbidity currents in the geologic record: Insights from active submarine channels. *Geology* 46, 563–566. <https://doi.org/10.1130/G40095.1>
- Hagen, R.A., Bergersen, D.D., Moberly, R., Colbourn, W.T., 1994. Morphology of a large meandering submarine canyon system on the Peru-Chile forearc. *Mar. Geol.* 119, 7–38. [http://dx.doi.org/10.1016/0025-3227\(94\)90138-4](http://dx.doi.org/10.1016/0025-3227(94)90138-4)
- Hansen, L.A.S., Callow, R.H.T., Kane, I.A., Gamberi, F., Rovere, M., Cronin, B.T., Kneller, B.C., 2015. Genesis and character of thin-bedded turbidites associated with submarine channels. *Mar. Petrol. Geol.* 67, 852–879. <https://doi.org/10.1016/j.marpetgeo.2015.06.007>
- Hansen, L., Janocko, M., Kane, I., Kneller, B., 2017. Submarine channel evolution, terrace development, and preservation of intra-channel thin-bedded turbidites: Mahin and Avon channels, offshore Nigeria. *Mar. Geol.* 383, 146–167. <https://doi.org/10.1016/j.margeo.2016.11.011>
- Harris, P.T., Whiteway, T., 2011. Global distribution of large submarine canyons: Geomorphic differences between active and passive continental margins. *Mar. Geol.* 285, 69–86. <https://doi.org/10.1016/j.margeo.2011.05.008>
- Harris, P., Macmillan-Lawler, M., Rupp, J., Baker, E., 2014. Geomorphology of the oceans. *Mar. Geol.* 352, 4–24. <https://doi.org/10.1016/j.margeo.2014.01.011>
- Harris, P.T., Macmillan-Lawler, M., 2015. Geomorphology of Mediterranean submarine canyons in a global context – Results from a multivariate analysis of canyon

- geomorphic statistics. In: Briand, F. (Ed.), *Submarine Canyon Dynamics*. CIESM, Sorrento, pp. 23–35.
- Heijnen, M.S., Mienis, F., Gates, A.R., Bett, B.J., Hall, R.A., Hunt, J., Kane, I.A., Pebody, C., Huvenne, V.A.I., Soutter, E.L., Clare, M.A., 2022. Challenging the highstand-dormant paradigm for land-detached submarine canyons. *Nat. Commun.* 13, 1–11. <https://doi.org/10.1038/s41467-022-31114-9>
- Heiniö, P., Davies, R.J., 2009. Trails of depressions and sediment waves along submarine channels on the continental margin of Espirito Santo Basin, Brazil. *Bull. Geol. Soc. Am.* 121, 698–711. <https://doi.org/10.1130/B26190.1>
- Hernandez, I., Davies, J.S., Huvenne, V.A.I., Dissanayake, A., 2022. Marine litter in submarine canyons: A systematic review and critical synthesis. *Front. Mar. Sci.* 9, 1–26. <https://doi.org/10.3389/fmars.2022.965612>
- Hernández-Molina, F.J., Somoza, L., Rey, J., Pomar, L., 1994. Late Pleistocene-Holocene sediments on the Spanish continental shelves: Model for very high resolution sequence stratigraphy. *Mar. Geol.* 120, 129–174. [https://doi.org/10.1016/0025-3227\(94\)90057-4](https://doi.org/10.1016/0025-3227(94)90057-4)
- Hernández-Molina, F.J., Fernández-Salas, L.M., Lobo, F., Somoza, L., Díaz-del-Río, V., Alveirinho Dias, J.M., 2000. The infralittoral prograding wedge: A new large-scale progradational sedimentary body in shallow marine environments. *Geo-Marine Lett.* 20, 109–117. <https://doi.org/10.1007/s003670000040>
- Herzer, R.H., Lewis, D.W., 1979. Growth and burial of a submarine canyon off Motunau, North Canterbury, New Zealand. *Sediment. Geol.* 24, 69–83. [https://doi.org/10.1016/0037-0738\(79\)90029-0](https://doi.org/10.1016/0037-0738(79)90029-0)
- Hesse, R., 1995. Long-distance correlation of spillover turbidites on the western levee of the Northwest Atlantic Mid-Ocean Channel (NAMOC), Labrador Sea. In: Pickering, K.T., Hiscott, R.N., Kenyon, N.H., Ricci Lucchi, F., Smith, R.D.A. (Eds.), *Atlas of deep water environments: architectural style in turbidite systems*. Chapman and Hall, pp. 276–281. https://doi.org/10.1007/978-94-011-1234-5_41
- Hesse, R., Rashid, H., Khodabakhsh, S., 2004. Fine-grained sediment lofting from meltwater-generated turbidity currents during Heinrich events. *Geology* 32, 449–452. <https://doi.org/10.1130/G20136.1>

- Hill, P.S., Fox, J.M., Crockett, J.S., Curran, K.J., Friedrichs, C.T., Geyer, W.R., Milligan, T.G., Ogston, A.S., Puig, P., Scully, M.E., Traykovski, P.A., Wheatcroft, R.A., 2009. Sediment Delivery to the Seabed on Continental Margins. In: Nittrouer, C.A., Austin, J.A., Field, M.E., Kravitz, J.H., Syvitski, J.P.M., Wiberg, P.L. (Eds.), *Continental Margin Sedimentation: From Sediment Transport to Sequence Stratigraphy*. IAS Special Publication 37, 49–99. <https://doi.org/10.1002/9781444304398.ch2>
- Hiscott, R., Hall, F.R., Pirmez, C., 1997. Turbidity-current overspill from the Amazon channel: texture of the silt/sand load, paleoflow from anisotropy of magnetic susceptibility and implications for flow processes. In: Flood, R., Piper, D., Klaus, A., Peterson, L. (Eds.), *Proceedings of the Ocean Drilling Program, Scientific Results 155*, pp. 53–78. <http://dx.doi.org/10.2973/odp.proc.sr.155.202.1997>
- Hiscott, R.N., Aksu, A.E., Flood, R.D., Kostylev, V., Yaşar, D., 2013. Widespread overspill from a saline density-current channel and its interaction with topography on the south-west Black Sea shelf. *Sedimentology* 60, 1639–1667. <https://doi.org/10.1111/sed.12071>
- Hizzett, J.L., Hughes Clarke, J.E., Sumner, E.J., Cartigny, M.J.B., Talling, P.J., Clare, M.A., 2018. Which triggers produce the most erosive, frequent and longest runout turbidity currents on deltas? *Geophys. Res. Lett.* 45, 855–863. <https://doi.org/10.1002/2017GL075751>
- Howarth, J.D., Orpin, A.R., Kaneko, Y., Strachan, L.J., Nodder, S.D., Mountjoy, J.J., Barnes, P.M., Bostock, H.C., Holden, C., Jones, K., Çağatay, M.N., 2021. Calibrating the marine turbidite palaeoseismometer using the 2016 Kaikōura earthquake. *Nat. Geosci.* 14, 161–167. <https://doi.org/10.1038/s41561-021-00692-6>
- Huang, Z., Nichol, S.L., Harris, P.T., Caley, M.J., 2014. Classification of submarine canyons of the Australian continental margin. *Mar. Geol.* 357, 362–383. <https://doi.org/10.1016/j.margeo.2014.07.007>
- Hubbard, S.M., Covault, J.A., Fildani, A., Romans, B.W., 2014. Sediment transfer and deposition in slope channels: Deciphering the record of enigmatic deep-sea processes from outcrop. *Bull. Geol. Soc. Am.* 126, 857–871. <https://doi.org/10.1130/B30996.1>
- Hughes Clarke, J.E., Marques, C.R.V., Pratomo, D., 2014. Imaging active mass-wasting and sediment flows on a fjord delta, Squamish, British Columbia. In: Krastel, S. (Ed.), *Submarine mass movements and their consequences: advances in natural and*

- technological hazards research. Springer, pp. 249–260. https://doi.org/10.1007/978-3-319-00972-8_22
- IUCN, 2019. Thematic Report – Conservation Overview of Mediterranean Deep-Sea Biodiversity: A Strategic Assessment. IUCN Gland, Switzerland and Malaga, Spain, pp. 122.
- Ivanov, V. V., Shapiro, G.I., Huthnance, J.M., Aleynik, D.L., Golovin, P.N., 2004. Cascades of dense water around the world ocean. *Prog. Oceanogr.* 60, 47–98. <https://doi.org/10.1016/j.pocean.2003.12.002>
- Izumi, N., 2004. The formation of submarine gullies by turbidity currents. *J. Geophys. Res. Ocean.* 109, 1–13. <https://doi.org/10.1029/2003jc001898>
- Jabaloy-Sánchez, A., Lobo, F.J., Azor, A., Martín-Rosales, W., Pérez-Peña, J. V., Bárcenas, P., Macías, J., Fernández-Salas, L.M., Vázquez-Vílchez, M., 2014. Six thousand years of coastline evolution in the Guadalfeo deltaic system (southern Iberian Peninsula). *Geomorphology* 206, 374–391. <https://doi.org/10.1016/j.geomorph.2013.08.037>
- Janocko, M., Nemec, W., Henriksen, S., Warchol, M., 2013. The diversity of deep-water sinuous channel belts and slope valley-fill complexes. *Mar. Petrol. Geol.* 41, 7–34. <http://dx.doi.org/10.1016/j.marpetgeo.2012.06.012>
- Jimenez-Espejo, F.J., Martinez-Ruiz, F., Rogerson, M., González-Donoso, J.M., Romero, O.E., Linares, D., Sakamoto, T., Gallego-Torres, D., Ruiz, J.L.R., Ortega-Huertas, M., Claros, J.A.P., 2008. Detrital input, productivity fluctuations, and water mass circulation in the westernmost Mediterranean Sea since the Last Glacial Maximum. *Geochem. Geophys. Geosy.* 9, Q11U02. <https://doi.org/10.1029/2008GC002096>
- Jobe, Z.R., Lowe, D.R., Uchytel, S.J., 2011. Two fundamentally different types of submarine canyons along the continental margin of Equatorial Guinea. *Mar. Petrol. Geol.* 28, 843–860. <https://doi.org/10.1016/j.marpetgeo.2010.07.012>
- Jobe, Z.R., Sylvester, Z., Parker, A.O., Howes, N., Slowey, N., Pirmez, C., 2015. Rapid adjustment of submarine channel architecture to changes in sediment supply. *J. Sediment. Res.* 85, 729–756. <https://doi.org/10.2110/jsr.2015.30>
- Jones, E.S., Ross, S.W., Robertson, C.M., Young, C.M., 2022. Distributions of microplastics and larger anthropogenic debris in Norfolk Canyon, Baltimore Canyon, and the

- adjacent continental slope (Western North Atlantic Margin, U.S.A.). *Mar. Pollut. Bull.* 174, 113047. <https://doi.org/10.1016/j.marpolbul.2021.113047>
- Juan, C., Ercilla, G., Javier Hernández-Molina, F., Estrada, F., Alonso, B., Casas, D., García, M., Farran, M., Llave, E., Palomino, D., Vázquez, J.T., Medialdea, T., Gorini, C., D'Acremont, E., El Moumni, B., Ammar, A., 2016. Seismic evidence of current-controlled sedimentation in the Alboran Sea during the Pliocene and Quaternary: Palaeoceanographic implications. *Mar. Geol.* 378, 292–311. <https://doi.org/10.1016/j.margeo.2016.01.006>
- Junta de Andalucía. Consejería de Medio Ambiente, 2019. [Plan Director Territorial de Gestión de Residuos no Peligrosos de Andalucía 2010–2019.](#)
- Kane, I.A., Fildani, A., 2021. Anthropogenic pollution in deep-marine sedimentary systems— A geological perspective on the plastic problem. *Geology* 49, 607–608. <https://doi.org/10.1130/focus052021.1>
- Kane, I.A., McCaffrey, W.D., Peakall, J., 2008. Controls on sinuosity evolution within submarine channels. *Geology* 36, 287–290. <https://doi.org/10.1130/G24588A.1>
- Kane, I.A., Clare, M.A., Miramontes, E., Wogelius, R., Rothwell, J.J., Garreau, P., Pohl, F., 2020. Seafloor microplastic hotspots controlled by deep-sea circulation. *Science* 368, 1140–1145. <https://doi.org/10.1126/science.aba5899>
- Katsanevakis, S., Verriopoulos, G., Nicolaidou, A., Thessalou-Legaki, M., 2007. Effect of marine litter on the benthic megafauna of coastal soft bottoms: A manipulative field experiment. *Mar. Pollut. Bull.* 54, 771–778. <https://doi.org/10.1016/j.marpolbul.2006.12.016>
- Keevil, G.M., Peakall, J., Best, J.L., Amos, K.J., 2006. Flow structure in sinuous submarine channels: Velocity and turbulence structure of an experimental submarine channel. *Mar. Geol.* 229, 241–257. <https://doi.org/10.1016/j.margeo.2006.03.010>
- Kertzus, V., Kneller, B., 2009. Clinoform quantification for assessing the effects of external forcing on continental margin development. *Basin Res.* 21, 738–758. <https://doi.org/10.1111/j.1365-2117.2009.00411.x>.
- Khripounoff, A., Vangriesheim, A., Babonneau, N., Crassous, P., Dennielou, B., Savoye, B., 2003. Direct observation of intense turbidity current activity in the Zaire submarine

- valley at 4000 m water depth. *Mar. Geol.* 194, 151–158.
[https://doi.org/10.1016/S0025-3227\(02\)00677-1](https://doi.org/10.1016/S0025-3227(02)00677-1)
- Khripounoff, A., Vangriesheim, A., Crassous, P., Etoubleau, J., 2009. High frequency of sediment gravity flow events in the Var submarine canyon (Mediterranean Sea). *Mar. Geol.* 263, 1–6. <https://doi.org/10.1016/j.margeo.2009.03.014>
- Khripounoff, A., Crassous, P., Lo Bue, N., Dennielou, B., Silva Jacinto, R., 2012. Different types of sediment gravity flows detected in the Var submarine canyon (northwestern Mediterranean Sea). *Prog. Oceanogr.* 106, 138–153.
<https://doi.org/10.1016/j.pocean.2012.09.001>
- Killworth P., 1983. Deep convection in the world oceans. *Rev. Geophys. Space Phys.* 21, 1–26. <https://doi.org/10.1029/RG021i001p00001>
- Kneller, B., McCaffrey, W.D., 1995. Modelling the effects of salt-induced topography on deposition from turbidity currents. In: GCSSEPM Foundation 16th Annual Research Conference Salt, Sediment and Hydrocarbons, SEPM 16, pp. 137–145.
<https://doi.org/10.5724/gcs.95.16.0137>
- Kneller, B., Buckee, C., 2000. The structure and fluid mechanics of turbidity currents: A review of some recent studies and their geological implications. *Sedimentology* 47, 62–94. <https://doi.org/10.1046/j.1365-3091.2000.047s1062.x>
- Kostic, S., 2011. Modeling of submarine cyclic steps: Controls on their formation, migration, and architecture. *Geosphere* 7, 294–304. <https://doi.org/10.1130/GES00601.1>
- Kostic, S., 2014. Upper flow regime bedforms on levees and continental slopes: turbidity current flow dynamics in response to fine-grained sediment waves. *Geosphere* 10, 1094–1103. <https://doi.org/10.1130/GES01015.1>
- Kostic, S., Parker, G., 2006. The response of turbidity currents to a canyon-fan transition: Internal hydraulic jumps and depositional signatures. *J. Hydraul. Res.* 44, 631–653.
<https://doi.org/10.1080/00221686.2006.9521713>
- Kostic, S., Sequeiros, O., Spinewine, B., Parker, G., 2010. Cyclic steps: a phenomenon of supercritical shallow flow from the high mountains to the bottom of the ocean. *J. Hydro Environ. Res.* 3, 167–172. <https://doi.org/10.1016/j.jher.2009.10.002>

- Kubo, Y., Nakajima, T., 2002. Laboratory experiments and numerical simulation of sediment-wave formation by turbidity currents. *Mar. Geol.* 192, 105–121. [https://doi.org/10.1016/S0025-3227\(02\)00551-0](https://doi.org/10.1016/S0025-3227(02)00551-0)
- La Violette, P.E., 1984. The advection of submesoscale thermal features in the Alboran Sea gyre. *J. Phys. Oceanogr.* 14, 550–565. [https://doi.org/10.1175/1520-0485\(1984\)014%3C0550:TAOSTF%3E2.0.CO;2](https://doi.org/10.1175/1520-0485(1984)014%3C0550:TAOSTF%3E2.0.CO;2)
- Lamb, M.P., Parsons, J.D., Mullenbach, B.L., Finlayson, D.P., Orange, D.L., Nittrouer, C.A., 2008. Evidence for superelevation, channel incision, and formation of cyclic steps by turbidity currents in Eel Canyon, California. *Bull. Geol. Soc. Am.* 120, 463–475. <https://doi.org/10.1130/B26184.1>
- Lamb, M.P., Finnegan, N.J., Scheingross, J.S., Sklar, L.S., 2015. New insights into the mechanics of fluvial bedrock erosion through flume experiments and theory. *Geomorphology* 244, 33–55. <https://doi.org/10.1016/j.geomorph.2015.03.003>
- Lario, J., Zazo, C., Goy, J. L., 1999. Fases de progradación y evolución morfosedimentaria de la flecha litoral de Calahonda (Granada) durante el Holoceno. *Estud. Geol.* 55, 247–250.
- Lastras, G., Canals, M., Urgeles, R., Amblas, D., Ivanov, M., Droz, L., Dennielou, B., Fabrès, J., Schoolmeester, T., Akhmetzhanov, A., Orange, D., García-García, A., 2007. A walk down the Cap de Creus canyon, Northwestern Mediterranean Sea: Recent processes inferred from morphology and sediment bedforms. *Mar. Geol.* 246, 176–192. <https://doi.org/10.1016/j.margeo.2007.09.002>
- Lastras, G., Arzola, R.G., Masson, D.G., Wynn, R.B., Huvenne, V.A.I., Hühnerbach, V., Canals, M., 2009. Geomorphology and sedimentary features in the Central Portuguese submarine canyons, Western Iberian margin. *Geomorphology* 103, 310–329. <https://doi.org/10.1016/j.geomorph.2008.06.01>
- Lastras, G., Canals, M., Amblas, D., Lavoie, C., Church, I., De Mol, B., Duran, R., Calafat, A.M., Hughes-Clarke, J.E., Smith, C.J., Heussner, S., 2011a. Understanding sediment dynamics of two large submarine valleys from seafloor data: Blanes and La Fonera canyons, northwestern Mediterranean Sea. *Mar. Geol.* 280, 20–39. <https://doi.org/10.1016/j.margeo.2010.11.005>

- Lastras, G., Acosta, J., Muñoz, A., Canals, M., 2011b. Submarine canyon formation and evolution in the Argentine Continental Margin between 44°30'S and 48°S. *Geomorphology* 128, 116–136. <https://doi.org/10.1016/j.geomorph.2010.12.027>
- Leeder, M.R., 1999. *Sedimentology and sedimentary basins: from turbulence to tectonics*. Blackwell Science, Wiley-Blackwell, 784 pp. <https://doi.org/10.1017/S0016756800224618>
- León, R., Somoza, L., Medialdea, T., González, F.J., Gimenez-Moreno, C.J., Pérez-López, R., 2014. Pockmarks on either side of the Strait of Gibraltar: formation from overpressured shallow contourite gas reservoirs and internal wave action during the last glacial sea-level lowstand? *Geo-Mar. Lett.* 34, 131–151. <https://doi.org/10.1007/s00367-014-0358-2>
- Lewis, K.B., Barnes, P.M., 1999. Kaikoura Canyon, New Zealand: active conduit from near-shore sediment zones to trench-axis channel. *Mar. Geol.* 162, 39–69. [https://doi.org/10.1016/S0025-3227\(99\)00075-4](https://doi.org/10.1016/S0025-3227(99)00075-4)
- Lewis, K.B., Pantin, H.M., 2002. Channel-axis, overbank and drift sediment waves in the southern Hikurangi Trough, New Zealand. *Mar. Geol.* 192, 123–151. [https://doi.org/10.1016/S0025-3227\(02\)00552-2](https://doi.org/10.1016/S0025-3227(02)00552-2)
- Li, L., Gong, C., 2018. Gradual Transition From Net Erosional to Net Depositional Cyclic Steps Along the Submarine Distributary Channel Thalweg in the Rio Muni Basin: A Joint 3-D Seismic and Numerical Approach. *J. Geophys. Res. Earth Surf.* 123, 2087–2106. <https://doi.org/10.1029/2017JF004513>
- Li, C., Ma, M., Lv, C., Zhang, G., Chen, G., Yan, Y., Bi, G., 2017. Sedimentary differences between different segments of the continental slope-parallel Central Canyon in the Qiongdongnan Basin on the northern margin of the South China Sea. *Mar. Petrol. Geol.* 88, 127–140. <https://doi.org/10.1016/j.marpetgeo.2017.08.009>
- Li, M.Z., Prescott, R.H., Robertson, A.G., 2019. Observation of internal tides and sediment transport processes at the head of Logan Canyon on central Scotian Slope, eastern Canada. *J. Mar. Syst.* 193, 103–125. <https://doi.org/10.1016/j.jmarsys.2019.02.007>
- Li, W., Li, S., Alves, T.M., Rebesco, M., Feng, Y., 2021. The role of sediment gravity flows on the morphological development of a large submarine canyon (Taiwan Canyon),

- north-east South China Sea. *Sedimentology* 68, 1091–1108.
<https://doi.org/10.1111/sed.12818>
- Li, S., Alves, T.M., Li, W., Wang, X., Rebesco, M., Li, J., Zhao, F., Yu, K., Wu, S., 2022. Morphology and evolution of submarine canyons on the northwest South China Sea margin. *Mar. Geol.* 443, 106695. <https://doi.org/10.1016/j.margeo.2021.106695>
- Li, J., Li, W., Alves, T.M., Rebesco, M., Wang, X., Li, S., Sun, J., Zhan, W., 2023. Controls on the morphology of closely spaced submarine canyons incising the continental slope of the northern South China Sea. *Geomorphology* 432, 108712. <https://doi.org/10.1016/j.geomorph.2023.108712>
- Liquete, C., Arnau, P., Canals, M., Colas, S., 2005. Mediterranean river systems of Andalusia, southern Spain, and associated deltas: A source to sink approach. *Mar. Geol.* 222–223, 471–495. <https://doi.org/10.1016/j.margeo.2005.06.033>
- Liquete, C., Canals, M., Ludwig, W., Arnau, P., 2009. Sediment discharge of the rivers of Catalonia, NE Spain, and the influence of human impacts. *J. Hydrol.* 366, 76–88. <https://doi.org/10.1016/j.jhydrol.2008.12.013>
- Liu, J.T., Liu, K.J., Huang, J.C., 2002. The effect of a submarine canyon on the river sediment dispersal and inner shelf sediment movements in southern Taiwan. *Mar. Geol.* 181, 357–386. [https://doi.org/10.1016/S0025-3227\(01\)00219-5](https://doi.org/10.1016/S0025-3227(01)00219-5)
- Liubartseva, S., Coppini, G., Lecci, R., Clementi, E., 2018. Tracking plastics in the Mediterranean: 2D Lagrangian model. *Mar. Pollut. Bull.* 129, 151–162. <https://doi.org/10.1016/j.marpolbul.2018.02.019>
- Lo Iacono, C. Lo, Sulli, A., Agate, M., Lo Presti, V., Pepe, F., Catalano, R., 2011. Submarine canyon morphologies in the Gulf of Palermo (Southern Tyrrhenian Sea) and possible implications for geo-hazard. *Mar. Geophys. Res.* 32, 127–138. <https://doi.org/10.1007/s11001-011-9118-0>
- Lo Iacono, C., Sulli, A., Agate, M., 2014. Submarine canyons of north-western Sicily (Southern Tyrrhenian Sea): Variability in morphology, sedimentary processes and evolution on a tectonically active margin. *Deep. Res. Part II Top. Stud. Oceanogr.* 104, 93–105. <https://doi.org/10.1016/j.dsr2.2013.06.018>
- Lo Iacono, C., Agate, M., Sulli, A., Cartigny, M., Robert, K., Gori, A., Russo, T., 2015. Development, human impact and habitat distribution in submarine canyons of the

- Central and Western Mediterranean. In: Briand, F. (Ed.), *Submarine Canyon Dynamics*. CIESM, Sorrento, pp. 87–96.
- Lo Iacono, C., Guillén, J., Guerrero, Q., Durán, R., Wardell, C., Hall, R.A., Aslam, T., Carter, G.D.O., Gales, J.A., Huvenne, V.A.I., 2020. Bidirectional bedform fields at the head of a submarine canyon (NE Atlantic). *Earth Planet. Sci. Lett.* 542, 116321. <https://doi.org/10.1016/j.epsl.2020.116321>
- Lobo, F. J., Fernandez-Salas, L. M., Moreno, I., Sanz, J. L., Maldonado, A., 2006. The sea-floor morphology of a Mediterranean shelf fed by small rivers, northern Alboran Sea margin. *Cont. Shelf Res.* 26, 2607–2628. <https://doi.org/10.1016/j.csr.2006.08.006>
- Lobo, F.J., Goff, J.A., Mendes, I., Bárcenas, P., Fernández-Salas, L.M., Martín-Rosales, W., Macías, J., Díaz del Río, V., 2015. Spatial variability of prodeltaic undulations on the Guadalfeo River prodelta: support to the genetic interpretation as hyperpycnal flow deposits. *Mar. Geophys. Res.* 36, 309–333. <https://doi.org/10.1007/s11001-014-9233-9>
- Lowe, D.R., 1982. Sediment gravity flows; II. Depositional models with special reference to the deposits of high- density turbidity currents. *J. Sediment. Res.*, 52, 279–297. <https://doi.org/10.1306/212F7F31-2B24-11D7-8648000102C1865D>
- Macdonald, H.A., Wynn, R.B., Huvenne, V.A., Peakall, J., Masson, D.G., Weaver, P.P., McPhail, S.D., 2011. New insights into the morphology, fill, and remarkable longevity (N0.2 my) of modern deep-water erosional scours along the northeast Atlantic margin. *Geosphere* 7, 845–867. <https://doi.org/10.1130/GES00611.1>
- Maier, K.L., Fildani, A., Paull, C.K., Graham, S.A., McHargue, T.R., Caress, D.W., McGann, M., 2011. The elusive character of discontinuous deep-water channels: new insights from Lucia Chica channel system, offshore California. *Geology* 39, 327–330. <https://doi.org/10.1130/G31589.1>
- Maier, K.L., Fildani, A., Paull, C.K., McHargue, T.R., Graham, S.A., Caress, D.W., 2013. Deep-sea channel evolution and stratigraphic architecture from inception to abandonment from high-resolution Autonomous Underwater Vehicle surveys offshore central California. *Sedimentology* 60, 935–960. <https://doi.org/10.1111/j.1365-3091.2012.01371.x>

- Maier, K.L., Johnson, S.Y., Hart, P., 2018. Controls on submarine canyon head evolution: Monterey Canyon, offshore central California. *Mar. Geol.* 404, 24–40. <https://doi.org/10.1016/j.margeo.2018.06.014>
- Maier, K.L., Rosenberger, K.J., Paull, C.K., Gwiazda, R., Gales, J., Lorenson, T., Barry, J.P., Talling, P.J., McGann, M., Xu, J., Lundsten, E., Anderson, K., Litvin, S.Y., Parsons, D.R., Clare, M.A., Simmons, S.M., Sumner, E.J., Cartigny, M.J.B., 2019. Sediment and organic carbon transport and deposition driven by internal tides along Monterey Canyon, offshore California. *Deep. Res. Part I Oceanogr. Res. Pap.* 153, 103108. <https://doi.org/10.1016/j.dsr.2019.103108>
- Maier, K.L., Paull, C.K., Caress, D.W., Anderson, K., Nieminski, N.M., Lundsten, E., Erwin, B.E., Gwiazda, R., Fildani, A., 2020. Submarine-fan development revealed by integrated high-resolution datasets from La Jolla fan, offshore California, U.S.A. *J. Sediment. Res.* 90, 468–479. <https://doi.org/10.2110/jsr.2020.22>
- Maillard, A., Gorini, C., Mauffret, A., Sage, F., Lofi, J., Gaullier, V., 2006. Offshore evidence of polyphase erosion in the Valencia Basin (Northwestern Mediterranean): Scenario for the Messinian Salinity Crisis. *Sediment. Geol.* 188–189, 69–91. <https://doi.org/10.1016/j.sedgeo.2006.02.006>
- Marchès, E., Mulder, T., Cremer, M., Bonnel, C., Hanquiez, V., Gonthier, E., Lecroart, P., 2007. Contourite drift construction influenced by capture of Mediterranean Outflow Water deep-sea current by the Portimão submarine canyon (Gulf of Cadiz, South Portugal). *Mar. Geol.* 242, 247–260. <https://doi.org/10.1016/j.margeo.2007.03.013>
- Marina, P., Rueda, J.L., Urra, J., Salas, C., Gofas, S., García Raso, J.E., Moya, F., García, T., López-González, N., Laiz-Carrión, R., Baro, J., 2015. Sublittoral soft bottom assemblages within a Marine Protected Area of the northern Alboran Sea. *J. Mar. Biol. Assoc. Uk.* 95, 871–884. <https://doi.org/10.1017/S0025315414002082>
- Marsset, T., Ballas, G., Munteanu, I., Aiken, C., Ion, G., Pitel-Roudaut, M., Dupont, P., 2022. Tectonic-sedimentary architecture of surficial deposits along the continental slope offshore Romania (North of the Viteaz Canyon, Western Black Sea): Impact on sediment instabilities. *Glob. Planet. Change* 208, 103708. <https://doi.org/10.1016/j.gloplacha.2021.103708>

- Martín, J., Puig, P., Palanques, A., Masqué, P., García-Orellana, J., 2008. Effect of commercial trawling on the deep sedimentation in a Mediterranean submarine canyon. *Mar. Geol.* 252, 150–155. <https://doi.org/10.1016/j.margeo.2008.03.012>
- Martín, J., Palanques, A., Vitorino, J., Oliveira, A., de Stigter, H.C., 2011. Near-bottom particulate matter dynamics in the Nazaré submarine canyon under calm and stormy conditions. *Deep. Res. Part II Top. Stud. Oceanogr.* 58, 2388–2400. <https://doi.org/10.1016/j.dsr2.2011.04.004>
- Martín, J., Puig, P., Palanques, A., Ribó, M., 2014. Trawling-induced daily sediment resuspension in the flank of a Mediterranean submarine canyon. *Deep. Res. Part II Top. Stud. Oceanogr.* 104, 174–183. <https://doi.org/10.1016/j.dsr2.2013.05.036>
- Martín-Lara, M.A., Godoy, V., Quesada, L., Lozano, E.J., Calero, M., 2021. Environmental status of marine plastic pollution in Spain. *Mar. Pollut. Bull.* 170, 112677. <https://doi.org/10.1016/j.marpolbul.2021.112677>
- Mas, V., Mulder, T., Dennielou, B., Schmidt, S., Khripounoff, A., Savoye, B., 2010. Multiscale spatio-temporal variability of sedimentary deposits in the Var turbidite system (North-Western Mediterranean Sea). *Mar. Geol.* 275, 37–52. <https://doi.org/10.1016/j.margeo.2010.04.006>
- Mascle, J., Migeon, S., Coste, M., Hassoun, V., Rouillard, P., 2015. “Rocky” versus “Sedimentary” canyons around the Mediterranean and the Black seas. In: Briand, F. (Ed.), *Submarine Canyon Dynamics in the Mediterranean and Tributary Seas*. CIESM, Monaco, pp. 37–48.
- Maselli, V., Kneller, B., Taiwo, O.L., Iacopini, D., 2019. Sea floor bedforms and their influence on slope accommodation. *Mar. Petrol. Geol.* 102, 625–637. <https://doi.org/10.1016/j.marpetgeo.2019.01.021>
- Maselli, V., Micallef, A., Normandeau, A., Oppo, D., Iacopini, D., Green, A., Ge, Z., 2021. Active faulting controls bedform development on a deep-water fan. *Geology* 49, 1495–1500. <https://doi.org/10.1130/G49206.1>
- Masqué, P., Fabres, J., Canals, M., Sanchez-Cabeza, J.A., Sanchez-Vidal, A., Cacho, I., Calafat, A.M., Bruach, J.M., 2003. Accumulation rates of major constituents of hemipelagic sediments in the deep Alboran Sea: A centennial perspective of

- sedimentary dynamics. *Mar. Geol.* 193, 207–233. [https://doi.org/10.1016/S0025-3227\(02\)00593-5](https://doi.org/10.1016/S0025-3227(02)00593-5)
- Masson, D.G., Huvenne, V.A.I., de Stigter, H.C., Arzola, R.G., LeBas, T.P., 2011. Sedimentary processes in the middle Nazaré Canyon. *Deep. Res. Part II Top. Stud. Oceanogr.* 58, 2369–2387. <https://doi.org/10.1016/j.dsr2.2011.04.003>
- Mateo-Ramírez, Á., Marina, P., Moreno D., Alcántara Valero, A.F., Aguilar, R., Báez, J.C., Bárcenas, P., Baro, J., Caballero-Herrera, J.A., Camiñas, J.A., Malouli Idrissi, M., de la Torriente, A., García, T., García Raso, J.E., Gofas, S., González-García, E., González García J.A., Moya-Urbano, E., Muñoz, A.R., Sánchez-Tocino, L., Salas, C., Templado, J., Tierno de Figueroa, J.M., Urra, J., Vázquez, J.T., Rueda, J.L., 2021. Marine Protected Areas and Key Biodiversity Areas of the Alboran Sea and adjacent areas. In: J.C. Báez, J.T. Vázquez, J.A. Camiñas, M. Malouli Idrissi (Eds.), *Alboran Sea – Ecosystems and Marine Resources*. Springer 25, 819–923. https://doi.org/10.1007/978-3-030-65516-7_25
- Mauchline, J., Gordon, J.D., 1984. Feeding and bathymetric distribution of the Gadoid and Morid fish of the rockall trough. *J. Mar. Biol. Assoc. United Kingdom* 64, 657–665. <https://doi.org/10.1017/S0025315400030320>
- Mauffrey, M. A., Berné, S., Jouet, G., Giresse, P., Gaudin, M., 2015. Sea-level control on the connection between shelf-edge deltas and the Bourcart canyon head (western Mediterranean) during the last glacial/interglacial cycle. *Mar. Geol.* 370, 1–19. <https://doi.org/10.1016/j.margeo.2015.09.010>
- Mauffrey, M. A., Urgeles, R., Berné, S., Canning, J., 2017. Development of submarine canyons after the Mid-Pleistocene Transition on the Ebro margin, NW Mediterranean: The role of fluvial connections. *Quaternary Sci. Rev.* 158, 77–93. <https://doi.org/10.1016/j.quascirev.2017.01.006>
- Mayall, M., Jones, E., Casey, M., 2006. Turbidite channel reservoirs-Key elements in facies prediction and effective development. *Mar. Petrol. Geol.* 23, 821–841. <https://doi.org/10.1016/j.marpetgeo.2006.08.001>
- Mazières, A., Gillet, H., Castelle, B., Mulder, T., Guyot, C., Garlan, T., Mallet, C., 2014. High-resolution morphobathymetric analysis and evolution of Capbreton submarine canyon head (Southeast Bay of Biscay-French Atlantic Coast) over the last decade

- using descriptive and numerical modeling. *Mar. Geol.* 351, 1–12.
<https://doi.org/10.1016/j.margeo.2014.03.001>
- Mecho, A., Francescangeli, M., Ercilla, G., Fanelli, E., Estrada, F., Valencia, J., Sobrino, I., Danovaro, R., Company, J.B., Aguzzi, J., 2020. Deep-sea litter in the Gulf of Cadiz (Northeastern Atlantic, Spain). *Mar. Pollut. Bull.* 153, 110969.
<https://doi.org/10.1016/j.marpolbul.2020.110969>
- Micallef, A., Ribó, M., Canals, M., Puig, P., Lastras, G., Tubau, X., 2014. Space-for-time substitution and the evolution of a submarine canyon-channel system in a passive progradational margin. *Geomorphology* 221, 34–50.
<https://doi.org/10.1016/j.geomorph.2014.06.008>
- Migeon, S., Savoye, B., Faugeres, J.C., 2000. Quaternary development of migrating sediment waves in the Var deep-sea fan: distribution, growth pattern, and implication for levee evolution. *Sediment. Geol.* 133, 265–293. [https://doi.org/10.1016/S0037-0738\(00\)00043-9](https://doi.org/10.1016/S0037-0738(00)00043-9)
- Migeon, S., Savoye, B., Zanella, E., Mulder, T., Faugères, J.C., Weber, O., 2001. Detailed seismic-reflection and sedimentary study of turbidite sediment waves on the var sedimentary ridge (SE France): Significance for sediment transport and deposition and for the mechanisms of sediment-wave construction. *Mar. Petrol. Geol.* 18, 179–208.
[https://doi.org/10.1016/S0264-8172\(00\)00060-X](https://doi.org/10.1016/S0264-8172(00)00060-X)
- Migeon, S., Savoye, B., Babonneau, N., Andersson, F.L.S., 2004. Processes of sediment-wave construction along the present Zaire deep-sea meandering channel: Role of meanders and flow stripping. *J. Sediment. Res.* 74, 580–598.
<https://doi.org/10.1306/091603740580>
- Migeon, S., Mulder, T., Savoye, B., Sage, F., 2006. The Var turbidite system (Ligurian sea, northwestern Mediterranean) - Morphology, sediment supply, construction of turbidite levee and sediment waves: Implications for hydrocarbon reservoirs. *Geo-mar. Lett.* 26, 361–371. <https://doi.org/10.1007/s00367-006-0047-x>
- Migeon, S., Mulder, T., Savoye, B., Sage, F., 2012. Hydrodynamic processes, velocity structure and stratification in natural turbidity currents: Results inferred from field data in the Var Turbidite System. *Sediment. Geol.* 245–246, 48–62.
<https://doi.org/10.1016/j.sedgeo.2011.12.007>

- Millot, C., 2009. Another description of the Mediterranean Sea outflow. *Prog. Oceanogr.* 82, 101–124. <https://doi.org/10.1016/j.pocean.2009.04.016>
- Millot, C., 2014. Heterogeneities of in-and out-flows in the Mediterranean Sea. *Prog. Oceanogr.* 120, 254–278. <https://doi.org/10.1016/j.pocean.2013.09.007>
- Ministerio de Pesca, Agricultura y Alimentación, 2002. Multibeam bathymetric grid. Ministerio de Pesca, Agricultura y Alimentación, Spanish government.
- Ministerio para la Transición Ecológica y el Reto Demográfico (MITECO-DGCM), 2021. [Programa de seguimiento de basuras marinas en playas. Informe de resultados. Dirección general de la costa y el mar, 290 pp.](#)
- Miralles, J., Radakovitch, O., Aloisi, J.C., 2005. ^{210}Pb sedimentation rates from the Northwestern Mediterranean margin. *Mar. Geol.* 216, 155–167. <https://doi.org/10.1016/j.margeo.2005.02.020>
- Miramontes, E., Déverchère, J., Pellegrini, C., Chiarella, D., 2023. Mediterranean Sea evolution and present-day physiography. *Oceanogr. Mediterr. Sea An Introd. Guid.* 13–39. <https://doi.org/10.1016/B978-0-12-823692-5.00006-6>
- Mitchell, N.C., 2005. Interpreting long-profiles of canyons in the USA Atlantic continental slope: *Mar. Geol.* 214, 75–99. <https://doi.org/10.1016/j.margeo.2004.09.005>
- Mitchell, N.C., 2006. Morphologies of knickpoints in submarine canyons. *Geol. Soc. Am. Bull.* 118, 589–605. <https://doi.org/10.1130/B25772.1>
- Mitchum, R.M.Jr., 1985. Seismic stratigraphic expression of submarine fan. In: Berg, O.R., Woolverton, D.G. (Eds.), *Seismic Stratigraphy II: An Integrated Approach to Hydrocarbon Exploration*, *Am. Assoc. Petr. Geol. B.* 39, pp. 117–136. <https://doi.org/10.1306/M39449C7>
- Miyake, H., Shibata, H., Furushima, Y., 2011. Deep-sea litter study using deep-sea observation tools. In: Omori, K., Guo, X., Yoshie, N., Fujii, N., Handoh, I.C., Isobre, A., Tanabre, A., *Interdisciplinary Studies on Environmental Chemistry — Marine Environmental Modeling and Analysis. TERRAPUB*, 261–269.
- Mohrig, D., Marr, J.G., 2003. Constraining the efficiency of turbidity current generation from submarine debris flows and slides using laboratory experiments. *Mar. Petrol. Geol.* 20, 883–899. <https://doi.org/10.1016/j.marpetgeo.2003.03.002>

- Morales-Caselles, C., Viejo, J., Martí, E., González-Fernández, D., Pragnell-Raasch, H., González-Gordillo, J.I., Montero, E., Arroyo, G.M., Hanke, G., Salvo, V.S., Basurko, O.C., Mallos, N., Lebreton, L., Echevarría, F., van Emmerik, T., Duarte, C.M., Gálvez, J.A., van Sebille, E., Galgani, F., García, C.M., Ross, P.S., Bartual, A., Ioakeimidis, C., Markalain, G., Isobe, A., Cózar, A., 2021. An inshore–offshore sorting system revealed from global classification of ocean litter. *Nat. Sustain.* 4, 484–493. <https://doi.org/10.1038/s41893-021-00720-8>
- Mordecai, G., Tyler, P.A., Masson, D.G., Huvenne, V.A.I., 2011. Litter in submarine canyons off the west coast of Portugal. *Deep. Res. Part II Top. Stud. Oceanogr.* 58, 2489–2496. <https://doi.org/10.1016/j.dsr2.2011.08.009>
- Morelli, E., Martorelli, E., Casalbore, D., Chiocci, F.L., 2022. Morpho-stratigraphic evolution of a tectonically controlled canyon-channel system in the Gioia Basin (Southern Tyrrhenian Sea). *Mar. Geol.* 451, 106881. <https://doi.org/10.1016/j.margeo.2022.106881>
- Morris, E.A., Hodgson, D.M., Brunt, R.L., Flint, S.S., 2014. Origin, evolution and anatomy of silt-prone submarine external levées. *Sedimentology* 61, 1734–1763. <https://doi.org/10.1111/sed.12114>
- Mosher, D.C., Piper, D.J.W., Campbell, C., Jenner, K.A., 2004. Near surface geology and sediment-failure geohazards of the central Scotian Slope. *AAPG Bull.* 88, 703–723. <https://doi.org/10.1306/01260403084>
- Mountjoy, J.J., Barnes, P.M., Pettinga, J.R., 2009. Morphostructure and evolution of submarine canyons across an active margin: Cook Strait sector of the Hikurangi Margin, New Zealand. *Mar. Geol.* 260, 45–68. <https://doi.org/10.1016/j.margeo.2009.01.006>
- Mountjoy, J.J., Howarth, J.D., Orpin, A.R., Barnes, P.M., Bowden, D.A., Rowden, A.A., Schimel, A.C.G., Holden, C., Horgan, H.J., Nodder, S.D., Patton, J.R., Lamarche, G., Gerstenberger, M., Micallef, A., Pallentin, A., Kane, T., 2018. Earthquakes drive large-scale submarine canyon development and sediment supply to deep-ocean basins. *Sci. Adv.* 4, eaar3748. <https://doi.org/10.1126/sciadv.aar3748>
- Mulder, T., Syvitski, J.P.M., 1995. Turbidity currents generated at river mouths during exceptional discharges to the world oceans. *J. Geol.* 103, 285–299. <http://doi.org/10.1086/629747>

- Mulder, T., Savoye, B., Syvitski, J.P.M., 1997. Numerical modelling of a mid-sized gravity flow: The 1979 Nice turbidity current (dynamics, processes, sediment budget and seafloor impact). *Sedimentology* 44, 305–326. <https://doi.org/10.1111/j.1365-3091.1997.tb01526.x>
- Mulder, T., Alexander, J., 2001. The physical character of subaqueous sedimentary density flow and their deposits. *Sedimentology* 48, 269–299. <https://doi.org/10.1046/j.1365-3091.2001.00360.x>
- Mulder, T., Syvitski, J.P.M., Migeon, S., Faugères, J.C., Savoye, B., 2003. Marine hyperpycnal flows: Initiation, behavior and related deposits. A review. *Mar. Petrol. Geol.* 20, 861–882. <https://doi.org/10.1016/j.marpetgeo.2003.01.003>
- Mulder, T., Zaragosi, S., Garlan, T., Mavel, J., Cremer, M., Sottolichio, A., Sénéchal, N., Schmidt, S., 2012. Present deep-submarine canyons activity in the Bay of Biscay (NE Atlantic). *Mar. Geol.* 295–298, 113–127. <https://doi.org/10.1016/j.margeo.2011.12.005>
- Mullenbach, B.L., Nittrouer, C.A., 2000. Rapid deposition of fluvial sediment in the El Canyon, northern California. *Cont. Shelf Res.* 20, 2191–2212. [https://doi.org/10.1016/S0278-4343\(00\)00067-4](https://doi.org/10.1016/S0278-4343(00)00067-4)
- Mullenbach, B.L., Nittrouer, C.A., Puig, P., Orange, D.L., 2004. Sediment deposition in a modern submarine canyon: Eel Canyon, northern California. *Mar. Geol.* 211, 101–119. <https://doi.org/10.1016/j.margeo.2004.07.003>
- Muñoz, A., Elvira, E., León, C., Acosta, J., Jiménez, P., 2017. Examples of Sediment Waves in and Around Submarine Canyons of the North Alboran Sea. In: Guillén, J., Acosta, J., Chiocci, F.L., Palanques, A. (Eds.), *Atlas of Bedforms in the Western Mediterranean*. Springer International Publishing, pp. 247–252. <https://doi.org/10.1007/978-3-319-33940-5>
- Murray, J.W., 1991. *Ecology and Palaeoecology of Benthic Foraminifera*. Longman Scientific & Technical, Routledge, 408 pp. <https://doi.org/10.4324/9781315846101>
- Murray, J.W., 2006. *Ecology and Applications of Benthic Foraminifera*. Cambridge University Press, Cambridge, 426 pp. <https://doi.org/10.1017/CBO9780511535529>

- Nakajima, T., Satoh, M., 2001. The formation of large mudwaves by turbidity currents on the levees of the Toyama deep-sea channel, Japan Sea. *Sedimentology* 48, 435–463. <https://doi.org/10.1046/j.1365-3091.2001.00373.x>
- Neves, D., Sobral, P., Pereira, T., 2015. Marine litter in bottom trawls off the Portuguese coast. *Mar. Pollut. Bull.* 99, 301–304. <https://doi.org/10.1016/j.marpolbul.2015.07.044>
- NOAA National Centers for Environmental Information, 2023. U.S. coastal relief model. [Coastal Relief Model | National Centers for Environmental Information \(NCEI\) \(noaa.gov\)](https://coastalreliefmodel.noaa.gov/)
- Normandeau, A., Lajeunesse, P., St-Onge, G., Bourgault, D., Drouin, S.S.O., Senneville, S., Bélanger, S., 2014. Morphodynamics in sediment-starved inner-shelf submarine canyons (Lower St. Lawrence Estuary, Eastern Canada). *Mar. Geol.* 357, 243–255. <https://doi.org/10.1016/j.margeo.2014.08.012>
- Normandeau, A., Lajeunesse, P., St-Onge, G., 2015. Submarine canyons and channels in the Lower St. Lawrence Estuary (Eastern Canada): Morphology, classification and recent sediment dynamics. *Geomorphology* 241, 1–18. <https://doi.org/10.1016/j.geomorph.2015.03.023>
- Normandeau, A., Lajeunesse, P., Poiré, A.G., Francus, P., 2016. Morphological expression of bedforms formed by supercritical sediment density flows on four fjord-lake deltas of the south-eastern Canadian Shield (Eastern Canada). *Sedimentology* 63, 2106–2129. <https://doi.org/10.1111/sed.12298>
- Normandeau, A., Campbell, D.C., Cartigny, M.J.B., 2019. The influence of turbidity currents and contour currents on the distribution of deep-water sediment waves offshore eastern Canada. *Sedimentology* 66, 1746–1767. <https://doi.org/10.1111/sed.12557>
- Normandeau, A., Lajeunesse, P., Ghienne, J.F., Dietrich, P., 2022. Detailed seafloor imagery of turbidity current bedforms reveals new insight into fine-scale near-bed processes. *Geophys. Res. Lett.* 49, e2021GL097389. <https://doi.org/10.1029/2021GL097389>
- Normandeau, A., Dafoe, L.T., Li, M.Z., Campbell, D.C., Jenner, K.A., 2023. Sedimentary record of bottom currents and internal tides in a modern highstand submarine canyon head. *Sedimentology*, 13165. <https://doi.org/10.1111/sed.13165>

- Normark, W.R., Hess, G.R., Stow, D.A.V., Bowen, A.J., 1980. Sediment waves on the Monterey fan levee: a preliminary physical interpretation. *Mar. Geol.* 37, 1–18. [https://doi.org/10.1016/0025-3227\(80\)90009-2](https://doi.org/10.1016/0025-3227(80)90009-2)
- Normark, W.R., Posamentier, H., Mutti, E., 1993. Turbidite systems: state of the art and future directions. *Rev. Geophys.* 31, 91–116. <https://doi.org/10.1029/93RG02832>
- Normark, W.R., Damuth, J.E., Leg 155 Sedimentology Group, 1997. Sedimentary facies and associated depositional elements of the Amazon fan. In: *Proc. ODP, Sci Results* (Flood, R.D., Piper, D.J.W., Klaus, A., Peterson, L.C. (Eds.), Ocean Drilling Program, College Station, TX 155, pp. 611–651.
- Normark, W.R., Piper, D.J., Posamentier, H., Pirmez, C., Migeon, S., 2002. Variability in form and growth of sediment waves on turbidite channel levees. *Mar. Geol.* 192, 23–58. [https://doi.org/10.1016/S0025-3227\(02\)00548-0](https://doi.org/10.1016/S0025-3227(02)00548-0)
- Normark, W.R., Carlson, P.R., 2003. Giant submarine canyons: is size any clue to their importance in the rock record? In: Chan, M.A., Archer, A.W. (Eds.), *Extreme Depositional Environments: Mega End Members in Geologic Time: Geological Society of America Special Paper, Colorado*, 170–190. <https://doi.org/10.1130/0-8137-2370-1.175>
- Normark, W.R., Piper, D.J.W., Romans, B.W., Covault, J.A., Dartnell, P., Sliter, R.W., 2009a. Submarine canyon and fan systems of the California Continental Borderland. *Spec. Pap. Geol. Soc. Am.* 454, 141–168. [https://doi.org/10.1130/2009.2454\(2.7\)](https://doi.org/10.1130/2009.2454(2.7))
- Normark, W.R., Paull, C.K., Caress, D.W., Ussler, W., Sliter, R., 2009b. Fine-scale relief related to late holocene channel shifting within the floor of the upper Redondo Fan, offshore Southern California. *Sedimentology* 56, 1690–1704. <https://doi.org/10.1111/j.1365-3091.2009.01052.x>
- Oberle, F.K.J., Puig, P., Martín, J., 2018. Fishing Activities. In: A. Micallef, S. Krastel, A. Savini (Eds.). *Submarine Geomorphology*. Springer, pp. 503–534. https://doi.org/10.1007/978-3-319-57852-1_25
- Oguz, T., Mourre, B., Tintoré, J., 2017. Modulation of frontogenetic plankton production along a meandering jet by zonal wind forcing: An application to the Alboran Sea. *J. Geophys. Res. Ocean.* 122, 6594–6610. <https://doi.org/10.1002/2017JC012866>

- Oliveira, A., Santos, A.I., Rodrigues, A., Vitorino, J., 2007. Sedimentary particle distribution and dynamics on the Nazaré canyon system and adjacent shelf (Portugal). *Mar. Geol.* 246, 105–122. <https://doi.org/10.1016/j.margeo.2007.04.017>
- Oliveira, F., Monteiro, P., Bentes, L., Henriques, N.S., Aguilar, R., Gonçalves, J.M.S., 2015. Marine litter in the upper São Vicente submarine canyon (SW Portugal): Abundance, distribution, composition and fauna interactions. *Mar. Pollut. Bull.* 97, 401–407. <https://doi.org/10.1016/j.marpolbul.2015.05.060>
- Ono, K., Naruse, H., Yao, Q., Cai, Z., Fukuda, S., Yokokawa, M., 2023. Multiple scours and upward fining caused by hydraulic jumps: Implications for the recognition of cyclic steps in the deepwater stratigraphic record. *J. Sediment. Res.* 93, 243–255. <https://doi.org/10.2110/jsr.2021.14>
- Ortega-Sánchez, M., Lobo, F.J., López-Ruiz, A., Losada, M.A., Fernández-Salas, L.M., 2014. The influence of shelf-indenting canyons and infralittoral prograding wedges on coastal morphology: The Carchuna system in Southern Spain. *Mar. Geol.* 347, 107–122. <https://doi.org/10.1016/j.margeo.2013.11.006>
- Palanques, A., El Khatab, M., Puig, P., Masqué, P., Sánchez-Cabeza, J.A., Isla, E., 2005. Downward particle fluxes in the Guadiaro submarine canyon depositional system (north-western Alboran Sea), a river flood dominated system. *Mar. Geol.* 220, 23–40. <https://doi.org/10.1016/j.margeo.2005.07.004>
- Miramontes, A., Durrieu de Madron, X., Puig, P., Fabres, J., Guillén, J., Calafat, A., Canals, M., Heussner, S., Bonnin, J., 2006. Suspended sediment fluxes and transport processes in the Gulf of Lions submarine canyons. The role of storms and dense water cascading. *Mar. Geol.* 234, 43–61. <https://doi.org/10.1016/j.margeo.2006.09.002>
- Palanques, A., Guillén, J., Puig, P., Durrieu de Madron, X., 2008. Storm-driven shelf-to-canyon suspended sediment transport at the southwestern Gulf of Lions. *Cont. Shelf Res.* 28, 1947–1956. <https://doi.org/10.1016/j.csr.2008.03.020>
- Palanques, A., Puig, P., Durrieu de Madron, X., Sanchez-Vidal, A., Pasqual, C., Martín, J., Calafat, A., Heussner, S., Canals, M., 2012. Sediment transport to the deep canyons and open-slope of the western Gulf of Lions during the 2006 intense cascading and open-sea convection period. *Prog. Oceanogr.* 106, 1–15. <https://doi.org/10.1016/j.pocean.2012.05.002>

- Palomino, D., Vazquez, J., Ercilla, G., Lopez-Gonzalez, N., 2016. Los montes submarinos de la plataforma marginal de Motril, Mar de Alborán: Interacción con las masas de agua profunda. *Boletín de La Academia Malagueña de Ciencias*, December, 73–85.
- Palomino, D., Alonso, B., Ercilla, G., Casas, D., López-González, N., Azpiroz-Zabala, M., Juan-Valenzuela, C., Fernández-Salas, L.M., Vázquez, J., The Fauces Team, 2019. Bedforms in the la Linea Turbidite System (NW Alboran Sea). 34th IAS Meeting of Sedimentology. Session 4.A, 655.
- Paradis, S., Lo Iacono, C., Masqué, P., Puig, P., Palanques, A., Russo, T., 2021. Evidence of large increases in sedimentation rates due to fish trawling in submarine canyons of the Gulf of Palermo (SW Mediterranean). *Mar. Pollut. Bull.* 172, 112861. <https://doi.org/10.1016/j.marpolbul.2021.112861>
- Parker, G., 1982. Conditions for the ignition of catastrophically erosive turbidity currents. *Mar. Geol.* 46, 307–327. [https://doi.org/10.1016/0025-3227\(82\)90086-X](https://doi.org/10.1016/0025-3227(82)90086-X)
- Parrilla, G., Kinder, T., 1987. Oceanografía física del Mar de Alborán. *Boletín del Instituto Español de Oceanografía* 4, 133–165.
- Parsons, J.D., Friedrichs, C.T., Traykovski, P.A., Mohrig, D., Imran, J., Syvitski, J.P.M., Parker, G., Puig, P., Buttle, J.L., García, M.H., 2007. The Mechanics of Marine Sediment Gravity Flows. *Int. Assoc. Sed. Spec. Pub.* 37, 275–337. <https://doi.org/10.1002/9781444304398.ch6>
- Paull, C.K., Ussler, W.I., Greene, H.G., Keaten, R., Mitts, P., Barry, J., 2002. Caught in the act: The 20 December 2001 gravity flow event in Monterey Canyon. *Geo-Marine Lett.* 22, 227–232. <https://doi.org/10.1007/s00367-003-0117-2>
- Paull, C.K., Mitts, P., Ussler, W.III., Greene, G.H., 2005. Trail of sand in upper Monterey canyon: Offshore California. *Aapg Bull.* 117, 1134–1145. <https://doi.org/10.1130/B25390.1>
- Paull, C.K., Ussler III, W., Caress, D.W., Lundsten, E., Covault, J.A., Maier, K.L., Xu, J., Augenstein, S., 2010. Origins of large crescent-shaped bedforms within the axial channel of Monterey Canyon, offshore California. *Geosphere* 6, 755–774. <https://doi.org/10.1130/GES00527.1>
- Paull, C.K., Caress, D.W., Ussler, W., Lundsten, E., Meiner-Johnson, M., 2011. High-resolution bathymetry of the axial channels within Monterey and Soquel submarine

- canyons, offshore central California. *Geosphere* 7, 1077–1101.
<https://doi.org/10.1130/GES00636.1>
- Paull, C.K., Caress, D.W., Lundsten, E., Gwiazda, R., Anderson, K., McGann, M., Conrad, J., Edwards, B., Sumner, E.J., 2013. Anatomy of the La Jolla Submarine Canyon system; offshore southern California. *Mar. Geol.* 335, 16–34.
<https://doi.org/10.1016/j.margeo.2012.10.003>
- Paull, C.K., McGann, M., Sumner, E.J., Barnes, P.M., Lundsten, E.M., Anderson, K., Gwiazda, R., Edwards, B., Caress, D.W., 2014. Sub-decadal turbidite frequency during the early Holocene: Eel Fan, offshore northern California. *Geology* 42, 855–858. <https://doi.org/10.1130/G35768.1>
- Paull, C.K., Talling, P.J., Maier, K.L., Parsons, D., Xu, J., Caress, D.W., Gwiazda, R., Lundsten, E.M., Anderson, K., Barry, J.P., Chaffey, M., O'Reilly, T., Rosenberger, K.J., Gales, J.A., Kieft, B., McGann, M., Simmons, S.M., McCann, M., Sumner, E.J., Clare, M.A., Cartigny, M.J., 2018. Powerful turbidity currents driven by dense basal layers. *Nat. Commun.* 9, 1–9. <https://doi.org/10.1038/s41467-018-06254-6>
- Peakall, J., McCaffrey, B., Kneller, B., 2000. A process model for the evolution, morphology, and architecture of sinuous submarine channels. *J. Sediment. Res.* 70, 434–448.
<https://doi.org/10.1306/2DC4091C-0E47-11D7-8643000102C1865D>
- Pearman, T.R.R., Robert, K., Callaway, A., Hall, R., Lo Iacono, C., Huvenne, V.A.I., 2020. Improving the predictive capability of benthic species distribution models by incorporating oceanographic data – Towards holistic ecological modelling of a submarine canyon. *Prog. Oceanogr.* 184, 102338.
<https://doi.org/10.1016/j.pocean.2020.102338>
- Pearman, T.R.R., Robert, K., Callaway, A., Hall, R.A., Mienis, F., Huvenne, V.A.I., 2023. Spatial and temporal environmental heterogeneity induced by internal tides influences faunal patterns on vertical walls within a submarine canyon. *Front. Mar. Sci.* 10, 1–20.
<https://doi.org/10.3389/fmars.2023.1091855>
- Peng, X., Dasgupta, S., Zhong, G., Du, M., Xu, H., Chen, M., Chen, S., Ta, K., Li, J., 2019. Large debris dumps in the northern South China Sea. *Mar. Pollut. Bull.* 142, 164–168.
<https://doi.org/10.1016/j.marpolbul.2019.03.041>

- Pérez-Asensio, J.N., Aguirre, J., 2010. Benthic foraminiferal assemblages in temperate coral-bearing deposits from the late Pliocene. *J. Foramin. Res.* 40, 61–78. <https://doi.org/10.2113/gsjfr.40.1.61>
- Pérez-Belzuz, F., Alonso, B., Ercilla, G., 1997. History of mud diapirism and trigger mechanisms in the Western Alboran Sea. *Tectonophysics* 282, 399–422. [https://doi.org/10.1016/S0040-1951\(97\)00226-6](https://doi.org/10.1016/S0040-1951(97)00226-6)
- Pérez-Belzuz, F., 1999. Geología del Margen y Cuenca del Mar de Alborán durante el Plio-Cuaternario: Sedimentación y Tectónica. Ph.D. Thesis Doctoral, University of Barcelona. Barcelona, Spain, 445 pp.
- Pérez-Belzuz, F., Alonso, B., 2000a. Evolución sedimentaria reciente de dos sistemas turbidíticos del área de Motril (NE Alborán). Parte I: sistema turbidítico de Calahonda. *Geotemas* 1, 203–206.
- Pérez-Belzuz, F., Alonso, B., 2000b. Evolución sedimentaria reciente de dos sistemas turbidíticos del área de Motril (NE Alborán). Parte II: sistema turbidítico de Sacratif. *Geotemas* 1, 207–211.
- Pérez-Belzuz, F., Alonso, B., Ercilla, G., 2000. Modelos de sistemas turbidíticos en el Área de Motril (NE Alborán). *Geotemas* 1, 213–216.
- Perkins, H., Kinder, T., La Violette, P., 1990. The Atlantic inflow in the Western Alboran Sea. *J. Phys. Oceanogr.* 20, 242–263. [https://doi.org/10.1175/1520-0485\(1990\)020](https://doi.org/10.1175/1520-0485(1990)020)
- Perri, F., Critelli, S., Dominici, R., Muto, F., Tripodi, V., Ceramicola, S., 2012. Provenance and accommodation pathways of late Quaternary sediments in the deep-water northern Ionian Basin, southern Italy. *Sediment. Geol.* 280, 244–259. <https://doi.org/10.1016/j.sedgeo.2012.01.007>
- Pham, C.K., Diogo, H., Menezes, G., Porteiro, F., Braga-Henriques, A., Vandepierre, F., Morato, T., 2014a. Deep-water longline fishing has reduced impact on Vulnerable Marine Ecosystems. *Sci. Rep.* 4. <https://doi.org/10.1038/srep04837>
- Pham, C.K., Ramirez-Llodra, E., Alt, C.H.S., Amaro, T., Bergmann, M., Canals, M., Company, J.B., Davies, J., Duineveld, G., Galgani, F., Howell, K.L., Huvenne, V.A.I., Isidro, E., Jones, D.O.B., Lastras, G., Morato, T., Gomes-Pereira, J.N., Purser, A., Stewart, H., Tojeira, I., Tubau, X., Van Rooij, D., Tyler, P.A., 2014b. Marine litter

- distribution and density in European seas, from the shelves to deep basins. PLoS One 9, e95839. <https://doi.org/10.1371/journal.pone.0095839>
- Pierdomenico, M., Martorelli, E., Dominguez-Carri6, C., Gili, J.M., Chiocci, F.L., 2016. Seafloor characterization and benthic megafaunal distribution of an active submarine canyon and surrounding sectors: The case of Gioia Canyon (Southern Tyrrhenian Sea). J. Mar. Syst. 157, 101–117. <https://doi.org/10.1016/j.jmarsys.2016.01.005>
- Pierdomenico, M., Cardone, F., Carluccio, A., Casalbore, D., Chiocci, F., Maiorano, P., D’Onghia, G., 2019a. Megafauna distribution along active submarine canyons of the central Mediterranean: Relationships with environmental variables. Prog. Oceanogr. 171, 49–69. <https://doi.org/10.1016/j.pocean.2018.12.015>
- Pierdomenico, M., Casalbore, D., Chiocci, F.L., 2019b. Massive benthic litter funnelled to deep sea by flash-flood generated hyperpycnal flows. Sci. Rep. 9, 1–10. <https://doi.org/10.1038/s41598-019-41816-8>
- Pierdomenico, M., Casalbore, D., Chiocci, F.L., 2020. The key role of canyons in funnelling litter to the deep sea: A study of the Gioia Canyon (Southern Tyrrhenian Sea). Anthropocene 30, 100237. <https://doi.org/10.1016/j.ancene.2020.100237>
- Pierdomenico, M., Ridente, D., Casalbore, D., Di Bella, L., Milli, S., Chiocci, F.L., 2022. Plastic burial by flash-flood deposits in a prodelta environment (Gulf of Patti, Southern Tyrrhenian Sea). Mar. Pollut. Bull. 181, 113819. <https://doi.org/10.1016/j.marpolbul.2022.113819>
- Pierdomenico, M., Bernhardt, A., Eggenhuisen, J.T., Clare, M.A., Lo Iacono, C., Casalbore, D., Davies, J.S., Kane, I., Huvenne, V.A.I., Harris, P.T., 2023. Transport and accumulation of litter in submarine canyons: a geoscience perspective. Front. Mar. Sci. 10, 1–22. <https://doi.org/10.3389/fmars.2023.1224859>
- Piper, D.J.W., Normark, W.R., 1983. Turbidite depositional patterns and flow characteristics, Navy depositional lobe, California Borderland. Sedimentology 30, 681–694. <https://doi.org/10.1111/j.1365-3091.1983.tb00702.x>
- Piper, D.J.W., Savoye, B., 1993. Processes of late quaternary turbidity current flow and deposition on the Var deep-sea fan, north-west Mediterranean Sea. Sedimentology 40, 557–582. <https://doi.org/10.1111/j.1365-3091.1993.tb01350.x>

- Piper, D.J.W., Cochonat, P., Morrison, M.L., 1999. The sequence of events around the epicentre of the 1929 Grand Banks earthquake: Initiation of debris flows and turbidity current inferred from sidescan sonar. *Sedimentology* 46, 79–97. <https://doi.org/10.1046/j.1365-3091.1999.00204.x>
- Piper, D.J.W., Normark, W.R., 2009. Processes that initiate turbidity currents and their influence on turbidites: A marine geology perspective. *J. Sediment. Res.* 79, 347–362. <https://doi.org/10.2110/jsr.2009.046>
- Platt, J.P., Viserres, R.L.M., 1986. Extensional collapse of thickened continental lithosphere: a working hypothesis for the Alboran Sea and Gibraltar Arc. *Geology* 17, 540–543. [https://doi.org/10.1130/0091-7613\(1989\)017%3C0540:ECOTCL%3E2.3.CO;2](https://doi.org/10.1130/0091-7613(1989)017%3C0540:ECOTCL%3E2.3.CO;2)
- Platt, J. P., Whitehouse, M. J., Kelley, S. P., Carter, A., Hollick, L., 2003. Simultaneous extensional exhumation across the Alboran Basin: Implications for the causes of late orogenic extension. *Geology* 31, 251–254. [https://doi.org/10.1130/0091-7613\(2003\)031<0251:SEEATA>2.0.CO;2](https://doi.org/10.1130/0091-7613(2003)031<0251:SEEATA>2.0.CO;2)
- Pohl, F., Eggenhuisen, J.T., Cartigny, M., Tilston, M.C., 2022. Initiation of deposition in supercritical turbidity currents downstream of a slope break. *Sedimentology* 1–55. <https://doi.org/10.31223/X5M35X>
- Poore, G.C.B., Ahyong, S.T., Taylor, J., 2011. The biology of squat lobsters. CSIRO, 363 pp. <https://doi.org/10.1071/9780643104341>
- Popescu, I., Lericolais, G., Panin, N., Normand, A., Dinu, C., Le Drezen, E., 2004. The Danube submarine canyon (Black Sea): Morphology and sedimentary processes. *Mar. Geol.* 206, 249–265. <https://doi.org/10.1016/j.margeo.2004.03.003>
- Popescu, I., Panin, N., Jipa, D., Lericolais, G., Ion, G., 2015. Submarine canyons of the Black Sea basin with a focus on the Danube Canyon. In: Briand, F. (Ed.), *Submarine Canyon Dynamics in the Mediterranean and Tributary Seas*. CIESM, Monaco, pp. 103–121.
- Posamentier, H.W., Vail, P.R., 1988. Eustatic controls on clastic deposition II: sequence and systems tract models. In: Wilgus, C.K., Hastings, B.S., Posamentier, H., Van Wagoner, J., Ross, C.A., Kendall, C.G. St.C. (Eds.), *Sea level changes: an integrated approach*. SEPM Special Publication, pp. 125–154. <https://doi.org/10.2110/pec.88.01.0125>

- Posamentier, H., Walker, R., 2006. Deep-water turbidites and submarine fans. In: Posamentier, H., Walker, R.G. (Eds.), *Facies models revisited*. SEPM Special Publication, pp. 397–520. <https://doi.org/10.2110/pec.06.84.0399>
- Post, A.L., Przeslawski, R., Nanson, R., Siwabessy, J., Smith, D., Kirkendale, L.A., Wilson, N.G., 2022. Modern dynamics, morphology and habitats of slope-confined canyons on the northwest Australian margin. *Mar. Geol.* 443, 106694. <https://doi.org/10.1016/j.margeo.2021.106694>
- Pratson, L.F., Coakley, B.J., 1996. A model for the headward erosion of submarine canyons induced by downslope-eroding sediment flows. *Bull. Geol. Soc. Am.* 108, 225–234. <https://doi.org/10.1130/0016-7606>
- Pratson, L.F., Imran, J., Parker, G., Syvitski, J.P.M., Hutton, E., 2000. Debris flows vs. turbidity currents: A modeling comparison of their dynamics and deposits. In: Bouma, A.H., Stone, C.G. (Eds.), *Fine-Grained Turbidite Systems*. SEPM Special Publication. AAPG Memoir. 72, 57–72. <http://dx.doi.org/10.1306/M72703C6>
- Prins, M.A., Postma, G., Cleveringa, J., Cramp, A., Kenyon, N.H., 2000. Controls on terrigenous sediment supply to the Arabian Sea during the late quaternary: The Indus fan. *Mar. Geol.* 169, 327–349. [https://doi.org/10.1016/S0025-3227\(00\)00086-4](https://doi.org/10.1016/S0025-3227(00)00086-4)
- Puga-Bernabéu, Á., Webster, J.M., Beaman, R.J., Guilbaud, V., 2011. Morphology and controls on the evolution of a mixed carbonate-siliciclastic submarine canyon system, Great Barrier Reef margin, north-eastern Australia. *Mar. Geol.* 289, 100–116. <https://doi.org/10.1016/j.margeo.2011.09.013>
- Puga-Bernabéu, Á., Webster, J.M., Beaman, R.J., Guilbaud, V., 2013. Variation in canyon morphology on the Great Barrier Reef margin, north-eastern Australia: The influence of slope and barrier reefs. *Geomorphology* 191, 35–50. <https://doi.org/10.1016/j.geomorph.2013.03.001>
- Puig, P., Ogston, A.S., Mullenbach, B.L., Nittrouer, C.A., Sternberg, R.W., 2003. Shelf-to-canyon sediment-transport processes on the Eel continental margin (northern California). *Mar. Geol.* 193, 129–149. [https://doi.org/10.1016/S0025-3227\(02\)00641-2](https://doi.org/10.1016/S0025-3227(02)00641-2)
- Puig, P., Palanques, A., Guillén, J., El Khatab, M., 2004. Role of internal waves in the generation of nepheloid layers on the northwestern Alboran slope: Implications for

- continental margin shaping. *J. Geophys. Res.* 109, C09011. <https://doi.org/10.1029/2004JC002394>
- Puig, P., Palanques, A., Orange, D.L., Lastras, G., Canals, M., 2008. Dense shelf water cascades and sedimentary furrow formation in the Cap de Creus Canyon, northwestern Mediterranean Sea. *Cont. Shelf Res.* 28, 2017–2030. <https://doi.org/10.1016/j.csr.2008.05.002>
- Puig, P., Canals, M., Company, J.B., Martín, J., Amblas, D., Lastras, G., Palanques, A., Calafat, A.M., 2012. Ploughing the deep sea floor. *Nature* 489, 286–289. <https://doi.org/10.1038/nature11410>
- Puig, P., Greenan, B.J.W., Li, M.Z., Prescott, R.H., Piper, D.J.W., 2013. Sediment transport processes at the head of Halibut Canyon, eastern Canada margin: An interplay between internal tides and dense shelf-water cascading. *Mar. Geol.* 341, 14–28. <https://doi.org/10.1016/j.margeo.2013.05.004>
- Puig, P., Palanques, A., Martín, J., 2014. Contemporary sediment-transport processes in submarine canyons. *Ann. Rev. Mar. Sci.* 6, 53–77. <https://doi.org/10.1146/annurev-marine-010213-135037>
- Puig, P., Martín, J., Masqué, P., Palanques, A., 2015. Increasing sediment accumulation rates in la Fonera (Palamós) submarine canyon axis and their relationship with bottom trawling activities. *Geophys. Res. Lett.* 42, 8106–8113. <https://doi.org/10.1002/2015GL065052>
- Puig, P., Durán, R., Muñoz, A., Elvira, E., Guillén, J., 2017. Submarine canyon-head morphologies and inferred sediment transport processes in the Alías-Almanzora canyon system (SW Mediterranean): On the role of the sediment supply. *Mar. Geol.* 393, 21–34. <http://dx.doi.org/10.1016/j.margeo.2017.02.009>
- Quattrini, A.M., Nizinski, M.S., Chaytor, J.D., Demopoulos, A.W.J., Roark, E.B., France, S.C., Moore, J.A., Heyl, T., Auster, P.J., Kinlan, B., Ruppel, C., Elliott, K.P., Kennedy, B.R.C., Lobecker, E., Skarke, A., Shank, T.M., 2015. Exploration of the canyon-incised continental margin of the northeastern United States reveals dynamic habitats and diverse communities. *PLoS One* 10, 1–32. <https://doi.org/10.1371/journal.pone.0139904>

- Ragnarsson, S.Á., Burgos, J.M., Kutti, T., van den Beld, I., Egilsdóttir, H., Arnaud-Haond, S., Grehan, A., 2017. The impact of anthropogenic activity on cold-water corals. In: Rossi, S., Bramanti, L., Gori, A., Orejas, C (Eds.), *Marine animal forests: the ecology of benthic biodiversity hotspots*. Springer, pp. 989–1023. https://doi.org/10.1007/978-3-319-21012-4_27
- Ramirez-Llodra, E., Tyler, P.A., Baker, M.C., Bergstad, O.A., Clark, M.R., Escobar, E., Levin, L.A., Menot, L., Rowden, A.A., Smith, C.R., van Dover, C.L., 2011. Man and the last great wilderness: Human impact on the deep sea. *PLoS One* 6, e22588. <https://doi.org/10.1371/journal.pone.0022588>
- Ramirez-Llodra, E., De Mol, B., Company, J.B., Coll, M., Sardà, F., 2013. Effects of natural and anthropogenic processes in the distribution of marine litter in the deep Mediterranean Sea. *Prog. Oceanogr.* 118, 273–287. <https://doi.org/10.1016/j.pocean.2013.07.027>
- Reading, H. G., Richards, M., 1994. Turbidite systems in deep-water basin margins classified by grain size and feeder system. *AAPG Bull.* 78, 792–822. <https://doi.org/10.1306/a25fe3bf-171b-11d7-8645000102c1865d>
- Rebesco, M., Neagu, R.C., Cuppari, A., Muto, F., Accettella, D., Dominici, R., Cova, A., Romano, C., Caburlotto, A., 2009. Morphobathymetric analysis and evidence of submarine mass movements in the western Gulf of Taranto (Calabria margin, Ionian Sea). *Int. J. Earth Sci.* 98, 791–805. <https://doi.org/10.1007/s00531-009-0429-1>
- Renault, L., Oguz, T., Pascual, A., Vizoso, G., Tintore, J., 2012. Surface circulation in the Alborn Sea (western Mediterranean) inferred from remotely sensed data. *J. Geophys. Res. Ocean.* 117, 1–11. <https://doi.org/10.1029/2011JC007659>
- Rennie, S.J., Pattiaratchi, C.B., McCauley, R.D., 2009a. Numerical simulation of the circulation within the Perth Submarine Canyon, Western Australia. *Cont. Shelf Res.* 29, 2020–2036. <https://doi.org/10.1016/j.csr.2009.04.010>
- Rennie, S., Hanson, C.E., McCauley, R.D., Pattiaratchi, C., Burton, C., Bannister, J., Jenner, C., Jenner, M.N., 2009b. Physical properties and processes in the Perth Canyon, Western Australia: Links to water column production and seasonal pygmy blue whale abundance. *J. Mar. Syst.* 77, 21–44. <https://doi.org/10.1016/j.jmarsys.2008.11.008>

- Ribó, M., Puig, P., Palanques, A., lo Iacono, C., 2011. Dense shelf water cascades in the cap de creus and palamós submarine canyons during winters 2007 and 2008. *Mar. Geol.* 284, 175–188. <https://doi.org/10.1016/j.margeo.2011.04.001>
- Richmond, R.H., 1993. Coral reefs: Present problems and future concerns resulting from anthropogenic disturbance. *Integr. Comp. Biol.* 33, 524–536. <https://doi.org/10.1093/icb/33.6.524>
- Rodriguez, M., Maleuvre, C., Jollivet-Castelot, M., d’Acremont, E., Rabaute, A., Lafosse, M., Ercilla, G., Vázquez, J.T., Alonso, B., Ammar, A., Gorini, C., 2017. Tsunamigenic submarine landslides along the Xauen-Tofiño banks in the Alboran Sea (Western Mediterranean Sea). *Geophys. J. Int.* 209, 266–281. <https://doi.org/10.1093/gji/ggx028>
- Rogers, K.G., Goodbred, S.L., Khan, S.R., 2015. Shelf-to-canyon connections: transport related morphology and mass balance at the shallow-headed, rapidly aggrading Swatch of No Ground (Bay of Bengal). *Mar. Geol.* 369, 288–299. <https://doi.org/10.1016/j.margeo.2015.09.011>
- Romans, B.W., Normark, W.R., McGann, M.M., Covault, J.A., Graham, S.A., 2009. Coarse-grained sediment delivery and distribution in the Holocene Santa Monica Basin, California: Implications for evaluating source-to-sink flux at millennial time scales. *Bull. Geol. Soc. Am.* 121, 1394–1408. <https://doi.org/10.1130/B26393.1>
- Rueda, J.L., Gofas, S., Aguilar, R., de la Torriente, A., García Raso, J.E., Lo Iacono, C., Luque, Á.A., Marina, P., Mateo-Ramírez, Á., Moya-Urbano, E., Moreno, D., Navarro-Barranco, C., Salas, C., Sánchez-Tocino, L., Templado, J., Urra, J., 2021. Benthic Fauna of Littoral and Deep-Sea Habitats of the Alboran Sea: A Hotspot of Biodiversity BT - Alboran Sea. In: J.C. Báez, J.T. Vázquez, J.A. Camiñas, M. Malouli Idrissi (Eds.), *Alboran Sea – Ecosystems and Marine Resources*. Springer, 9, 285–358. https://doi.org/10.1007/978-3-030-65516-7_9
- Ryan, W.B.F., Hsu, K.J., Cita, M.B., Dumitricia, P., Lort, J., Maync, W., Nesteroff, W.D., Pautot, G., Stradner, H., Wezel, F.C., 1973. Western Alboran Basin — Site 121. Initial Reports of the Deep Sea Drilling Project 13. U.S. Govt. Printing Office, Washington, D.C. 1447.
- Saldías, G.S., Allen, S.E., 2020. The influence of a submarine canyon on the circulation and cross-shore exchanges around an upwelling front. *J. Phys. Oceanogr.* 50, 1677–1698. <https://doi.org/10.1175/JPO-D-19-0130.1>

- Sánchez, P., Masó, M., Sáez, R., de Juan, S., Muntadas, A., Demestre, M., 2013. Baseline study of the distribution of marine debris on soft-bottom habitats associated with trawling grounds in the northern Mediterranean. *Sci. Mar.* 77, 247–255. <https://doi.org/10.3989/scimar03702.10A>
- Sarhan, T., Lafuente, J.G., Vargas, M., Vargas, J.M., Plaza, F., 2000. Upwelling mechanisms in the northwestern Alborán Sea. *J. Mar. Syst.* 23, 317–331. [https://doi.org/10.1016/S0924-7963\(99\)00068-8](https://doi.org/10.1016/S0924-7963(99)00068-8)
- Scacchia, E., Tinterri, R., Gamberi, F., 2022. The Influence of Channel Planform and Slope Topography on Turbidity Current Overbank Processes: The Example of the Acquarone Fan (Southeastern Tyrrhenian Sea). *Front. Earth Sci.* 9, 1–22. <https://doi.org/10.3389/feart.2021.785164>
- Schattner, U., Lazar, M., 2016. Hierarchy of source-to-sink systems — Example from the Nile distribution across the eastern Mediterranean. *Sediment. Geol.* 343, 119–131. <https://doi.org/10.1016/j.sedgeo.2016.08.006>
- Schlining, K., von Thun, S., Kuhn, L., Schlining, B., Lundsten, L., Jacobsen Stout, N., Chaney, L., Connor, J., 2013. Debris in the deep: Using a 22-year video annotation database to survey marine litter in Monterey Canyon, central California, USA. *Deep. Res. Part I Oceanogr. Res. Pap.* 79, 96–105. <https://doi.org/10.1016/j.dsr.2013.05.006>
- Schmiedl, G., de Bovée, F., Buscail, R., Charrière, B., Hemleben, C., Medernach, L., Picon, P., 2000. Trophic control of benthic foraminiferal abundance and microhabitat in the bathyal Gulf of Lions, western Mediterranean Sea. *Mar. Micropaleontol.* 40, 167–188. [https://doi.org/10.1016/S0377-8398\(00\)00038-4](https://doi.org/10.1016/S0377-8398(00)00038-4)
- Schulten, I., Micallef, A., Krastel, S., Urlaub, M., Gutscher, M.A., Kopp, H., 2023. Reconstruction of the 1908 Messina gravity flow (central Mediterranean Sea) from geophysical and sedimentological data. *Mar. Geol.* 459, 107047. <https://doi.org/10.1016/j.margeo.2023.107047>
- Serra, C.S., Martínez-Loriente, S., Gràcia, E., Urgeles, R., Vizcaino, A., Perea, H., Bartolome, R., Pallàs, R., Lo Iacono, C., Díez, S., Dañobeitia, J., Terrinha, P., Zitellini, N., 2020. Tectonic evolution, geomorphology and influence of bottom currents along a large submarine canyon system: The São Vicente Canyon (SW Iberian margin). *Mar. Geol.* 426, 106219. <https://doi.org/10.1016/j.margeo.2020.106219>

- Serrano, M.A., Díez-Minguito, M., Valle-Levinson, A., Ortega-Sanchez, M., 2020. Circulation in a Short, Microtidal Submarine Canyon in the Alborán Sea. *J. Coast. Res.* 95, 1531–1535. <https://doi.org/10.2112/SI95-295.1>
- Shanmugam, G., 1997. The Bouma Sequence and the turbidite mind set. *Earth-Science Rev.* 42, 201–229. [https://doi.org/10.1016/S0012-8252\(97\)81858-2](https://doi.org/10.1016/S0012-8252(97)81858-2)
- Shanmugam, G., 2019. Slides, Slumps, Debris Flows, Turbidity Currents, Hyperpycnal Flows, and Bottom Currents. In: Kirk Cochran, J., Bokuniewicz, H.J., Yager, P.L. (Eds.), *Encyclopedia of Ocean Sciences*. Academic Press 4, 228–257. <https://doi.org/10.1016/B978-0-12-409548-9.10884-X>
- Shepard, F.P., 1981. Submarine canyons: multiple causes and long-time persistence. *Am. Assoc. Petr. Geol. B.* 65, 1062–1077. <https://doi.org/10.1306/03B59459-16D1-11D7-8645000102C1865D>
- Shepard, F.P., Emery, K.O., 1941. Submarine Topography off the California Coast: Canyons and Tectonic Interpretation. *Geol. Soc. Am. Spec. Pap.* 31, 171. <https://doi.org/10.1130/SPE31>
- Slootman, A., Cartigny, M.J.B., 2020. Cyclic steps: Review and aggradation-based classification. *Earth-sci. Rev.* 201, 102949. <https://doi.org/10.1016/j.earscirev.2019.102949>
- Smith, D.P., Ruiz, G., Kvitek, R., Iampietro, P.J., 2005. Semi-annual patterns of erosion and deposition in upper Monterey Canyon from serial multibeam bathymetry. *Bull. Geol. Soc. Am.* 117, 1123–1133. <https://doi.org/10.1130/B25510.1>
- Smith, D.P., Kvitek, R., Iampietro, P.J., Wong, K., 2007. Twenty-nine months of geomorphic change in upper Monterey Canyon (2002-2005). *Mar. Geol.* 236, 79–94. <https://doi.org/10.1016/j.margeo.2006.09.024>
- Smith, D.P., Kvitek, R., Iampietro, P.J., Wong, K., 2017. Twenty-nine months of geomorphic change in upper Monterey Canyon (2002-2005). *Mar. Geol.* 236, 79–94. <https://doi.org/10.1016/j.margeo.2006.09.024>
- Smith, M.E., Werner, S.H., Buscombe, D., Finnegan, N.J., Sumner, E.J., Mueller, E.R., 2018. Seeking the Shore: Evidence for Active Submarine Canyon Head Incision Due to Coarse Sediment Supply and Focusing of Wave Energy. *Geophys. Res. Lett.* 45, 12,403–12,413. <https://doi.org/10.1029/2018GL080396>

- Somoza, L., Medialdea, T., León, R., Ercilla, G., Vázquez, J.T., Farran, M., Hernández-Molina, F.J., González, J., Juan, C., Fernández-Puga, M.C., 2012. Structure of mud volcano systems and pockmarks in the region of the Ceuta Contourite Depositional System (Western Alborán Sea). *Mar. Geol.* 332–334, 4–26. <https://doi.org/10.1016/j.margeo.2012.06.002>
- Sotomayor-García, A., Rueda, J.L., Sánchez-Guillamón, O., Urrea, J., Vázquez, J.T., Palomino, D., Fernández-Salas, L.M., López-González, N., González-Porto, M., Santana-Casiano, J.M., González-Dávila, M., Presas-Navarro, C., Fraile-Nuez, E., 2019. First macro-colonizers and survivors around tagoro Submarine Volcano, Canary Islands, Spain. *Geosci.* 9, 52. <https://doi.org/10.3390/geosciences9010052>
- Soutter, E. L., Kane, I. A., Hodgson, D. M., Flint, S., 2021. The concavity of submarine canyon longitudinal profiles. *J. Geophys. Res.-earth.* 126, e2021JF006185. <https://doi.org/10.1029/2021JF006185>
- Stacey, C.D., Hill, P.R., Talling, P.J., Enkin, R.J., Hughes Clarke, J., Lintern, D.G., 2019. How turbidity current frequency and character varies down a fjord-delta system: Combining direct monitoring, deposits and seismic data. *Sedimentology* 66, 1–31. <https://doi.org/10.1111/sed.12488>
- Stanley, D.J., Kelling, G., Juan-Antonio Vera, J.-A.V., Sheng, H., 1975. Sands in the Alboran Sea: A model of input in a deep marine basin. *Smithson. Contrib. to Earth Sci.* 1–51. <https://doi.org/10.5479/si.00810274.15.1>
- Stefatos, A., Charalampakis, M., Papatheodorou, G., Ferentinos, G., 1999. Marine debris on the seafloor of the Mediterranean Sea: Examples from two enclosed gulfs in western Greece. *Mar. Pollut. Bull.* 38, 389–393. [https://doi.org/10.1016/S0025-326X\(98\)00141-6](https://doi.org/10.1016/S0025-326X(98)00141-6)
- Sumner, E.J., Peakall, J., Parsons, D.R., Wynn, R.B., Darby, S.E., Dorrell, R.M., McPhail, S.D., Perrett, J., Webb, A., White, D., 2013. First direct measurements of hydraulic jumps in an active submarine density current. *Geophys. Res. Lett.* 40, 5904–5908. <https://doi.org/10.1002/2013GL057862>
- Sun, T., Parker, G., 2005. Transportational cyclic steps created by flow over an erodible bed. Part 2. Theory and numerical simulation. *J. Hydraul. Res.* 43, 502–514. <https://doi.org/10.1080/00221680509500148>

- Sun, Y., Wang, D., Canals, M., Alves, T.M., Wang, W., Zhu, Y., Qin, Y., Zeng, F., Zheng, Y., 2023. Bedform evolution along a submarine canyon in the South China Sea: New insights from an autonomous underwater vehicle survey. *Sedimentology*, 13152. <https://doi.org/10.1111/sed.13152>
- Sunamura, T., 2018. A fundamental equation for describing the rate of bedrock erosion by sediment-laden fluid flows in fluvial, coastal, and aeolian environments. *Earth Surf. Process. Land.* 43, 3022–3041. <https://doi.org/10.1002/esp.4467>
- Susanth, S., Kurian, P.J., Bijesh, C.M., Twinkle, D., Tyagi, A., Rajan, S., 2021. Controls on the evolution of submarine canyons in steep continental slopes: geomorphological insights from Palar Basin, southeastern margin of India. *Geo-Mar. Lett.* 41. <https://doi.org/10.1007/s00367-021-00685-9>
- Sweet, M.L., Blum, M.D., 2016. Connections between fluvial to shallow marine environments and submarine canyons: Implications for sediment transfer to deep water. *J. Sediment. Res.* 86, 1147–1162. <http://dx.doi.org/10.2110/jsr.2016.64>
- Sylvester, Z., Deptuck, M., Prather, B., Pirmez, C., O’Byrne, C., Mohrig, D., Van Hoorn, B., Wynn, R., 2012. Seismic stratigraphy of a shelf-edge delta and linked submarine channels in the northeastern Gulf of Mexico. Application of the principles of seismic geomorphology to continental-slope and base-of-slope systems: case studies from seafloor and near-seafloor analogues. *SEPM Special Publication*, 99, 31–59. <https://doi.org/10.2110/pec.12.99.0031>
- Symons, W.O., Sumner, E.J., Talling, P.J., Cartigny, M.J., Clare, M.A., 2016. Large-scale sediment waves and scours on the modern seafloor and their implications for the prevalence of supercritical flows. *Mar. Geol.* 371, 130–148. <https://doi.org/10.1016/j.margeo.2015.11.009>
- Symons, W.O., Sumner, E.J., Paull, C.K., Cartigny, M.J.B., Xu, J.P., Maier, K.L., Lorenson, T.D., Talling, P.J., 2017. A new model for turbidity current behavior based on integration of flow monitoring and precision coring in a submarine canyon. *Geology* 45, 367–370. <https://doi.org/10.1130/G38764.1>
- Taki, K., Parker, G., 2005. Transportational cyclic steps created by flow over an erodible bed. Part 1. Experiments. *J. Hydraul. Res.* 43, 488–501. <https://doi.org/10.1080/00221680509500147>

- Talling, P.J., 2014. On the triggers, resulting flow types and frequencies of subaqueous sediment density flows in different settings. *Mar. Geol.* 352, 155–182. <https://doi.org/10.1016/j.margeo.2014.02.006>
- Talling, P.J., Masson, D.G., Sumner, E.J., Malgesini, G., 2012. Subaqueous sediment density flows: Depositional processes and deposit types. *Sedimentology* 59, 1937–2003. <https://doi.org/10.1111/j.1365-3091.2012.01353.x>
- Talling, P.J., Baker, M.L., Pope, E.L., Ruffell, S.C., Jacinto, R.S., Heijnen, M.S., Hage, S., Simmons, S.M., Hasenhündl, M., Heerema, C.J., McGhee, C., Apprioual, R., Ferrant, A., Cartigny, M.J.B., Parsons, D.R., Clare, M.A., Tshimanga, R.M., Trigg, M.A., Cula, C.A., Faria, R., Gaillot, A., Bola, G., Wallance, D., Griffiths, A., Nunny, R., Urlaub, M., Peirce, C., Burnett, R., Neasham, J., Hilton, R.J., 2022. Longest sediment flows yet measured show how major rivers connect efficiently to deep sea. *Nat. Commun.* 13, 1–15. <https://doi.org/10.1038/s41467-022-31689-3>
- Tarrés, M., Cerdà-Domènech, M., Pedrosa-Pàmies, R., Rumín-Caparrós, A., Calafat, A., Canals, M., Sanchez-Vidal, A., 2022. Particle fluxes in submarine canyons along a sediment-starved continental margin and in the adjacent open slope and basin in the SW Mediterranean Sea. *Prog. Oceanogr.* 203, 102783. <https://doi.org/10.1016/j.pocean.2022.102783>
- Taviani, M., Foglini, F., Castellan, G., Montagna, P., McCulloch, M.T., Trotter, J.A., 2023. First assessment of anthropogenic impacts in submarine canyon systems off southwestern Australia. *Sci. Total Environ.* 857, 159243. <https://doi.org/10.1016/j.scitotenv.2022.159243>
- Tek, D.E., McArthur, A.D., Poyatos-Moré, M., Colombero, L., Allen, C., Patacci, M., McCaffrey, W.D., 2022. Controls on the architectural evolution of deep-water channel overbank sediment wave fields: insights from the Hikurangi Channel, offshore New Zealand. *New Zeal. J. Geol. Geophys.* 65, 141–178. <https://doi.org/10.1080/00288306.2021.1978509>
- Templado, J., Ballesteros, E., Galparsoro, I., Borja, Á., Serrano, A., Martín, L., Brito, A., 2013. [*Inventario Español de Hábitats y Especies Marinos. Guía interpretativa: Inventario Español de Hábitats Marinos. Universidades 230.*](#)

- Thiel, M., Gutow, L., 2005. The ecology of rafting in the marine environment. II. The rafting organisms and community. *Oceanogr. Mar. Biol.* 43, 279–418. <https://doi.org/10.1201/9781420037449.ch7>
- Thompson, R.C., Olson, Y., Mitchell, R.P., Davis, A., Rowland, S.J., John, A.W.G., McGonigle, D., Russell, A.E., 2004. Lost at Sea: Where Is All the Plastic? *Science* 304, 838. <https://doi.org/10.1126/science.1094559>
- Thushari, G.G.N., Senevirathna, J.D.M., 2020. Plastic pollution in the marine environment. *Heliyon* 6, e04709. <https://doi.org/10.1016/j.heliyon.2020.e04709>
- Tintoré, J., La Violette, P. E., Blade, I., Cruzado, A., 1988. A Study of an Intense Density Front in the Eastern Alboran Sea: The Almeria Oran Front. *J. Phys. Oceanogr.* 18, 1384–1397. [http://dx.doi.org/10.1175/1520-0485\(1988\)018%3C1384:ASOAIID%3E2.0.CO;2](http://dx.doi.org/10.1175/1520-0485(1988)018%3C1384:ASOAIID%3E2.0.CO;2)
- Trenkel, V.M., Le Loc'h, F., Rochet, M.J., 2007. Small-scale spatial and temporal interactions among benthic crustaceans and one fish species in the Bay of Biscay. *Mar. Biol.* 151, 2207–2215. <https://doi.org/10.1007/s00227-007-0655-7>
- Trestrail, C., Nuggeoda, D., Shimeta, J., 2020. Invertebrate responses to microplastic ingestion: Reviewing the role of the antioxidant system. *Sci. Total Environ.* 734, 138559. <https://doi.org/10.1016/j.scitotenv.2020.138559>
- Trincardi, F., Foglini, F., Verdicchio, G., Asioli, A., Correggiari, A., Minisini, D., Piva, A., Remia, A., Ridente, D., Taviani, M., 2007. The impact of cascading currents on the Bari Canyon System, SW-Adriatic Margin (Central Mediterranean). *Mar. Geol.* 246, 208–230. <https://doi.org/10.1016/j.margeo.2007.01.013>
- Tubau, X., Lastras, G., Canals, M., Micallef, A., Amblas, D., 2013. Significance of the fine drainage pattern for submarine canyon evolution: The Foix Canyon System, Northwestern Mediterranean Sea. *Geomorphology* 184, 20–37. <https://doi.org/10.1016/j.geomorph.2012.11.007>
- Tubau, X., Paull, C. K., Lastras, G., Caress, D. W., Canals, M., Lundsten, E., Anderson, K., Gwiazda, R., Amblas, D., 2015a. Submarine canyons of Santa Monica Bay, Southern California: Variability in morphology and sedimentary processes. *Mar. Geol.* 365, 61–79. <https://doi.org/10.1016/j.margeo.2015.04.004>

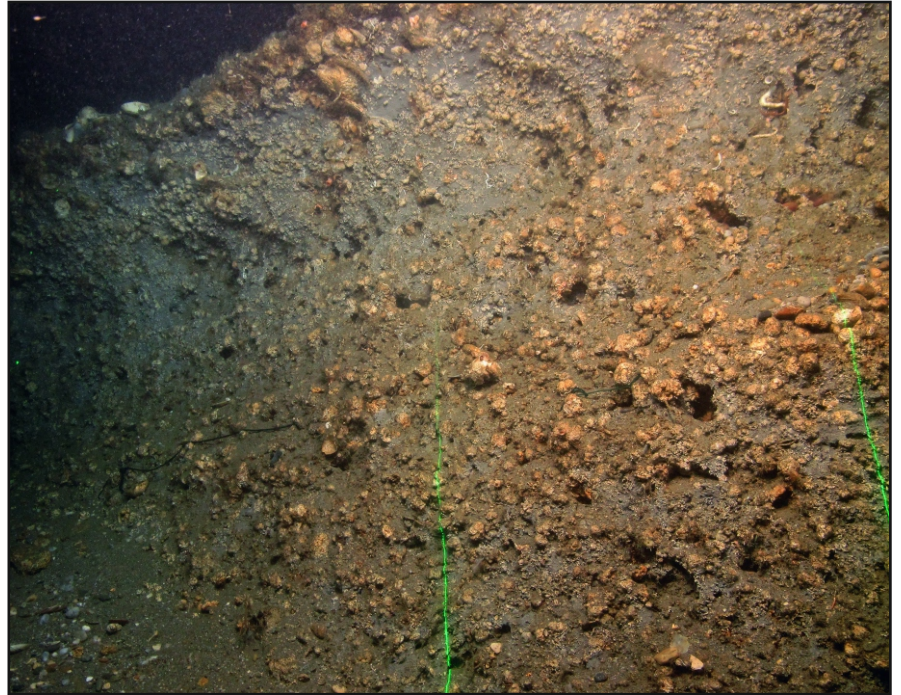
- Tubau, X., Canals, M., Lastras, G., Rayo, X., Rivera, J., Amblas, D., 2015b. Marine litter on the floor of deep submarine canyons of the Northwestern Mediterranean Sea: The role of hydrodynamic processes. *Prog. Oceanogr.* 134, 379–403. <https://doi.org/10.1016/j.pocean.2015.03.013>
- Turchetto, M., Boldrin, A., Langone, L., Miserocchi, S., Tesi, T., Foglini, F., 2007. Particle transport in the Bari Canyon (southern Adriatic Sea). *Mar. Geol.* 246, 231–247. <https://doi.org/10.1016/j.margeo.2007.02.007>
- Udden, J.A. 1914. Mechanical composition of clastic sediments. *Bull. Geol. Soc. Am.* 25, 655–744. <https://doi.org/10.1130/GSAB-25-655>
- Uiblein, F., Lorance, P., Latrouite, D., 2003. Behaviour and habitat utilisation of seven demersal fish species on the Bay of Biscay continental slope, NE Atlantic. *Mar. Ecol. Prog. Ser.* 257, 223–232. <https://doi.org/10.3354/meps257223>
- United Nations 2021. United Nations Environmental Program. [From pollution to solution: A global assessment of marine litter and plastic pollution](#)
- Vail, P.R., 1987. Part 1: Seismic stratigraphy interpretation procedure. In: Bally, A.W. (Ed.), *Atlas of Seismic Stratigraphy*, Am. Assoc. Petr. Geol. B. 27, pp. 1–10.
- van den Beld, I.M.J., Guillaumont, B., Menot, L., Bayle, C., Arnaud-Haond, S., Bourillet, J.F., 2017. Marine litter in submarine canyons of the Bay of Biscay. *Deep. Res. Part II Top. Stud. Oceanogr.* 145, 142–152. <https://doi.org/10.1016/j.dsr2.2016.04.013>
- Vangriesheim, A., Khripounoff, A., Crassous, P., 2009. Turbidity events observed in situ along the Congo submarine channel. *Deep. Res. Part II Top. Stud. Oceanogr.* 56, 2208–2222. <https://doi.org/10.1016/j.dsr2.2009.04.004>
- Vargas-Yáñez, M., García-Martínez, M.C., Moya, F., Balbín, R., López-Jurado, J.L., 2021. The oceanographic and climatic context. In: J.C. Báez, J.T. Vázquez, J.A. Camiñas, M. Malouli Idrissi (Eds.), *Alboran Sea – Ecosystems and Marine Resources*. Springer, Cham 26, pp. 85–110.
- Vázquez, J.T., 2001. Estructura del margen continental del Mar de Alborán. Ph.D. Thesis Doctoral, Complutense University of Madrid. Madrid, Spain, 422 pp.
- Vázquez, J.T., Ercilla, G., Alonso, B., Juan, C., Rueda, J.L., Palomino, D., Fernández-Salas, L.M., Bárcenas, P., Casas, D., Díaz-del-Río, V., Estrada, F., Farran, M., García, M., González, E., López-González, N., El Moumni, B., Contouriber, M.a.M.t., 2015.

- Submarine canyons and related features in the Alboran Sea: continental margins and major isolated reliefs. In: Briand, F. (Ed.), *Submarine Canyon Dynamics in the Mediterranean and Tributary Seas*. CIESM, Monaco, pp. 183–196.
- Vieira, R.P., Raposo, I.P., Sobral, P., Gonçalves, J.M.S., Bell, K.L.C., Cunha, M.R., 2015. Lost fishing gear and litter at Gorringe Bank (NE Atlantic). *J. Sea Res.* 100, 91–98. <https://doi.org/10.1016/j.seares.2014.10.005>
- Vitorino, J., Oliveira, A., Beja, J., 2005. Physical processes in the Nazare Canyon area and related sedimentary impacts. *Geophys. Res. Abstr.* 7, 10187. [SRef-ID: 1607-7962/gra/EGU05-A-10187](https://doi.org/10.1029/2005EGU05-A-10187)
- von Lom-Keil, H., Spieß, V., Hopfauf, V., 2002. Fine-grained sediment waves on the western flank of the Zapiola Drift, Argentine Basin: evidence for variations in Late Quaternary bottom flow activity. *Mar. Geol.* 192, 239–258. [http://dx.doi.org/10.1016/S0025-3227\(02\)00055-1](http://dx.doi.org/10.1016/S0025-3227(02)00055-1)
- Walsh, J.P., Nittrouer, C.A., 2003. Contrasting styles of off-shelf sediment accumulation in New Guinea. *Mar. Geol.* 196, 105–125. [https://doi.org/10.1016/S0025-3227\(03\)00069-0](https://doi.org/10.1016/S0025-3227(03)00069-0)
- Wan, L., Hurter, S., Bianchi, V., Li, P., Wang, J., Salles, T., 2022. The roles and seismic expressions of turbidites and mass transport deposits using stratigraphic forward modeling and seismic forward modeling. *J. Asian Earth Sci.* 232, 105110. <https://doi.org/10.1016/j.jseaes.2022.105110>
- Wang, X., Wang, Y., He, M., Chen, W., Zhuo, H., Gao, S., Wang, M., Zhou, J., 2017. Genesis and evolution of the mass transport deposits in the middle segment of the Pearl River canyon, South China Sea: Insights from 3D seismic data. *Mar. Petrol. Geol.* 88, 555–574. <https://doi.org/10.1016/j.marpetgeo.2017.08.036>
- Warrick, J.A., 2014. Eel River margin source-to-sink sediment budgets: Revisited. *Mar. Geol.* 351, 25–37. <https://doi.org/10.1016/j.margeo.2014.03.008>
- Warrick, J.A., Farnsworth, K.L., 2009. Dispersal of river sediment in the Southern California Bight. In: Lee, H.J., and Normark, W.R. (Eds.), *Ocean: The Southern California Continental Borderland*. Spec. Pap. Geol. Soc. Am. 454, 53–67. [https://doi.org/10.1130/2009.2454\(2.3\)](https://doi.org/10.1130/2009.2454(2.3))

- Watters, D.L., Yoklavich, M.M., Love, M.S., Schroeder, D.M., 2010. Assessing marine debris in deep seafloor habitats off California. *Mar. Pollut. Bull.* 60, 131–138. <https://doi.org/10.1016/j.marpolbul.2009.08.019>
- Weaver, P.P.E., Pujol, C., 1988. History of the last deglaciation in the Alboran sea (western Mediterranean) and adjacent north Atlantic as revealed by coccolith floras. *Palaeogeogr. Palaeoclimatol. Palaeoecol.* 64, 35–42. [https://doi.org/10.1016/0031-0182\(88\)90140-X](https://doi.org/10.1016/0031-0182(88)90140-X)
- Wei, C.L., Rowe, G.T., Nunnally, C.C., Wicksten, M.K., 2012. Anthropogenic “Litter” and macrophyte detritus in the deep Northern Gulf of Mexico. *Mar. Pollut. Bull.* 64, 966–973. <https://doi.org/10.1016/j.marpolbul.2012.02.015>
- Wentworth, C.K., 1922. A scale of grade and class terms for clastic sediments. *J. Geol.* 30, 377–392.
- Wiles, E., Green, A., Watkeys, M., Botes, R., Jokat, W., 2019. Submarine canyons of NW Madagascar: A first geomorphological insight. *Deep. Res. Part II Top. Stud. Oceanogr.* 161, 5–15. <https://doi.org/10.1016/j.dsr2.2018.06.003>
- Wijeratne, S., Pattiaratchi, C., Proctor, R., 2018. Estimates of surface and subsurface boundary current transport around Australia. *J. Geophys. Res. Ocean.* 123, 3444–3466. <https://doi.org/10.1029/2017JC013221>
- Wilkin, J., Cuthbertson, A., Dawson, S., Stow, D., Stephen, K., Nicholson, U., Penna, N., 2023. The response of high density turbidity currents and their deposits to an abrupt channel termination at a slope break: Implications for channel-lobe transition zones. *Sedimentology* 70, 1164–1194. <https://doi.org/10.1111/sed.13073>
- Wunsch, M., Betzler, C., Lindhorst, S., Lüdmann, T., Eberli, G.P., 2017. Sedimentary dynamics along carbonate slopes (Bahamas archipelago). *Sedimentology* 64, 631–657. <https://doi.org/10.1111/sed.12317>
- Wynn, R.B., Stow, D.A.V., 2002. Classification and characterisation of deep-water sediment waves. *Mar. Geol.* 192, 7–22. [https://doi.org/10.1016/S0025-3227\(02\)00547-9](https://doi.org/10.1016/S0025-3227(02)00547-9)
- Wynn, R.B., Weaver, P.P., Ercilla, G., Stow, D.A., Masson, D.G., 2000. Sedimentary processes in the selvage sediment-wave field, NE Atlantic: new insights into the formation of sediment waves by turbidity currents. *Sedimentology* 47, 1181–1197. <https://doi.org/10.1046/j.1365-3091.2000.00348.x>

- Wynn, R.B., Kenyon, N.H., Masson, D.G., Stow, D.A.V., Weaver, P.P.E., 2002a. Characterization and recognition of deep-water channel-lobe transition zones. *AAPG Bull.* 86, 1441–1462. <https://doi.org/10.1306/61eedcc4-173e-11d7-8645000102c1865d>
- Wynn, R.B., Piper, D.J.W., Gee, M.J.R., 2002b. Generation and migration of coarse-grained sediment waves in turbidity current channels and channel-lobe transition zones. *Mar. Geol.* 192, 59–78. [https://doi.org/10.1016/S0025-3227\(02\)00549-2](https://doi.org/10.1016/S0025-3227(02)00549-2)
- Xu, J.P., 2011. Measuring currents in submarine canyons: Technological and scientific progress in the past 30 years. *Geosphere* 7, 868876. <https://doi.org/10.1130/GES00640.1>
- Xu, J.P., Noble, M., Eittreim, S.L., Rosenfeld, L.K., Schwing, F.B., Pilskaln, C.H., 2002. Distribution and transport of suspended particulate matter in Monterey Canyon, California. *Mar. Geol.* 181, 215–234. [https://doi.org/10.1016/S0025-3227\(01\)00268-7](https://doi.org/10.1016/S0025-3227(01)00268-7)
- Xu, J.P., Wong, F.L., Kvitek, R., Smith, D.P., Paull, C.K., 2008. Sandwave migration in Monterey Submarine Canyon, Central California. *Mar. Geol.* 248, 193–212. <https://doi.org/10.1016/j.margeo.2007.11.005>
- Xu, J.P., Swarzenski, P.W., Noble, M., Li, A.C., 2010. Event-driven sediment flux in Hueneme and Mugu submarine canyons, southern California. *Mar. Geol.* 269, 74–88. <https://doi.org/10.1016/j.margeo.2009.12.007>
- Xu, J.P., Barry, J.P., Paull, C.K., 2013. Small-scale turbidity currents in a big submarine canyon. *Geology* 41, 143–46. <https://doi.org/10.1130/G33727.1>
- Xu, J.P., Sequeiros, O.E., Noble, M.A., 2014. Sediment concentrations, flow conditions, and downstream evolution of two turbidity currents, Monterey Canyon, USA. *Deep. Res. Part I Oceanogr. Res. Pap.* 89, 11–34. <https://doi.org/10.1016/j.dsr.2014.04.001>
- Yin, S., Lin, L., Pope, E.L., Li, J., Ding, Weifeng, Wu, Z., Ding, Weiwei, Gao, J., Zhao, D., 2019. Continental slope-confined canyons in the Pearl River Mouth Basin in the South China Sea dominated by erosion, 2004–2018. *Geomorphology* 344, 60–74. <https://doi.org/10.1016/j.geomorph.2019.07.016>
- Zhang, J., Wu, S., Hu, G., Fan, T. en, Yu, B., Lin, P., Jiang, S., 2018. Sea-level control on the submarine fan architecture in a deepwater sequence of the Niger Delta Basin. *Mar. Petrol. Geol.* 94, 179–197. <https://doi.org/10.1016/j.marpetgeo.2018.04.002>

- Zhang, S., Zhu, J., Jia, Y., Li, S., Chen, R., Chen, X., Ou, X., Li, Q., 2022. Submarine small-scale features of cyclic steps in the Penghu Canyon: Implications for the migration of canyon. *J. Mar. Sci. Eng.* 10, 1301. <https://doi.org/10.3390/jmse10091301>
- Zhong, G., Peng, X., 2021. Transport and accumulation of plastic litter in submarine canyons—The role of gravity flows. *Geology* 49, 581–586. <https://doi.org/10.1130/g48536.1>
- Zhong, G., Cartigny, M.J., Kuang, Z., Wang, L., 2015. Cyclic steps along the South Taiwan Shoal and West Penghu submarine canyons on the northeastern continental slope of the South China Sea. *Geol. Soc. Am. Bull.* 127, 804–824. <https://doi.org/10.1130/B31003.1>
- Zhou, W., Chiarella, D., Zhuo, H., Wang, Y., Tang, W., Zou, M., Xu, Q., 2021. Genesis and evolution of large-scale sediment waves in submarine canyons since the Penultimate Glacial Maximum (ca. 140 ka), northern South China Sea margin. *Mar. Petrol. Geol.* 134, 105381. <https://doi.org/10.1016/j.marpetgeo.2021.105381>
- Zhu, M., Graham, S., Pang, X., McHargue, T., 2010. Characteristics of migrating submarine canyons from the middle Miocene to present: Implications for paleoceanographic circulation, northern South China Sea. *Mar. Petrol. Geol.* 27, 307–319. <https://doi.org/10.1016/j.marpetgeo.2009.05.005>
- Zúñiga, D., Flexas, M.M., Sanchez-Vidal, A., Coenjaerts, J., Calafat, A., Jordà, G., García-Orellana, J., Puigdefàbregas, J., Canals, M., Espino, M., Sardà, F., Company, J.B., 2009. Particle fluxes dynamics in Blanes submarine canyon (Northwestern Mediterranean). *Prog. Oceanogr.* 82, 239–251. <https://doi.org/10.1016/j.pocean.2009.07.002>



**Sedimentary and litter transfer processes in the
northern margin of the Alboran Sea:**
The role of shelf-incised submarine canyon
geomorphological characteristics

Javier Cerrillo Escoriza
PhD Thesis, 2024